University of Alberta

PRACTICAL DIVERSITY COMBINING SCHEMES FOR GENERALIZED FADING CHANNELS

by

Sasan Haghani

A thesis submitted to the Faculty of Graduate Studies and Research in partial fulfillment of the requirements for the degree of Doctor of Philosophy

Department of Electrical and Computer Engineering

Edmonton, Alberta

Fall 2007

Your file Votre référence
ISBN: 978-0-494-47639-0
Our file Notre référence
ISBN: 978-0-494-47639-0

To Laleh,

My love, soul mate and best friend

Abstract

Spatial diversity employing multiple antennas is an effective method for mitigating the effects of fading in mobile communication systems. One of the simplest and lowest complexity diversity methods used for the mitigation of the deleterious effects of fading channels is switch-and-stay combining (SSC). In the first part of this thesis, we study the performances of predetection and postdetection SSC receivers in correlated fading channels. Tractable analytical expressions are obtained for the average symbol error rate (SER) of various modulation formats of practical interest. It is shown that the performance gain of postdetection SSC over predetection SSC can be as much as 1.1 dB in average signal-to-noise power ratio (SNR). In the second part, we examine the performances of noncoherent modulation schemes with L branch signal-*plus*-noise $(S+N)$ selection combining (SC) receivers in independent as well as correlated fading channels. We compare the performances of $S+N$ SC receivers with the classical SC receiver and show that, unlike as suggested by previously published results, the performances of $S+N$ SC receivers are not always superior to the performance of the classical SC receiver, if the receiver is operating in the low SNR region. However, for moderate to large average SNR, we show that $S+N$ SC can have a gain of 1.5 dB in average SNR over classical SC, when operating in correlated fading channels.

In the last part of this thesis, we propose and examine the performance of a dual-branch decorrelator receiver in correlated fading channels. It is shown that the receiver

does not need any knowledge of channel statistics to perform the decorrelation. It is observed that the decorrelator receiver when combined with switched combining and classical SC is superior to the performance of a conventional switched combining and classical SC receiver, respectively. The gain of the decorrelator receiver over the conventional receiver is shown to be as much 2.8 dB in average SNR when SSC is employed.

Acknowledgments

I would like to express my sincere gratitude to my supervisor Dr. Norman C. Beaulieu for his valuable guidance, encouragement, technical advice, financial support and friendship during my studies at the University of Alberta. It has been a true privilage for me studying under his supervision. His depth of knowledge, clarity in thinking and unfaltering standards of excellence have been a true inspiration for me. I would also like to thank the members of the *i*CORE Wireless Communications Laboratory for their friendship and support. Also, my sincere thanks to Sharon Walker for her valuable friendship and help with the administrative work during my studies at the University of Alberta.

I would like to thank Dr. Mohamed-Slim Alouini of Texas A&M University who has agreed to serve as my external examiner. I am honored to have him on my Ph.D defense committee. I am also deeply grateful to Drs. Ioanis Nikolaidis, Chintha Tellambura, Masoud Ardakani and Venkata Dinavahi for reading my thesis and serving on my Ph.D. defense committee.

I am indebted to my parents for their continuous love and moral support during my studies. My heartful thanks go to my loving wife, Laleh, whose patience, love and support have been instrumental in the completion of this work.

Finally, I would like to acknowledge the financial support I have received from the Alberta Informatics Circle of Research Excellence (*i*CORE), Alberta Ingenuity Fund,

the Natural Science and Engineering Research Council of Canada (NSERC) and the J. Gordin Kaplan Graduate Student Award at the University of Alberta.

Contents

1 Introduction 1

1.1 Fading Channels 1

1.1.1 Slow and Fast Fading Channels 2

1.1.2 Small- and Large-Scale Fading Channels 2

1.1.3 Frequency-Selective Fading Channels 3

1.1.4 Frequency Non-selective Fading Channels 3

1.1.4.1 Rayleigh Distribution 4

1.1.4.2 Rice Distribution 4

1.1.4.3 Nakagami-m Distribution 5

1.2 Diversity Methods 5

1.2.1 Classical Selection Combining 6

1.2.2 Signal-plus-Noise $(S + N)$ Selection Combining 7

1.2.3 Maximal Ratio Combining 7

1.2.4 Equal Gain Combining 7

1.2.5 Square-Law Combining 8

1.2.6 Switch-and-Stay Combining 8

1.3 System Performance Measures 8

1.3.1 Mean Output SNR 8

1.3.2 Outage Probability 9
1.3.3 Average Bit Error Probability 9
1.4 Thesis Outline and Contributions 9

2 Predetection Switched Combining in Correlated Rician Fading 13
2.1 Introduction 13
2.2 Switching Mechanism 14
2.3 Error Rate Analysis 16
2.3.1 Moment Generating Function 17
2.3.2 Mean Output SNR 18
2.3.3 Average SER 20
2.3.4 Outage Probability 23
2.4 Numerical Examples 23
2.5 Conclusion 30

3 Performance of Postdetection Switch-and-Stay Combining Schemes in Correlated Rayleigh and Rician Fading 31
3.1 Postdetection SSC Model 1 32
3.1.1 System Model 32
3.1.2 Average BER Analysis 34
3.1.2.1 Rayleigh Fading 35
3.1.2.2 Rician Fading 41
3.2 Postdetection SSC Model 2 44
3.2.1 System Model 44
3.2.2 Average Symbol Error Rate 46
3.2.2.1 Rayleigh Fading 48

3.2.2.2 Rician Fading 51
3.3 Numerical Examples and Discussion 53
3.4 Conclusion 64

4 Performance of $S+N$ Selection Combining Receivers in Independent Nakagami and Rician Fading 65

4.1 Performance of $S + N$ SC Receiver Model 1 66
4.1.1 Rician Fading 69
4.1.2 Nakagami-m Fading 70
4.1.3 Rayleigh Fading 73
4.2 Performance of $S + N$ SC Receiver Model 2 73
4.2.1 Rician Fading 76
4.2.2 Nakagami-m Fading 78
4.2.3 Rayleigh Fading 79
4.3 Performance Analysis of noncoherent MFSK with Classical Selection Combining 80
4.3.1 Rician Fading 81
4.3.2 Nakagami-m Fading 81
4.3.3 Rayleigh Fading 82
4.4 Numerical Examples and Discussion 83
4.5 Conclusions 98

5 Performance of $S + N$ Selection Diversity Receivers in Correlated Rayleigh and Rician Fading 99

5.1 Average SER of $S + N$ SC Model 1 100
5.1.1 Rayleigh Fading 102

5.1.2 Rician Fading 105
5.2 Average BER of $S+N$ SC Model 2 106
5.2.1 Rayleigh Fading 108
5.2.2 Rician Fading 110
5.3 Numerical Examples 112
5.4 Conclusion 123

6 On Decorrelation in Dual-Branch Diversity Systems 124

6.1 Introduction 124
6.2 System Model 128
6.3 Selection Combining 129
6.3.1 Output SNR CDF 130
6.3.2 Output SNR PDF 130
6.3.3 Output SNR MGF 130
6.3.4 Mean Output SNR 131
6.3.5 Average Error Rate 131
6.3.6 Outage Probability 133
6.4 Switch-and-Stay Combining 134
6.4.1 Output SNR CDF 134
6.4.2 Output SNR PDF 135
6.4.3 Output SNR MGF 135
6.4.4 Mean Output SNR 136
6.4.5 Average Error Rate 136
6.5 Square-Law Combining 138
6.6 Equal Gain Combining 139
6.7 Numerical Examples 140

6.8 Conclusion 154

7 Conclusion **155**

7.1 Conclusions 155

7.2 Suggestions for Future Research 157

References **160**

Appendix A **178**

Appendix B **181**

Vita **183**

List of Figures

2.1 The average SER of QFSK as a function of the average SNR per symbol per branch in correlated Rician fading for $K = 5$ and $\rho = 0.2, 0.4$ and 0.8. The optimum switching threshold values that minimize the SER are used to plot the curves. 25

2.2 The optimum switching threshold of QFSK as a function of the average SNR per symbol per branch for $\rho = 0.4$ and $K = 0, 3, 6$ and 9. 26

2.3 The optimum switching threshold of QFSK as a function of the average SNR per symbol per branch for $\rho = 0, 0.3, 0.6$ and 0.8 and for $K = 2$ and 10. 27

2.4 The average SER of QFSK as a function of the switching threshold for several values of ρ and $\bar{\gamma}$. 28

2.5 The optimum outage probability of dual-branch predetection SSC as a function of the normalized switching threshold for $\rho = 0.35$ and 0.55 and for $K = 3, 5$ and 7. 29

3.1 The block diagram of postdetection SSC receiver Model 1 (after [10, Fig. 1]). 33

3.2 The average BER versus the normalized switching thresholds of noncoherent BFSK with postdetection SSC Model 1 in non-identically distributed correlated Rayleigh fading with $\rho = 0.7$, $\bar{\gamma}_1 = 10$ dB and $\bar{\gamma}_2 = 5.48$ dB ($\delta = 0.6$). 40

3.3 The block diagram of postdetection SSC receiver Model 2 (after [24, Fig. 1]). 44

3.4 The average BER of BFSK with postdetection SSC Model 2 in correlated Rayleigh fading with average fading power imbalance for $\rho = 0.5$, $\bar{\gamma}_1 = 15$ dB and $\bar{\gamma}_2 = 13.2$ dB ($\delta = 0.4$). 50

3.5 The average BER of BFSK with postdetection SSC Model 1 as a function of switching threshold in correlated Rician fading for $\bar{\gamma} = 10$ dB, 15 dB and 25 dB and $\rho = 0, 0.4$ and 0.8. 56

3.6 The average BER of BFSK with postdetection SSC Model 2 as a function of switching threshold in correlated Rician fading for $\bar{\gamma} = 10$ dB, 15 dB and 25 dB and $\rho = 0, 0.4$ and 0.8. 57

3.7 The average BER of MFSK with postdetection SSC Model 2 as a function of switching threshold in correlated Rician fading with $\rho = 0.6$ and $K = 5$ for $M = 2, 4, 8, 16$ and 32. 58

3.8 The average BER of QFSK with postdetection SSC Model 2 and predetection SSC as a function of the average SNR per bit per branch in identically distributed correlated Rician fading with $\rho = 0.5$ and $K = 0, 3, 6$ and 10. 59

3.9 The average BER of QFSK with postdetection SSC Model 2 and predetection SSC as a function of the average SNR per bit per branch in identically distributed correlated Rician fading branches with $K = 5$ for several values of correlation $\rho = 0, 0.3, 0.5$ and 0.8. 60

3.10 The average BER of MFSK with postdetection SSC Model 2 and predetection SSC as a function of the average SNR per bit per branch in identically distributed correlated Rician fading branches with $K = 5$ and $\rho = 0.6$ for $M = 4, 16$ and 64. 61

3.11 The average BER of BFSK with postdetection SSC Model 1 and 2 and predetection SSC as a function of average SNR per bit per branch in identically distributed correlated Rician fading with $K = 5$ for $\rho = 0, 0.4$ and 0.8. 62

3.12 Comparison of postdetection SSC Model 1 and Model 2 in correlated Rayleigh fading with average fading power imbalance for several values of ρ. 63

4.1 The structure of the noncoherent MFSK $S + N$ Selection Receiver Model 1. 67

4.2 The structure of the noncoherent BFSK $S+N$ Selection Receiver Model 2 (after [7, Fig. 3]). 74

4.3 The average BER of noncoherent QFSK with 4-branch $S + N$ SC receiver Model 1 and classical SC in i.i.d Nakagami-m fading with $m = 1, 3$ and 6. 87

4.4 The average BER of noncoherent QFSK with 4-branch $S + N$ SC receiver Model 1 and classical SC in i.n.d Nakagami-m fading with $m = 1, 3$ and 6 and $\beta = 0.8$. 88

4.5 The average SER of noncoherent QFSK over 4-branch i.n.d Rician fading with an average decay factor $\beta = 0.5$ for $K = 0, 3$ and 6. . . . 89

4.6 The average SER of noncoherent QFSK in 4-branch i.n.d Rician fading with an average decay factor $\beta = 1$ for $K = 0, 3$ and 6. 90

4.7 The average BER of noncoherent MFSK with 4-branch $S + N$ SC receiver Model 1 and classical SC in i.i.d Nakagami-m fading with $m = 2$ for $M = 4, 8$ and 16. 91

4.8 The average BER of noncoherent MFSK with 4-branch $S + N$ SC receiver Model 1 and classical SC in i.n.d Nakagami-m fading with $m = 2$ and $\beta = 0.8$ for $M = 4, 8$ and 16. 92

4.9 The average BER of noncoherent BFSK with $S + N$ SC Model 1 in i.n.d Rician fading with $L = 2, 4$ and 8, an average decay factor of $\beta = 0.5$ and $K = 3$. 93

4.10 The average BER of noncoherent 16-ary FSK with 4-branch $S + N$ SC receiver Model 1 and classical SC in i.n.d Nakagami-m fading with $m = 4$ and $\beta = 0, 0.3$ and 0.8. 94

4.11 The average BER of noncoherent BFSK with 4-branch $S + N$ SC receiver Model 2 and classical SC in i.n.d Nakagami-m fading with $m = 5$ and $\beta = 0, 0.3$ and 0.8. 95

4.12 The average BER of noncoherent 8-ary FSK in L-branch i.i.d Nakagami-m fading with $S + N$ SC receiver Model 1, classical SC and SLC for $m = 3$ and $L = 3, 4$ and 5. 96

4.13 The average BER of noncoherent BFSK in L-branch i.i.d Nakagami-m fading with $S + N$ SC receiver Model 1, $S + N$ SC receiver Model 2 and SLC for $m = 5$ and $L = 3, 4$ and 5. 97

5.1 The average BER of QFSK with $S+N$ SC Model 1 and classical SC as a function of average SNR per bit per branch in equally correlated identically distributed Rician fading for $K=4$, $\rho=0.5$ and $L=2,4$ and 6. 116

5.2 The average BER of QFSK with $S+N$ SC Model 1 and classical SC as a function of average SNR per bit per branch in equally correlated Rician fading for $K=0,5,10$ and $\rho=0.6$. 117

5.3 The average BER of 4-branch MFSK with $S+N$ SC Model 1 and classical SC as a function of average SNR per bit per branch in correlated Rayleigh fading with $M=2,4$ and 16. 118

5.4 The average BER of QFSK with $S+N$ SC Model 1 and classical SC as a function of the average SNR per bit of the first branch in correlated Rayleigh fading with $\beta=0,0.5$ and 1. 119

5.5 The average BER of 3-branch BFSK with $S+N$ SC Model 1 and $S+N$ SC Model 2 in correlated Rayleigh fading for several values of average decay factor $\beta=0,0.6$ and 1.2. 120

5.6 The average BER of 4-branch BFSK with $S+N$ SC Model 1, $S+N$ SC Model 2 and classical SC as a function of average SNR per bit per branch in equally correlated Rician fading with $K=5$ and $\rho=0.2,0.4$ and 0.6 121

5.7 The average BER of 2-, 3-, and 4-branch BFSK with classical SC, $S+N$ SC Model 1 and $S+N$ SC Model 2 as a function of average SNR per bit per branch in equally correlated Rician fading with $K=10$ and $\rho=0.6$. 122

6.1 The structure of the dual-branch decorrelator receiver. 127

6.2 The normalized mean output SNRs of the conventional and decorrelator EGC receivers as a function of the correlation, ρ, for $K = 3, 6$ and 9. 144

6.3 The average BER of BPSK for the conventional and decorrelator SC receivers as a function of the average SNR per bit per branch in correlated Rician fading with $\rho = 0.55$ for $K = 0, 5$ and 10. 145

6.4 The average BER of BPSK for the conventional and the decorrelator SC receivers as a function of the average SNR per bit per branch in correlated Rician fading with $K = 5$ for $\rho = 0.1, 0.5$ and 0.9. 146

6.5 The outage probability of conventional and decorrelator SC receivers as a function of the average SNR per branch in correlated Rician fading with $\rho = 0.5$ for $K = 0, 5$ and 10. 147

6.6 The outage probability of conventional and decorrelator SC receivers as a function of the average SNR per branch in correlated Rician fading with $K = 6$ for $\rho = 0.1, 0.4$ and 0.8. 148

6.7 The average output SNR of the conventional and the decorrelator receivers in correlated Rician fading with $\rho = 0.5$ for $K = 0, 5$ and 10. . 149

6.8 The average BER of QFSK for the conventional and decorrelator SSC receivers in correlated Rician fading with $\rho = 0.6$ for $K = 0, 5$ and 10. 150

6.9 The average BER of QFSK for the decorrelator SSC receiver as a function of the switching threshold in correlated Rician fading with $K = 5$ and $\rho = 0.1, 0.5$ and 0.9 for $\bar{\gamma} = 10, 15$ and 25 dB. 151

6.10 The average BER of MFSK for the conventional and the decorrelator SSC receivers in correlated Rician fading with $\rho = 0.6$ and $K = 4$ for $M = 2, 4$ and 16. 152

6.11 The average output SNR of the conventional and the decorrelator SSC receivers as a function of the average SNR per symbol in correlated Rician fading with $K = 10$ for $\rho = 0.15, 0.45$ and 0.75. 153

Acronyms

AWGN	additive white Gaussian noise
BER	bit error rate
BFSK	binary frequency shift keying
BPSK	binary phase shift keying
CDF	cumulative distribution function
CDMA	code division multiple access
DPSK	differential phase shift keying
EGC	equal gain combining
FDMA	frequency division multiple access
GDC	general diversity combining
H-S/MRC	hybrid-selection/maximal ratio combining
LOS	line of sight
MFSK	M-ary frequency shift keying
MGF	monent generating function
MIP	multipath intensity profile
MPSK	M-ary phase shift keying
MQAM	M-ary quadrature amplitude modulation
MRC	maximal ratio combining

PDF	probability density function
QDPSK	quadrature differential phase shift keying
QFSK	quaternary frequency shift keying
RF	radio frequency
RV	random variable
SC	selection combining
SER	symbol error rate
$S+N$ SC	signal-*plus*-noise selection combining
SLC	square-law combining
SNR	signal-to-noise power ratio
SSC	switch-and-stay Combining

List of Symbols

E_s	Energy per symbol
E_b	Energy per bit
$\mathbb{E}[\cdot]$	Expectation operation
f_i	The frequency matched to ith symbol
f_X	PDF of the RV X
$f_{X\|Z}$	Conditional PDF of the RV X given Z
$f_{\gamma_{\mathrm{SSC}}}$	PDF of the SSC output SNR
$f_{\gamma_{\mathrm{SC}}}$	PDF of the SC output SNR
$F_X(\cdot)$	CDF of the RV X
$F_{X\|Z}(\cdot)$	Conditional CDF of the RV X given Z
$F_{X_1,X_2}(\cdot,\cdot)$	Joint CDF of the RVs X_1 and X_2
$F_{\gamma_{\mathrm{SSC}}}(\cdot)$	CDF of the SSC output SNR
g_i	The complex channel gain on the ith branch
G_i	The complex channel gain on the ith branch
$I_0(\cdot)$	Zero-order Modified Bessel function of the first kind
$I_1(\cdot)$	First-order Modified Bessel function of the first kind
j	The imaginary number $\sqrt{-1}$
K	Rician fading parameter
K_i	Rician fading parameter on the ith branch

L	Total number of diversity branches
L_c	Number of diversity branches selected in H-S/MRC
$L_k(\cdot)$	The Laguerre polynomial
m	Nakagami fading parameter
m_i	Nakagami fading parameter on the ith branch
M	Modulation order
N_0	One-sided power spectral density of white Gaussian noise
N_{ij}	Complex Gaussian noise of the jth square-law detector on the ith branch
n_i	Complex Gaussian noise on the ith branch
P_{out}	Outage Probability
$P_b(E)$	Average BER
$P_s(E)$	Average SER
$Q(\cdot)$	The area under the tail of the Gaussian PDF
$Q_1(\cdot,\cdot)$	The first order Marcum-Q function
T	Time interval between switching times
T_0	Channel coherence time
T_s	Time duration of a symbol transmission
w_{T_i}	Switching threshold on the ith branch
W_{ij}	The output of the jth square-law detector on the ith branch
α	Fading amplitude
α_i	The fading amplitude on the ith branch
β	Average power decay factor
Ω	Average fading power
Ω_i	Average fading power on the ith branch

γ_{SC}	The output SNR of selection combining
γ_{MRC}	The output SNR of maximal ratio combining
γ_{SSC}	The output SNR of switch-and-stay combining
γ_{th}	Outage probability threshold
$\bar{\gamma}$	Average SNR
$\bar{\gamma}_{\text{SSC}}$	The mean output SNR of the SSC receiver
$\bar{\gamma}_{\text{SC}}$	The mean output SNR of the SC receiver
$\bar{\gamma}_{\text{EGC}}$	The mean output SNR of the EGC receiver
η_T	Switching threshold
η_{T_i}	Normalized switching threshold on the ith branch
η^*	The optimum switching threshold
ρ	Correlation coefficient
ρ_η	Power correlation
$\Phi_{\gamma_{\text{SSC}}}$	The MGF of the predetection SSC output SNR
$\Phi_{\gamma_{\text{SC}}}$	The MGF of the decorrelator SC output SNR
ψ_i	The channel phase on the ith branch

Chapter 1

Introduction

Wireless technology is the foundation for the much anticipated ubiquitous communication systems that allow people and machines to transfer and receive information on the move, anytime and anywhere. Wireless systems operate on complex and time varying channels that introduce severe multipath and shadow fading to the propagating signal. This places fundamental limitations on the performances of mobile communication systems. Many methods such as linear diversity combining techniques are used to overcome the effects of fading.

In this chapter, we first give a brief review of fading channels and we introduce some linear diversity combining techniques which are used to overcome the effects of fading. Next, we introduce system performance measures which are widely used in assessing the performance of various digital communication systems. Finally, we conclude this chapter with the thesis outline and a summary of contributions.

1.1 Fading Channels

When a steady-state, single-frequency, radio wave is transmitted over a multipath channel, the envelope amplitude of the received signal is observed to fluctuate in

time. This phenomenon is known as fading [1] and its existence constitutes one of the limitations of mobile communication design. In the following sections, fading channels are categorized.

1.1.1 Slow and Fast Fading Channels

Fading channels can be categorized as fast fading or slow fading channels [2], [3]. The terminology fast fading is used to describe channels in which the channel coherence time, T_0, is less than the time duration of a symbol transmission, T_s. The coherence time is a measure of the expected time duration over which the channels response is essentially invariant. In fast fading channels $T_0 < T_s$, and the time in which the channel behaves in a correlated manner is shorter than the time duration of the symbol. In contrast, under slow fading $T_0 > T_s$, and so the channel state will virtually remain unchanged during the time in which the symbol is transmitted.

1.1.2 Small- and Large-Scale Fading Channels

Another categorization of fading channels is large-scale and small-scale fading [2], [3]. Large-scale fading represents the average signal power attenuation or path loss due to the transmission of the signal over large areas. The statistics of large-scale fading provide a way of comparing an estimate of the path loss as a function of distance, where path loss is defined as the received power expressed in the terms of transmitted power. Small-scale fading refers to dramatic changes in signal amplitude and phase that can be experienced as a result of small changes (as small as one-half wavelength) in the spatial separation between the receiver and the transmitter. Small-scale fading is further categorized as frequency selective and frequency non-selective fading.

1.1.3 Frequency-Selective Fading Channels

In frequency-selective fading, as the name suggests, the frequency components of the transmitted signal are not attenuated equally by the channel. Frequency-selective fading is found in wide-band systems where the bandwidth is greater than the coherence bandwidth. Coherence bandwidth is defined as the range of frequencies over which the fading effect introduced by the channel is highly correlated [3]. In other words, the coherence bandwidth represents a range of frequency over which the channel passes all spectral components with approximately equal gain and linear phase. One of the consequences of frequency-selective channels is the time dispersion in the transmitted signal which limits the system performance by causing intersymbol interference in the detection process.

1.1.4 Frequency Non-selective Fading Channels

A fading channel is called non-selective if all the frequencies are affected in the same manner. Narrowband systems, where the transmission bandwidth occupied by the signal is smaller than the coherence bandwidth, experience non-selective fading.

In a frequency non-selective channel the phase and the amplitude of the signal are affected. The phase is usually assumed to have a uniform distribution in $[0, 2\pi]$. For the envelope of the transmitted signal, however, many different distribution models have been proposed in the literature. The most well known distributions are the Rayleigh, Rician and Nakagami-m distributions. The probability density function (PDF) for each of these distributions and short descriptions of the environments in which these models are used, are given below.

1.1.4.1 Rayleigh Distribution

In a rich scattering environment where there is no line of sight (LOS) between the receiver and the transmitter, the envelope of the fading signal is modeled with a Rayleigh probability density function (PDF) [4], [5]. The PDF of the fading amplitude, α, is given by

$$f(\alpha, \Omega) = \frac{2\alpha}{\Omega} \exp(-\frac{\alpha^2}{\Omega}), \quad \alpha \geq 0 \tag{1.1}$$

where $\Omega = \mathbb{E}[\alpha^2]$ is the average fading. Note that $\mathbb{E}[\cdot]$ denotes the expectation operation.

1.1.4.2 Rice Distribution

Some types of scattering environments have a specular or LOS component. This happens in microcellular urban and suburban land mobile, picocellular indoor and factory environments. In these environments the Rice distribution is used to model the fading amplitude α and its PDF is given by [4]

$$f(\alpha; \Omega, K) = \frac{2\alpha(1+K)}{\Omega} \exp\left(-K - \frac{(1+K)\alpha^2}{\Omega}\right) I_0\left(2\alpha\sqrt{\frac{K(1+K)}{\Omega}}\right), \quad \alpha \geq 0 \tag{1.2}$$

where K is the Rice factor defined as

$$K = \frac{\text{Specular component power}}{\text{Scattered component power}} = \frac{s^2}{\Omega} \tag{1.3}$$

and $\mathbb{E}[\alpha^2] = s^2 + \Omega$ and where $I_0(\cdot)$ denotes the modified Bessel function of the first kind of order zero. Note that for $K = 0$, this model reduces to the Rayleigh model and for $K = \infty$, the channel does not exhibit fading at all.

1.1.4.3 Nakagami-m Distribution

The Nakagami-m model was first developed by Nakagami in early 1940's. It is often the best fit to land mobile and indoor mobile multipath propagation as well as ionospheric radio links [4]. The PDF of the fading amplitude α is given by [4]

$$f(\alpha;\Omega,m)=\frac{2m^m\alpha^{2m-1}}{\Omega^m\Gamma(m)}\exp\left(-\frac{m\alpha^2}{\Omega}\right),\quad \alpha\geq 0 \tag{1.4}$$

where m is the fading parameter defined as

$$m=\frac{\Omega^2}{\mathbb{E}[(R^2-\Omega)^2]},\qquad m\geq\frac{1}{2}.$$

As was stated earlier the Nakagami-m distribution has better accuracy in matching experimental data than the Rayleigh and the Rice distributions. The parameter m controls a wide range of fading models. For $m=\frac{1}{2}$ and $m=1$ the Nakagami-m distribution reduces to the one-sided Gaussian and Rayleigh distributions, respectively. Also, as m approaches $+\infty$ the pdf becomes an impulse function located at $\sqrt{\Omega}$, which corresponds to a channel with no fading.

1.2 Diversity Methods

Diversity is an effective method that exploits the principle of providing the receiver with multiple faded replicas of the same information bearing signal [4]. To understand why diversity can be an effective method to improve the system performance, assume that the receiver has L independent copies of the transmitted signal. Then if p denotes the probability of any given branch being in a deep fade, then the probability of having an all the branches being in deep fades will be p^L [6].

Diversity can be achieved by several methods. Some are antenna diversity, angle

diversity, polarization diversity and frequency diversity. The most well known diversity method used in wireless communication systems is antenna diversity. Diversity combining schemes can be categorized as predetection and postdetection combining schemes. Diversity combining that takes effect at radio frequency (RF) is called predetection combining, while diversity combining that takes effect at baseband is called postdetection combining.

Lets assume that there are L diversity branches at the receiver and each branch undergoes frequency nonselective fading. The signals that are received at the diversity branches could be combined in different ways. Depending on the bit error rate (BER) requirements of the system and the constraints on the complexity one can choose a diversity combining technique.

1.2.1 Classical Selection Combining

In selection combining (SC) the input having the largest signal-to-noise ratio (SNR) among L possible branches is selected for data detection. The output SNR of SC can be expressed as

$$\gamma_{\text{SC}} \triangleq \max_i \{\gamma_i\} = \gamma_{(1)}. \tag{1.5}$$

where $\gamma_{(i)}$'s are the ordered SNR's of the diversity branches, i.e., $\gamma_{(1)} > \gamma_{(2)} > \cdots > \gamma_{(L)}$. Note that in the analysis of classical SC, such as that presented in [5], it is assumed that in measuring the largest SNR, the average noise power, computed as

$$\overline{n^2(t)} = \frac{1}{\tau}\int_0^\tau n^2(t)dt \tag{1.6}$$

is taken over a sufficiently long time τ such that it can be assumed constant over all branches [7]. Therefore, in the analysis of classical SC, choosing the largest signal magnitude is considered equivalent to choosing the largest SNR.

1.2.2 Signal-plus-Noise ($S + N$) Selection Combining

In a practical communication system employing classical SC, one needs to measure the SNR on each diversity branch in order to choose the largest for data recovery. This however, might be expensive or difficult especially for high signaling rates. As a result, the branch with the largest signal-plus-noise ($S + N$) sample at the output of the matched filter is selected for data recovery. We refer to this combining scheme as $S + N$ SC.

1.2.3 Maximal Ratio Combining

In this method, the signals from L branches are weighted proportionally to their SNRs, co-phased and then summed. Brennan [1] has proved that the output SNR of the MRC combiner is equal to the sum of the branch SNRs, that is

$$\gamma_{\text{MRC}} = \sum_{i=1}^{L} \gamma_i.$$

If the branches are independent and identically distributed and the signals have equal energy, then it can be shown that MRC is equivalent to maximum likelihood (ML) detection [4, pp. 280-281]. Note that MRC is used with coherent modulation systems.

1.2.4 Equal Gain Combining

In MRC, the receiver has to estimate both the phase and the amplitude of the complex channel gain and is expensive to implement. Equal gain combining (EGC) is a simpler diversity method, where the branches are co-phased and are equally weighted, alleviating the need to estimate the amplitude of the channel.

1.2.5 Square-Law Combining

In square-law combining (SLC), the outputs of the square-law detectors are summed to form the final decision. For orthogonal digital modulation with noncoherent demodulation and independent and identically distributed (i.i.d) diversity branches, the optimum diversity combining technique is SLC [8].

1.2.6 Switch-and-Stay Combining

Switch-and-Stay Combining (SSC) is a combining scheme designed to simplify the complexity of a classical selection combiner. As mentioned earlier, in a classical SC receiver the system has to monitor all the branches to find the branch with the best fading conditions. In SSC, however, the receiver selects a particular antenna until its quality drops below a predetermined threshold. When this happens, the receiver switches to another antenna and stays connected to it until the signal quality drops below the threshold, regardless of whether the quality of that antenna is above or below the predetermined threshold.

We note that switching transients will cause "dead times" (locally generated outages) in the receiver. However, switching rate analyses of SC and SSC systems have only been recently considered in the literature [9], [10], [11]. For example, Beaulieu has obtained analytical expressions for the switching rates of dual-branch SC and SSC systems [11]. We do not consider the deleteroius effects of switching transients in this thesis.

1.3 System Performance Measures

In this section we briefly introduce three measures which are widely used in evaluating the performance of wireless communication systems.

1.3.1 Mean Output SNR

One of the most well known performance measures of a communication system is the mean output SNR at the combiner output. The mean output SNR is often used as a comparative performance measure in communication systems and can be obtained as [12]

$$\bar{\gamma} = \int_0^\infty x f_\gamma(x) dx \tag{1.7}$$

where $f_\gamma(\cdot)$ denotes the pdf of the combiner output.

1.3.2 Outage Probability

The outage probability of a system is defined as the probability that the instantaneous error probability exceeds a specified value or equivalently, when the probability of γ falls below a certain threshold γ_{th} [12]. That is,

$$P_{\text{out}} = \int_0^{\gamma_{\text{th}}} f_\gamma(\gamma) d\gamma. \tag{1.8}$$

1.3.3 Average Bit Error Probability

The most well known performance measures of a communication system are it's average BER and average symbol error rate (SER). One way of obtaining the average BER/SER is by averaging the the conditional bit error probability in a static (non

fading) channel over the signal fading. That is

$$P_b(E) = \int_0^\infty P_b(E|\gamma) f_\gamma(\gamma) d\gamma. \tag{1.9}$$

The average BER/SER is a very good indicator of the system behaviour and the one most often illustrated in documents containing system performance evaluations [12].

1.4 Thesis Outline and Contributions

In Chapter 2 we study the performance of predetection dual-branch SSC in correlated Rician fading. Analytical expressions are derived for the average SER of several modulation formats of practical interest with predetection SSC in correlated Rician fading. Analytical expressions are also derived for the mean output SNR and the outage probability of dual-branch predetection SSC in correlated Rician fading.

In Chapter 3 the performances of two dual-branch postdetection SSC receivers operating in slow, frequency nonselective correlated Rayleigh and Rician fading channels are analyzed. For each receiver structure analytical expressions are derived for the average BER and average SER of noncoherent binary frequency shift keying (BFSK) and noncoherent M-ary frequency shift keying (MFSK) in correlated Rayleigh and Rician fading. For Rayleigh fading, the impact of fading power imbalance is also studied. The effects of important parameters, such as the correlation coefficient, fading power imbalance and fading factor, on the performances of these postdetection SSC receivers are analyzed. The performances of the postdetection SSC receivers are compared to the performance of the predetection SSC receiver obtained in Chapter 2 and it is observed that postdetection SSC outperforms predetection SSC.

In Chapter 4 we study the performance of two $S+N$ SC receivers with noncoherent BFSK and noncoherent MFSK in independent but not necessarily identical (i.n.d)

Rician, Nakagami-m and Rayleigh fading channels. For each receiver, we obtain average SER and BER expressions in terms of single integrals with finite integration limits. In addition, we analyze the performance of classical SC in i.n.d fading channels. Our analytical expressions are validated using extensive Monte Carlo simulations. Our results indicate that, unlike as suggested by previously published results, the performances of $S+N$ SC receivers are not always superior to that of classical SC in fading and depend on the value of the SNR, the modulation order, the diversity order, the multipath intensity profile and the fading parameter of the channel. It is further shown that increasing the number of diversity branches in a $S+N$ SC receiver does not necessarily decrease the probability of error if the system is operating in the low SNR region. The performances of $S+N$ SC schemes are also compared to the performances of EGC and SLC receivers.

In Chapter 5 we generalize the results of Chapter 4 to correlated Rayleigh and Rician fading channels. The branches are assumed to be equally correlated for Rician fading. For Rayleigh fading, the correlation model is more general than the equally correlated scenario and includes it as a special case. For each receiver structure, we obtain analytical results for the average BER of noncoherent BFSK and noncoherent MFSK in the format of double integrals which can be easily computed using Gaussian quadrature techniques. The effects of diversity order, correlation and the fading parameter on the performances of $S+N$ SC receivers are studied. Several numerical examples are presented to compare the performances of $S+N$ SC receivers with classical SC. For example, in the case of equally correlated Rician branches, it is shown that the performance gap between $S+N$ SC and classical SC increases as the correlation among the diversity branches increases.

In Chapter 6, we propose a new dual-branch decorrelation receiver and analyze

its performance with classical SC, SSC, EGC and SLC in correlated slow, frequency nonselective Rayleigh and Rician fading channels. We show that the decorrelator receiver, when combined with classical SC and SSC, can improve the performance of the system as much as 2.83 dB in average SNR. It is shown that the decorrelator receiver and the conventional dual-branch receiver have the same performance if SLC is employed. For the decorrelator receiver with SC and SSC important performance measures such as the average BER of several modulation schemes of practical interest, mean output SNR and outage probability are computed. Our results show that the outage probability of the decorrelator receiver can be reduced by as much as one-sixth relative to the outage of the conventional receiver in some scenarios. On the other hand, it is shown that decorrelation has no benefit for dual-branch MRC and negative benefit for dual-branch EGC.

Finally, the conclusions and a summary of the thesis is presented in Chapter 7 as well as some suggestions for future research.

Chapter 2

Predetection Switched Combining in Correlated Rician Fading

2.1 Introduction

The application of SSC systems has been suggested for low complexity receivers where the number of diversity branches is equal to two [13]. In this chapter, we consider the performance of dual-branch predetection SSC in correlated Rician fading in conjunction with several modulation formats of practical interest. The performance of predetection SSC systems has been thoroughly investigated in correlated Rayleigh and Nakagami-m fading channels [14], [15]. However, the performance of predetection SSC in correlated Rician fading is not well studied in the literature. To the best of the author's knowledge the only reference that has results on the subject is [16], where the performance of noncoherent BFSK is analyzed. In [16], the authors have used the probability density function of the bivariate Rician distribution to obtain their results which are in the form of triple integrals and are difficult to compute. In this chapter, using a different approach to that of [16], we obtain analytical expressions for the average SER of several types of modulation formats in correlated Rician

fading. For example, for noncoherent BFSK, our result is given in closed-form and is much easier to compute than the triple integral given in [16].

Using these analytical expressions, optimum switching thresholds that minimize the average SER can be obtained. The validity of our analytical results are tested using Monte Carlo simulation. The performance of predetection SSC is compared to classical SC. The effects of correlation coefficient, fading parameter and switching threshold on the performance of predetection SSC systems are investigated.

The remainder of this chapter is organized as follows. In Section 2.2, the system model and the structure of the receiver are introduced. In Section 2.3, analytical expressions are derived for the performance of various modulation formats with dual-branch predetection SSC in correlated Rician fading and optimum switching thresholds that minimize the average SER are obtained. Furthermore, analytical expressions for the output average SNR and outage probability are derived. In Section 2.4, some numerical examples are given and the validity of our analytical results are tested via Monte Carlo simulation. In addition, the effects of fading correlation and fading parameter on the performance of SSC systems are demonstrated via some numerical examples. Finally, some conclusions are given in Section 2.5.

2.2 Switching Mechanism

The switching mechanism is as follows. We assume that the switching is performed at discrete instants of time $t = nT$ where n is an integer and T is the time interval between switching times [17]. For instance, in a packet based communication system T could be the time between the transmission of packets. The fading on each diversity branch is assumed to be slow and frequency nonselective and the Rician model is used

to characterize the fading statistics. The fadings on the two branches are assumed to be correlated with correlation coefficient ρ.

Let $\gamma_{\text{SSC}}(n)$ denote the output of the switch at time $t = nT$ and let $\gamma_1(n)$ and $\gamma_2(n)$ denote, respectively, the instantaneous SNR on channels 1 and 2 at time $t = nT$. We assume that the fadings on the two diversity branches are correlated. We further assume that the average SNR on the two branches are identical, i.e., $\bar{\gamma} = \bar{\gamma_1} = \bar{\gamma_2}$. Let $\gamma_{\text{SSC}}(n)$ denote the instantaneous SNR at the output of the switch at time $t = nT$. The system operates as follows. Suppose that the switch is connected to Antenna 1(Antenna 2), i.e., $\gamma_{\text{SSC}}(n) = \gamma_1(n)(\gamma_{\text{SSC}}(n) = \gamma_2(n))$. The switch will remain connected to Antenna 1 (Antenna 2) as long as the SNR on channel 1 (channel 2) is above a predetermined threshold. If the SNR on channel 1 (channel 2) falls below the predetermined threshold, the system will switch to Antenna 2 (Antenna 1) regardless of the value of SNR on that branch. In mathematical terms, $\gamma_{\text{SSC}}(n)$ can be written as [17, eq. (3)]

$$\gamma_{\text{SSC}}(n) = \gamma_1(n) \text{ iff } \begin{cases} \gamma_{\text{SSC}}(n-1) = \gamma_1(n-1) & \gamma_1(n) \geq \eta_T \\ \gamma_{\text{SSC}}(n-1) = \gamma_2(n-1) & \gamma_2(n) < \eta_T \end{cases} \tag{2.1a}$$

$$\gamma_{\text{SSC}}(n) = \gamma_2(n), \quad \text{as above with interchanging } \gamma_1 \text{ and } \gamma_2 \tag{2.1b}$$

where η_T is the switching threshold on either channel. Following the analysis in [16], the CDF of γ_{SSC} can be written as

$$F_{\gamma_{\text{SSC}}}(x) = \Pr(\eta_T < \gamma_1 < x) + \Pr(\gamma_1 < x, \gamma_2 < \eta_T) \tag{2.2}$$

where we have dropped the dependence on n for notational simplicity. Eq. (2.2) can be alternatively written as

$$F_{\gamma_{\text{SSC}}}(x) = (F_\gamma(x) - F_\gamma(\eta_T))\, u(x - \eta_T) + F_{\gamma_1,\gamma_2}(x, \eta_T) \tag{2.3}$$

where $u(\cdot)$ denotes the unit step function and $F_\gamma(\cdot) \triangleq F_{\gamma_1}(\cdot) = F_{\gamma_2}(\cdot)$ and $F_{\gamma_1,\gamma_2}(\cdot,\cdot)$ denote the marginal and the joint distributions of the RVs γ_1 and γ_2, respectively.

2.3 Error Rate Analysis

For a Rician faded environment, with fading parameter K, one can show that $F_\gamma(\cdot)$ is given by

$$F_\gamma(x) = 1 - Q_1\left(\sqrt{2K}, \sqrt{\frac{2(1+K)x}{\bar{\gamma}}}\right) \tag{2.4}$$

where $Q_1(\cdot,\cdot)$ is the first order Marcum-Q function and is defined as [18, eq. (4.11)]

$$Q_1(a,b) = \int_b^\infty x \exp\left(-\frac{x^2+a^2}{2}\right) I_0(ax)dx \tag{2.5}$$

and where $I_0(\cdot)$ is the zero-order modified Bessel function of the first kind [19, Section 8.43] given by

$$I_0(x) = \sum_{k=0}^{\infty} \frac{(x/2)^{2k}}{(k!)^2}. \tag{2.6}$$

Following the procedure in [20, Section III.A], one can show that $F_{\gamma_1,\gamma_2}(x,\eta_T)$ can be written as

$$\begin{aligned} F_{\gamma_1,\gamma_2}(x,\eta_T) = \int_0^\infty & \left(1 - Q_1\left(\sqrt{\frac{2\rho v}{1-\rho}}, \sqrt{\frac{2(1+K)x}{\bar{\gamma}(1-\rho)}}\right)\right) \\ & \times \left(1 - Q_1\left(\sqrt{\frac{2\rho v}{1-\rho}}, \sqrt{\frac{2(1+K)\eta_T}{\bar{\gamma}(1-\rho)}}\right)\right) \\ & \times \exp\left(-v - \frac{K}{\rho}\right) I_0\left(\sqrt{\frac{4Kv}{\rho}}\right) dv. \end{aligned} \tag{2.7}$$

Using [18, eq. (B.31)], (2.7) can be simplified as

$$F_{\gamma_1,\gamma_2}(x,\eta_T) = 1 - Q_1\left(\sqrt{2K}, \sqrt{\frac{2(1+K)x}{\bar{\gamma}}}\right) - Q_1\left(\sqrt{2K}, \sqrt{\frac{2(1+K)\eta_T}{\bar{\gamma}}}\right) + \int_0^\infty \exp\left(-v - \frac{K}{\rho}\right) \times Q_1\left(\sqrt{\frac{2\rho v}{1-\rho}}, \sqrt{\frac{2(1+K)x}{\bar{\gamma}(1-\rho)}}\right) Q_1\left(\sqrt{\frac{2\rho v}{1-\rho}}, \sqrt{\frac{2(1+K)\eta_T}{\bar{\gamma}(1-\rho)}}\right) I_0\left(\sqrt{\frac{4Kv}{\rho}}\right) dv. \tag{2.8}$$

Substituting (2.4) and (2.8) in (2.3), we obtain a general expression for the CDF of γ_{SSC} in correlated Rician fading as

$$\begin{aligned} F_{\gamma_{\text{SSC}}}(x) = {} & 1 + Q_1\left(\sqrt{2K}, \sqrt{\frac{2(1+K)x}{\bar{\gamma}}}\right)(u(x-\eta_T) - 1) \\ & - Q_1\left(\sqrt{2K}, \sqrt{\frac{2(1+K)\eta_T}{\bar{\gamma}}}\right)(u(x-\eta_T) + 1) \\ & + \int_0^\infty \exp\left(-v - \frac{K}{\rho}\right) Q_1\left(\sqrt{\frac{2\rho v}{1-\rho}}, \sqrt{\frac{2(1+K)x}{\bar{\gamma}(1-\rho)}}\right) \\ & \times Q_1\left(\sqrt{\frac{2\rho v}{1-\rho}}, \sqrt{\frac{2(1+K)\eta_T}{\bar{\gamma}(1-\rho)}}\right) I_0\left(\sqrt{\frac{4Kv}{\rho}}\right) dv. \end{aligned} \tag{2.9}$$

2.3.1 Moment Generating Function

The moment generating function (MGF) is calculated in this section. The MGF can be used in the calculation of the average SER as well as in the calculation of the moments of the predetection SSC output SNR. The MGF of predetection SSC can be obtained using

$$\Phi_{\text{ssc}}(s) = \int_0^\infty \exp(sx) f_{\gamma_{\text{SSC}}}(x) dx. \tag{2.10}$$

To avoid calculating $f_{\gamma_{\text{SSC}}}(\cdot)$, using integration by parts, we transform (2.10) into

$$\Phi_{\text{ssc}}(s) = s\int_0^\infty \exp(sx) F_{\gamma_{\text{SSC}}}(x) dx. \tag{2.11}$$

Substituting (2.9) in (2.11), changing the order of integration where necessary and after many mathematical manipulations and integral evaluations we obtain a closed-form expression for the MGF of predetection SSC in correlated Rician fading as

$$\begin{aligned}\Phi_{\text{ssc}}(s) &= \Upsilon_1(K,s,\bar{\gamma}) \\ &\times \left(1+Q_1\left(\sqrt{\frac{2K(1+K)}{s\bar{\gamma}+1+K}},\sqrt{\frac{2(s\bar{\gamma}+K+1)\eta_T}{\bar{\gamma}}}\right)\right. \\ &\left.-Q_1\left(\sqrt{\Upsilon_2(K,s,\bar{\gamma})},\sqrt{\Upsilon_3(K,s,\bar{\gamma})\eta_T}\right)\right)\end{aligned} \tag{2.12a}$$

where

$$\Upsilon_1(K,s,\bar{\gamma}) = \frac{1+K}{1+K-s\bar{\gamma}}\exp\left(\frac{Ks\bar{\gamma}}{1+K-s\bar{\gamma}}\right) \tag{2.12b}$$

$$\Upsilon_2(K,s,\bar{\gamma}) = \frac{2K(1+K-s\bar{\gamma}(1-\rho))^2}{(1+K-s\bar{\gamma})(1+K-s\bar{\gamma}(1-\rho^2))} \tag{2.12c}$$

$$\Upsilon_3(K,s,\bar{\gamma}) = \frac{2(1+K)(1+K-s\bar{\gamma})}{\bar{\gamma}(1+K-s\bar{\gamma}(1-\rho^2))}. \tag{2.12d}$$

2.3.2 Mean Output SNR

The mean output SNR can be obtained from the MGF as

$$\bar{\gamma}_{\text{SSC}} = \left.\frac{d\Phi_{\text{ssc}(s)}}{ds}\right|_{s=0}. \tag{2.13}$$

Substituting (2.9) in (2.13), using

$$\begin{aligned}\frac{dQ_1\left(\sqrt{g_1(x)},\sqrt{g_2(x)}\right)}{dx} &= \frac{1}{2}\exp\left(-\frac{g_1(x)+g_2(x)}{2}\right) \\ &\times\left(\frac{dg_1(x)}{dx}\sqrt{\frac{g_2(x)}{g_1(x)}}I_1\left(\sqrt{g_1(x)g_2(x)}\right)-\frac{dg_2(x)}{dx}\right. \\ &\left.\times I_0\left(\sqrt{g_1(x)g_2(x)}\right)\right)\end{aligned} \tag{2.14}$$

and after some mathematical simplifications, we obtain the following expression for the mean output SNR in correlated Rician fading as

$$\bar{\gamma}_{\text{SSC}} = \bar{\gamma} + \exp\left(-K - \frac{(K+1)\eta_T}{\bar{\gamma}}\right)\left[(1-\rho)^2\sqrt{\frac{K\bar{\gamma}\eta_T}{1+K}}\right.$$
$$\left.\times I_1\left(\sqrt{\Upsilon_4(K,\bar{\gamma})\eta_T}\right) + (1-\rho^2)\eta_T I_0\left(\sqrt{\Upsilon_4(K,\bar{\gamma})\eta_T}\right)\right] \tag{2.15a}$$

where $I_1(\cdot)$ is the first-order modified Bessel function of the first kind [19] and

$$\Upsilon_4(K,\bar{\gamma}) = \frac{4K(K+1)}{\bar{\gamma}}. \tag{2.15b}$$

The optimum switching threshold, $\eta^*_{T_{\text{SNR}}}$, that maximizes the mean output SNR can now be obtained by finding the root of $\frac{d\bar{\gamma}_{\text{SSC}}}{d\eta_T} = 0$. Unlike correlated or uncorrelated Nakagami and Rayleigh fading where $\eta^*_{T_{\text{SNR}}} = \bar{\gamma}$, [14], one can show that the optimum switching threshold in correlated Rician fading is not equal to $\bar{\gamma}$. However, our numerical calculations have shown that the optimum switching threshold is close to $\bar{\gamma}$. For example, for $K = 5$, $\rho = 0.8$ and $\bar{\gamma} = 10$ dB, $\eta^*_{T_{\text{SNR}}} = 10.55$ (10.23 dB).

For $\rho = 0$ which corresponds to independent fading, (2.15a) reduces to

$$\bar{\gamma}_{\text{SSC}} = \bar{\gamma} + \exp\left(-K - \frac{(K+1)\eta_T}{\bar{\gamma}}\right)\left(\sqrt{\frac{K\bar{\gamma}\eta_T}{1+K}}\right.$$
$$\left.\times I_1\left(\sqrt{\Upsilon_4(K,\bar{\gamma})\eta_T}\right) + \eta_T I_0\left(\sqrt{\Upsilon_4(K,\bar{\gamma})\eta_T}\right)\right) \tag{2.16}$$

which is equivalent to, but easier to compute than the expression given in [14, eq. (21)].

Interestingly note that unlike correlated Rician fading, for uncorrelated Rician fading, $\eta^*_{T_{\text{SNR}}} = \bar{\gamma}$.

2.3.3 Average SER

In a slow fading environment the average symbol error rate is usually computed by averaging the static SER, $P_s(e|\gamma)$ over the PDF of γ_{SSC}. That is

$$P_e = \int_0^\infty P_s(e|\gamma) f_{\gamma_{\text{SSC}}}(\gamma) d\gamma. \tag{2.17}$$

In this section, we take a different approach to compute the average SER, which does not involve the computation of the PDF of γ_{SSC}. Using integration by parts one can write (2.17) as

$$P_s = -\int_0^\infty P_s'(e|\gamma) F_{\gamma_{\text{SSC}}}(\gamma) d\gamma. \tag{2.18}$$

where $P_s'(e|\gamma)$ denotes the derivative of the static error rate. Alternatively, we can use a MGF-based approach [12] to calculate the average SER in fading channels. In the following we derive the average SER of various modulation techniques with dual-branch predetection SSC in correlated Rician fading.

1. For coherent BFSK and M-ary pulse amplitude modulation (MPAM) the static SER is given by [20, eq. (33)]

$$P_s(e|\gamma) = aQ(\sqrt{b\gamma}) \tag{2.19}$$

where $(a, b) = (1, 2)$ for BPSK, $(a, b) = (1, 1)$ for coherent BFSK and $(a, b) = (2(M-1)/M, 6/(M^2-1))$ for MPAM, and $Q(\cdot)$ is the area under the tail of the Gaussian PDF defined at [21, eq. (2-1-97)]. Substituting (2.19) in (2.18), the average SER is obtained as

$$P_s = \frac{a\sqrt{b}}{2\sqrt{2\pi}} \int_0^\infty \frac{1}{\sqrt{\gamma}} \exp\left(-\frac{1}{2}b\gamma\right) F_{\gamma_{\text{SSC}}}(\gamma) d\gamma \tag{2.20}$$

2. For 4-ary PSK, M-ary quadrature amplitude modulation (MQAM), minimum shift keying (MSK) and coherently detected binary differentially PSK (DPSK),

the static SER is given in [20, eq. (39)] as

$$P_s(e|\gamma) = aQ(\sqrt{b\gamma}) - cQ^2(\sqrt{b\gamma}) \tag{2.21}$$

where $(a, b, c) = (2, 2, 1)$ for 4PSK or MSK, $(a, b, c) = (2, 2, 2)$ for coherently detected DPSK and $(a, b, c) = (\frac{4(\sqrt{M}-1)}{\sqrt{M}}, \frac{3\log_2 M}{M-1}, \frac{4(\sqrt{M}-1)^2}{M})$ for MQAM. Substituting (2.21) in (2.18), we obtain the average SER as

$$P_s = \sqrt{\frac{b}{2\pi}} \int_0^\infty \frac{1}{\sqrt{\gamma}} \exp\left(-\frac{1}{2}b\gamma\right) \left(\frac{a}{2} - cQ\left(\sqrt{b\gamma}\right)\right) F_{\gamma_{\text{SSC}}}(\gamma) d\gamma \tag{2.22}$$

3. For $\frac{\pi}{4}$-quadrature differential PSK (QDPSK) and noncoherent correlated BFSK, the static SER is given in [20, eq. (41)] as

$$P_s(e|\gamma) = Q_1(a\sqrt{\gamma}, b\sqrt{\gamma}) - \frac{1}{2} \exp\left(-\frac{(a^2+b^2)\gamma}{2}\right) I_0(ab\gamma) \tag{2.23}$$

where $(a, b) = (\sqrt{2-\sqrt{2}}, \sqrt{2+\sqrt{2}})$ and $(a, b) = (\sqrt{\frac{1-\sqrt{1-\lambda^2}}{2}}, \sqrt{\frac{1-\sqrt{1+\lambda^2}}{2}})$ for $\frac{\pi}{4}$-DQPSK and noncoherent correlated BFSK, respectively and where λ is the correlation between the binary signals in noncoherent correlated BFSK. Using (2.23) in (2.18), the average SER in this case can be evaluated using

$$P_s = \frac{a^2 - b^2}{4} \int_0^\infty \exp\left(-\frac{(a^2+b^2)\gamma}{2}\right) I_0(ab\gamma) F_{\gamma_{\text{SSC}}}(\gamma) d\gamma \tag{2.24}$$

4. For noncoherent MFSK, using the moment generating function method, one can obtain a closed-form expression for the average SER as

$$\begin{aligned} P_s = & \sum_{n=1}^{M-1} \frac{(-1)^{n+1}\binom{M-1}{n}}{n+1} \Upsilon_1(K, \beta(n), \bar{\gamma}) \\ & \times \left(Q_1\left(\sqrt{\frac{2K(1+K)}{\beta(n)\bar{\gamma}+1+K}}, \sqrt{\frac{2(\beta(n)\bar{\gamma}+K+1)\eta_T}{\bar{\gamma}}}\right) \right. \\ & \left. - Q_1\left(\sqrt{\Upsilon_2(K, \beta(n), \bar{\gamma})}, \sqrt{\Upsilon_3(K, \beta(n), \bar{\gamma})\eta_T}\right) + 1 \right) \end{aligned} \tag{2.25}$$

where $\beta(n) = -n/(n+1)$. For $M = 2$, which corresponds to BFSK (2.25) reduces to

$$\begin{aligned} P_s = & \Upsilon_1(K, \frac{1}{2}, \bar{\gamma}) \\ & \times \left(1 + Q_1\left(\sqrt{\frac{4K(1+K)}{\bar{\gamma}+2+2K}}, \sqrt{\frac{(\bar{\gamma}+2K+2)\eta_T}{\bar{\gamma}}}\right)\right. \\ & \left. - Q_1\left(\sqrt{\Upsilon_2(K, \frac{1}{2}, \bar{\gamma})}, \sqrt{\Upsilon_3(K, \frac{1}{2}, \bar{\gamma})\eta_T}\right)\right) \end{aligned} \tag{2.26}$$

which is much simpler to compute than [17, eq. (18)], which requires triple integration.

It is clear that the average SER of any modulation format with predetection SSC is a function of the switching threshold. In general, the optimum switching threshold that minimizes the average SER will be different from the optimum switching threshold that maximizes SNR. An optimum switching threshold that minimizes the average SER can be obtained by finding the root of $\frac{dP_s}{d\eta_T} = 0$. For example, for MFSK the optimum switching threshold is the root of

$$\begin{aligned} & \sum_{n=1}^{M-1} \frac{(-1)^{n+1}\binom{M-1}{n}}{n+1} \Upsilon_1 \left[\frac{\Upsilon_2}{2} \exp\left(-\frac{\Upsilon_2}{2} - \frac{\Upsilon_3\eta_T}{2}\right)\right. \\ & \times I_0\left(\sqrt{\Upsilon_2\Upsilon_3\eta_T}\right) - \frac{\beta(n)\bar{\gamma}+K+1}{\bar{\gamma}} I_0\left(\sqrt{\Upsilon_4\eta_T}\right) \\ & \left. \times \exp\left(-\frac{K(K+1)}{\beta(n)\bar{\gamma}+K+1} - \frac{(\beta(n)\bar{\gamma}+K+1)\eta_T}{\bar{\gamma}}\right)\right] = 0 \end{aligned} \tag{2.27}$$

which was obtained by differentiating (2.25) with respect to η_T. Note that for notational simplicity we have removed the dependence of Υ_i on $K, \beta(n)$ and $\bar{\gamma}$.

2.3.4 Outage Probability

The outage probability is the probability that the output instantaneous SNR, γ_{SSC}, falls below a given threshold γ_{th} and is given by

$$P_{out} = \Pr(0 < \gamma_{\text{SSC}} < \gamma_{\text{th}}) = F_{\gamma_{\text{SSC}}}(\gamma_{\text{th}}). \tag{2.28}$$

where $F_{\gamma_{\text{SSC}}}(\eta_{\text{th}})$ was obtained in (2.9). It follows from (2.3) that the value of switching threshold, $\eta^*_{T_{\text{out}}}$, for which the outage probability attains its optimum (minimum) value is $\eta^*_{T_{\text{out}}} = \gamma_{\text{th}}$ [14]. Thus, the optimum outage probability is given by

$$P_{out} = F_{\gamma_1,\gamma_2}(\gamma_{\text{th}}, \gamma_{\text{th}}) \tag{2.29}$$

which is equal to the outage probability of classical SC.

2.4 Numerical Examples

In this section, we give some numerical examples. In Fig. 2.1, the average SER of noncoherent QFSK with SSC and classical SC is plotted as a function of the average SNR per symbol per branch for several values of ρ and for $K = 5$. For SSC, we have used (2.25) to plot the analytical curves in Fig. 2.1 where for each value of SNR, the optimum switching thresholds the minimize the average SER have been used. These optimum switching thresholds have been calculated by obtaining the roots of (2.27) numerically. Note that there is excellent agreement between our theoretical results and simulations. Also plotted in Fig. 2.1, is the average SER of QFSK with classical SC in correlated Rician fading. As expected, the average SER of classical SC is always less than the average SER of predetection SSC and the SNR gap between predetection SSC and classical SC does not change significantly with ρ.

In Fig. 2.2, the optimum switching thresholds that minimize the average SER of QFSK are plotted as a function of the average SNR per symbol per branch for several values of K and for $\rho = 0.4$. Fig. 2.2 shows that the optimum switching threshold increases as the channel is less faded. Fig. 2.2 also shows that for a given K, the optimum switching threshold increases as the average SNR on the branches increase.

In Fig. 2.3, the optimum switching thresholds that minimize the average SER of QFSK are plotted as a function of the average SNR per symbol per branch for several values of ρ and for $K = 2$ and $K = 10$. Fig. 2.3 shows that for a fixed K, the optimum switching threshold decreases as correlation increases.

In Fig. 2.4, the average SER of QFSK is plotted as a function of the switching threshold for several values of ρ for $\bar{\gamma} = 5, 10$ and 15 dB. Fig. 2.4 shows that as correlation increases, and for a given $\bar{\gamma}$, the average SER becomes less sensitive to the switching threshold.

Finally, in Fig. 2.5, the optimum outage probability of SSC is plotted as a function of normalized SNR $(\gamma_{\text{th}}/\bar{\gamma})$ for several values of K and ρ. As expected, the outage probability decreases as ρ decreases or K increases.

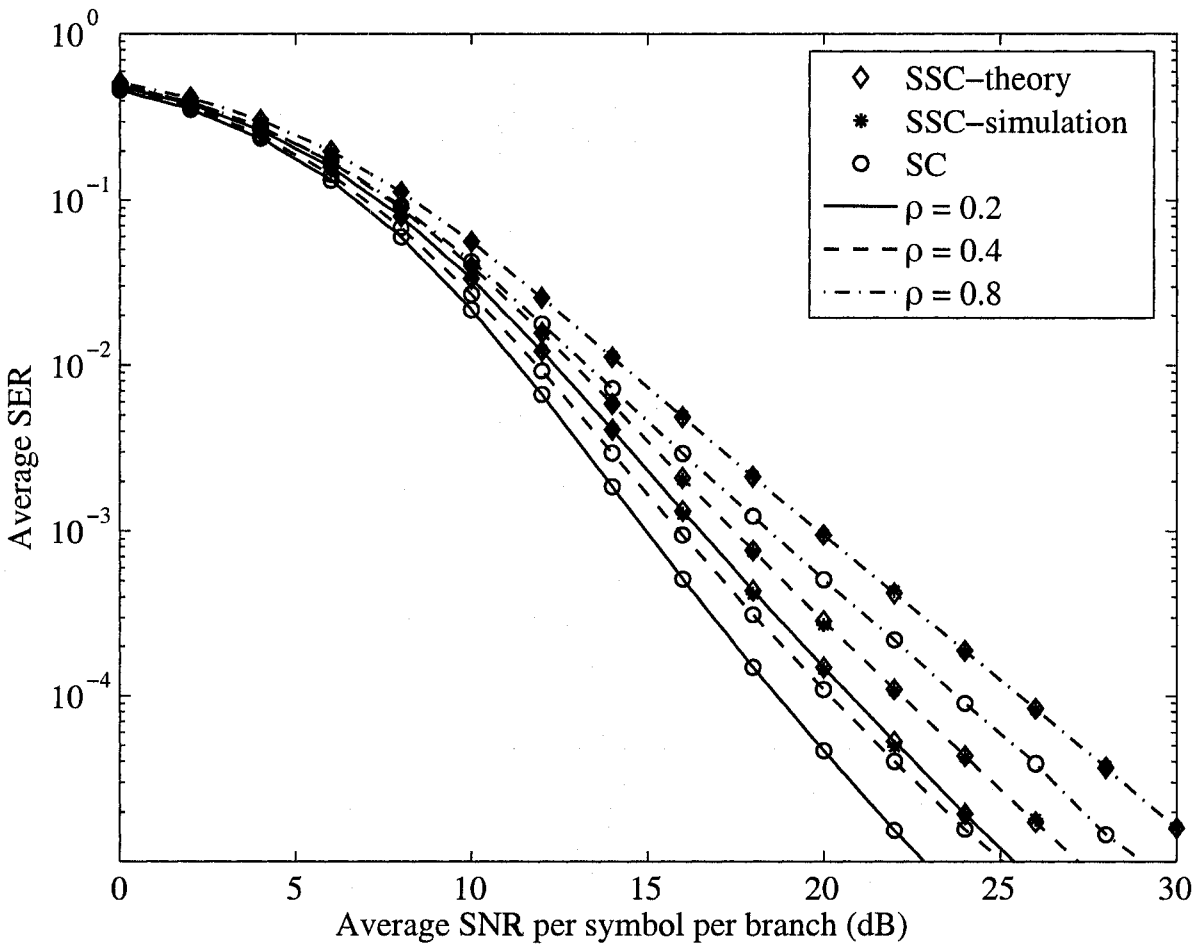

Figure 2.1: The average SER of QFSK as a function of the average SNR per symbol per branch in correlated Rician fading for $K = 5$ and $\rho = 0.2, 0.4$ and 0.8. The optimum switching threshold values that minimize the SER are used to plot the curves.

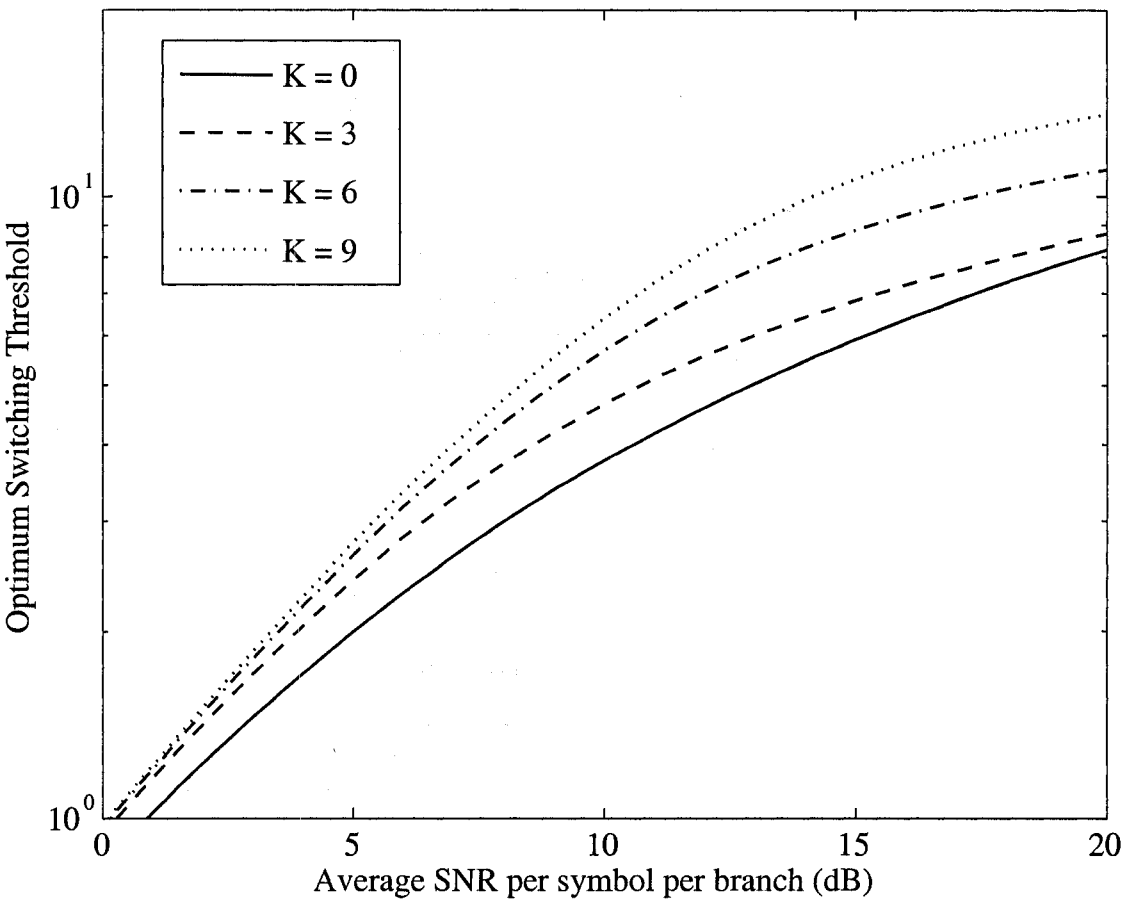

Figure 2.2: The optimum switching threshold of QFSK as a function of the average SNR per symbol per branch for $\rho = 0.4$ and $K = 0, 3, 6$ and 9.

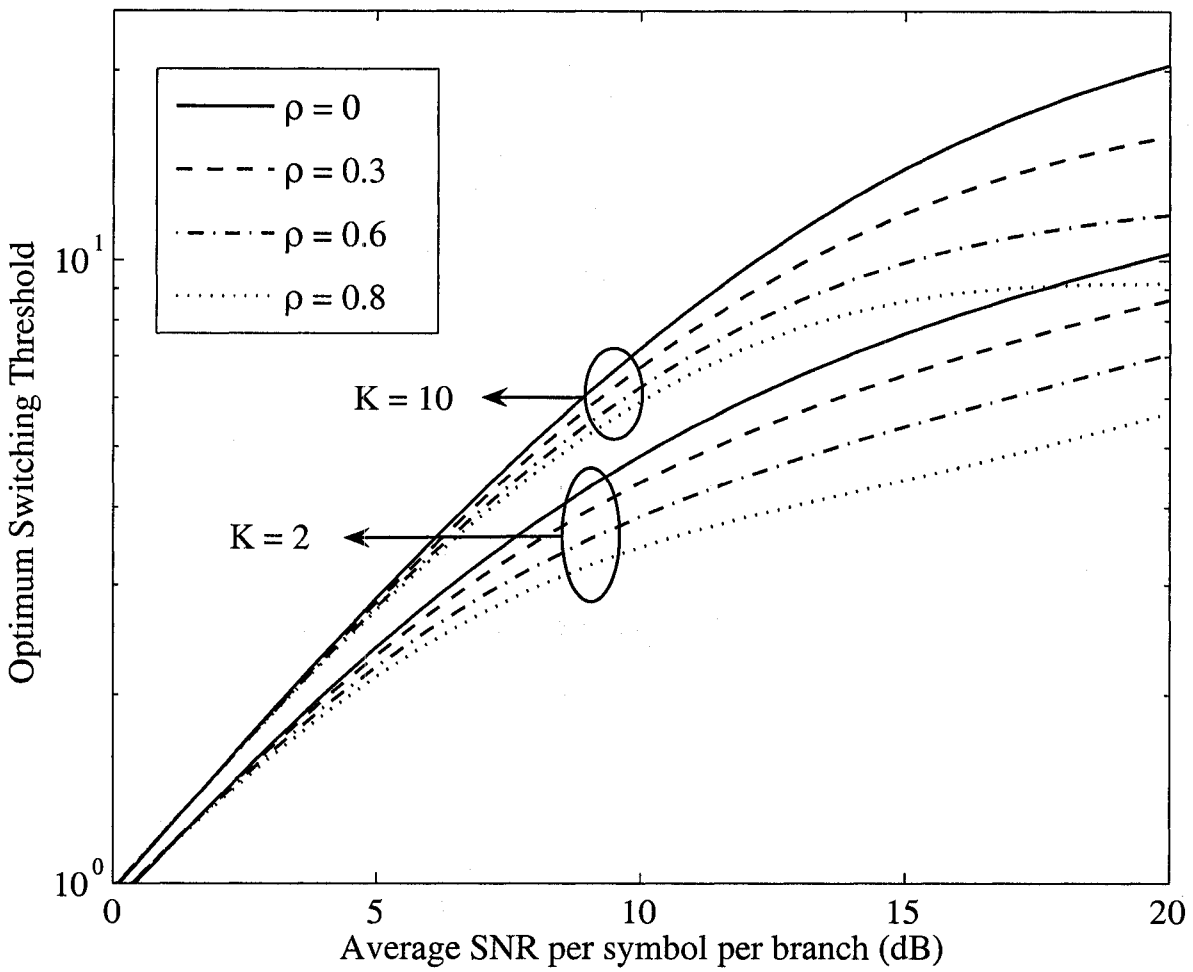

Figure 2.3: The optimum switching threshold of QFSK as a function of the average SNR per symbol per branch for $\rho = 0, 0.3, 0.6$ and 0.8 and for $K = 2$ and 10.

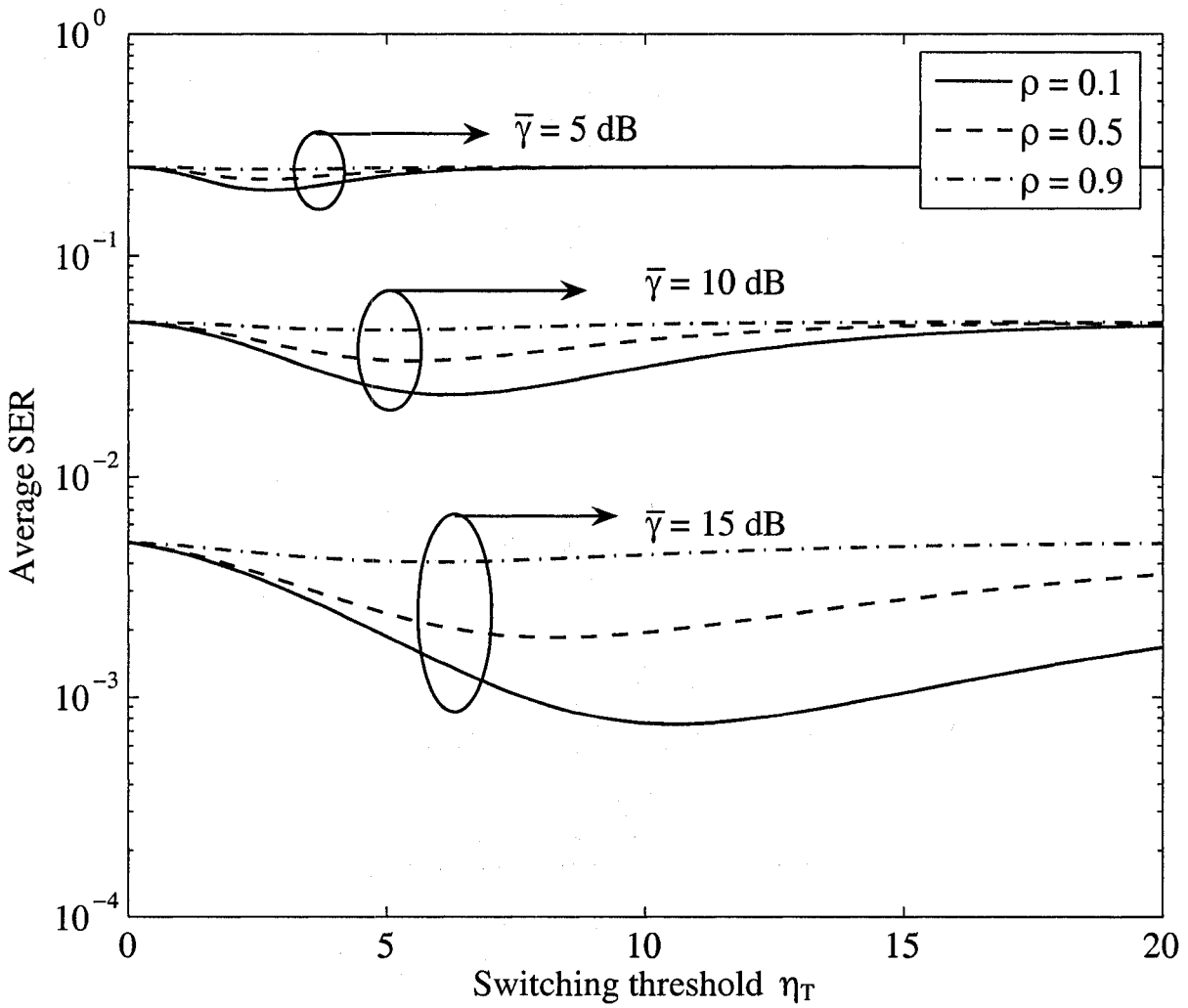

Figure 2.4: The average SER of QFSK as a function of the switching threshold for several values of ρ and $\bar{\gamma}$.

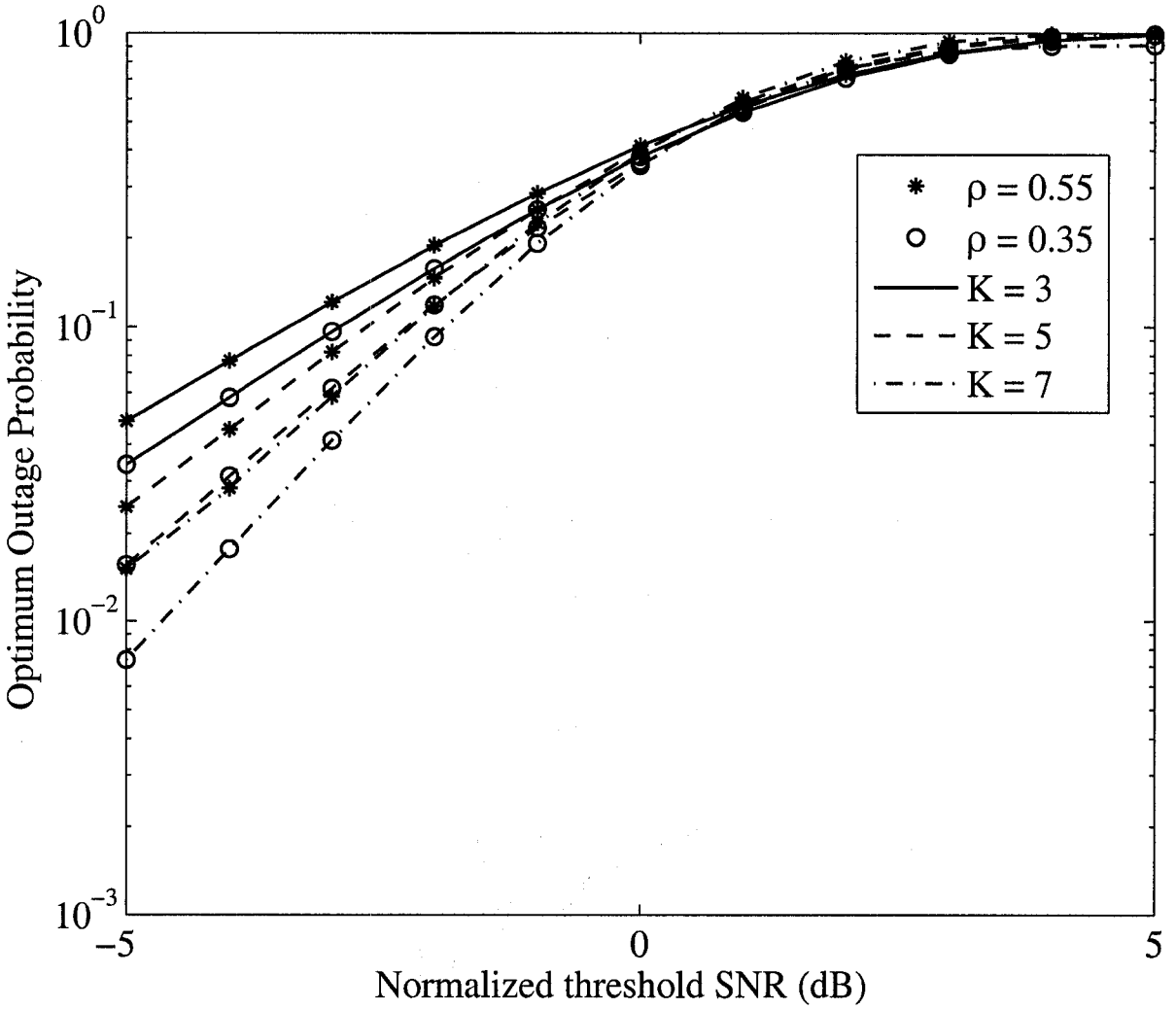

Figure 2.5: The optimum outage probability of dual-branch predetection SSC as a function of the normalized switching threshold for $\rho = 0.35$ and 0.55 and for $K = 3, 5$ and 7.

2.5 Conclusion

The performance of dual-branch predetection SSC in correlated Rician fading was studied. Analytical expressions for the average SER were derived for a number of modulation formats of practical interest. Analytical expressions were also derived for the output average SNR and outage probability of dual-branch predetection SSC in correlated Rician fading. As a practical example, the effects of correlation, fading parameter and switching threshold on the performance of QFSK were demonstrated. It was shown that for large correlation, as the average SNR decreases, the average SER becomes less sensitive to the switching threshold.

Chapter 3

Performance of Postdetection Switch-and-Stay Combining Schemes in Correlated Rayleigh and Rician Fading

In the previous chapter, we studied the performance of predetection SSC system in correlated Rician fading, In this chapter, we study the performance of binary frequency-shift keying (BFSK) and M-ary frequency shift keying (MFSK) with dual-branch postdetection switch-and-stay combining (SSC) in correlated Rayleigh and Rician fading.

Although the performance of predetection SSC is well studied both in independent as well as correlated fading channels [14]- [17], [22]- [26], to the best of the author's knowledge, the performance of postdetection SSC receivers has only been studied in independent fading channels [13], [27]- [29]. In practice, however, the assumption of independence among the diversity branches may not be accurate particularly if the antennas are placed closely as in many portable communication devices.

In this chapter, two postdetection SSC receivers are studied. We refer to these

receivers as postdetection SSC Model 1 and postdetection SSC Model 2. The performances of binary frequency shift keying (BFSK) and M-ary frequency shift keying (MFSK) with postdetection SSC Model 1 and Model 2 are analyzed in both correlated Rayleigh and Rician fading channels. In the Rayleigh fading scenario we also consider the case where the average fading powers are not necessarily equal. Closed-form expressions are derived for the average BER of noncoherent BFSK and MFSK with Postdetection SSC Model 1 and Model 2 in Rayleigh and Rician fading channels. The validity of our analytical expressions are tested using extensive Monte Carlo simulation results. Using these analytical expressions, optimum switching thresholds that minimize the average BER are obtained. The performances of postdetection SSC Model 1 and Model 2 are compared to the performance of predetection SSC.

The remainder of this chapter is organized as follows. In Section 3.1, the structure of postdetection SSC Model 1 is given and the performance using BFSK in this receiver structure is analyzed in correlated Rayleigh and Rician fading channels. In Section 3.2, we analyze the performance of MFSK with postdetection SSC Model 2 in correlated Rayleigh and Rician fading channels. Some numerical examples are given in Section 3.3 and the performances of postdetection SSC Model 1 and Model 2 are compared to the performance of predetection SSC in correlated fading channels. Finally, some conclusions are given in Section 3.4.

3.1 Postdetection SSC Model 1

3.1.1 System Model

The signaling transmission is assumed to be BFSK over a slow, flat fading channel. The equiprobable binary symbols zero and one are transmitted around the carrier

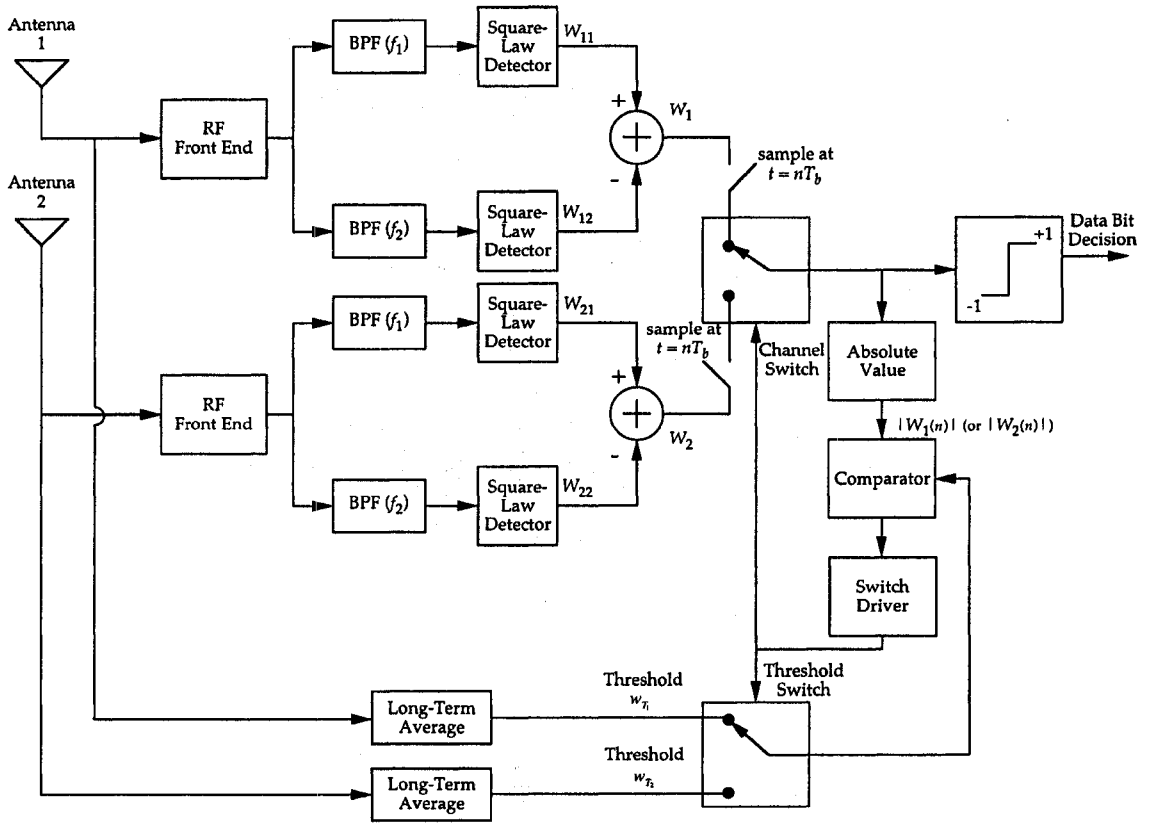

Figure 3.1: The block diagram of postdetection SSC receiver Model 1 (after [10, Fig. 1]).

frequencies f_1 and f_2, respectively, with energy E_b.

A block diagram of a BFSK system with dual-branch postdetection SSC is given in Fig. 3.1 (after [13, Fig. 1]). Noncoherent modulation is employed on each diversity branch consisting of two bandpass filters, one tuned to frequency f_1 and the other to frequency f_2 followed by square-law detectors [13]. Let $W_{ik}(n), i, k = 1, 2$ denote the output of the jth square-law detector on the ith branch in the nth symboling interval. The receiver computes the decision variables $W_1 = W_{11} - W_{12}$ and $W_2 = W_{21} - W_{22}$ which are also the inputs to the switch. If the switch is connected to W_i and $W_i > 0$, the receiver selects the binary symbol corresponding to frequency f_1, otherwise the

symbol corresponding to frequency f_2 is selected.

Let w_{T_1} and w_{T_2} denote the switching thresholds on channel 1 and channel 2, respectively. In mathematical terms the operation of the switch can be written as [13, eqs. (1)-(2)]

$$W(n) = W_i(n) = \text{if} \begin{cases} W(n-1) = W_i(n-1) \quad \text{and} \quad |W_i(n)| \geq w_{T_i}, \quad i = 1,2 \\ \qquad\qquad\qquad\qquad \text{or} \\ W(n-1) = W_{\bar{i}}(n-1) \quad \text{and} \quad |W_{\bar{i}}(n)| \leq w_{T_{\bar{i}}}, \quad i = 1,2 \end{cases} \tag{3.1}$$

where $\bar{i}$ denotes the 2's complement of i.

3.1.2 Average BER Analysis

Following the analysis in [13], the average BER of noncoherent BFSK with dual-branch postdetection SSC can be written as [13, eq. (7)]

$$\begin{aligned} P_b(E) = {} & p_1 F_{W_1}(-w_{T_1}) + p_2 F_{W_2}(-w_{T_2}) \\ & + p_1 (F_{W_1,W_2}(w_{T_1}, 0) - F_{W_1,W_2}(-w_{T_1}, 0)) \\ & + p_2 (F_{W_1,W_2}(0, w_{T_2}) - F_{W_1,W_2}(0, -w_{T_2})) \end{aligned} \tag{3.2a}$$

where $F_{W_1,W_2}(\cdot,\cdot)$ denotes the joint cumulative distribution function (CDF) of the random variables (RVs) W_1 and W_2, F_{W_i} is the marginal CDF of the RV W_i, $i = 1,2$ and p_1 and p_2 are defined as [13, eq. (13)]

$$p_1 = \frac{F_{|W_2|}(w_{T_2})}{F_{|W_1|}(w_{T_1}) + F_{|W_2|}(w_{T_2})} \tag{3.2b}$$

$$p_2 = \frac{F_{|W_1|}(w_{T_1})}{F_{|W_1|}(w_{T_1}) + F_{|W_2|}(w_{T_2})}. \tag{3.2c}$$

In the case of identically distributed branches, $F_{W_1}(\cdot) = F_{W_2}(\cdot) \triangleq F_W(\cdot)$, $w_{T_1} = w_{T_2} \triangleq w_T$, $p_1 = p_2 = 1/2$ and (3.2a) can be further simplified to

$$P_b(E) = F_W(-w_T) + (F_{W_1,W_2}(w_T, 0) - F_{W_1,W_2}(-w_T, 0)). \tag{3.3}$$

Assume, without loss of generality, that the symbol corresponding to frequency f_1 is transmitted. Then the RVs W_1 and W_2 can be written as [13]

$$W_1 = W_{11} - W_{12} = |2E_bG_1 + N_{11}|^2 - |N_{12}|^2 \tag{3.4}$$

$$W_2 = W_{21} - W_{22} = |2E_bG_2 + N_{21}|^2 - |N_{22}|^2 \tag{3.5}$$

where E_b is the energy per bit per symbol, $N_{ik}, i, k = 1, 2$ are independent and identically distributed (i.i.d) zero-mean Gaussian random variables (RVs) with variance $4E_bN_0$ and G_1 and G_2 denote the complex channel gains on channel 1 and channel 2, respectively. We assume that the average fading powers, $\Omega_i = E[|G_i|^2]$, $i = 1, 2$, are not necessarily equal, i.e., they are non-identically distributed. We further assume that the channel gains are correlated and we denote the fading correlation between G_1 and G_2 as ρ.

To proceed, we need to calculate the joint CDF of W_1 and W_2 and the marginal CDFs. To calculate the joint CDF of W_1 and W_2, we transform W_1 and W_2 into conditionally independent RVs so that their conditional joint CDF can be written as the product of the conditional marginal CDFs [20], [30] and subsequently the joint CDF is obtained by removing the conditioning. Assume that W_1 and W_2 are conditionally independent given a positive RV Z. Then, their joint CDF can be calculated as

$$F_{W_1,W_2}(w_1, w_2) = \int_0^\infty F_{W_1|Z}(w_1)F_{W_2|Z}(w_2)f_Z(z)dz. \tag{3.6}$$

3.1.2.1 Rayleigh Fading

To begin our analysis, we write $G_i, i = 1, 2$ as

$$G_i = \sqrt{\Omega_i}(\sqrt{1-\rho}X_i + \sqrt{\rho}X_0 + j(\sqrt{1-\rho}Y_i + \sqrt{\rho}Y_0)) \tag{3.7}$$

where $j = \sqrt{-1}$ and X_i and Y_i are *independent* zero-mean Gaussian RVs with variance $\frac{1}{2}$. The definitions given in (3.7) guarantee that G_1 and G_2 are Rayleigh distributed with $E[|G_i|^2] = \Omega_i \; i = 1, 2$. Furthermore, one can easily show that the cross-correlation between G_1 and G_2 is equal to ρ. Note that the power correlation, ρ_η, is equal to the square of the fading gain correlation, i.e., $\rho_\eta = \rho^2$ [31].

Using (3.7), we can write W_{11} defined in (3.4) as

$$W_{11} = (2E_b\sqrt{\Omega_1}(\sqrt{1-\rho}X_1 + \sqrt{\rho}X_0) + N_{11}^I)^2 + (2E_b\sqrt{\Omega_1}(\sqrt{1-\rho}Y_1 + \sqrt{\rho}Y_0) + N_{11}^Q)^2 \tag{3.8}$$

where N_{11}^I and N_{11}^Q are zero-mean Gaussian RVs with variance $2E_bN_0$. Similarly W_{21} can be written as

$$W_{21} = (2E_b\sqrt{\Omega_2}(\sqrt{1-\rho}X_2 + \sqrt{\rho}X_0) + N_{21}^I)^2 + (2E_b\sqrt{\Omega_2}(\sqrt{1-\rho}Y_2 + \sqrt{\rho}Y_0) + N_{21}^Q)^2. \tag{3.9}$$

Let $\mathbb{X}_2(a, \sigma^2)$ denote a non-central chi-squared RV with non-centrality parameter a^2 and assume that X_0 and Y_0 are fixed. Then W_{11} is a non-central chi-squared RV with two degrees of freedom with non-centrality parameter $a_1^2 = 4E_b^2\Omega_1\rho Z$ and $\sigma_1^2 = 2E_bN_0(1+\bar{\gamma}_1(1-\rho))$, where $\bar{\gamma}_i = E_b\Omega_i/N_0$ is the average SNR on the ith channel and

$$Z = X_0^2 + Y_0^2. \tag{3.10}$$

Similarly, one can show that W_{21} is a non-central chi-squared RV with non-centrality parameter $a_2^2 = 4E_b^2\Omega_2\rho Z$ and $\sigma_2^2 = 2E_bN_0(1 + \bar{\gamma}_2(1-\rho))$. Noting that W_{12} and W_{22} are independent central chi-squared RVs with two degrees of freedom and parameter $2E_bN_0$, one can see that the RVs W_1 and W_2 are now conditionally independent given Z. Furthermore, $W_1|Z$ and $W_2|Z$ are the difference between a non-central and a central chi-squared RV. Therefore using [13, eq. (51)] and after

some mathematical manipulations and simplifications, their CDFs can be written as

$$F_{W_i|Z}(w) = \begin{cases} Y_1(\bar{\gamma}_i, \rho, z) \exp\left(\frac{w}{4E_bN_0}\right), & w < 0 \\ 1 - Q_1\left(\sqrt{Y_2(\bar{\gamma}_i, \rho, z)}, \sqrt{\frac{w}{2E_bN_0(1+(1-\rho)\bar{\gamma}_i}}\right) & \\ +Y_1(\bar{\gamma}_i, \rho, z) \exp\left(\frac{w}{4E_bN_0}\right) \times & \\ Q_1\left(\sqrt{Y_3(\bar{\gamma}_i, \rho, z)}, \sqrt{\frac{Y_4(\bar{\gamma}_i, \rho, z)w}{2E_bN_0}}\right), & w > 0 \end{cases} \tag{3.11a}$$

where

$$Y_1(\bar{\gamma}, \rho, z) = \frac{1}{2+(1-\rho)\bar{\gamma}} \exp\left(-\frac{\bar{\gamma}\rho z}{2+(1-\rho)\bar{\gamma}}\right) \tag{3.11b}$$

$$Y_2(\bar{\gamma}, \rho, z) = \frac{2\rho\bar{\gamma}z}{(1+(1-\rho)\bar{\gamma})} \tag{3.11c}$$

$$Y_3(\bar{\gamma}, \rho, z) = \frac{2\rho\bar{\gamma}z}{(1+(1-\rho)\bar{\gamma})(2+(1-\rho)\bar{\gamma})} \tag{3.11d}$$

$$Y_4(\bar{\gamma}, \rho, z) = \frac{2+(1-\rho)\bar{\gamma}}{1+(1-\rho)\bar{\gamma}}. \tag{3.11e}$$

The unconditional CDF of W_i can now be calculated by integrating $F_{W_i|Z}(w)$ over the probability density function of Z given by

$$f_Z(z) = \exp(-z), \quad z > 0. \tag{3.12}$$

The result, after some algebra, is

$$F_{W_i}(w) = \begin{cases} \frac{1}{2+\bar{\gamma}_i} \exp\left(\frac{w}{4E_bN_0}\right), & w < 0 \\ 1 - \frac{1+\bar{\gamma}_i}{2+\bar{\gamma}_i} \exp\left(-\frac{w}{4E_bN_0(1+\bar{\gamma}_i)}\right), & w > 0 \end{cases} \tag{3.13}$$

which, as expected, is equal to [13, eq. 17] and [13, eq. 18] for $i = 1$ and $i = 2$, respectively.

To obtain the average BER, we now calculate the terms in (3.2a). We begin by evaluating p_1 and p_2 defined in (3.2b) and (3.2c), respectively. Substituting (3.13) in (3.2b) and (3.2c) and noting that $F_{|W_i|}(w_{T_i}) = F_{W_i}(w_{T_i}) - F_{W_i}(-w_{T_i})$, results in

$$p_1 = \frac{\mathcal{F}_0(\bar{\gamma}_2, \eta_{T_2})}{\mathcal{F}_0(\bar{\gamma}_1, \eta_{T_1}) + \mathcal{F}_0(\bar{\gamma}_2, \eta_{T_1})} \tag{3.14}$$

$$p_2 = \frac{\mathcal{F}_0(\bar{\gamma}_1, \eta_{T_1})}{\mathcal{F}_0(\bar{\gamma}_1, \eta_{T_1}) + \mathcal{F}_0(\bar{\gamma}_2, \eta_{T_2})} \tag{3.15}$$

where $\eta_{T_i} = w_{T_i}/(\Omega_i E_b^2)$ is the normalized switching threshold on the ith channel and $\mathcal{F}_0(x,y)$ is defined as

$$\mathcal{F}_0(x,y) = 1 - \frac{1+x}{2+x}\exp\left(-\frac{xy}{4(1+x)}\right) - \frac{1}{2+x}\exp\left(-\frac{xy}{4}\right). \tag{3.16}$$

Next, substituting (3.11) in (3.6), using [18, eq. (B.18)], and after some mathematical manipulation and integral evaluations, we obtain closed-form expressions for $F_{W_1,W_2}(w_{T_1},0)$ and $F_{W_1,W_2}(-w_{T_1},0)$ as

$$\begin{aligned} F_{W_1,W_2}(w_{T_1},0) = \frac{1}{2+\bar{\gamma}_2}\left(1-\exp\left(-\frac{w_{T_1}\mathcal{F}_1(\bar{\gamma}_1,\bar{\gamma}_2,\rho)}{4E_bN_0}\right)\right) \\ + \mathcal{F}_2(\bar{\gamma}_1,\bar{\gamma}_2,\rho)\exp\left(-\frac{w_{T_1}\mathcal{F}_1(\bar{\gamma}_1,\bar{\gamma}_2,\rho)}{4E_bN_0}\right) \end{aligned} \tag{3.17}$$

and

$$F_{W_1,W_2}(-w_{T_1},0) = \mathcal{F}_2(\bar{\gamma}_1,\bar{\gamma}_2,\rho)\exp\left(-\frac{w_{T_1}}{4E_bN_0}\right) \tag{3.18}$$

respectively, where $\mathcal{F}_1(x,y,z)$ and $\mathcal{F}_2(x,y,z)$ are defined as

$$\mathcal{F}_1(x,y,z) = \frac{2+y}{xy(1-z^2)+2x+y+2} \tag{3.19}$$

$$\mathcal{F}_2(x,y,z) = \frac{1}{(2+(1-z)x)(2+(1+z)y)}. \tag{3.20}$$

Similarly, we can derive analytical expressions for $F_{W_1,W_2}(0,w_{T_2})$ and $F_{W_1,W_2}(0,-w_{T_2})$ as

$$\begin{aligned} F_{W_1,W_2}(0,w_{T_2}) = \frac{1}{2+\bar{\gamma}_1}\left(1-\exp\left(-\frac{w_{T_2}\mathcal{F}_1(\bar{\gamma}_2,\bar{\gamma}_1,\rho)}{4E_bN_0}\right)\right) \\ + \mathcal{F}_2(\bar{\gamma}_1,\bar{\gamma}_2,\rho)\exp\left(-\frac{w_{T_2}\mathcal{F}_1(\bar{\gamma}_1,\bar{\gamma}_2,\rho)}{4E_bN_0}\right) \end{aligned} \tag{3.21}$$

and

$$F_{W_1,W_2}(0,-w_{T_2}) = \mathcal{F}_2(\bar{\gamma}_2,\bar{\gamma}_1,\rho)\exp\left(-\frac{w_{T_2}}{4E_bN_0}\right) \tag{3.22}$$

respectively. A closed-form expression can now be obtained for the average BER of BFSK with postdetection SSC in correlated Rayleigh fading with average fading

power imbalance as

$$P_b(E) = \sum_{i=1}^{2} \frac{\mathcal{F}_0(\bar{\gamma}_{\bar{i}}, \eta_{T_{\bar{i}}})}{\mathcal{F}_0(\bar{\gamma}_i, \eta_{T_i}) + \mathcal{F}_0(\bar{\gamma}_{\bar{i}}, \eta_{T_{\bar{i}}})} \times \left\{ \frac{1}{2+\bar{\gamma}_i} \exp\left(-\frac{\eta_{T_i}\bar{\gamma}_i}{4}\right) + \frac{1}{2+\bar{\gamma}_{\bar{i}}} \left(1 - \exp\left(-\frac{\eta_{T_i}\bar{\gamma}_i}{4}\mathcal{F}_1(\bar{\gamma}_i, \bar{\gamma}_{\bar{i}}, \rho)\right)\right) \right. \\ \left. + \mathcal{F}_2(\bar{\gamma}_i, \bar{\gamma}_{\bar{i}}, \rho) \left(\exp\left(-\frac{\eta_{T_i}\bar{\gamma}_i}{4}\mathcal{F}_1(\bar{\gamma}_i, \bar{\gamma}_{\bar{i}}, \rho)\right) - \exp\left(-\frac{\eta_{T_i}\bar{\gamma}_i}{4}\right)\right) \right\} \tag{3.23}$$

where $\bar{i} = (i+1) \mod 3$, i.e., $\bar{1} = 2$ and $\bar{2} = 1$. For $\rho = 0$, one can show that (3.23) reduces to the result given in [13], as expected.

For the case of identical correlated fading, i.e., $\bar{\gamma}_1 = \bar{\gamma}_2 = \bar{\gamma}$, $\eta_{T_1} = \eta_{T_2} \triangleq \eta_T$, $p_1 = p_2 = 1/2$ and (3.23) reduces to

$$P_b(E) = \frac{1}{2+\bar{\gamma}} \left\{ 1 + \exp\left(-\frac{\eta_T\bar{\gamma}}{4}\right) - \exp\left(-\frac{\eta_T\bar{\gamma}}{4}\mathcal{F}_1(\bar{\gamma}, \bar{\gamma}, \rho)\right) \right\} \\ - \mathcal{F}_2(\bar{\gamma}, \bar{\gamma}, \rho) \left(\exp\left(-\frac{\eta_T\bar{\gamma}}{4}\right) - \exp\left(-\frac{\eta_T\bar{\gamma}}{4}\mathcal{F}_1(\bar{\gamma}, \bar{\gamma}, \rho)\right)\right). \tag{3.24}$$

For $\rho = 0$ one can easily show that (3.24) reduces to [13, eq. (20)], as expected.

As a check on the validity of our results, we see that for both extremes $\eta_T = 0$ and $\eta_T = \infty$, (3.24) reduces to the BER of a single-branch noncoherent BFSK receiver given by

$$P_b(E) = \frac{1}{2+\bar{\gamma}}. \tag{3.25}$$

The average BER in (3.24) can now be minimized by obtaining an optimal switching threshold, η_T^*, which is the solution to the equation [13]

$$\frac{dP_b(E)}{d\eta_T}\Big|_{\eta=\eta_T^*} = 0. \tag{3.26}$$

Substituting (3.24) in (3.26), leads to the desired solution as

$$\eta_T^* = \frac{4(\bar{\gamma}^2(1-\rho^2) + 3\bar{\gamma} + 2)}{(2+\bar{\gamma}(1-\rho^2))\bar{\gamma}^2} \ln\left(\frac{\bar{\gamma}^2(1-\rho^2) + 3\bar{\gamma} + 2}{2+\bar{\gamma}}\right) \tag{3.27}$$

The minimum BER can now be obtained by substituting (3.27) in (3.24).

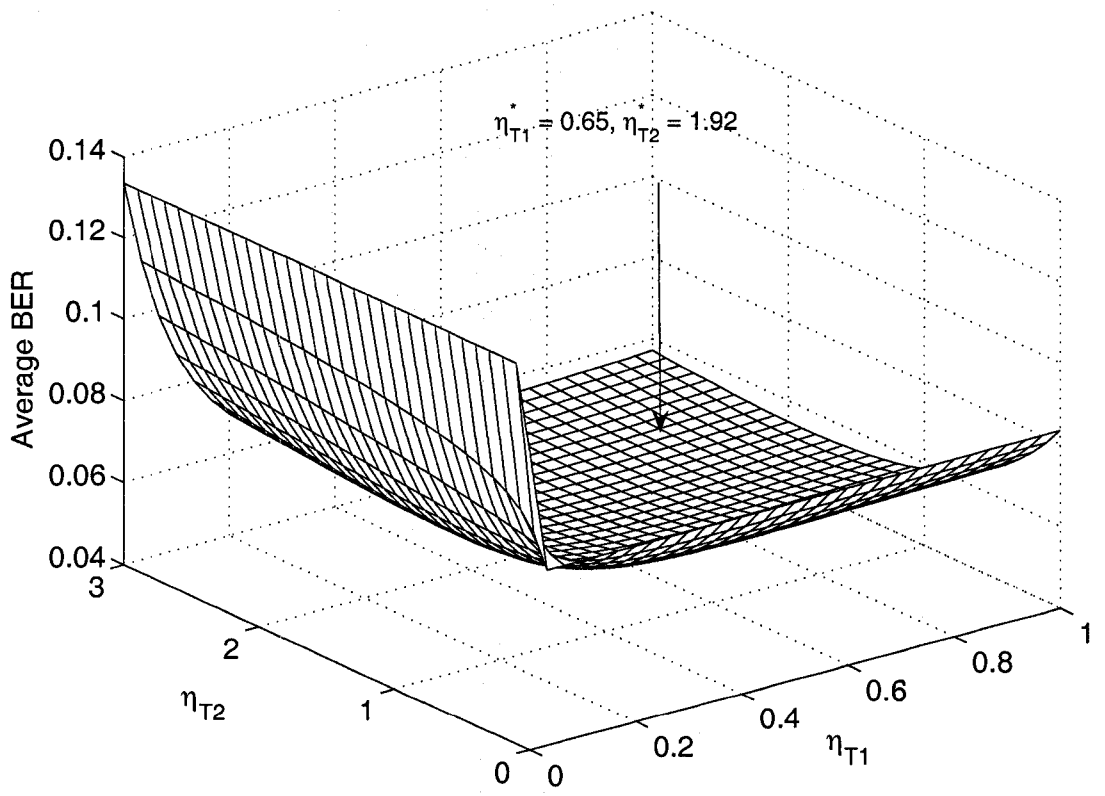

Figure 3.2: The average BER versus the normalized switching thresholds of noncoherent BFSK with postdetection SSC Model 1 in non-identically distributed correlated Rayleigh fading with $\rho = 0.7$, $\bar{\gamma}_1 = 10$ dB and $\bar{\gamma}_2 = 5.48$ dB ($\delta = 0.6$).

In the case of average fading power imbalance between the diversity paths, the average BER given in (3.23), is a function of η_{T_1} and η_{T_2} and the expression has to be minimized with respect to both parameters to reach a global solution. For example, Fig. 3.2 shows the average BER of postdetection SSC Model 1 as a function of η_{T_1} and η_{T_2} for $\bar{\gamma}_1 = 10$ dB and $\bar{\gamma}_2 = 5.48$ dB where the average SNR on the second branch is related to the average SNR on the first branch as $\bar{\gamma}_2 = \bar{\gamma}_1 \exp(-\delta)$ where $\delta = 0.6$ is the average decay factor. The optimum values of the normalized switching thresholds that minimize the average BER are shown in the figure.

3.1.2.2 Rician Fading

In the case of Rician fading, the complex channel gains can be written as

$$G_i = \sqrt{1-\rho}X_i + \sqrt{\rho}X_0 + \nu_1 + j(\sqrt{1-\rho}Y_i + \sqrt{\rho}Y_0 + \nu_2) \tag{3.28}$$

where X_i and Y_i are zero-mean Gaussian RVs with variance $\sigma^2 = \Omega/(2(K+1))$ and ν_1 and ν_2 correspond to the in-phase and quadrature component of the line of sight component and are related to the Rician factor K through $K = (\nu_1^2 + \nu_2^2)/(2\sigma^2)$. Using the representation given in (3.28), one can show that the fading correlation between G_1 and G_2 is equal to ρ and $E[|G_i|^2] = \Omega, i = 1, 2$. In addition, the power correlation between $|G_1|^2$ and $|G_2|^2$ can be obtained as

$$\rho_\eta = \rho\frac{2K+\rho}{2K+1}. \tag{3.29}$$

Define

$$Z = (X_0 + \frac{\nu_1}{\sqrt{\rho}})^2 + (Y_0 + \frac{\nu_2}{\sqrt{\rho}})^2. \tag{3.30}$$

Then assuming that Z is fixed, one can show, similar to the derivation in the previous section and after some mathematical simplification, that the conditional CDF of $W_i, i = 1, 2$ given Z, i.e., $F_{W_i|Z}(w)$ can be written as

$$F_{W_i|Z}(w) = \begin{cases} H_1(\bar{\gamma}, K, \rho, z)\exp\left(\frac{w}{4E_bN_0}\right), & w < 0 \\ 1 - Q_1\left(\sqrt{H_2(\bar{\gamma}_i, K, \rho, z)}, \sqrt{H_3(\bar{\gamma}, K, \rho)\frac{w}{2E_bN_0}}\right) \\ +H_1(\bar{\gamma}, K, \rho, z)\exp\left(\frac{w}{4E_bN_0}\right) \times \\ Q_1\left(\sqrt{H_4(\bar{\gamma}_i, K, \rho, z)}, \sqrt{H_5(\bar{\gamma}, K, \rho)\frac{w}{2E_bN_0}}\right), & w > 0 \end{cases} \tag{3.31a}$$

where

$$H_1(\bar{\gamma}, K, \rho, z) = \frac{1+K}{2(1+K)+\bar{\gamma}(1-\rho)} \exp\left(-\frac{\bar{\gamma}\rho(1+K)z}{2(1+K)+\bar{\gamma}(1-\rho)}\right) \quad (3.31b)$$

$$H_2(\bar{\gamma}, K, \rho, z) = \frac{2\bar{\gamma}\rho(1+K)z}{1+K+\bar{\gamma}(1-\rho)} \quad (3.31c)$$

$$H_3(\bar{\gamma}, K, \rho) = \frac{1}{1+K+\bar{\gamma}(1-\rho)} \quad (3.31d)$$

$$H_4(\bar{\gamma}, K, \rho, z) = \frac{2\bar{\gamma}\rho(1+K)^2 z}{(1+K+\bar{\gamma}(1-\rho))(2(1+K)+\bar{\gamma}(1-\rho))} \quad (3.31e)$$

$$H_5(\bar{\gamma}, K, \rho) = \frac{2(1+K)+\bar{\gamma}(1-\rho)}{1+K+\bar{\gamma}(1-\rho)}. \quad (3.31f)$$

Similar to the approach taken in the previous section, using the PDF of Z, given by

$$f_Z(z) = (K+1)\exp\left(-\frac{K}{\rho} - (K+1)z\right) I_0\left(2\sqrt{\frac{K(K+1)z}{\rho}}\right) \quad (3.32)$$

and after much mathematical manipulations and integral evaluations, we obtain the BER of BFSK in correlated Rician fading as

$$P_b = R_1(K,\bar{\gamma})\left(\exp\left(-\frac{\eta_T\bar{\gamma}}{4}\right) + 1 - Q_1\left(\sqrt{R_2(K,\bar{\gamma},\rho)}, \sqrt{\eta_T R_3(K,\bar{\gamma},\rho)}\right)\right)$$
$$+ R_4(K,\bar{\gamma},\rho)\left[Q_1\left(\sqrt{R_5(K,\bar{\gamma},\rho)}, \sqrt{\eta_T R_6(K,\bar{\gamma},\rho)}\right)\exp\left(\frac{\eta_T\bar{\gamma}}{4}\right) - \exp\left(-\frac{\eta_T\bar{\gamma}}{4}\right)\right] \quad (3.33a)$$

where

$$R_1(K,\bar{\gamma}) = \frac{1+K}{2(1+K)+\bar{\gamma}} \exp\left(-\frac{K\bar{\gamma}}{2(1+K)+\bar{\gamma}}\right) \tag{3.33b}$$

$$R_2(K,\bar{\gamma},\rho) = \frac{2K\bar{\gamma}(2(1+K)+\bar{\gamma}(1-\rho))^2}{(2(1+K)+\bar{\gamma})(\bar{\gamma}^2(1-\rho^2)+3\bar{\gamma}(1+K)+2(1+K)^2)} \tag{3.33c}$$

$$R_3(K,\bar{\gamma},\rho) = \frac{\bar{\gamma}(1+K)(2(1+K)+\bar{\gamma})}{2(\bar{\gamma}^2(1-\rho^2)+3\bar{\gamma}(1+K)+2(1+K)^2)} \tag{3.33d}$$

$$R_4(K,\bar{\gamma},\rho) = \frac{(1+K)^2}{(2(1+K)+\bar{\gamma}(1-\rho))(2(1+K)+\bar{\gamma}(1+\rho))} \times \exp\left(-\frac{2K\bar{\gamma}}{2(1+K)+\bar{\gamma}(1+\rho)}\right) \tag{3.33e}$$

$$R_5(K,\bar{\gamma},\rho) = \frac{2K\bar{\gamma}(1+K)(2(1+K)+\bar{\gamma}(1-\rho)}{(2(K+1)+\bar{\gamma}(1+\rho))} \times \frac{1}{(\bar{\gamma}^2(1-\rho^2)+3\bar{\gamma}(1+K)+2(1+K)^2)} \tag{3.33f}$$

$$R_6(K,\bar{\gamma},\rho) = \frac{\bar{\gamma}(2(1+K)+\bar{\gamma}(1-\rho))(2(1+K)+\bar{\gamma}(1+\rho))}{2(\bar{\gamma}^2(1-\rho^2)+3\bar{\gamma}(1+K)+2(1+K)^2)}. \tag{3.33g}$$

As a check on the validity of our result one can show that for $\rho = 0$, (3.33) reduces to [13, eq. (9)], as expected. Also note that for $K = 0$, which corresponds to Rayleigh fading, (3.33) reduces to (3.24).

The optimum switching threshold that minimizes the average BER can now be calculated by substituting (3.33) in (3.26) and obtaining η_T^*. Using [13, eq. (39)], we obtain

$$R_1(K,\bar{\gamma})\Bigg(-\frac{\bar{\gamma}}{4}\exp\left(-\frac{\eta_T\bar{\gamma}}{4}\right)+\frac{R_3(K,\bar{\gamma},\rho)\eta_T}{2}\exp\left(-\frac{R_2(K,\bar{\gamma},\rho)+R_3(K,\bar{\gamma},\rho)\eta_T}{2}\right) \times I_0\left(\sqrt{R_2(K,\bar{\gamma},\rho)R_3(K,\bar{\gamma},\rho)\eta_T}\right)\Bigg)+R_4(K,\bar{\gamma},\rho)\Bigg[\frac{\bar{\gamma}}{4}\exp\left(-\frac{\eta_T\bar{\gamma}}{4}\right)+\exp\left(\frac{\eta_T\bar{\gamma}}{4}\right) \times\Bigg\{\frac{\bar{\gamma}}{4}Q_1\left(\sqrt{R_5(K,\bar{\gamma},\rho)},\sqrt{R_6(K,\bar{\gamma},\rho)\eta_T}\right)-\frac{R_6(K,\bar{\gamma},\rho)\eta_T}{2} \times\exp\left(-\frac{R_5(K,\bar{\gamma},\rho)+R_6(K,\bar{\gamma},\rho)\eta_T}{2}\right)I_0\left(\sqrt{R_5(K,\bar{\gamma},\rho)R_6(K,\bar{\gamma},\rho)\eta_T}\right)\Bigg\}\Bigg]=0 \tag{3.34}$$

whose solution is the optimum switching threshold η_T^*.

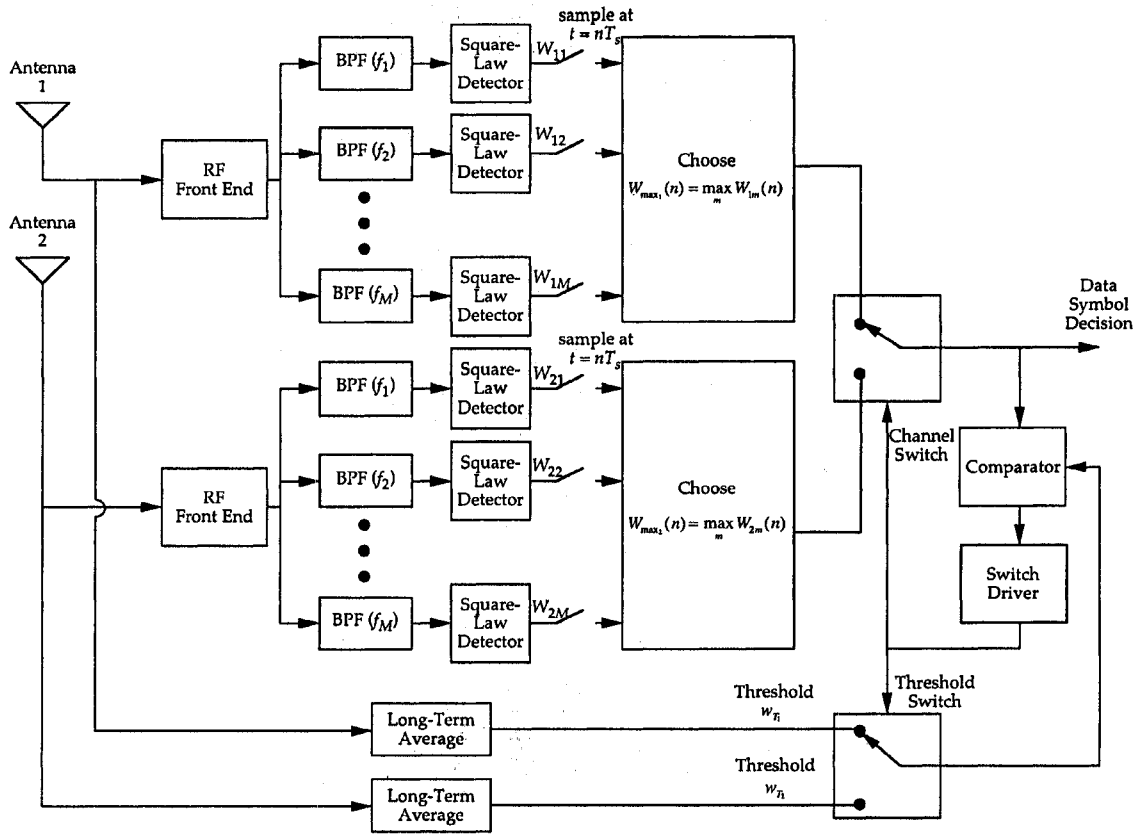

Figure 3.3: The block diagram of postdetection SSC receiver Model 2 (after [24, Fig. 1]).

3.2 Postdetection SSC Model 2

3.2.1 System Model

The modulation format is considered to be MFSK. The structure of the receiver is depicted in Fig. 3.3 (after [27, Fig. 1]). Let $W_{ij}(n), i = 1, 2, j = 1, \cdots, M$ denote the outputs of the M square law detectors of the receiver at the sampling instant $t = nT_s$, where T_s is the symboling time and where the subscript i in W_{ij} denotes the diversity branch. The square-law detectors are matched to frequencies f_1 through f_M. Assume

that the first symbol of the alphabet is transmitted. Then W_{ij} can be written as

$$W_{i1}(n) = |2E_sG_i + N_{i1}|^2 \tag{3.35}$$

$$W_{ik}(n) = |N_{ik}|^2, i = 1, 2, k = 2, 3, \cdots, M \tag{3.36}$$

where E_s is the transmitted energy per symbol, G_1 and G_2 are the complex channel gains on channels 1 and 2 and N_{ik} are zero-mean complex Gaussian RVs with variance $4E_sN_0$. Note that the definition of G_i is given in (3.7) and (3.28) for the cases of Rayleigh and Rician fading, respectively. The switching mechanism is based on comparison of the maximum of the square-law detector output on each branch with a predetermined threshold w_{T_i}. For example if the switch is connected to Antenna 1, it will stay connected to Antenna 1 as long as $\max W_{1k}(n) > w_{T_i}$. If $\max W_{1k}(n) < w_{T_1}$ the system will switch to Antenna 2 regardless of whether $\max W_{2k}(n)$ is greater or less than the predetermined threshold w_{T_2}. Note that the difference between postdetection SSC Model 1 and postdetection SSC Model 2 is that in postdetection SSC Model 1 a summing process occurs on the outputs of the square-law detectors before data detection, while in postdetection SSC Model 2 the outputs of the square-law detectors are directly used for data detection. Note also that BFSK signaling can be used with both postdetection SSC Model 1 and Model 2 whereas MFSK signaling can be used only with postdetection SSC Model 2.

3.2.2 Average Symbol Error Rate

Assume that the switch is connected to Antenna 1. Then the probability of a correct decision can be written as [27]

$$\begin{aligned} P_{s1}(C) &= \Pr\left(W_{11}(n) \geq w_{T_1}, W_{12}(n) < W_{11}(n), \cdots, W_{1M}(n) < W_{11}(n)\right) \\ &\quad + \Pr\left(W_{\max_1}(n) \leq w_{T_1}, W_{22}(n) < W_{21}(n), \cdots, W_{2M}(n) < W_{21}(n)\right) \\ &\triangleq P_{s1}^1(C) + P_{s1}^2(C) \end{aligned} \tag{3.37}$$

where $W_{\max_1}(n) \triangleq \max W_{1k}, k = 1, \cdots, M$. Noting that $W_{1k}, k = 1, \cdots, M$ are independent and $W_{1k}, k = 2, \cdots, M$ are i.i.d, we can write $P_{s1}^1(C)$ as

$$P_{s1}^1(C) = \int_{w_{T_1}}^{\infty} f_{W_{11}}(w)[F_{W_{12}}(w)]^{M-1} dw. \tag{3.38}$$

Let $Y = \max W_{2i}, i \neq 1$. Then, $P_{s1}^2(C)$ can be written as

$$\begin{aligned} P_{s1}^2(C) &= [F_{W_{12}}(w_{T_1})]^{M-1} \Pr(W_{11} < w_{T_1}, W_{21} > Y) \\ &= [F_{W_{12}}(w_{T_1})]^{M-1} [F_{W_{11}}(w_{T_1}) - \int_0^{\infty} F_{W_{11},W_{21}}(w_{T_1}, y) f_Y(y) dy] \end{aligned} \tag{3.39}$$

where $F_{W_{11},W_{21}}(w_1, w_2)$ is the joint CDF of the RVs W_{11} and W_{21}, and $f_Y(y)$ is the PDF of the RV Y defined earlier. Note that in obtaining the second equality in (3.39) we have used the total probability theorem. Now assume that the RVs W_{11} and W_{21} are independent given RV Z defined in the previous section in (3.10) and (3.30) for the cases of Rayleigh and Rician fading, respectively. Then (3.39) can be written as

$$\begin{aligned} P_{s1}^2(C) = [F_{W_{12}}(w_{T_1})]^{M-1} \Bigg[& F_{W_{11}}(w_{T_1}) - (M-1) \\ & \times \int_0^{\infty} \left\{ \int_0^{\infty} F_{W_{11}|Z}(w_{T_1}) F_{W_{21}|Z}(w) f_Z(z) dz \right\} (F_{W_{22}}(w))^{M-2} f_{W_{22}}(w) dw \Bigg] \end{aligned} \tag{3.40}$$

where $f_Y(w) = (M-1)(F_{W_{22}}(w))^{M-2} f_{W_{22}}(w)$ has been used. Combining (3.38) and (3.40), the probability of correct decision assuming the switch is connected to Antenna

1 becomes

$$P_{s1}(C) = \int_{w_{T_1}}^{\infty} f_{W_{11}}(w)[F_{W_{12}}(w)]^{M-1}dw + [F_{W_{12}}(w_{T_1})]^{M-1}\left[F_{W_{11}}(w_{T_1}) - (M-1)\right.$$
$$\left.\times \int_0^{\infty}\left\{\int_0^{\infty} F_{W_{11}|Z}(w_{T_1})F_{W_{21}|Z}(w)f_Z(z)dz\right\}(F_{W_{22}}(w))^{M-2}f_{W_{22}}(w)dw\right]. \tag{3.41}$$

Similarly if the switch is connected to Antenna 2, the probability of correct decision becomes

$$P_{s2}(C) = \int_{w_{T_2}}^{\infty} f_{W_{21}}(w)[F_{W_{22}}(w)]^{M-1}dw + [F_{W_{22}}(w_{T_2})]^{M-1}\left[F_{W_{21}}(w_{T_2}) - (M-1)\right.$$
$$\left.\times \int_0^{\infty}\left\{\int_0^{\infty} F_{W_{21}|Z}(w_{T_2})F_{W_{11}|Z}(w)f_Z(z)dz\right\}(F_{W_{12}}(w))^{M-2}f_{W_{12}}(w)dw\right]. \tag{3.42}$$

Let p_i denote the percentage of time that the switch is connected to Antenna i. Then, using a two-state Markov chain, similar to the one presented in [15], one can compute p_1 and p_2 as

$$p_1 = \frac{F_{W_{21}}(w_{T_2})[F_{W_{22}}(w_{T_2})]^{M-1}}{F_{W_{21}}(w_{T_2})[F_{W_{22}}(w_{T_2})]^{M-1} + F_{W_{11}}(w_{T_1})[F_{W_{12}}(w_{T_1})]^{M-1}} \tag{3.43}$$

$$p_2 = \frac{F_{W_{11}}(w_{T_1})[F_{W_{12}}(w_{T_1})]^{M-1}}{F_{W_{21}}(w_{T_2})[F_{W_{22}}(w_{T_2})]^{M-1} + F_{W_{11}}(w_{T_1})[F_{W_{12}}(w_{T_1})]^{M-1}}. \tag{3.44}$$

The probability of correct decision can now be obtained as $P_s(C) = p_1P_{s1}(C) + p_2P_{s2}(C)$. Thus the SER can be computed as

$$P_s(E) = 1 - P_s(C) = 1 - \sum_{i=1}^{2} \frac{F_{W_{\bar{i}1}}(w_{T_{\bar{i}}})[F_{W_{\bar{i}2}}(w_{T_{\bar{i}}})]^{M-1}}{F_{W_{i1}}(w_{T_i})[F_{W_{i2}}(w_{T_i})]^{M-1} + F_{W_{\bar{i}1}}(w_{T_{\bar{i}}})[F_{W_{\bar{i}2}}(w_{T_{\bar{i}}})]^{M-1}}$$
$$\times\left(\int_{w_{T_i}}^{\infty} f_{W_{i1}}(w)[F_{W_{i2}}(w)]^{M-1}dw + [F_{W_{i2}}(w_{T_i})]^{M-1}\left[F_{W_{i1}}(w_{T_i}) - (M-1)\right.\right.$$
$$\left.\left.\times \int_0^{\infty}\left\{\int_0^{\infty} F_{W_{i1}|Z}(w_{T_i})F_{W_{\bar{i}1}|Z}(w)f_Z(z)dz\right\}(F_{W_{i2}}(w))^{M-2}f_{W_{i2}}(w)dw\right]\right). \tag{3.45}$$

To proceed, one needs to obtain $F_{W_{i1}|Z}(\cdot), F_{W_{i1}}(\cdot), F_{W_{i2}}(\cdot)$ and $f_{W_{i2}}(\cdot)$. These CDFs and PDFs are obtained for the cases of Rayleigh and Rician fading below.

Note that the average BER can be obtained from the average SER using [21]

$$P_b(E) = \frac{M}{2(M-1)} P_s(E). \tag{3.46}$$

3.2.2.1 Rayleigh Fading

In this case, using (3.10) and similar to the approach in the previous section, one can show that $F_{W_{i1}|Z}(\cdot)$ is given by

$$F_{W_{i1}|Z}(w) = 1 - Q_1\left(\sqrt{\frac{2\bar{\gamma}_i \rho z}{1+\bar{\gamma}_i(1-\rho)}}, \sqrt{\frac{w}{2E_s N_0(1+\bar{\gamma}_i(1-\rho))}}\right). \tag{3.47}$$

Integrating (3.47) over the PDF of Z given in (3.10) we obtain $F_{W_{i1}}(\cdot)$ as

$$F_{W_{i1}}(w) = 1 - \exp\left(-\frac{w}{4E_s N_0(1+\bar{\gamma}_i)}\right). \tag{3.48}$$

The PDF of W_{i1} can be obtained from (3.48) by differentiation as

$$f_{W_{i1}}(w) = \frac{1}{4E_s N_0(1+\bar{\gamma}_i)} \exp\left(-\frac{w}{4E_s N_0(1+\bar{\gamma}_i)}\right). \tag{3.49}$$

The PDF and CDF of W_{i2} can be calculated as

$$F_{W_{i2}}(w) = 1 - \exp\left(-\frac{w}{4E_s N_0}\right) \tag{3.50}$$

and

$$f_{W_{i2}}(w) = \frac{1}{4E_s N_0} \exp\left(-\frac{w}{4E_s N_0}\right) \tag{3.51}$$

respectively. A closed-form expression for the average SER of MFSK in unbalanced correlated Rayleigh fading is

$$P_s(E) = 1 - \sum_{i=1}^{2} \frac{1}{1+\kappa(\eta_{T_i},\bar{\gamma}_i)} \left\{ \sum_{i=0}^{M-1} \binom{M-1}{i} \frac{(-1)^i}{1+i(1+\bar{\gamma}_i)} \right.$$
$$\times \exp\left(-\frac{\eta_{T_i}\bar{\gamma}_i(1+i(1+\bar{\gamma}_i))}{4(1+\bar{\gamma}_i)}\right) + \left(1-\exp\left(-\frac{\eta_{T_i}\bar{\gamma}_i}{4}\right)\right)^{M-1}$$
$$\times \left(1-\exp\left(-\frac{\eta_{T_i}\bar{\gamma}_i}{4(1+\bar{\gamma}_i)}\right) - \sum_{i=0}^{M-2} \frac{(M-1)\binom{M-2}{i}(-1)^i}{(i+1)((i+1)(1+\bar{\gamma}_{\bar{i}})+1)}\right.$$
$$\left.\left. \times \left[1-\exp\left(-\frac{\bar{\gamma}_i\eta_{T_i}(i\bar{\gamma}_{\bar{i}}+\bar{\gamma}_{\bar{i}}+i+2)}{4(\bar{\gamma}_i\bar{\gamma}_{\bar{i}}(1-\rho^2)(i+1)+2(1+\bar{\gamma}_i)+(\bar{\gamma}_i+\bar{\gamma}_{\bar{i}})(i+1)+i-\bar{\gamma}_i)}\right)\right]\right)\right\} \tag{3.52a}$$

where $\eta_{T_i} = w_{T_i}/(\Omega_i E_s^2)$ is the normalized switching threshold and

$$\kappa(\eta_{T_i},\bar{\gamma}_i) = \frac{\left(1-\exp\left(-\frac{\eta_{T_i}\bar{\gamma}_i}{4}\right)\right)^{M-1}\left(1-\exp\left(-\frac{\eta_{T_i}\bar{\gamma}_i}{4(1+\bar{\gamma}_i)}\right)\right)}{\left(1-\exp\left(-\frac{\eta_{T_{\bar{i}}}\bar{\gamma}_{\bar{i}}}{4}\right)\right)^{M-1}\left(1-\exp\left(-\frac{\eta_{T_{\bar{i}}}\bar{\gamma}_{\bar{i}}}{4(1+\bar{\gamma}_{\bar{i}})}\right)\right)}. \tag{3.52b}$$

The details of the derivation of (3.52) are given in Appendix A. The average BER can be obtained from the average SER using (3.46). Similar to postdetection SSC Model 1, we obtain optimum switching thresholds $\eta_{T_1}^*$ and $\eta_{T_2}^*$ that minimize the average BER. For example, in Fig. 3.4, the average BER of BFSK with postdetection SSC Model 2 with average fading power imbalance is plotted as a function of η_{T_1} and η_{T_2} for $\rho = .5$, $\bar{\gamma}_1 = 15$ dB and $\bar{\gamma}_2 = 13.2$ dB ($\delta = 0.4$). The optimum switching thresholds that minimize the average BER are shown in the figure.

In the case of identically distributed branches, $\bar{\gamma}_1 = \bar{\gamma}_2 = \bar{\gamma}$, $\eta_{T_1} = \eta_{T_2} = \eta_T$ and

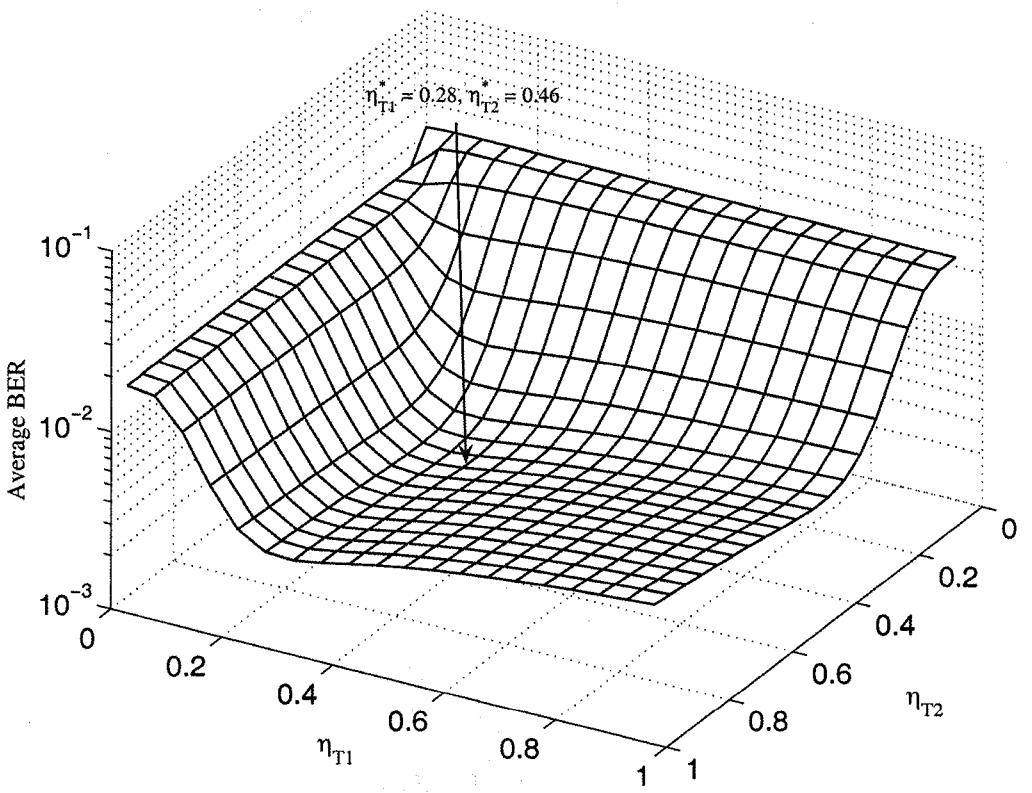

Figure 3.4: The average BER of BFSK with postdetection SSC Model 2 in correlated Rayleigh fading with average fading power imbalance for $\rho = 0.5$, $\bar{\gamma}_1 = 15$ dB and $\bar{\gamma}_2 = 13.2$ dB ($\delta = 0.4$).

(3.52) reduces to

$$\begin{aligned} P_s(E) = 1 - \Bigg\{ & \sum_{i=0}^{M-1} \binom{M-1}{i} \frac{(-1)^i}{1+i(1+\bar{\gamma})} \exp\left(-\frac{\eta_T \bar{\gamma}(1+i(1+\bar{\gamma}))}{4(1+\bar{\gamma})}\right) \\ & + \left(1 - \exp\left(-\frac{\eta_T \bar{\gamma}}{4}\right)\right)^{M-1} \left(1 - \exp\left(-\frac{\eta_T \bar{\gamma}}{4(1+\bar{\gamma})}\right)\right. \\ & - \sum_{i=0}^{M-2} \frac{(M-1)\binom{M-2}{i}(-1)^i}{(i+1)((i+1)(1+\bar{\gamma})+1)} \\ & \left. \times \left[1 - \exp\left(-\frac{\bar{\gamma}\eta_T(i\bar{\gamma}+\bar{\gamma}+i+2)}{4(\bar{\gamma}^2(1-\rho^2)(i+1)+2(1+\bar{\gamma})+2\bar{\gamma}(i+1))}\right)\right]\right)\Bigg\}. \end{aligned} \tag{3.53}$$

Substituting (3.53) in (3.26) one obtains

$$\sum_{i=0}^{M-1}\binom{M-1}{i}\frac{(-1)^{i+1}\bar{\gamma}}{4(1+\bar{\gamma})}\exp\left(-\frac{\eta_T\bar{\gamma}_i(1+i(1+\bar{\gamma}_i))}{4(1+\bar{\gamma}_i)}\right)+\frac{\bar{\gamma}}{4}\exp\left(-\frac{\eta_T\bar{\gamma}}{4}\right)$$
$$\times\left(1-\exp\left(-\frac{\eta_T\bar{\gamma}}{4}\right)\right)^{M-2}\left(1-\exp\left(-\frac{\eta_T\bar{\gamma}_i}{4(1+\bar{\gamma}_i)}\right)-\sum_{i=0}^{M-2}\frac{(M-1)\binom{M-2}{i}(-1)^i}{(i+1)((i+1)(1+\bar{\gamma}_i)+1)}\right.$$
$$\left.\times\left[1-\exp\left(-\frac{\bar{\gamma}_i\eta_T(i\bar{\gamma}_i+\bar{\gamma}_i+i+2)}{4(\bar{\gamma}_i^2(1-\rho^2)(i+1)+2(1+\bar{\gamma}_i)+2\bar{\gamma}_i(i+1))}\right)\right]\right)$$
$$+\left(1-\exp\left(-\frac{\eta_T\bar{\gamma}}{4}\right)\right)^{M-1}\left[\frac{\bar{\gamma}}{4(1+\bar{\gamma})}\exp\left(-\frac{\eta_T\bar{\gamma}}{4(1+\bar{\gamma})}\right)\right.$$
$$-\sum_{i=0}^{M-2}\frac{(M-1)\binom{M-2}{i}(-1)^i\bar{\gamma}}{4(i+1)(\bar{\gamma}^2(1-\rho^2)(i+1)+2(1+\bar{\gamma})+2\bar{\gamma}(i+1))}$$
$$\left.\times\exp\left(-\frac{\bar{\gamma}\eta_T(i\bar{\gamma}+\bar{\gamma}+i+2)}{4(\bar{\gamma}^2(1-\rho^2)(i+1)+2(1+\bar{\gamma})+2\bar{\gamma}(i+1))}\right)\right]=0 \tag{3.54}$$

whose solution is the optimum switching threshold η_T^* and can be easily obtained using the bisection method.

3.2.2.2 Rician Fading

For Rician fading, using (3.32), $F_{W_{i1}|Z}(\cdot)$ can be written as

$$F_{W_{i1}|Z}(w)=1-Q_1\left(\sqrt{\frac{2\bar{\gamma}_i\rho(1+K)z}{1+K+\bar{\gamma}_i(1-\rho)}},\sqrt{\frac{(1+K)w}{2E_sN_0(1+K+\bar{\gamma}_i(1-\rho))}}\right). \tag{3.55}$$

Next we calculate $F_{W_{i1}}(\cdot)$ by integrating (3.55) over the PDF of Z given in (3.32). The result is

$$F_{W_{i1}}(w)=1-Q_1\left(\sqrt{\frac{2K\bar{\gamma}}{\bar{\gamma}+K+1}},\sqrt{\frac{w(K+1)}{2E_sN_0(\bar{\gamma}+K+1)}}\right) \tag{3.56}$$

The PDF of W_{i1} can be obtained from (3.56) as

$$f_{W_{i1}}(w)=\frac{K+1}{4E_sN_0(\bar{\gamma}+K+1)}\exp\left(-\frac{(K+1)w}{4E_sN_0(\bar{\gamma}+K+1)}-\frac{K\bar{\gamma}}{\bar{\gamma}+K+1}\right)$$
$$\times I_0\left(\sqrt{\frac{K\bar{\gamma}(K+1)w}{E_sN_0(\bar{\gamma}+K+1)^2}}\right). \tag{3.57}$$

Now substituting (3.50), (3.51) and (3.55)-(3.57) in (3.45), using [18, eqs. (B.27) and (B.31)], and after much mathematical manipulations and integral evaluations similar to the procedure in the appendix, the average SER of MFSK with identically correlated Rician fading is obtained as

$$
\begin{aligned}
P_s(E) = 1 - \sum_{i=0}^{M-1} (-1)^i \binom{M-1}{i} \frac{K+1}{T_0(K,\bar{\gamma},i)} \exp\left(-\frac{Ki\bar{\gamma}}{T_0(K,\bar{\gamma},i)}\right) \\
\times Q_1\left(\sqrt{\frac{2K(K+1)\bar{\gamma}}{(\bar{\gamma}+K+1)T_0(K,\bar{\gamma},i)}}, \sqrt{\frac{\eta_T\bar{\gamma}T_0(K,\bar{\gamma},i)}{2(\bar{\gamma}+K+1)}}\right) - \left(1-\exp\left(-\frac{\eta_T\bar{\gamma}}{4}\right)\right)^{M-1} \\
\times \left\{1 - Q_1\left(\sqrt{\frac{2K\bar{\gamma}}{\bar{\gamma}+K+1}}, \sqrt{\frac{\bar{\gamma}\eta_T(K+1)}{2(\bar{\gamma}+K+1)}}\right) - (M-1)\sum_{i=0}^{M-2}\binom{M-2}{i}(-1)^i \right. \\
\times \frac{K+1}{(i+1)T_1(K,\bar{\gamma},i)} \exp\left(-\frac{K\bar{\gamma}(i+1)}{T_1(K,\bar{\gamma},i)}\right) \\
\left. \times \left[1 - Q_1\left(\sqrt{\frac{2K\bar{\gamma}(T_2(K,\bar{\gamma},i,\rho))^2}{T_1(K,\bar{\gamma},i)T_3(K,\bar{\gamma},i,\rho)}}, \sqrt{\frac{\bar{\gamma}\eta_T(1+K)T_1(K,\bar{\gamma},i)}{2T_3(K,\bar{\gamma},i,\rho)}}\right)\right]\right\}
\end{aligned}
\tag{3.58a}
$$

where

$$T_0(K,\bar{\gamma},i) = (K+1)(i+1) + i\bar{\gamma} \tag{3.58b}$$

$$T_1(K,\bar{\gamma},i) = (K+1)(i+2) + \bar{\gamma}(i+1) \tag{3.58c}$$

$$T_2(K,\bar{\gamma},i,\rho) = (K+1)(i+2) + \bar{\gamma}(i+1)(1-\rho) \tag{3.58d}$$

$$
\begin{aligned}
T_3(K,\bar{\gamma},i,\rho) &= (K+1)^2(i+2) + 2i\bar{\gamma}(K+1) \\
&+ 3\bar{\gamma}(K+1) + \bar{\gamma}^2(1-\rho^2)(1+i).
\end{aligned}
\tag{3.58e}
$$

As a check on our result, one can show that for $\rho = 0$, (3.58a) reduces to [29, eq. (17)], as expected.

Substituting (3.58a) in (3.26) and using the identity

$$\mathcal{Q}(a,b,z) \triangleq \frac{\delta}{\delta z} Q_1\left(\sqrt{a}, \sqrt{bz}\right) = -\frac{b}{2}\exp\left(-\frac{a}{2} - \frac{bz}{2}\right) I_0\left(\sqrt{abz}\right) \tag{3.59}$$

a transcendental equation whose solution is the optimum switching threshold is obtained as

$$\sum_{i=0}^{M-1} \frac{(-1)^i \binom{M-1}{i}(K+1)}{T_0(K,\bar{\gamma},i)} \exp\left(-\frac{Ki\bar{\gamma}}{T_0(K,\bar{\gamma},i)}\right)$$
$$\times \mathcal{Q}\left(\frac{2K(K+1)\bar{\gamma}}{(\bar{\gamma}+K+1)T_0(K,\bar{\gamma},i)}, \frac{\bar{\gamma}T_0(K,\bar{\gamma},i)}{2(\bar{\gamma}+K+1)}, \eta_T\right) + \frac{(M-1)\bar{\gamma}}{4}\exp\left(-\frac{\eta_T\bar{\gamma}}{4}\right)$$
$$\times \left(1-\exp\left(-\frac{\eta_T\bar{\gamma}}{4}\right)\right)^{M-2}\left\{1-Q_1\left(\sqrt{\frac{2K\bar{\gamma}}{\bar{\gamma}+K+1}}, \sqrt{\frac{\bar{\gamma}\eta_T(K+1)}{2(\bar{\gamma}+K+1)}}\right)\right.$$
$$-\sum_{i=0}^{M-2}\frac{(M-1)\binom{M-2}{i}(-1)^i(K+1)}{(i+1)T_1(K,\bar{\gamma},i)}\exp\left(-\frac{K\bar{\gamma}(i+1)}{T_1(K,\bar{\gamma},i)}\right)$$
$$\left.\times\left[1-Q_1\left(\sqrt{\frac{2K\bar{\gamma}(T_2(K,\bar{\gamma},i,\rho))^2}{T_1(K,\bar{\gamma},i)T_3(K,\bar{\gamma},i,\rho)}}, \sqrt{\frac{\bar{\gamma}\eta_T(1+K)T_1(K,\bar{\gamma},i)}{2T_3(K,\bar{\gamma},i,\rho)}}\right)\right]\right\}$$
$$+\left(1-\exp\left(-\frac{\eta_T\bar{\gamma}}{4}\right)\right)^{M-1}\left\{\frac{\bar{\gamma}(K+1)}{4(\bar{\gamma}+K+1)}\exp\left(-\frac{K\bar{\gamma}}{\bar{\gamma}+K+1}\right)\right.$$
$$\times\exp\left(-\frac{(K+1)\bar{\gamma}\eta_T}{4(\bar{\gamma}+K+1)}\right)I_0\left(\sqrt{\frac{K(K+1)\bar{\gamma}\eta_T}{(\bar{\gamma}+K+1)^2}}\right)$$
$$-(M-1)\sum_{i=0}^{M-2}\binom{M-2}{i}(-1)^i\frac{K+1}{(i+1)T_1(K,\bar{\gamma},i)}$$
$$\left.\times\exp\left(-\frac{K\bar{\gamma}(i+1)}{T_1(K,\bar{\gamma},i)}\right)F\left(\frac{2K\bar{\gamma}(T_2(K,\bar{\gamma},i,\rho))^2}{T_1(K,\bar{\gamma},i)T_3(K,\bar{\gamma},i,\rho)}, \frac{\bar{\gamma}(1+K)T_1(K,\bar{\gamma},i)}{2T_3(K,\bar{\gamma},i,\rho)}, \eta_T\right)\right\} = 0. \tag{3.60}$$

The solution to (3.60) can be obtained using the bisection method.

3.3 Numerical Examples and Discussion

In this section, we present some numerical examples. Monte Carlo simulation results are also presented to test the validity of our analytical results obtained in Sections 3.1 and 3.2.

The average BER of dual-diversity BFSK in correlated Rician fading is plotted as

a function of the normalized switching threshold in Figs. 3.5 and 3.6 for postdetection SSC Model 1 and postdetection SSC Model 2, respectively, for several values of average SNR and correlation factor. The optimum normalized switching thresholds for each average SNR and correlation factor are given in the figures. Figs. 3.5 and 3.6 show that for a fixed value of correlation as the average SNR increases the optimum switching threshold decreases. Also note that as correlation increases, and for a fixed value of average SNR, the optimum switching threshold decreases. Comparing Figs. 3.5 and 3.6 we see that the optimum switching threshold for postdetection SSC Model 1 is smaller than the optimum switching thresholds for postdetection SSC Model 2, implying that postdetection SSC Model 1 switches more often than postdetection SSC Model 2. Figs. 3.5 and 3.6 also show that the average BER changes significantly with a small change in the optimum switching threshold for large values of average SNR.

Fig. 3.7 shows the effect of modulation order, M, on the optimum switching threshold of MFSK with postdetection SSC Model 2 in correlated Rician fading for $K = 5$ and $\rho = 0.6$. Note that as the modulation order increases the optimum switching threshold decreases.

In Fig. 3.8, the performance of quaternary FSK (QFSK) with postdetection SSC Model 2 is compared to the performance of QFSK in predetection SSC for several values of fading parameter K where it can be seen that the performance gap of postdetection SSC Model 2 over predetection SSC increases as the channel becomes less faded. The effect of correlation on the performance of postdetection SSC Model 2 and predetection SSC is shown in Fig. 3.9 for QFSK. Fig. 3.9 indicates that the performance gap between postdetection SSC Model 2 and predetection SSC decreases as the correlation increases. For predetection SSC, we have used the analytical expression

given in [32] to plot the curves in Fig. 3.8

Fig. 3.10 shows the average BER of MFSK with postdetection SSC Model 2 and predetection SSC for several values of M in correlated Rician fading with $K = 5$, $\rho = 0.6$ and for several values of M. Fig. 3.10 shows that the performance gap between the two diversity receivers remains almost constant as the modulation order increases.

To compare the performances of postdetection SSC Model 1 with postdetection SSC Model 2 and predetection SSC, we have plotted in Fig. 3.11 the average BER of BFSK in correlated Rician fading for several values of correlation. Fig. 3.11 shows that the BER of postdetection SSC Model 1 is superior to the performance of postdetection SSC Model 2 and predetection SSC in all cases. Fig. 3.11 also indicates that as correlation increases the performance gap between postdetection SSC Model 1 and postdetection SSC Model 2 decreases. For example, at an average BER of 10^{-4} the SNR gap between postdetection SSC Model 1 and postdetection SSC Model 2 is 0.79 dB, 0.50 dB and .45 dB for $\rho = 0$, $\rho = 0.4$ and $\rho = 0.8$, respectively.

Finally Fig. 3.12 studies the effects of average fading power imbalance on the performance of postdetection SSC Model 1 and 2 in correlated Rayleigh fading. In Fig. 3.12 the BER of BFSK is plotted as a function of the average SNR of the first branch for several values of ρ. The average SNR on the second branch is related to the first branch as $\bar{\gamma}_2 = \bar{\gamma}_1 \exp(-\delta)$ where $\delta = 0.5$. Comparing Fig. 3.12 with Fig. 3.11 shows that the gap between postdetection SSC Model 1 and Model 2 decreases when there is average fading power imbalance between the branches.

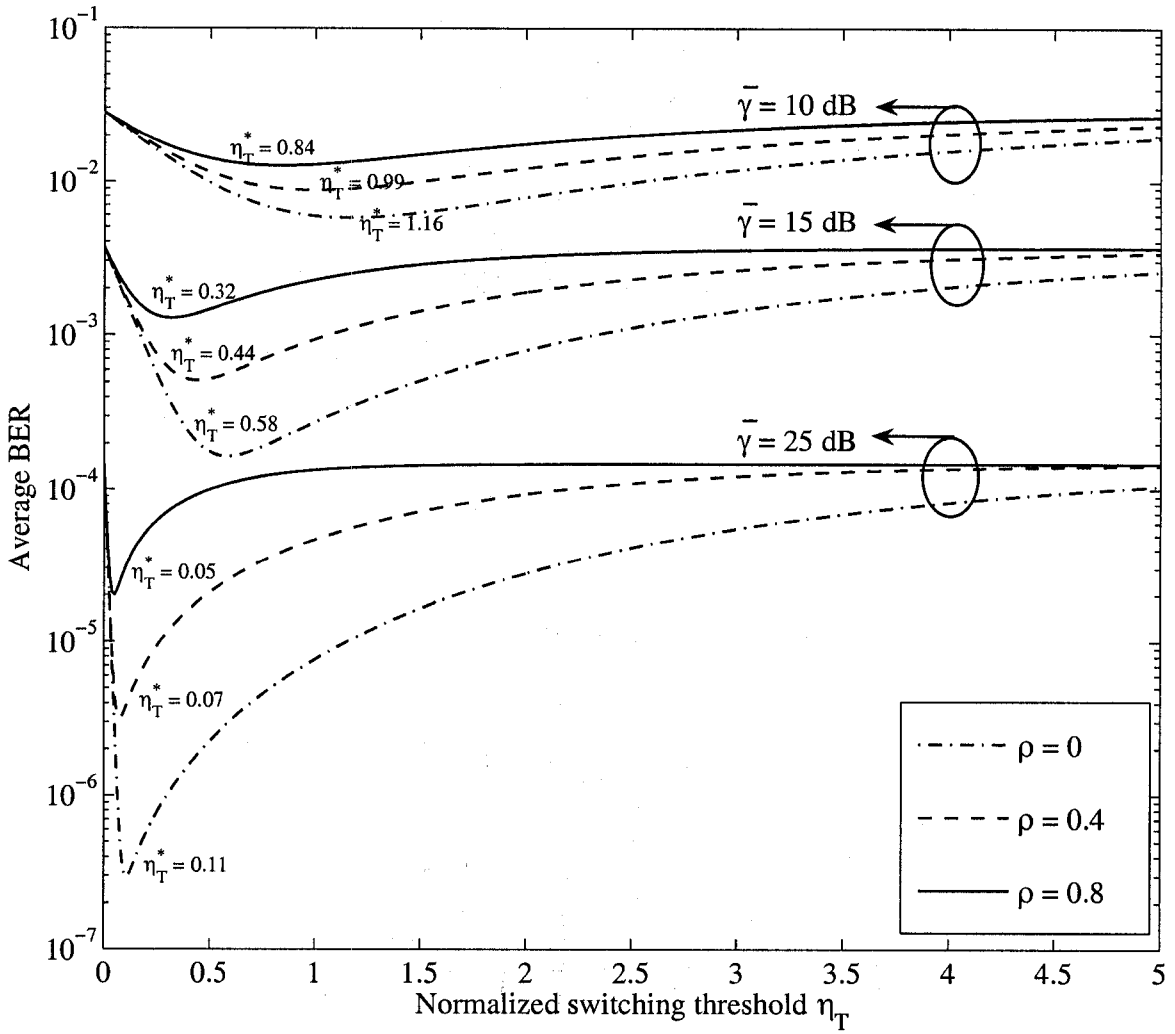

Figure 3.5: The average BER of BFSK with postdetection SSC Model 1 as a function of switching threshold in correlated Rician fading for $\bar{\gamma}$ = 10 dB, 15 dB and 25 dB and $\rho = 0, 0.4$ and 0.8.

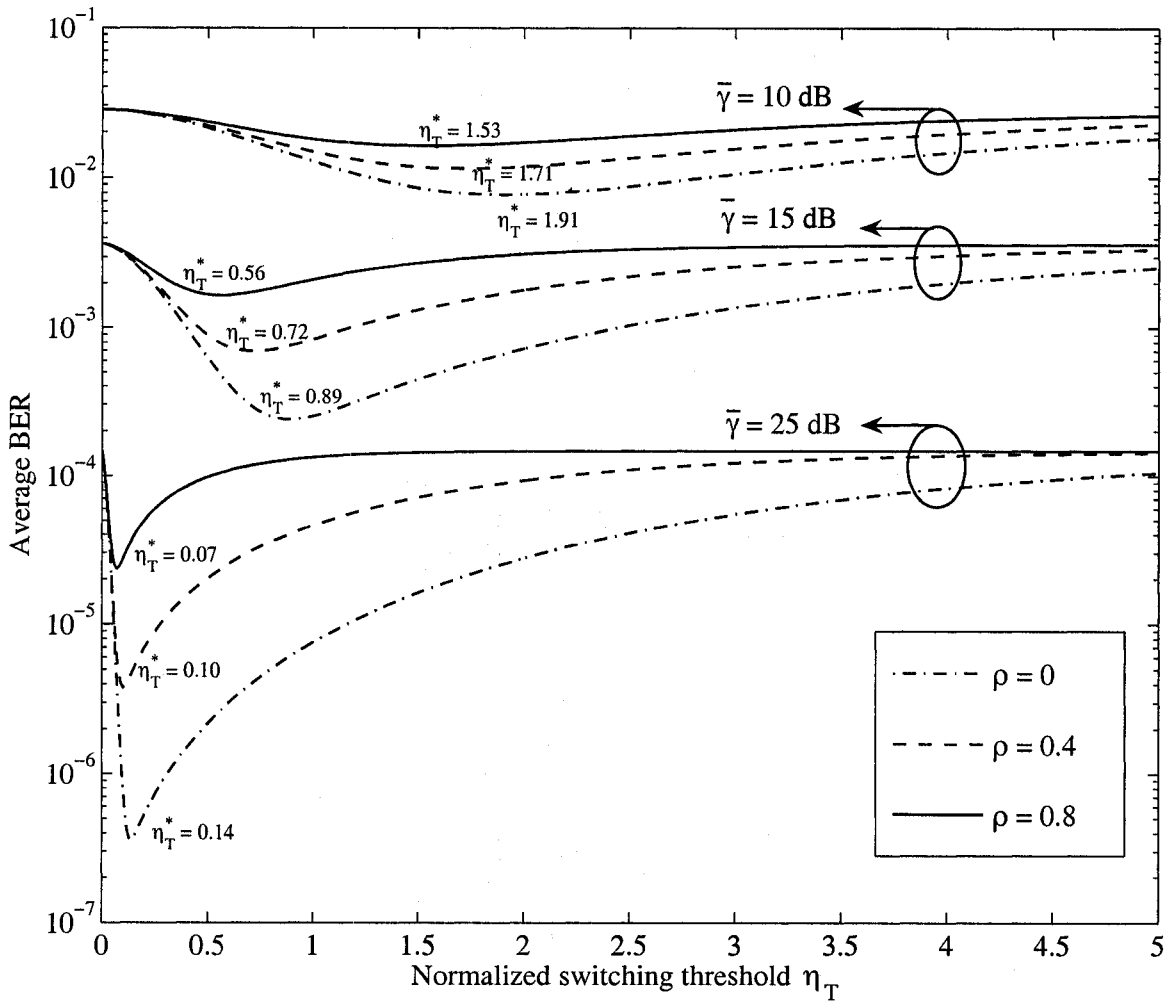

Figure 3.6: The average BER of BFSK with postdetection SSC Model 2 as a function of switching threshold in correlated Rician fading for $\bar{\gamma}$ = 10 dB, 15 dB and 25 dB and $\rho = 0, 0.4$ and 0.8.

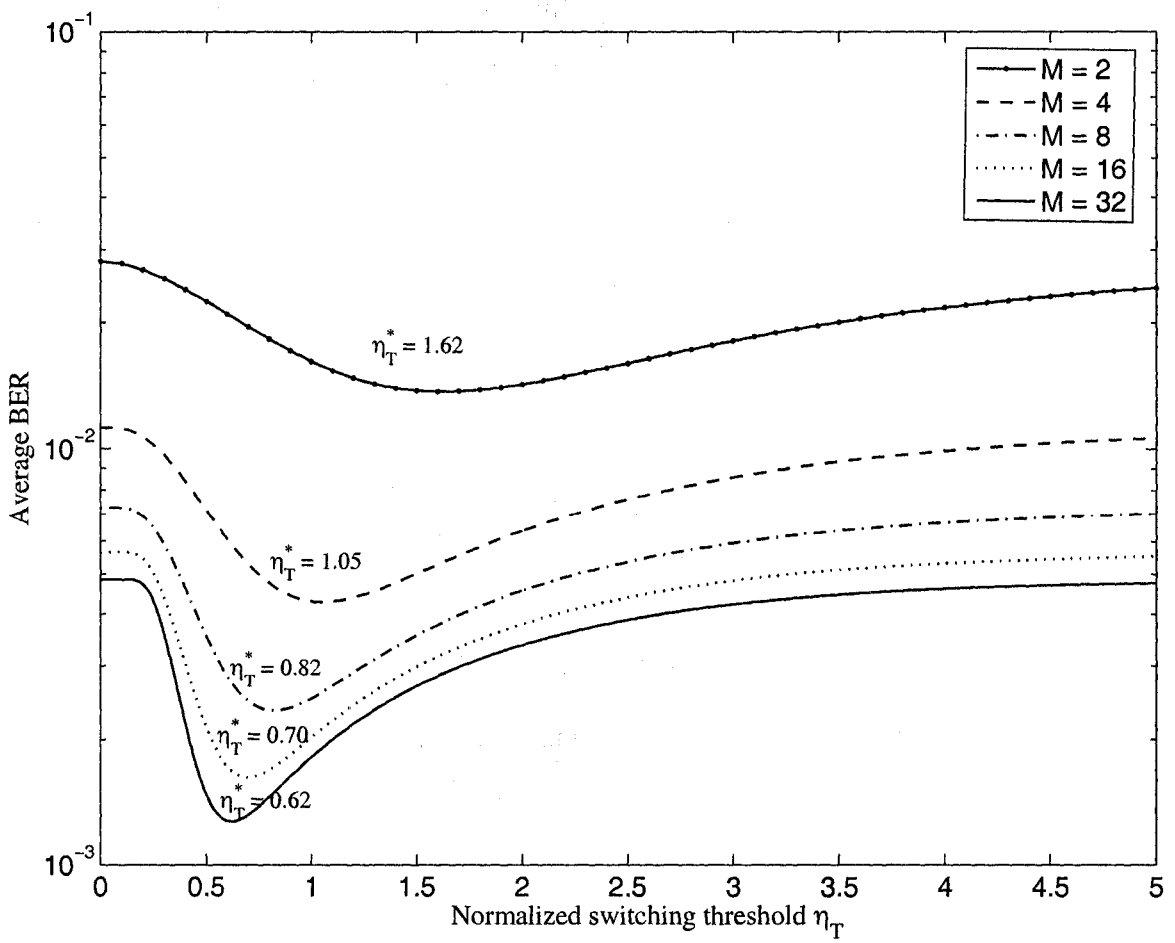

Figure 3.7: The average BER of MFSK with postdetection SSC Model 2 as a function of switching threshold in correlated Rician fading with $\rho = 0.6$ and $K = 5$ for $M = 2, 4, 8, 16$ and 32.

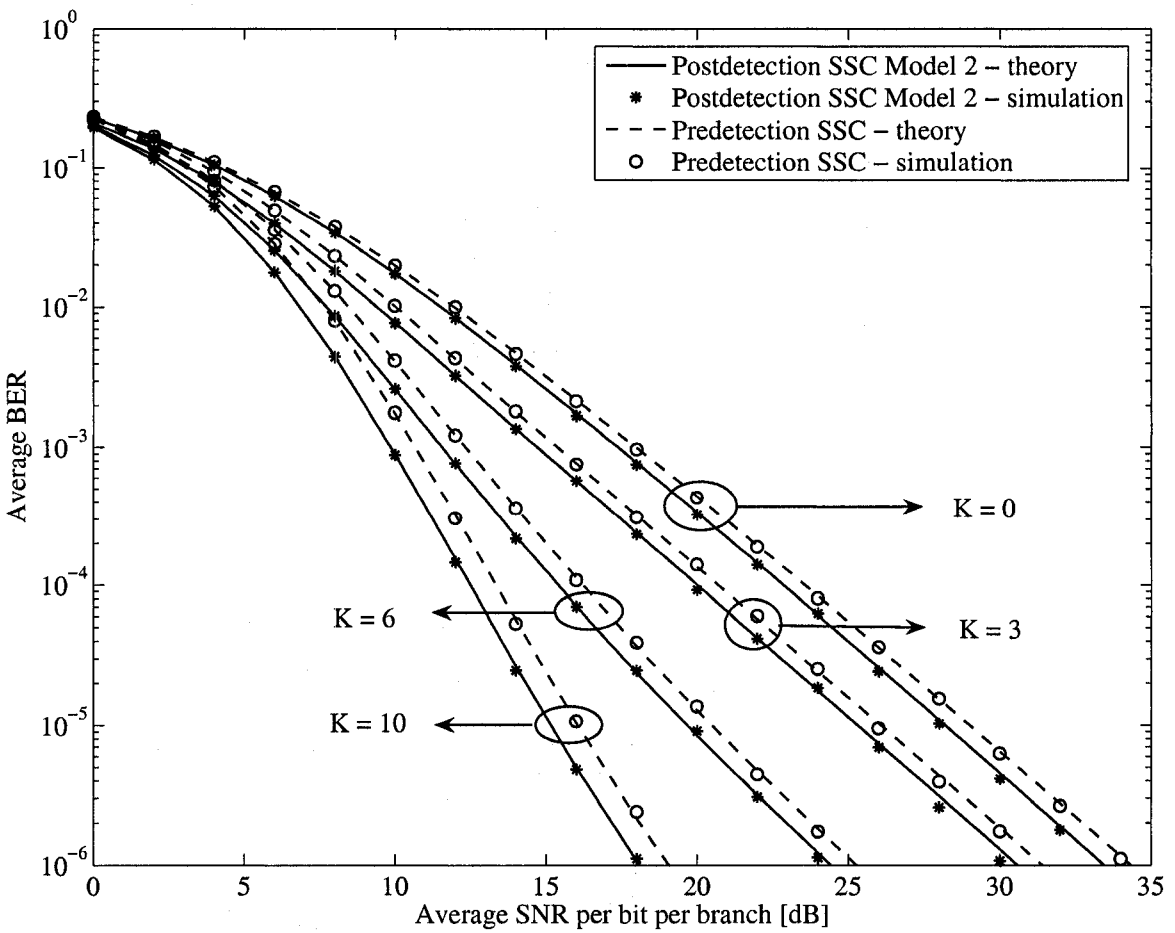

Figure 3.8: The average BER of QFSK with postdetection SSC Model 2 and predetection SSC as a function of the average SNR per bit per branch in identically distributed correlated Rician fading with $\rho = 0.5$ and $K = 0, 3, 6$ and 10.

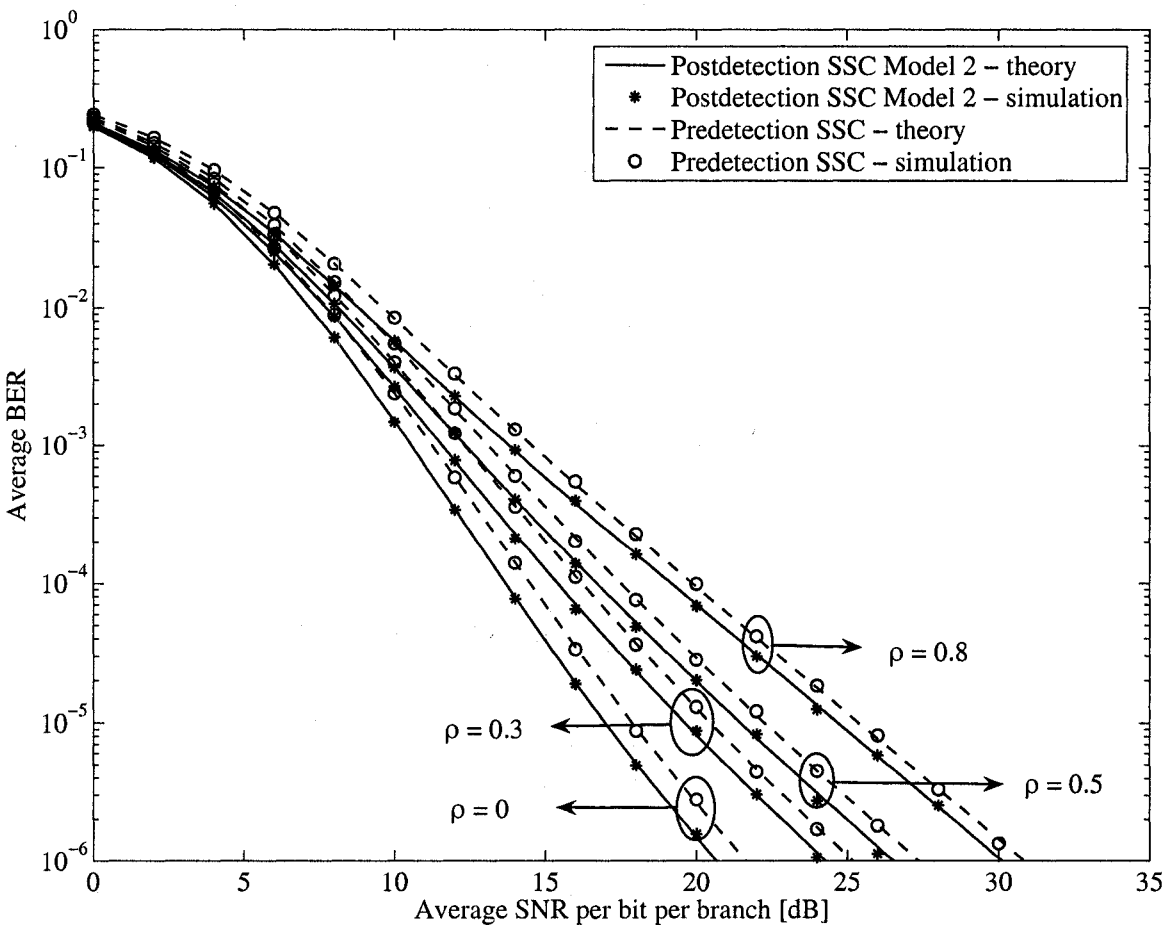

Figure 3.9: The average BER of QFSK with postdetection SSC Model 2 and predetection SSC as a function of the average SNR per bit per branch in identically distributed correlated Rician fading branches with $K = 5$ for several values of correlation $\rho = 0, 0.3, 0.5$ and 0.8.

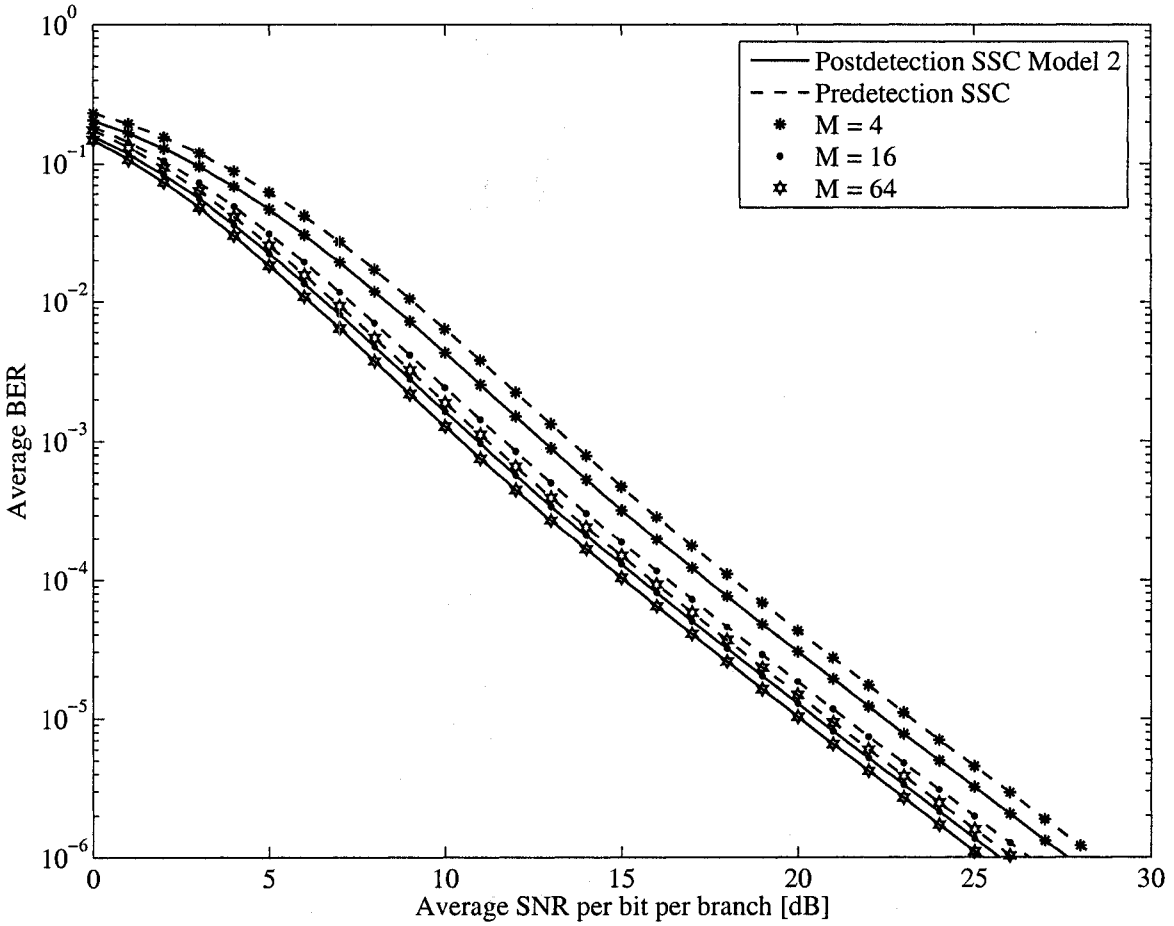

Figure 3.10: The average BER of MFSK with postdetection SSC Model 2 and predetection SSC as a function of the average SNR per bit per branch in identically distributed correlated Rician fading branches with $K = 5$ and $\rho = 0.6$ for $M = 4, 16$ and 64.

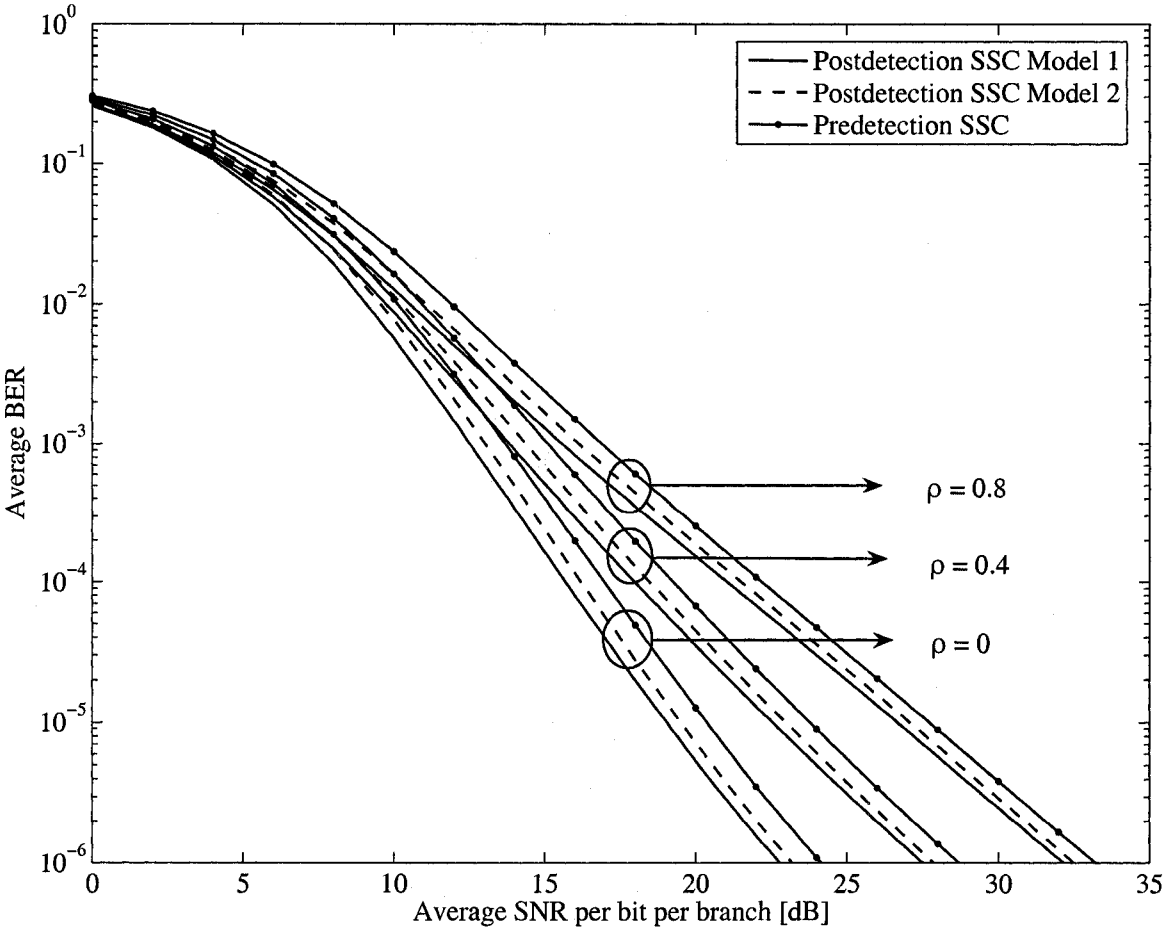

Figure 3.11: The average BER of BFSK with postdetection SSC Model 1 and 2 and predetection SSC as a function of average SNR per bit per branch in identically distributed correlated Rician fading with $K = 5$ for $\rho = 0, 0.4$ and 0.8.

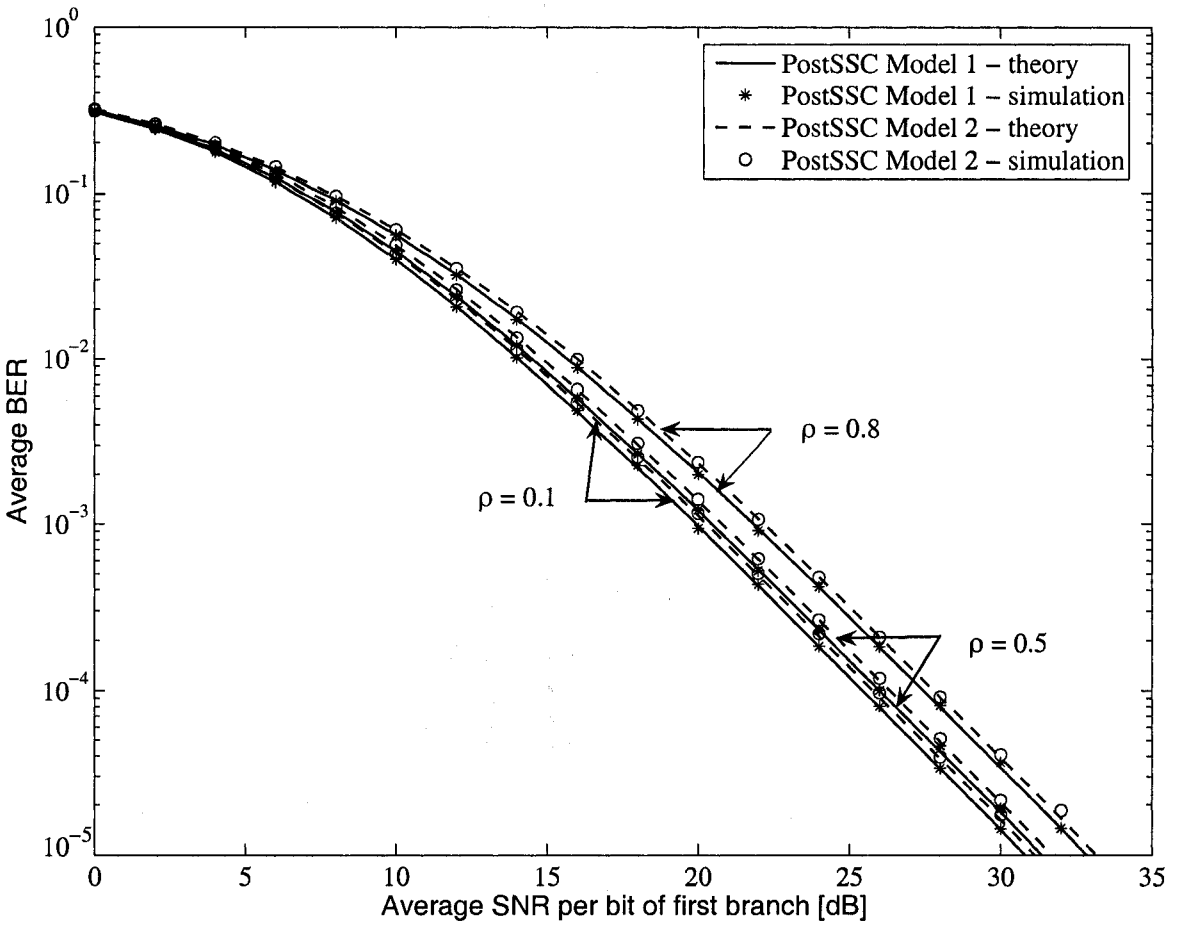

Figure 3.12: Comparison of postdetection SSC Model 1 and Model 2 in correlated Rayleigh fading with average fading power imbalance for several values of ρ.

3.4 Conclusion

In this chapter, the performances of two postdetection SSC receivers in correlated Rayleigh and Rician fading channels were studied. Closed-form expressions for the average BER of BFSK and MFSK with postdetection SSC Model 1 and Model 2 were derived. Optimum switching thresholds that minimize the probability of error were obtained. The effects of correlation, switching threshold and average fading power imbalance on the performance of postdetection SSC were examined. The performances of postdetection SSC Model 1 and Model 2 were compared with the performance of predetection SSC and it was shown that similar to the case of independent dual-diversity branches, postdetection SSC outperforms predetection SSC in correlated fading for all values of SNR. Our results indicate the the performance gain of postdetection SSC Model 1 over postdetection SSC Model 2 in Rayleigh fading decreases when the average fading power on the branches is not balanced.

Chapter 4

Performance of $S+N$ Selection Combining Receivers in Independent Nakagami and Rician Fading

In this chapter, we study the performances of $S+N$ SC receivers in independent Nakagami and Rician fading channels. Some previous studies related to $S+N$ SC employing noncoherent MFSK are as follows. In [33], the authors analyzed the performance of noncoherent MFSK with $S+N$ SC in independent and identically distributed (i.i.d) Rayleigh fading. In [7], two new $S+N$ SC models were presented and the performance of noncoherent BFSK was obtained for the case of i.i.d. Rayleigh fading channels. A comparison of various selection combining schemes for noncoherent BFSK operating on independent and non-identically distributed (i.n.d) Rayleigh fading channels was given in [34].

In this chapter, we consider two $S+N$ receiver models which we refer to as $S+N$ SC Model 1 and $S+N$ SC Model 2. We analyze the performance of noncoherent MFSK and the performance of noncoherent BFSK with L branch diversity with $S+N$ SC models 1 and 2, respectively. We assume that the diversity branches are

independent but not necessarily identically distributed (i.n.d). Analytical expressions are derived for the average BER and average SER of noncoherent MFSK in Rician and Nakagami-m fading with $S+N$ SC and classical SC in the form of single integrals with finite integration limits. Extensive Monte Carlo simulation results are presented to validate our analytical expressions.

The remainder of this chapter is organized as follows. In Section 4.1, the structure of the $S+N$ SC Model 1 is presented and the performance of noncoherent MFSK with $S+N$ SC Model 1 in i.n.d Rician, Nakagami and Rayleigh fading channels is obtained. In Section 4.2, the performance of $S+N$ SC Model 2 with noncoherent BFSK is analyzed in i.n.d fading channels. Section 4.3 reviews the performance of noncoherent MFSK with classical SC in i.n.d Rician, Nakagami and Rayleigh fading channels. Numerical examples, comparing the performances of $S+N$ SC receivers with classical SC, are presented in Section 4.4. Finally, some conclusions are given in Section 4.5.

4.1 Performance of $S+N$ SC Receiver Model 1

The receiver structure is depicted in Fig. 4.1. We assume that the fading process is slow and frequency nonselective and the diversity branches are i.n.d. Furthermore, we assume that the signals are equiprobable with the same energy E_s. An optimum receiver for each diversity reception is implemented in the format of a matched filter followed by a square-law envelope detector.

Let $X_{im}, m = 1, \cdots, M, i = 1, \cdots, L$ denote the output of the square-law detector for the mth symbol of the ith diversity branch. Assume, without loss of generality,

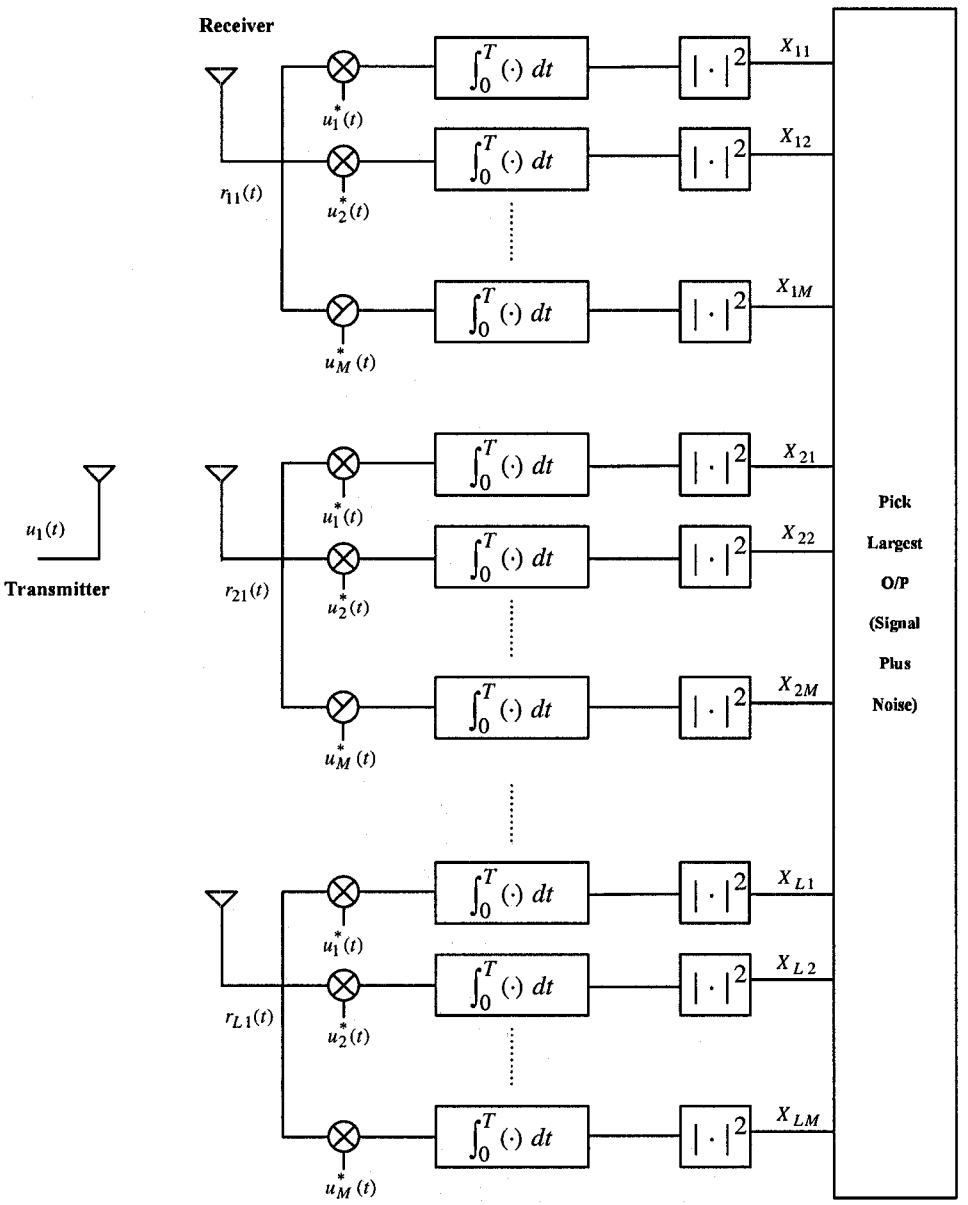

Figure 4.1: The structure of the noncoherent MFSK $S+N$ Selection Receiver Model 1.

that the first symbol in the alphabet is transmitted. Then, the outputs of the square-law combiners can be written as [33]

$$X_{i1} = |2E_s\alpha_i \exp(j\psi_i) + N_{i1}|^2 \tag{4.1}$$

$$X_{im} = |N_{im}|^2, \quad i = 1, \cdots, L, m = 2, \cdots, M \tag{4.2}$$

where $N_{im}, i = 1, \cdots, L, m = 1, \cdots, M$ are independent and identically distributed, zero-mean complex Gaussian RVs with variance $4E_sN_0$ and $\alpha_i \exp(j\psi_i), i = 1, \cdots, L$ are the complex channel gains. Then, the average SER can be written as

$$P_s = \Pr\left[\max_i\{X_{i1}\} < \max_{\substack{i,m \\ m\neq 1}}\{X_{im}\}\right] \tag{4.3a}$$

$$= L(M-1)\int_0^\infty \left(\prod_{i=1}^{L} F_{X_{i1}}(x)\right)\left(F_{X_{22}}(x)\right)^{LM-L-1} f_{X_{22}}(x)dx \tag{4.3b}$$

where $F_X(\cdot)$ and $f_X(\cdot)$ represent the cumulative distribution function (CDF) and probability density function (PDF) of the RV X, respectively. Note that to obtain (4.3b) from (4.3a), we have used the fact that the RVs $X_{im}, i = 1, \cdots, L, m = 2, \cdots, M$ are i.i.d. For noncoherent MFSK, The average BER can be computed from the average SER using [21]

$$P_b = \frac{M}{2(M-1)}P_s. \tag{4.4}$$

To proceed, we first obtain the PDF and CDF of X_{22} which are independent of the fading model. From (4.2), one notes that X_{22} is a central chi-squared RV with two degrees of freedom. Hence, its PDF and CDF is given by [35]

$$f_{X_{22}}(w) = \frac{1}{4E_sN_0}\exp\left(-\frac{w}{4E_sN_0}\right) \tag{4.5}$$

and

$$F_{X_{22}}(w) = 1 - \exp\left(-\frac{w}{4E_sN_0}\right) \tag{4.6}$$

respectively. To obtain the PDF and CDF of $X_{i1}, i = 1, \cdots, L$ we consider two fading scenarios: Rician and Nakagami-m fading. Rayleigh fading is considered also as a special case of either Rician or Nakagami-m fading scenarios.

4.1.1 Rician Fading

In this case $\alpha_i \exp(j\psi_i)$ can be written as [4]

$$\alpha_i \exp(j\psi_i) = Z_{i1} + jZ_{i2}, \quad i = 1, \cdots, L \tag{4.7}$$

where Z_{i1} and Z_{i2} are Gaussian RVs with means m_{i1} and m_{i2} and variance σ_i^2, respectively. The Rice factor K_i can be written in terms of m_{i1}, m_{i2} and $\sigma_{Z_i}^2$ as [4]

$$K_i = \frac{m_{i1}^2 + m_{i2}^2}{2\sigma_{Z_i}^2}. \tag{4.8}$$

Next, we obtain the CDF of $X_{i1}, i = 1, \cdots, N$. Substituting (4.7) in (4.1), we obtain

$$X_{i1} = |2E_s Z_{i1} + N_{i1}^I|^2 + |2E_s Z_{i2} + N_{i2}^Q|^2 \tag{4.9}$$

where N_{i1}^I and N_{i2}^Q are independent zero-mean Gaussian RVs with variance $2E_sN_0$. From (4.9), one can see that $X_{i1}, i = 1, \cdots, L$ are non-central chi-squared RVs with non-centrality parameters s_i^2 and variance σ_i^2 given by

$$s_i^2 = \frac{4E_sN_0K_i\bar{\gamma}_i}{K_i + 1} \tag{4.10}$$

$$\sigma_i^2 = 2E_sN_0\frac{\bar{\gamma}_i + K_i + 1}{K_i + 1} \tag{4.11}$$

where $\bar{\gamma}_i$ is the average signal-to-noise ratio (SNR) on the ith diversity branch. Therefore, the CDF of X_{i1} can be written as

$$F_{X_{i1}}(x) = 1 - Q_1\left(\sqrt{P_1(K_i, \bar{\gamma}_i)}, \sqrt{\frac{P_2(K_i, \bar{\gamma}_i)x}{4E_sN_0}}\right), \quad i = 1, \cdots, N \tag{4.12a}$$

where

$$P_1(K_i, \bar{\gamma}_i) = \frac{2K_i\bar{\gamma}_i}{\bar{\gamma}_i + K_i + 1} \tag{4.12b}$$

$$P_2(K, \bar{\gamma}_i) = \frac{2(K_i+1)}{(\bar{\gamma}_i + K_i + 1)}. \tag{4.12c}$$

Substituting (4.5), (4.6) and (4.12) in (4.3) and making the change of variable $y = x/(4E_sN_0)$, we obtain

$$\begin{aligned} P_e = L(M-1)\int_0^{\infty} \left[\prod_{i=1}^{L}\left\{1 - Q_1\left(\sqrt{P_1(K_i,\bar{\gamma}_i)}, \sqrt{P_2(K_i,\bar{\gamma}_i)y}\right)\right\}\right] \\ \times (1-\exp(-y))^{LM-L-1}\exp(-y)dy. \end{aligned} \tag{4.13}$$

For numerical calculations it is desirable to transform the integral in (4.13) into an integral with a finite range of integration. This is accomplished by making the change of variable $y = \tan(\theta)$ in (4.13). Thus, we obtain the average SER of noncoherent MFSK with $S+N$ selection combining as

$$\begin{aligned} P_e = L(M-1)\int_0^{\frac{\pi}{2}} \left[\prod_{i=1}^{L}\left\{1 - Q_1\left(\sqrt{P_1(K_i,\bar{\gamma}_i)}, \sqrt{P_2(K_i,\bar{\gamma}_i)\tan(\theta)}\right)\right\}\right] \\ \times [1-\exp(-\tan(\theta))]^{LM-L-1}\exp(-\tan(\theta))\sec^2(\theta)d\theta. \end{aligned} \tag{4.14}$$

For i.i.d Rician fading $K_1 = \cdots = K_L = K$, $\bar{\gamma}_1 = \cdots = \bar{\gamma}_L = \bar{\gamma}$ and (4.14) reduces to

$$\begin{aligned} P_e = L(M-1)\int_0^{\frac{\pi}{2}} \left[\left\{1 - Q_1\left(\sqrt{P_1(K,\bar{\gamma})}, \sqrt{P_2(K,\bar{\gamma})\tan(\theta)}\right)\right\}\right]^L \\ \times [1-\exp(-\tan(\theta))]^{LM-L-1}\exp(-\tan(\theta))\sec^2(\theta)d\theta. \end{aligned} \tag{4.15}$$

4.1.2 Nakagami-m Fading

To obtain the CDF of $X_{i1}, i = 1, \cdots, L$, we first write it as

$$\begin{aligned} X_{i1} &= |2E_s\alpha_i e^{j\theta_i} + N_{i1}|^2 \\ &= |2E_s\alpha_i + e^{-j\theta_i}N_{i1}|^2|e^{j\theta_i}|^2 \\ &= |2E_s\alpha_i + N_i|^2 \\ &= |2E_s\alpha_i + N_i^I|^2 + |N_i^Q|^2 \end{aligned} \tag{4.16}$$

where $N_i = e^{-j\theta_i} N_{i1}$ and the fixed phase term $e^{-j\theta_i}$ is absorbed in the noise term N_{i1} without changing its statistics [21, p. 292] to yield N_i. Under the static channel condition, X_{i1} is a non-central chi-squared RV with two degrees of freedom and its CDF is given by

$$F_{X_{i1}|\alpha_i,\theta_i}(x) = 1 - Q_1\left(\frac{2E_s\alpha_i}{\sigma}, \frac{\sqrt{x}}{\sigma}\right) \tag{4.17}$$

where $\sigma = \sqrt{2E_sN_0}$.

To obtain the unconditional CDF of X_{i1}, we average $F_{X_{i1}|\alpha_i,\theta_i}(w)$ over the joint pdf of (α_i, θ_i) to get

$$\begin{aligned} F_{X_{i1}}(x) &= \int_{\alpha_i=0}^{\infty}\int_{\theta_i=0}^{2\pi} F_{X_{i1}|\alpha_i,\theta_i}(x) f(\alpha_i,\theta_i) d\alpha_i d\theta_i & \text{(4.18a)} \\ &= \int_{\alpha_i=0}^{\infty}\left(1 - Q_1\left(\frac{2E_s\alpha_i}{\sigma}, \frac{\sqrt{x}}{\sigma}\right)\right)\left\{\int_{\theta_i=0}^{2\pi} f(\alpha_i,\theta_i)d\theta_i\right\} d\alpha_i & \text{(4.18b)} \\ &= \int_{\alpha_i=0}^{\infty}\left(1 - Q_1\left(\frac{2E_s\alpha_i}{\sigma}, \frac{\sqrt{x}}{\sigma}\right)\right) f(\alpha_i) d\alpha_i. & \text{(4.18c)} \end{aligned}$$

Note that in obtaining (4.18c) no assumption is made about the phase of the Nakagami-m distribution. In a Nakagami-m fading environment, the marginal PDF of α_i is given by [12, eqn. (2.20)]

$$p_{\alpha_i}(\alpha_i) = \frac{2\alpha_i^{2m_i-1}}{\Gamma(m_i)}\left(\frac{m_i}{\Omega_i}\right)^{m_i} \exp\left(-\frac{m_i\alpha_i^2}{\Omega_i}\right) \tag{4.19}$$

where m_i is the fading parameter on the ith channel and $\Omega_i = E[\alpha_i^2]$.

Substituting (4.19) in (4.18c) and using [36, eq. (9)], and after some mathematical simplifications, we obtain the unconditional CDF of X_{i1} as

$$\begin{aligned} F_{X_{i1}}(x) = 1 &- \frac{\bar{\gamma}_i}{m_i+\bar{\gamma}_i}\exp\left(-\frac{x}{2\sigma^2}\frac{m_i}{m_i+\bar{\gamma}_i}\right) \\ &\times \sum_{k=0}^{m_i-1}\epsilon_k(m_i,\bar{\gamma}_i)\left(\frac{m_i}{m_i+\bar{\gamma}_i}\right)^k L_k\left(-\frac{x}{2\sigma^2}\frac{\bar{\gamma}_i}{m_i+\bar{\gamma}_i}\right) \end{aligned} \tag{4.20a}$$

where $L_k(\cdot)$ is the Laguerre polynomial defined as [19, eq. (8.970.1)]

$$L_k(x) = \sum_{l=0}^{k}(-1)^l\binom{k}{k-l}\frac{x^l}{l!} \tag{4.20b}$$

and $\epsilon_k(m_i, \bar{\gamma}_i)$ is given by

$$\epsilon_k(m_i, \bar{\gamma}_i) = \begin{cases} 1, & k < m_i - 1 \\ \dfrac{m_i + \bar{\gamma}_i}{\bar{\gamma}_i}, & k = m_i - 1 \end{cases} . \tag{4.20c}$$

For notational simplicity we define $C_{k,l}$ as

$$C_{k,l}(m_i, \bar{\gamma}_i) = \frac{\epsilon_k(m_i, \bar{\gamma}_i)}{l!} \binom{k}{k-l} \left(\frac{\bar{\gamma}_i}{m_i + \bar{\gamma}_i}\right)^{l+1} \left(\frac{m_i}{m_i + \bar{\gamma}_i}\right)^{k} \tag{4.21}$$

and we rewrite $F_{X_{i1}}(x)$ in (4.20a) as

$$F_{X_{i1}}(x) = 1 - \exp\left(-\frac{x}{2\sigma^2}\frac{m_i}{m_i + \bar{\gamma}_i}\right) \sum_{k=0}^{m_i-1} \sum_{l=0}^{k} C_{k,l}(m_i, \bar{\gamma}_i) \left(\frac{x}{2\sigma^2}\right)^{l} \tag{4.22}$$

where we have replaced the Laguerre polynomial with its definition given in (4.20b).

The average SER of noncoherent MFSK with $S + N$ SC receiver Model 1 in Nakagami-m fading can now be computed by substituting (4.5), (4.6) and (4.20) in (4.3). The result is

$$P_s(E) = L(M-1) \int_0^{\infty} \prod_{i=1}^{L} \left(1 - \exp\left(-\frac{m_i}{m_i + \bar{\gamma}_i} x\right) \sum_{k=0}^{m_i-1} \sum_{l=0}^{k} C_{k,l_i}(m_i, \bar{\gamma}_i) (x)^{l}\right) \times (1 - \exp(-x))^{L} \exp(-x) dx. \tag{4.23}$$

For i.i.d Nakagami-m fadings, using the binomial theorem and after some mathematical manipulation and integral evaluations, the integral in (4.23) reduces to a closed-form expression as

$$P_s(E) = L(M-1) \sum_{v=0}^{LM-L-1} \sum_{n=0}^{L} (-1)^{v+n} \binom{ML-L-1}{v} \binom{L}{n} \exp\left(-\left(\frac{nm}{m+\bar{\gamma}} + 1 + v\right)\right) \times \sum_{\underline{k}^L=\underline{0}^L}^{\underline{m-1}^L} \sum_{\underline{l}^L=\underline{0}^L}^{\underline{k}^L} \left\{\prod_{p=1}^{n} C_{k_p,l_p}\right\} \frac{\left(\sum_{p=1}^{n} l_p\right)!}{\left(\frac{nm}{m+\bar{\gamma}} + 1 + v\right)^{1+\sum_{p=1}^{n} l_p}} \tag{4.24}$$

where $\underline{C}^L$ is a constant vector of dimension L with each element being C and we define the summation $\sum_{\underline{\kappa}^L=\underline{\eta}^L}^{\underline{\nu}^L}$ as

$$\sum_{\underline{\kappa}^L=\underline{\eta}^L}^{\underline{\nu}^L} \triangleq \sum_{\kappa_1=\eta_1}^{\nu_1} \sum_{\kappa_2=\eta_2}^{\nu_2} \cdots \sum_{\kappa_N=\eta_L}^{\nu_L}. \tag{4.25}$$

4.1.3 Rayleigh Fading

For Rayleigh fading it can be shown that setting $K_i = 0, i = 1, \cdots, L$ in (4.14) and setting $m_i = 1, i = 1, \cdots, L$ in (4.23), and after some mathematical simplifications we obtain a closed-form expression for the average SER of noncoherent MFSK with $S + N$ SC model 1. The result is

$$\begin{aligned} P_e = J \sum_{j=0}^{J} \binom{J-1}{j} (-1)^j \Bigg\{ & \frac{1}{J-j} - \sum_{i_1=1}^{L} \frac{1}{J-j+c_{i_1}} \\ & + \sum_{i_1,i_2=1}^{L} \frac{1}{J-j+c_{i_1}+c_{i_2}} + \cdots + (-1)^L \frac{1}{J-j+\sum_{i=1}^{N} c_i} \Bigg\} \end{aligned} \tag{4.26}$$

where $c_i = \frac{1}{1+\bar{\gamma}_i}$ and $J = LM - L - 1$. For the case of noncoherent BFSK (4.26) reduces to [34, eq. (21)] as expected.

For i.i.d Rayleigh fading, one can show that (4.15) reduces to

$$P_e = \sum_{n=0}^{L} (-1)^n \binom{L}{n} \prod_{l=1}^{L(M-1)} \frac{l}{l + n/(1+\bar{\gamma})} \tag{4.27}$$

which is equal to [33, eq. (11)], as expected.

4.2 Performance of $S + N$ SC Receiver Model 2

In this section, we derive the BER of binary orthogonal signaling with $S+N$ SC Model 2. The receiver structure is depicted in Fig. 4.2 (after [7, Fig. 3]). Notice that this receiver structure is limited to binary signaling and therefore, in this section we only

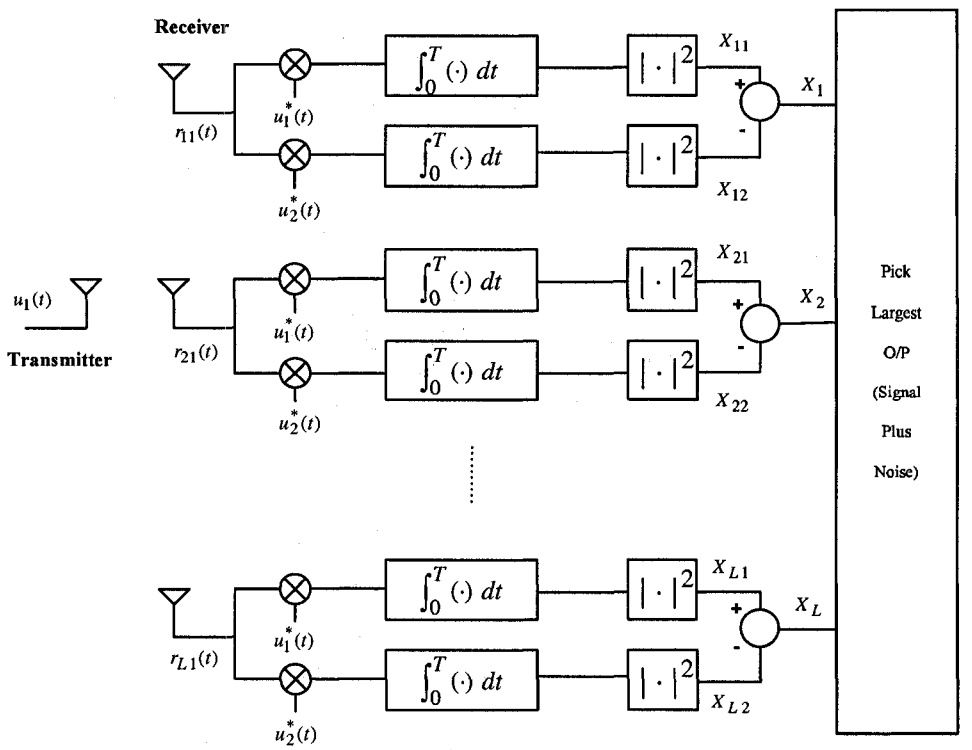

Figure 4.2: The structure of the noncoherent BFSK $S + N$ Selection Receiver Model 2 (after [7, Fig. 3]).

consider noncoherent BFSK. The receiver bases its decision on the RVs $X_i = X_{i1} - X_{i2}$ where X_{i1} and X_{i2} are expressed as

$$X_{i1} = |2E_b\alpha_i \exp(j\psi_i) + N_{i1}|^2 \tag{4.28}$$

$$X_{i2} = |N_{i2}|^2, \quad i = 1, \cdots, N, \tag{4.29}$$

where E_b denotes energy per transmitted bit, $\alpha_i \exp(j\psi_i)$ is the complex channel gain and N_{i1} and N_{i2} are zero-mean complex Gaussian RVs with variance $\sigma^2 = 2E_bN_0$ per dimension.

Assuming that $u_1(t)$, corresponding to a "1" bit, is transmitted, an error occurs if from the L statistics $X_j = X_{j1} - X_{j2}$, the one with the largest magnitude is negative. Mathematically, the BER can be written as

$$P_e = \sum_{i=1}^{L} \Pr\left(\max_{j\neq i} |X_j| < |X_i|, X_i < 0\right). \tag{4.30}$$

To proceed, we write (4.30) as

$$\begin{aligned} P_e &= \sum_{i=1}^{L} \Pr\left(\max_{j\neq i} |X_i| + X_i < 0\right) \\ &= \sum_{i=1}^{L} \int_0^\infty f_{X_i}(-x) \prod_{\substack{j=1 \\ j\neq i}}^{L} \left(F_{X_j}(x) - F_{X_j}(-x)\right) dx. \end{aligned} \tag{4.31}$$

For i.i.d fading, (4.31) reduces to

$$P_e = L \int_0^\infty f_{X_1}(-x) \left(F_{X_1}(x) - F_{X_1}(-x)\right)^{L-1} dx. \tag{4.32}$$

Note that (4.32) is equal to [7, eq. (8)], as expected. Eqs. (4.31) and (4.32) show that we need to compute the CDF and PDF of X_i to compute the BER. These are computed in the following subsections for Rician, Nakagami-m and Rayleigh fading channels.

4.2.1 Rician Fading

In this case, the RV X_i is the difference between a non-central chi-squared and a central chi-squared RV. In [13], an expression is obtained for the CDF of the difference of a non-central and a central chi-squared RV. Using [13, eq. (51)], we obtain the CDF of X_i as

$$F_{X_i}(x) = \begin{cases} Y_1(K_i, \bar{\gamma}_i) \exp\left(\dfrac{x}{4E_bN_0}\right), & x < 0 \\ 1 - Q_1\left(\sqrt{P_1(K_i, \bar{\gamma}_i)}, \sqrt{\dfrac{P_2(K_i, \bar{\gamma}_i)x}{4E_bN_0}}\right) & \\ +Y_1(K_i, \bar{\gamma}_i) \exp\left(\dfrac{x}{4E_bN_0}\right) Q_1\left(\sqrt{Y_2(K_i, \bar{\gamma}_i)}, \sqrt{\dfrac{Y_3(K_i, \bar{\gamma}_i)x}{4E_bN_0}}\right), & x > 0 \end{cases} \tag{4.33a}$$

where

$$Y_1(K, \bar{\gamma}) = \frac{K+1}{2K+2+\bar{\gamma}} \exp\left(-\frac{\bar{\gamma}K}{2K+2+\bar{\gamma}}\right) \tag{4.33b}$$

$$Y_2(K, \bar{\gamma}) = \frac{2\bar{\gamma}K(K+1)}{(\bar{\gamma}+K+1)(\bar{\gamma}+2+2K)} \tag{4.33c}$$

$$Y_3(K, \bar{\gamma}) = \frac{2(\bar{\gamma}+2+2K)}{\bar{\gamma}+K+1}. \tag{4.33d}$$

The PDF of X_i is computed from its CDF as

$$f_{X_i}(x) = \frac{1}{4E_bN_0} Y_1(K_i, \bar{\gamma}_i) \exp\left(\frac{x}{4E_bN_0}\right), \quad x < 0. \tag{4.34}$$

Note that to compute the BER, eq. (4.31) shows that one only needs the PDF of $f_{X_i}(x)$ for negative arguments. Therefore, $f_{X_i}(x)$ is only given for $x < 0$ in (4.34). Substituting (4.33a) and (4.34) in (4.31) and making a simple change of variable, we obtain the BER of noncoherent BFSK with $S+N$ selection Model 2 in Rician fading

as a single integral with finite integration range as

$$P_e = \sum_{i=1}^{L} Y_1(K_i, \bar{\gamma}_i) \int_0^{\frac{\pi}{2}} e^{-\tan(x)} \prod_{\substack{j=1 \\ j \neq i}}^{L} \Bigg\{ 1 - Y_1(K_j, \bar{\gamma}_j) e^{-\tan(x)} \\ - Q_1\left(\sqrt{P_1(K_j, \bar{\gamma}_j)}, \sqrt{P_2(K_j, \bar{\gamma}_j)\tan(x)}\right) \\ + Y_1(K_j, \bar{\gamma}_j) e^{\tan(x)} Q_1\left(\sqrt{Y_2(K_j, \bar{\gamma}_j)}, \sqrt{Y_3(K_j, \bar{\gamma}_j)\tan(x)}\right) \Bigg\} \sec^2(x) dx. \tag{4.35}$$

For i.i.d Rician fading, (4.35) can be simplified as

$$P_e = L Y_1(K, \bar{\gamma}) \int_0^{\frac{\pi}{2}} \exp(-\tan(x)) \\ \times \left(1 - Y_1(K, \bar{\gamma}) e^{-\tan(x)} - Q_1\left(\sqrt{P_1(K, \bar{\gamma})}, \sqrt{P_2(K, \bar{\gamma})\tan(x)}\right) \right. \\ \left. + Y_1(K, \bar{\gamma}) \exp(\tan(x)) Q_1\left(\sqrt{Y_2(K, \bar{\gamma})}, \sqrt{Y_3(K, \bar{\gamma})\tan(x)}\right)\right)^{L-1} \sec^2(x) dx. \tag{4.36}$$

For dual-branch diversity (4.35) reduces to a closed-form expression, namely

$$P_e = \sum_{i=1}^{2} Y_1(K_{\bar{i}}, \bar{\gamma}_{\bar{i}}) \Bigg\{ 1 - f_1\Big(P_1(K_i, \bar{\gamma}_i), P_2(K_i, \bar{\gamma}_i), 1\Big) \\ + Y_1(K_i, \bar{\gamma}_i) f_2\Big(Y_2(K_i, \bar{\gamma}_i), Y_3(K_i, \bar{\gamma}_i)\Big) - \frac{Y_1(K_i, \bar{\gamma}_i)}{2} \Bigg\} \tag{4.37a}$$

where $f_1(a, b, c)$ and $f_2(a, b)$ are defined as

$$f_1(a, b, c) = \int_0^{\infty} Q_1(\sqrt{a}, \sqrt{bx}) \exp(-cx) dx \\ = \frac{2c + b - b \exp\left(-\dfrac{ac}{2c+b}\right)}{c(2c+b)} \quad a, b, c > 0 \tag{4.37b}$$

$$f_2(a, b) = \int_0^{\infty} Q_1\left(\sqrt{a}, \sqrt{bx}\right) dx = \frac{2 + a}{b}, \quad a, b > 0 \tag{4.37c}$$

and where $\bar{i}$ denotes the 2's complement of i, i.e., if $i = 1$ then $\bar{i} = 2$ and vice versa. The proof of the integral identities in (4.37b) and (4.37c) is given in [37].

4.2.2 Nakagami-m Fading

In this case, it is shown in [38] that the CDF of X_i is given by

$$F_{X_i}(x) = \begin{cases} 1 - \sum_{k=0}^{m_i-1} \sum_{l=0}^{k} D_{k,l}(m_i, \bar{\gamma}_i) \exp\left(\frac{x}{2\sigma^2}\right) \\ \times \Gamma\left(l+1, \left(\frac{m_i}{m_i+\bar{\gamma}_i}+1\right)\frac{x}{2\sigma^2}\right), & x > 0 \\ \exp\left(\frac{x}{2\sigma^2}\right) C(m_i, \bar{\gamma}_i), & x < 0 \end{cases} \tag{4.38a}$$

where $\Gamma(\cdot,\cdot)$ is the incomplete Gamma function defined as [19, eq. (8.352.2)]

$$\Gamma(n+1, z) = n! \exp(-z) \sum_{k=0}^{n} \frac{z^k}{k!}, \quad n \in \mathbb{N} \tag{4.38b}$$

and where for notational simplicity we have defined D_{k_i,l_i} and $C(m, \bar{\gamma})$ as

$$D_{k,l}(m_i, \bar{\gamma}_i) = \frac{C_{k,l}(m_i, \bar{\gamma}_i)}{\left(1 + \frac{m_i}{m_i+\bar{\gamma}_i}\right)^{l_i+1}} \tag{4.38c}$$

$$C(m_i, \bar{\gamma}) = 1 - \sum_{k=0}^{m_i-1} \sum_{l=0}^{k} D_{k,l}(m_i, \bar{\gamma}_i)\Gamma(l+1) \tag{4.38d}$$

where $\Gamma(n) = \Gamma(n, 0)$.

From the CDF of X_i, we derive the PDF of X_i by differentiation. The result is

$$f_{X_i}(x) = \frac{1}{2\sigma^2} \exp\left(\frac{x}{2\sigma^2}\right) C(m_i, \bar{\gamma}_i), \quad x < 0. \tag{4.39}$$

The PDF in (4.39) is given for $x < 0$, as we only need the pdf for negative arguments for the calculation of the BER in (4.31) and (4.32). Now substituting (4.38) and (4.39) in (4.31), we obtain the BER of noncoherent BFSK with $S+N$ SC receiver Model 2 in Nakagami-m fading as

$$\begin{aligned} P_b = \sum_{i=1}^{L} C(m_i, \bar{\gamma}_i) \int_0^{\infty} \exp(-x) \prod_{\substack{j=1 \\ j\neq i}}^{L} \Big[1 - \sum_{k=0}^{m-1} \sum_{l=0}^{k} D_{k,l}(m_j, \bar{\gamma}_j) \\ \times \exp(x)\Gamma\left(l+1, \left(\frac{m_j}{m_j+\bar{\gamma}_j}+1\right)x\right) - C(m_j, \bar{\gamma}_j)\exp(-x)\Big] dx. \end{aligned} \tag{4.40}$$

For i.i.d Nakagami-m fading the BER becomes

$$P_b = LC(m,\bar{\gamma}) \int_0^{\infty} \exp(-x) \Big[1 - \sum_{k=0}^{m-1} \sum_{l=0}^{k} D_{k,l}(m,\bar{\gamma}) \times \exp(x) \Gamma\left(l+1, \left(\frac{m}{m+\bar{\gamma}}+1\right)x\right) - C(m,\bar{\gamma})\exp(-x) \Big]^{L-1} dx. \tag{4.41}$$

4.2.3 Rayleigh Fading

For i.n.d Rayleigh fading, setting $K_i = 0, i = 1, \cdots, L$ in (4.35) and $m_i = 1, i = 1, \cdots, L$ in (4.40), we obtain the BER of noncoherent BFSK with i.n.d Rayleigh fading as

$$P_e = \sum_{i=1}^{L} \frac{1}{2+\bar{\gamma}_i} \int_0^{\infty} \exp(-x) \prod_{\substack{j=1 \\ j\neq i}}^{L} \left[1 - \frac{\exp(-x) + \exp\left(-\frac{x}{1+\bar{\gamma}_j}\right)(3+\bar{\gamma}_j)}{2+\bar{\gamma}_j} \right] dx. \tag{4.42}$$

Note that the expression given in (4.42) is simpler to compute than the expression given in [34, eq. (22)] for the BER of $S+N$ SC receiver Model 2 in i.n.d Rayleigh fading. Notice that for a given N, (4.42) reduces to a closed-form expression. For example, for the important case of dual-branch diversity, (4.42) reduces to

$$P_e = \frac{8 + 5\bar{\gamma}_1 + 5\bar{\gamma}_2 + 3\bar{\gamma}_1\bar{\gamma}_2}{(2+\bar{\gamma}_1)^2(2+\bar{\gamma}_2)^2} \tag{4.43}$$

which is equal to [39, eq. (12)] and [34, eq. (22)], as expected.

For i.i.d Rayleigh fading, one can show that (4.41) reduces to

$$P_e = L \sum_{n=0}^{L-1} \binom{L-1}{n} \frac{(-1)^n}{(\bar{\gamma}+2)^{n+1}} \sum_{i=0}^{n} \binom{n}{i} \frac{(\bar{\gamma}+1)^{i+1}}{\bar{\gamma}(n-i+1)+n+1} \tag{4.44}$$

which is equal to [7, eq. (9)], as expected.

4.3 Performance Analysis of noncoherent MFSK with Classical Selection Combining

In this section, we derive the average SER of noncoherent MFSK with classical SC in i.n.d fading. To compute the average SER, we average the static error rate, denoted as $P_s(e|\gamma)$ over the PDF of the largest SNR, $f_{\gamma_{\max}}(x)$, where $\gamma_{\max} = \max\{\gamma_1, \gamma_2, \cdots, \gamma_N\}$. That is

$$P_s = \int_0^\infty P_s(e|\gamma) f_{\gamma_{\max}}(\gamma) d\gamma. \tag{4.45}$$

The SER of noncoherent MFSK in an additive white Gaussian channel noise channel is given in [21] as

$$P_s(e|\gamma) = \sum_{n=1}^{M-1} \frac{(-1)^{n+1}\binom{M-1}{n}}{n+1} \exp\left(-\frac{n\gamma}{n+1}\right) \tag{4.46}$$

where γ is the instantaneous SNR per branch.

The CDF of $\gamma_{\max}$ can be written as

$$F_{\gamma_{\max}}(x) = \prod_{i=1}^{L} F_{\gamma_i}(x) \tag{4.47}$$

where $F_{\gamma_i}(x)$ is the CDF of the SNR on the i$^{\text{th}}$ branch. Differentiating the CDF of $\gamma_{\max}$ in (4.47), we obtain its PDF as

$$f_{\gamma_{\max}}(x) = \sum_{i=1}^{L} f_{\gamma_i}(x) \prod_{\substack{j=1 \\ j\neq i}}^{L} F_{\gamma_j}(x). \tag{4.48}$$

Substituting (4.46) and (4.48) in (4.45), we obtain a general expression for the SER of classical SC as

$$P_s = \sum_{n=1}^{M-1} \sum_{i=1}^{L} \frac{(-1)^{n+1}\binom{M-1}{n}}{n+1} \int_0^\infty \exp\left(-\frac{nx}{n+1}\right) f_{\gamma_i}(x) \prod_{\substack{j=1 \\ j\neq i}}^{L} F_{\gamma_j}(x) dx. \tag{4.49}$$

Note that in obtaining (4.49), we have assumed the diversity branches go through i.n.d fading. We now, obtain SER expressions for Rician, Rayleigh and Nakagami-m fading scenarios.

4.3.1 Rician Fading

For Rician fading, the PDF and CDF of γ_i can be written as

$$f_{\gamma_i}(x) = \frac{(K_i+1)}{\bar{\gamma}_i} \exp\left(-K_i - \frac{(K_i+1)x}{\bar{\gamma}_i}\right) I_0\left(2\sqrt{\frac{K_i(K_i+1)x}{\bar{\gamma}_i}}\right) \tag{4.50}$$

and

$$F_{\gamma_i}(x) = 1 - Q_1\left(\sqrt{2K_i}, \sqrt{\frac{2(1+K_i)x}{\bar{\gamma}_i}}\right) \tag{4.51}$$

respectively, where $\bar{\gamma}_i$ is the average SNR on the ith branch.

Substituting (4.50) and (4.51) in (4.49), and making the change of variable, $x = \tan(\theta)$, we obtain the SER of selection combining with i.n.d Rician fading as

$$P_s = \sum_{n=1}^{M-1} \frac{(-1)^{n+1}\binom{M-1}{n}}{n+1} \sum_{i=1}^{L} \frac{K+1}{\bar{\gamma}_i} \exp(-K) \int_0^{\frac{\pi}{2}} \exp\left(-\left(\frac{n}{n+1} + \frac{K+1}{\bar{\gamma}_i}\right)\tan(\theta)\right) \times \prod_{\substack{j=1 \\ j\neq i}}^{L} \left[1 - Q_1\left(\sqrt{2K}, \sqrt{\frac{2(1+K)\tan(\theta)}{\bar{\gamma}_j}}\right)\right] \sec^2(\theta) d\theta. \tag{4.52}$$

4.3.2 Nakagami-m Fading

In the case of Nakagami-m fading, the PDF and CDF of γ_i are given by [12]

$$f_{\gamma_i}(x) = \frac{\left(\frac{m_i}{\bar{\gamma}_i}\right)^{m_i}}{\Gamma(m_i)} \exp\left(-\frac{m_i x}{\bar{\gamma}_i}\right) x^{m_i - 1} \tag{4.53}$$

and

$$F_{\gamma_i}(x) = 1 - \frac{\Gamma\left(m_i, \frac{m_i x}{\bar{\gamma}_i}\right)}{\Gamma(m_i)} \tag{4.54}$$

respectively. Substituting (4.53) and (4.54) in (4.49), we obtain the average SER of noncoherent MFSK with classical SC in i.n.d Nakagami-m fading as

$$P_s = \sum_{n=1}^{M-1} \sum_{i=1}^{L} \frac{(-1)^{n+1}\binom{M-1}{n}}{n+1} \frac{\left(\frac{m_i}{\bar{\gamma}_i}\right)^{m_i}}{\Gamma(m_i)} \int_0^{\infty} x^{m_i - 1} \exp\left(-\left(\frac{m_i}{\bar{\gamma}_i} + \frac{n}{n+1}\right) x\right) \times \prod_{\substack{j=1 \\ j\neq i}}^{L} \left(1 - \frac{\Gamma\left(m_j, \frac{m_j x}{\bar{\gamma}_j}\right)}{\Gamma(m_j)}\right) dx. \tag{4.55}$$

For i.i.d Nakagami-m fading, (4.55) reduces to [40, eq. (18)], as expected. For i.i.d Nakagami-m fadings with integer values of m, using the multinomial theorem and after some mathematical simplification and integral evaluations, (4.55) reduces to a closed-form expression given by

$$\begin{aligned} P_s = L \sum_{n=1}^{M-1} \frac{(-1)^{n+1}\binom{M-1}{n}}{n+1} \frac{\left(\frac{m}{\bar{\gamma}}\right)^m}{\Gamma(m)} \\ \times \sum_{l=0}^{L} (-1)^l \binom{L}{l} \sum_{k=0}^{l(m-1)} \delta_{kl} \left(\frac{m}{\bar{\gamma}}\right)^k \frac{\Gamma(m+k)}{\left(\frac{m}{\bar{\gamma}} + \frac{n}{n+1} + \frac{lm}{\bar{\gamma}}\right)^{m+k}} \end{aligned} \tag{4.56a}$$

where δ_{kl} can be computed using [41]

$$\delta_{kl} = \sum_{i=k-m+1}^{k} \frac{\delta_{i(l-1)}}{(k-i)!} I_{[0,(l-1)(m-1)]}(l) \tag{4.56b}$$

where $\delta_{00} = \delta_{0l} = 1$, $\delta_{k1} = \frac{1}{k!}$, $\delta_{1l} = l$ and $I_{[a,b]}(x)$ is defined as

$$I_{[a,b]}(x) = \begin{cases} 1, & a \leq x \leq b \\ 0, & \text{otherwise} \end{cases} . \tag{4.56c}$$

which is equal to [40, eq. (19)], as expected.

4.3.3 Rayleigh Fading

For Rayleigh fading, it can be shown that (4.52) and (4.55) reduce to a closed-form expression as

$$\begin{aligned} P_s = \sum_{n=1}^{M-1} \frac{(-1)^{n+1}\binom{M-1}{n}}{n+1} \sum_{i=1}^{L} \frac{1}{\bar{\gamma}_i} \Bigg\{ \frac{1}{a_i} - \sum_{\substack{i_1=1 \\ i_1 \neq i}}^{L} \frac{1}{a_i + \beta_{i_1}} \\ + \sum_{\substack{i_1,i_2=1 \\ i_1 \neq i_2 \neq i}}^{L} \frac{1}{a_i + \beta_{i_1} + \beta_{i_2}} + \cdots + (-1)^L \frac{1}{a_i + \sum_{\substack{i_1=1 \\ i_1 \neq i}}^{L}} \Bigg\} \end{aligned} \tag{4.57}$$

where $a_i = \frac{n}{n+1} + \frac{1}{\bar{\gamma}_i}$ and $\beta_i = \frac{1}{\bar{\gamma}_i}$. For i.i.d Rayleigh fading, the SER can be written as

$$P_s = \sum_{n=1}^{M-1} \frac{(-1)^{n+1}\binom{M-1}{n}}{n+1} \prod_{j=1}^{L} \frac{j}{j + \frac{n\bar{\gamma}}{n+1}} \tag{4.58}$$

which is equal to [33, eq. (6)], as expected.

In [33, Section V] it is concluded that $S+N$ SC always outperforms classical SC. Comparing (4.58) with (4.27) one can show, unlike previously concluded in [33, Section V], that the SER performance of $S+N$ SC model 1 is not always smaller than that of classical SC in i.i.d Rayleigh fading. For example, in the case of noncoherent 16-ary FSK with 2 branches the performance of classical SC is superior to that of $S+N$ SC Model 1 for the SNR range of 0 to a crossover value of 6.97 dB. One can also show using numerical calculations of (4.58) and (4.27) that for a fixed value of M, as the number of diversity branches increases this crossover value decreases. For example, considering noncoherent 16-ary FSK, the crossover value is 6.97 dB, 3.87 dB and 2.67 dB for $L = 2, 4$ and $L = 6$, respectively. For a fixed number of diversity branches, increasing the modulation order decreases the SNR cross-over value. For example, if $L = 4$, the cross-over value is 4.21 dB, 4.08 dB and 3.88 dB for noncoherent 4-ary, 8-ary and 16-ary FSK.

4.4 Numerical Examples and Discussion

In this section, some numerical examples are presented to compare the performances of the $S+N$ SC receivers with those of classical SC and SLC in i.i.d and i.n.d Rician and Nakagami-m fading. For i.n.d fading we assume an exponentially decaying multipath intensity profile (MIP), i.e., $\bar{\gamma}_i = \bar{\gamma}_1 \exp(-\beta(i-1)), i = 1, \cdots, L$ where β is the average power decay factor. We also present examples to compare the performances

of the systems in i.i.d and i.n.d fading. Monte Carlo simulation results are presented to test the validity of our analytical expressions. We study the effects of the modulation order, the diversity order, the fading parameter and the average power decay factor on the relative performance of $S+N$ SC Model 1 and Model 2 with classical SC and SLC.

We begin with examining the effect of the fading parameter m on the system performance for both i.i.d and i.n.d Nakagami-m fading employing $S+N$ SC Model 1. In Figs. 4.3 and 4.4, we have plotted the average BER of noncoherent QFSK with 4 diversity branches in i.i.d and i.n.d Nakagami-m channels, respectively, where $m = 1, 3$ and 6 and $\beta = 0.8$. Both figures indicate that as the severity of fading decreases, and for a given BER, the SNR difference between $S+N$ SC Model 1 and classical SC increases. For example, in Fig. 4.3 and at a average BER of 10^{-4}, the SNR difference is 0.72 dB, 1.37 dB and 1.63 dB for $m = 1$, $m = 3$ and $m = 6$, respectively. Comparing Fig. 4.4 with Fig. 4.3, one can see that in i.n.d fading, in contrast to the i.i.d case, the performance of $S+N$ SC Model 1 is inferior to that of classical SC when the average SNR is small. The differences are small, however, and they occur for large values of error rate, so that the $S+N$ model 1 receiver will be preferred for practical implementations.

The effect of average decay factor on the relative performance of $S+N$ SC Model 1 to classical SC in presented in Figs. 4.5 and 4.6 where the SER of noncoherent QFSK is plotted as a function of the average SNR per bit of the first branch $\bar{\gamma}_1$ for $\beta = .5$ and $\beta = 1$ and for $K = 0, 3$ and 6. Comparing Figs. 4.5 and 4.6, one can observe the effect of average decay factor on the relative performance of the two selection combining receivers. For example when $K = 0$, which corresponds to Rayleigh fading, Fig. 4.5 shows that $S+N$ SC Model 1 outperforms SC for the range of SNR given. However,

in Fig. 4.6, classical SC has superior performance over $S+N$ model 1 for small values of SNR up to a crossover value of 8.4 dB. Fig. 4.6 also shows that as the channel becomes better, this crossover value decreases.

Figs. 4.7 and 4.8 study the effect of modulation order on the performances of $S+N$ SC Model 1 and classical SC in i.i.d and i.n.d Nakagami-m fading channels. While Fig. 4.7 shows that $S+N$ SC Model 1 outperforms classical SC for the range of SNR given, we see in Fig. 4.8 that similar to Fig. 4.4, classical SC has superior performance over $S+N$ SC Model 1 for small values of SNR. Fig. 4.8 also shows that the value of SNR at which the error rate curves of classical SC and $S+N$ SC Model 1 cross, decreases as M increases. For example, the cross-over value is 3.4 dB, 2.7 dB and 2.3 dB for $M = 4, 8$ and 16, respectively.

In Fig. 4.9, the average BER of noncoherent BFSK with $S+N$ SC model 1 is plotted as a function of the average SNR in i.n.d Rician fading with an average decay factor of $\beta = 0.5$ and for $K = 3$ for several values of L. It is interesting to note that unlike the case of i.i.d fading, the performance of the system does not necessarily improve as we increase the diversity order. For example, Fig. 4.9 shows that the performance of the $S+N$ SC Model 1 with 4-branch diversity is superior to the performance of 8-branch $S+N$ SC Model 1 for the SNR range of 0 to 13 dB. This phenomena can be explained as follows. In the small SNR region the noise term is dominant and $S+N$ SC receiver is basically choosing the branch which is mostly affected by noise. Therefore, in the small SNR region, increasing the diversity order does not necessarily improve the performance of the system.

In Fig. 4.10, the effect of the average delay factor, β, on the relative performances of $S+N$ SC Model 1 and classical SC is examined, where the BER of noncoherent 16-ary FSK is plotted as a function of SNR per bit on the first diversity branch for

4-branch $S+N$ SC Model 1 and classical SC in Nakagami-m fading with $m=4$. Notice that as β increases, the performance gain of $S+N$ SC Model 1 over classical SC decreases. Also, it is important to notice that for the region of small SNR and for large β classical SC performs better that $S+N$ SC Model 1. This is because for larger β, we get weaker diversity branches in terms of signal strength and the noise in the system becomes the dominant factor. Therefore, by choosing the largest output of square-law detectors, the $S+N$ SC receiver is in fact choosing a branch mostly affected by noise resulting in an inferior performance compared to classical SC. The same phenomena is in evidence in Fig. 4.11, where for large β and in the small SNR region, classical SC outperforms $S+N$ SC Model 1 and $S+N$ SC Model 2, while in the moderate to high SNR region $S+N$ SC Model 2 outperforms both $S+N$ SC Model 1 and $S+N$ SC Model 2. Furthermore, Fig. 4.11 shows that S+N SC Model 2 has superior performance over $S+N$ Model 1 in all cases.

Finally, we compare the performance of $S+N$ SC Models 1 and 2 with square-law combining (SLC). Fig. 4.12 shows the average BER performance of noncoherent 8-ary FSK with 3, 4 and 5 branch diversity with $S+N$ SC Model 1, classical SC and SLC in i.i.d Nakagami-m fading. For SLC, we have used the analytical expressions given in [42] to plot the curves in Fig. 4.12. Fig. 4.12 shows that as we increase the number of diversity branches, the performance gap between $S+N$ SC Model 1 and SLC increases. For example at an average BER of 10^{-3}, the SNR difference between $S+N$ SC Model 1 with SLC is 1.18 dB, 1.57 dB and 1.9 dB for $N=3,4$ and 5, respectively. The performance gap between $S+N$ SC Model 2 and SLC also increases as the number of diversity branches is increased, as illustrated in Fig. 4.13. For example, at an average BER of 10^{-3} the SNR difference between the two systems is 0.29 dB, 0.57 dB and 0.92 dB, for $L=3,4$ and 5, respectively.

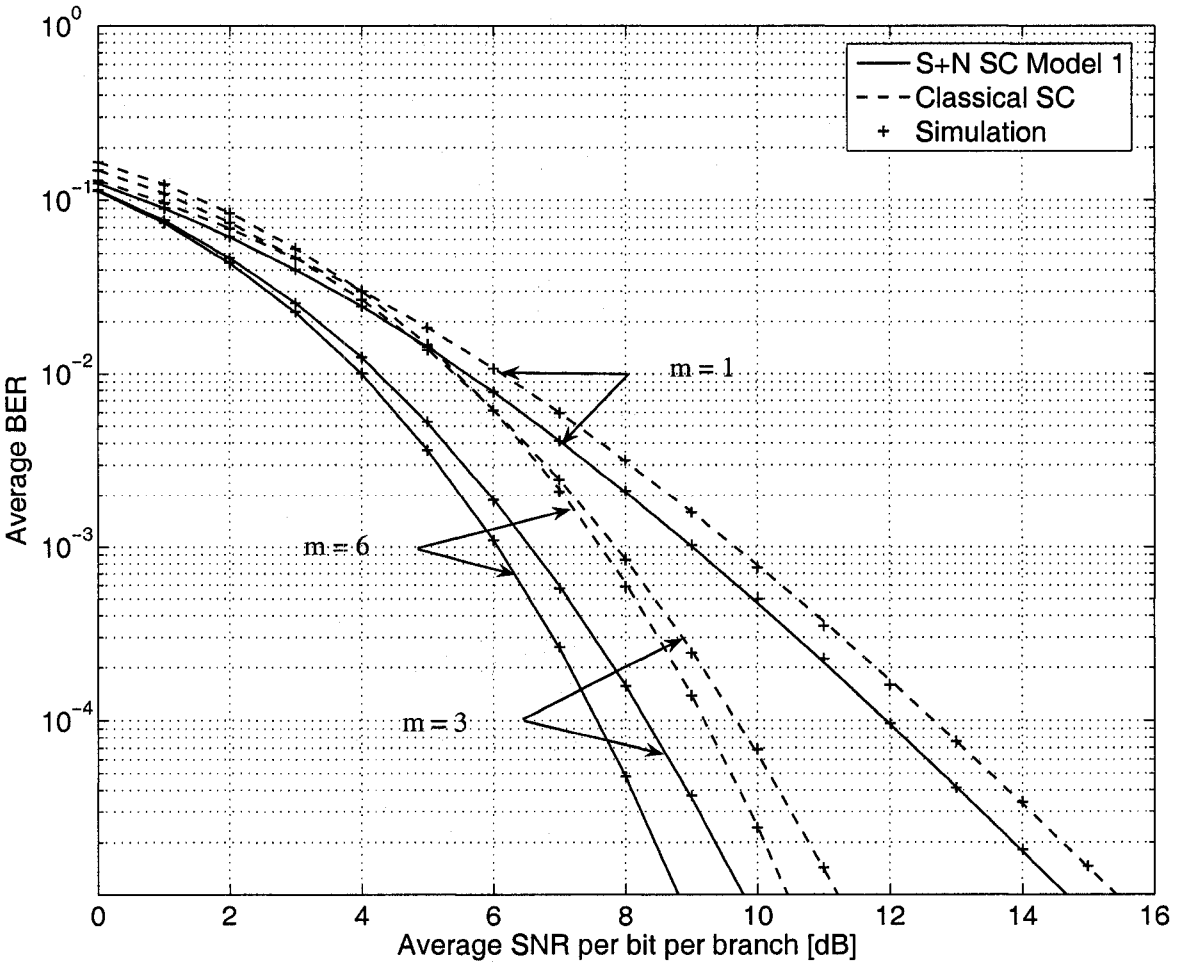

Figure 4.3: The average BER of noncoherent QFSK with 4-branch $S+N$ SC receiver Model 1 and classical SC in i.i.d Nakagami-m fading with $m = 1, 3$ and 6.

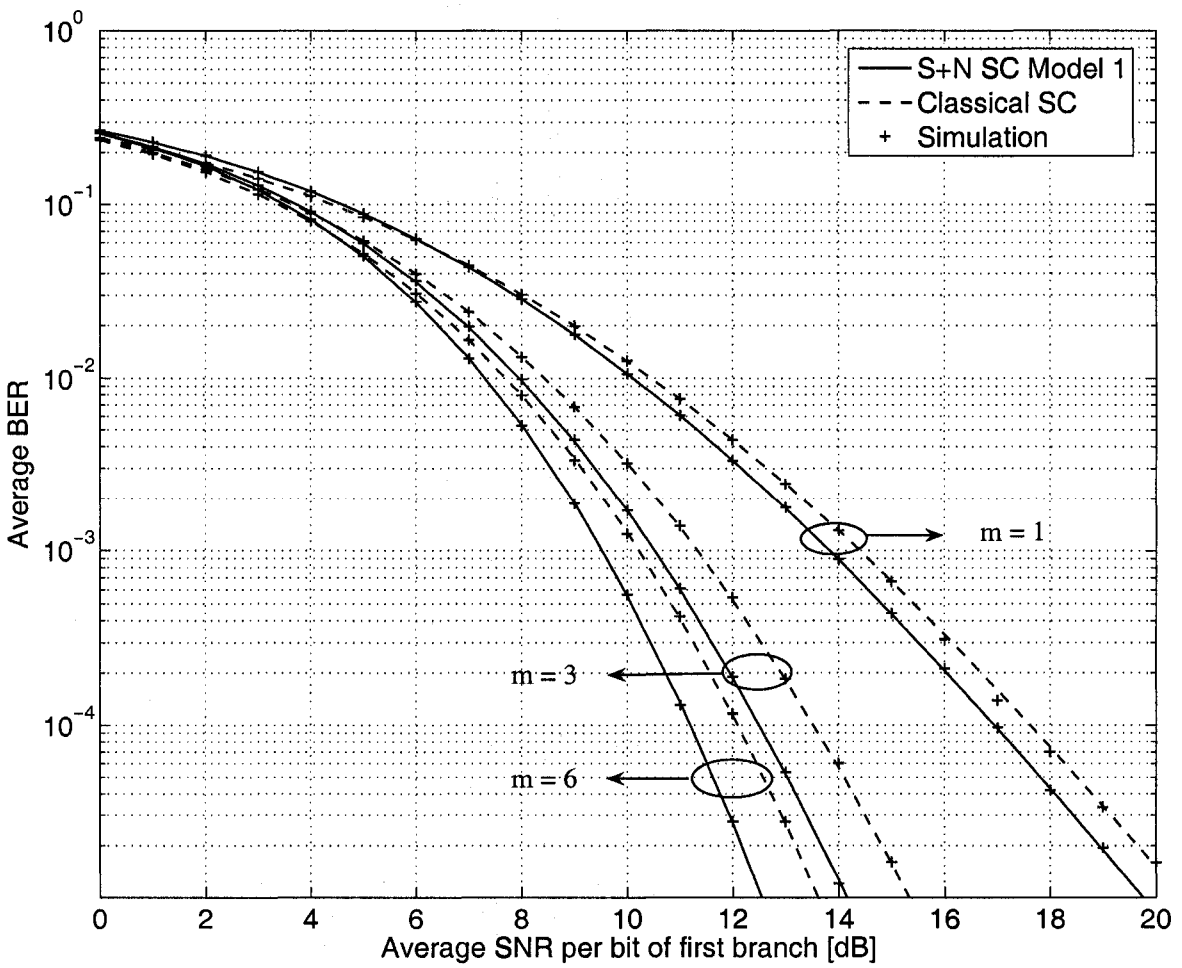

Figure 4.4: The average BER of noncoherent QFSK with 4-branch $S+N$ SC receiver Model 1 and classical SC in i.n.d Nakagami-m fading with $m = 1, 3$ and 6 and $\beta = 0.8$.

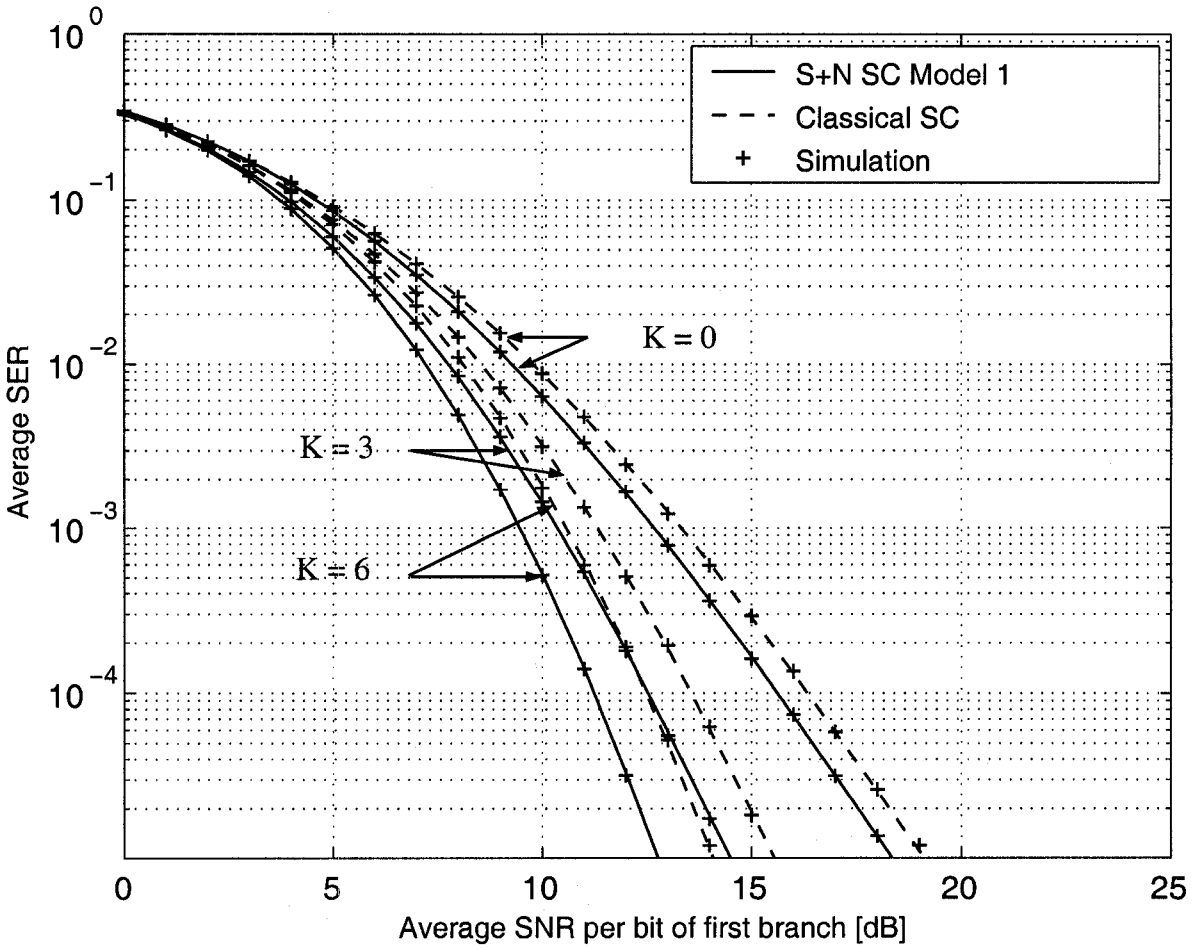

Figure 4.5: The average SER of noncoherent QFSK over 4-branch i.n.d Rician fading with an average decay factor $\beta = 0.5$ for $K = 0, 3$ and 6.

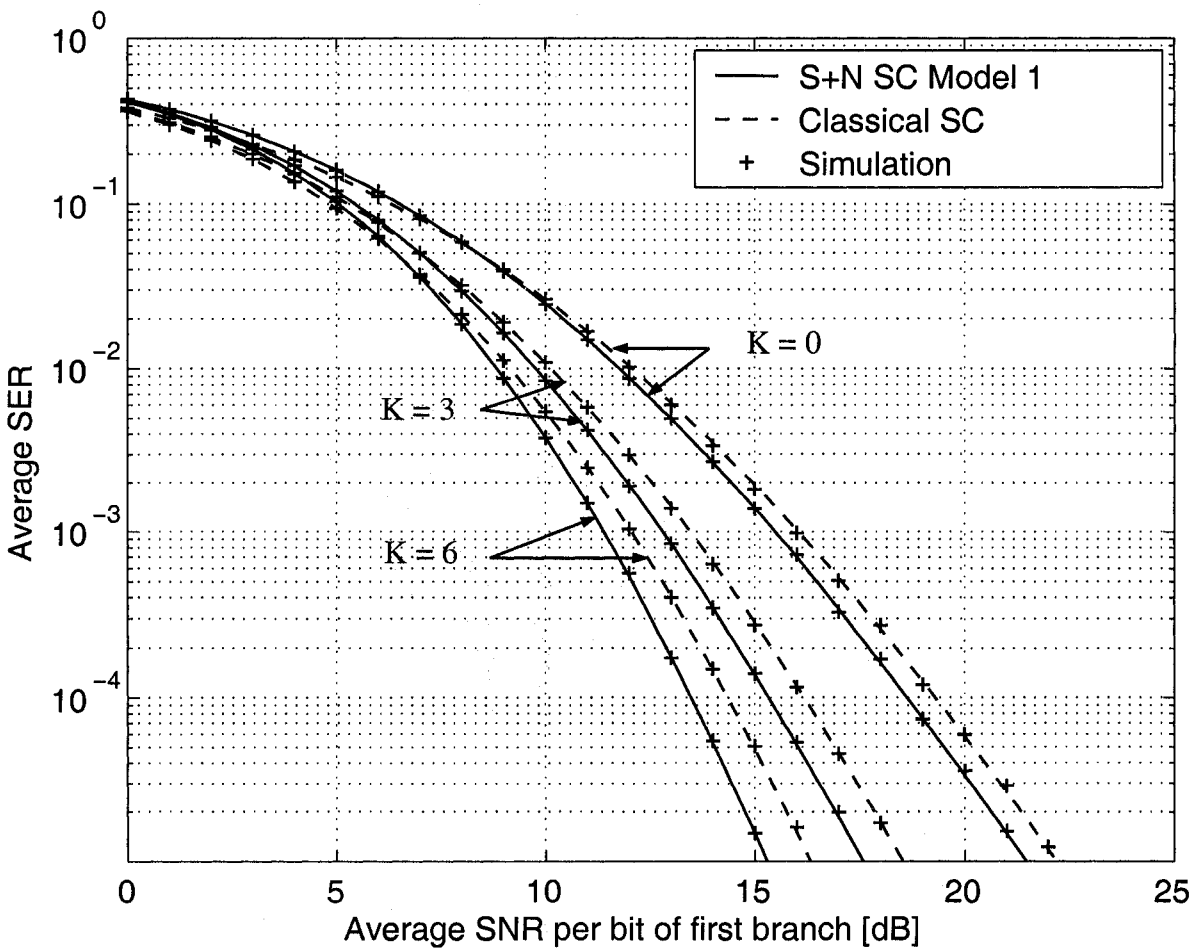

Figure 4.6: The average SER of noncoherent QFSK in 4-branch i.n.d Rician fading with an average decay factor $\beta = 1$ for $K = 0, 3$ and 6.

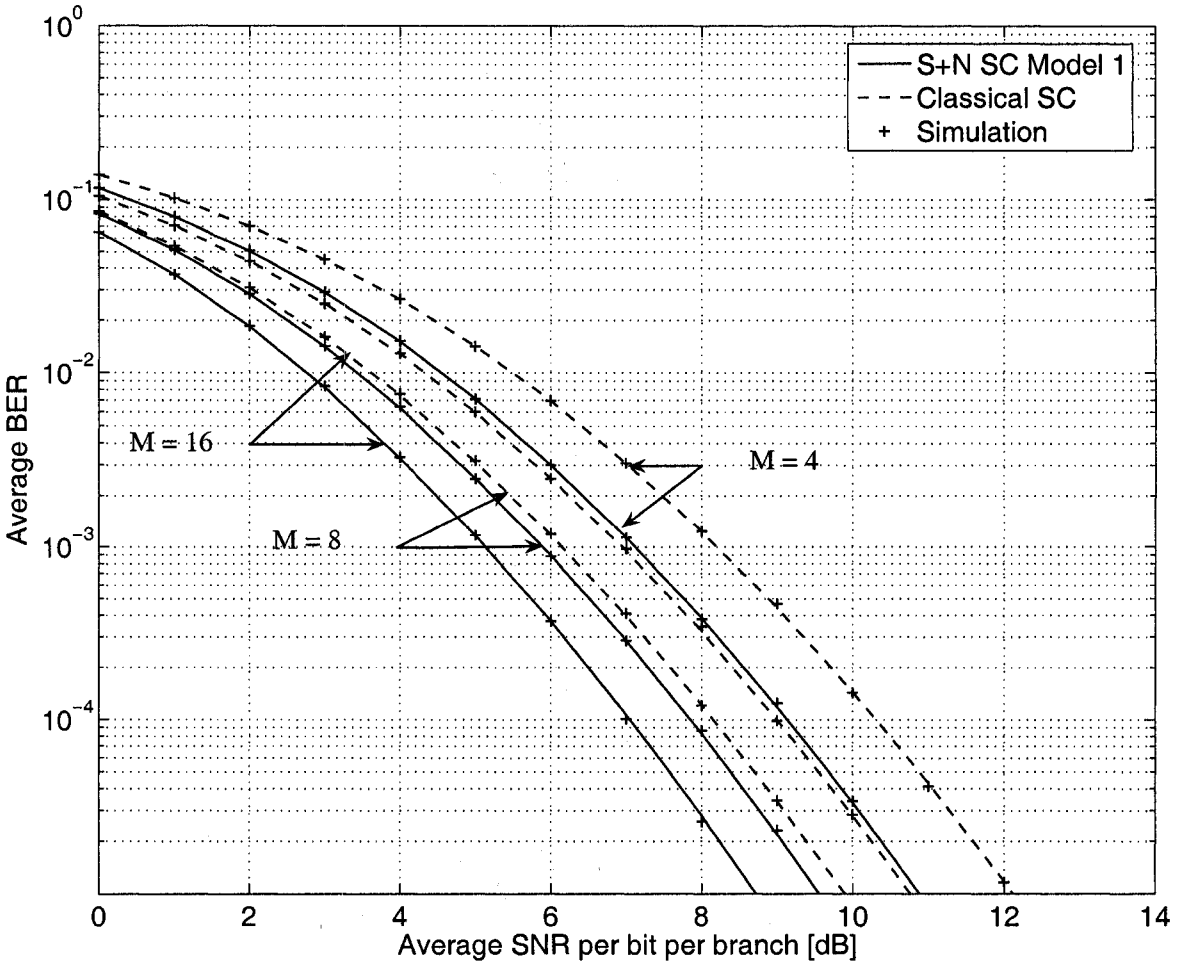

Figure 4.7: The average BER of noncoherent MFSK with 4-branch $S+N$ SC receiver Model 1 and classical SC in i.i.d Nakagami-m fading with $m = 2$ for $M = 4, 8$ and 16.

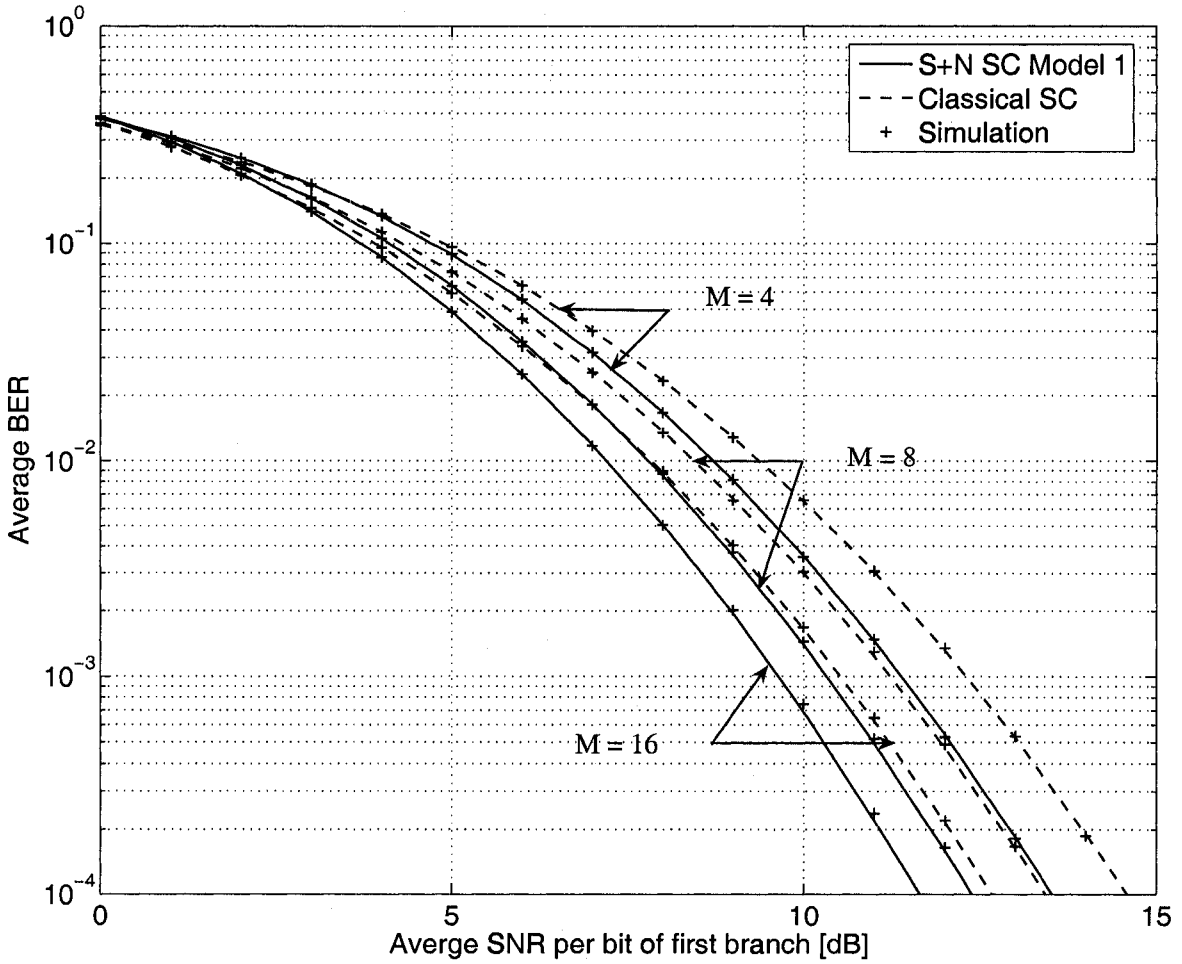

Figure 4.8: The average BER of noncoherent MFSK with 4-branch $S+N$ SC receiver Model 1 and classical SC in i.n.d Nakagami-m fading with $m = 2$ and $\beta = 0.8$ for $M = 4, 8$ and 16.

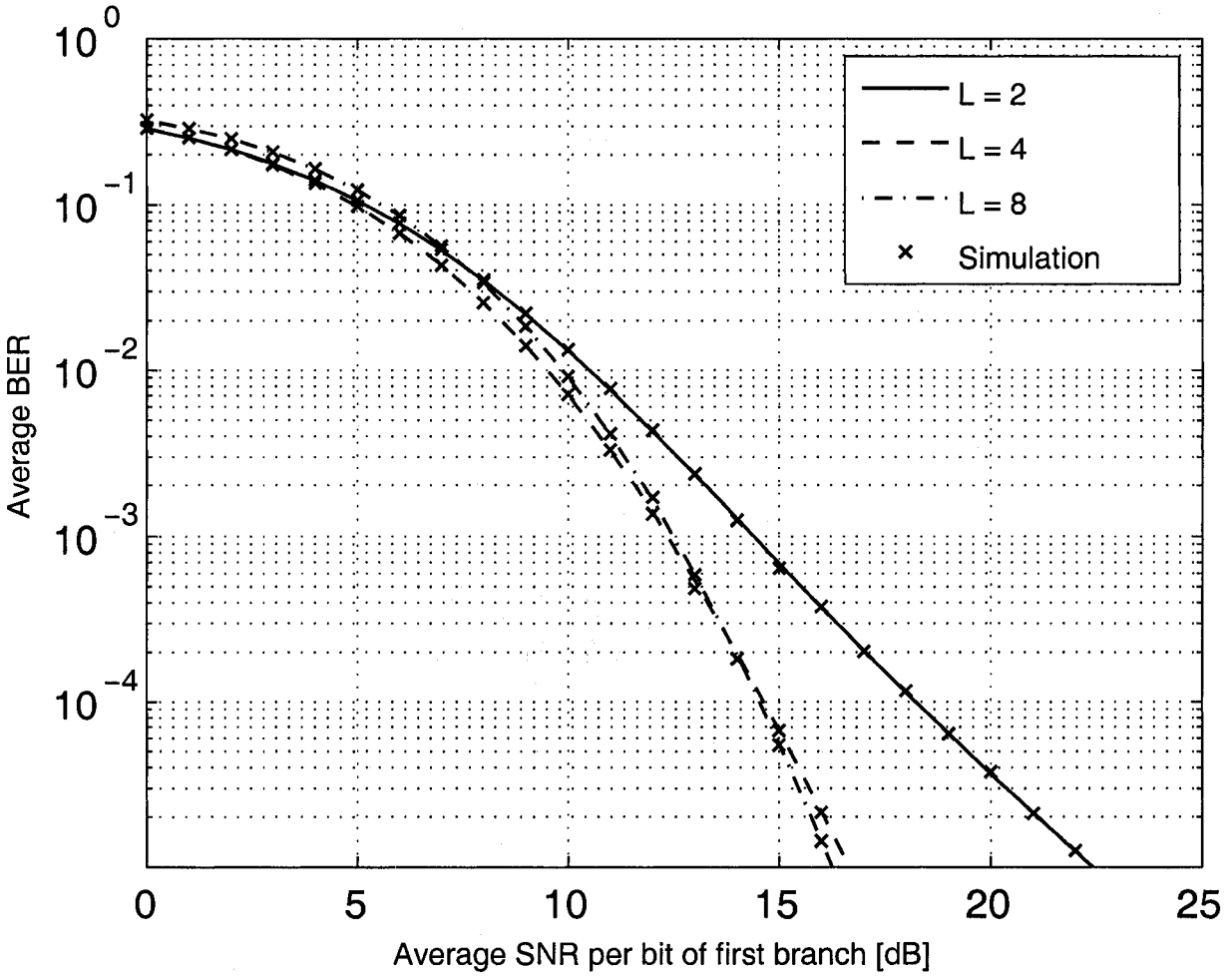

Figure 4.9: The average BER of noncoherent BFSK with $S+N$ SC Model 1 in i.n.d Rician fading with $L = 2, 4$ and 8, an average decay factor of $\beta = 0.5$ and $K = 3$.

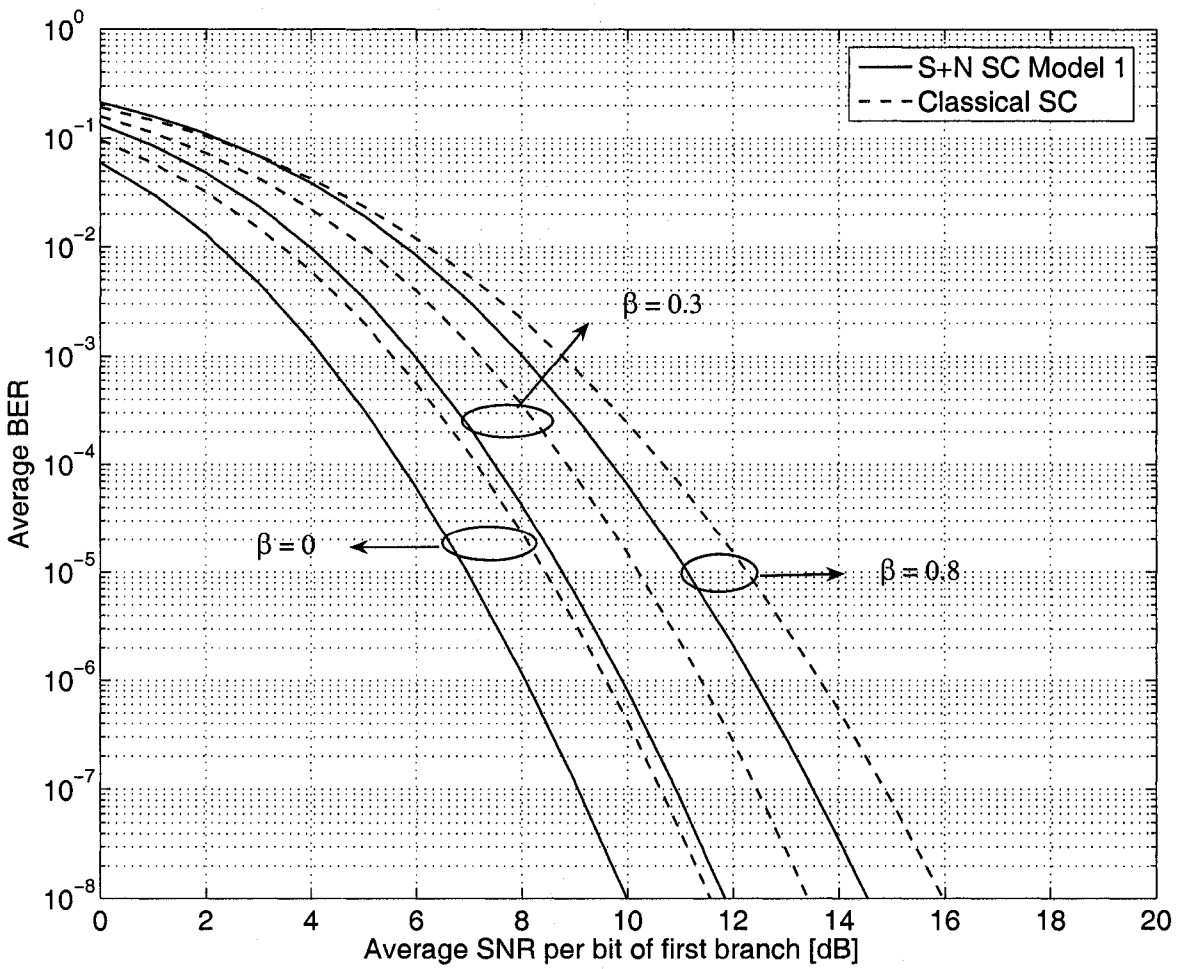

Figure 4.10: The average BER of noncoherent 16-ary FSK with 4-branch $S+N$ SC receiver Model 1 and classical SC in i.n.d Nakagami-m fading with $m = 4$ and $\beta = 0, 0.3$ and 0.8.

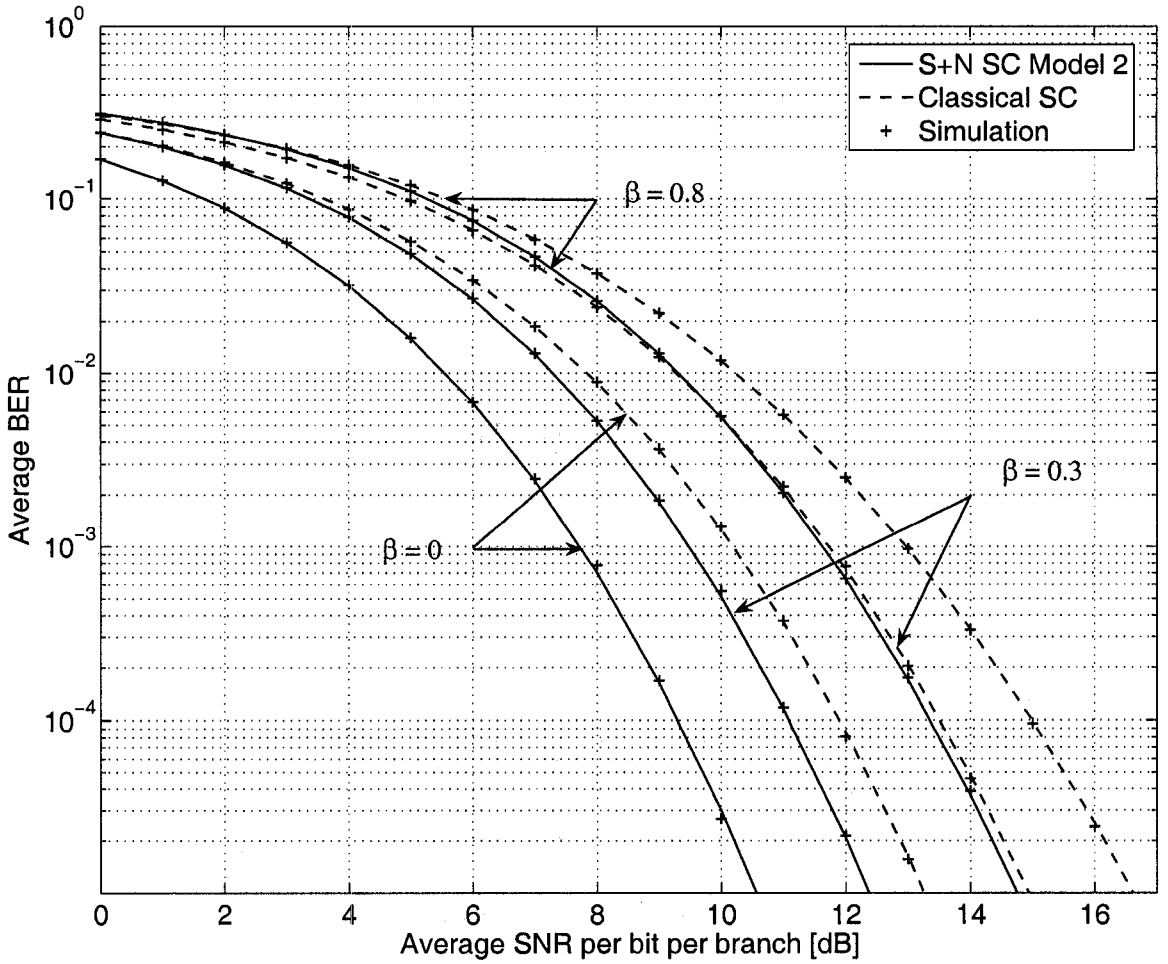

Figure 4.11: The average BER of noncoherent BFSK with 4-branch $S+N$ SC receiver Model 2 and classical SC in i.n.d Nakagami-m fading with $m = 5$ and $\beta = 0, 0.3$ and 0.8.

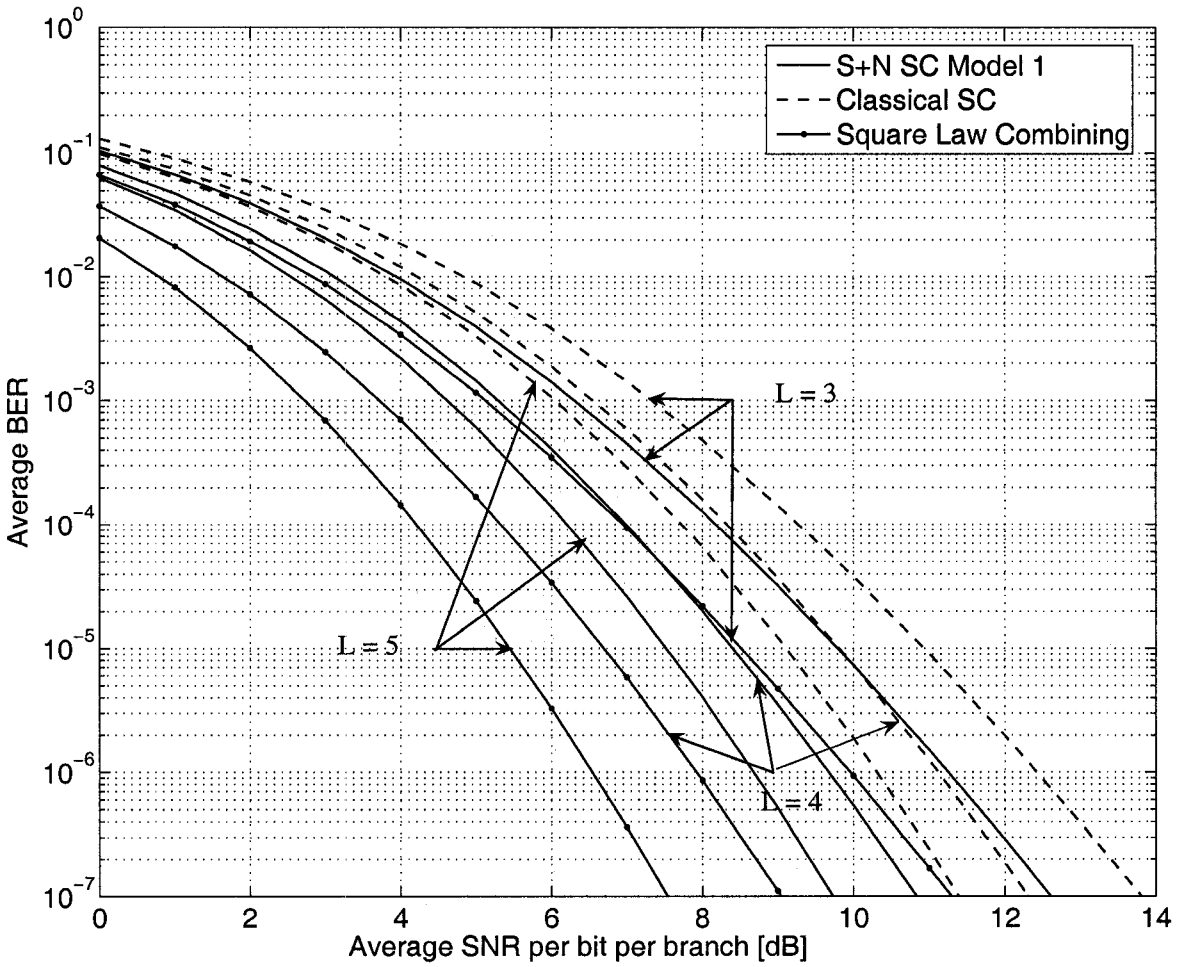

Figure 4.12: The average BER of noncoherent 8-ary FSK in L-branch i.i.d Nakagami-m fading with $S+N$ SC receiver Model 1, classical SC and SLC for $m = 3$ and $L = 3, 4$ and 5.

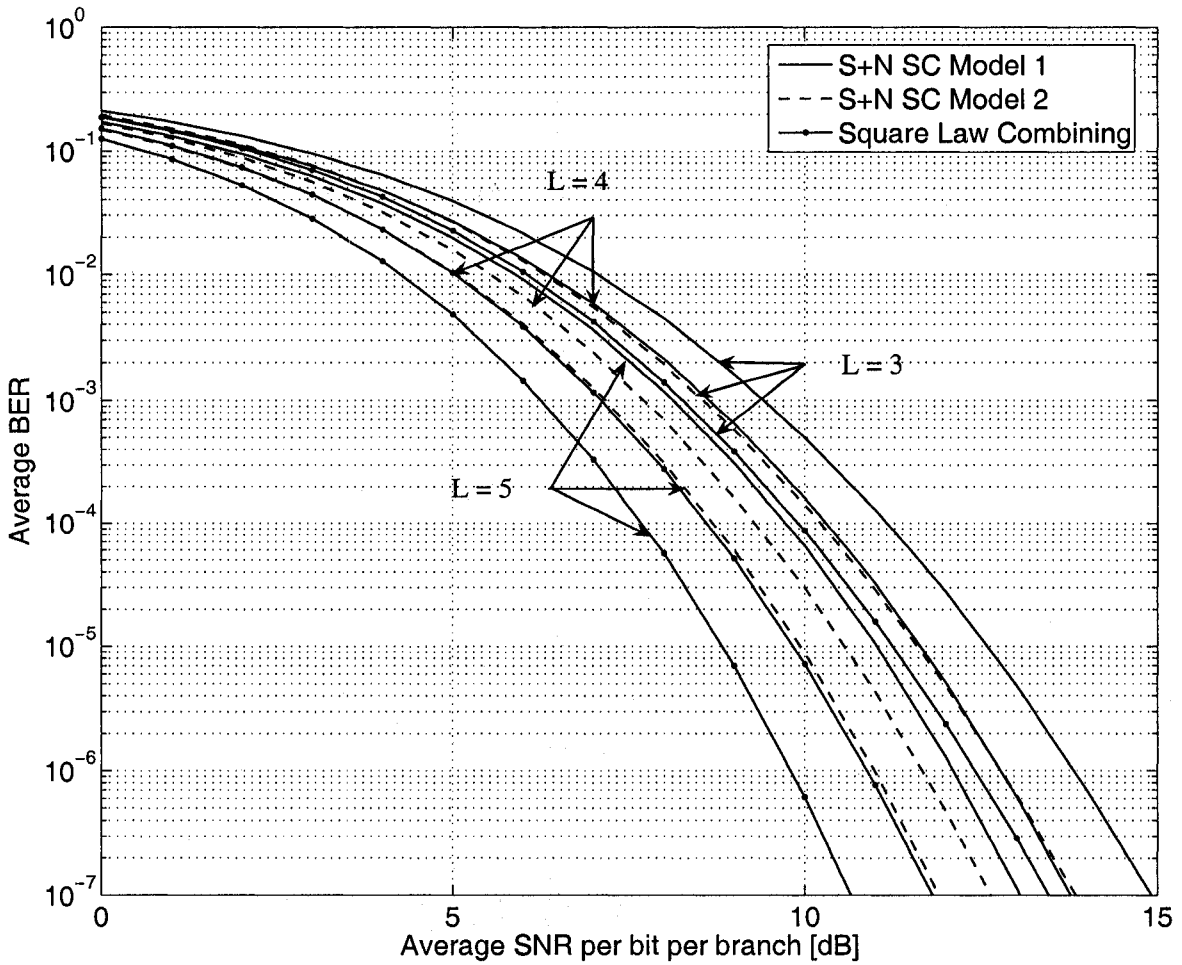

Figure 4.13: The average BER of noncoherent BFSK in L-branch i.i.d Nakagami-m fading with $S + N$ SC receiver Model 1, $S + N$ SC receiver Model 2 and SLC for $m = 5$ and $L = 3, 4$ and 5.

4.5 Conclusions

The performances of two $S+N$ SC receivers in i.n.d Rician, Nakagami and Rayleigh fading channels were analyzed. For each receiver, analytical expressions were derived for the average BER in terms of single integrals. These analytical expressions were verified using extensive Monte Carlo simulation results. It was shown that, unlike previously published results, the performance of $S+N$ SC receivers are not always superior to the performance of the classical SC receiver when the receiver is operating in the low SNR region. The effects of diversity order, modulation order and average fading power imbalance on the performances of the two $S+N$ SC receivers was examined. Interestingly, it was shown that the performance of the $S+N$ SC receiver does not necessarily improve with the addition of diversity branches when the receiver is operating in the low SNR region. The performances of the $S+N$ SC receivers were compared to the performances of classical SC and SLC.

Chapter 5

Performance of $S+N$ Selection Diversity Receivers in Correlated Rayleigh and Rician Fading

In Chapter 4, we studied the performances of two $S+N$ SC receivers in i.n.d Rician, Nakagami and Rayleigh fading channels. In this chapter, we generalize the results of the previous chapter to correlated Rayleigh and Rician fading channels. For Rician fading we assume that the branches are equally correlated. For Rayleigh fading, the correlation model is more general and includes the equally correlated scenario as a special case. For each $S+N$ SC receiver structure, we obtain easy to compute analytical expressions for the average BER, which are verified using Monte Carlo simulation results.

For Rayleigh fading, we assume that the correlation structure follows the model given in [30, eq. (8.1.5)], [43], which includes the case of equally correlated fading as a special case. We also consider the general scenario that the fading powers on the channels are not necessarily identical. For Rician fading, our analysis considers the case of equally correlated branches, where for each receiver structure analytical

expressions are derived for the average BER. The effects of correlation, fading power imbalance and fading parameter on the performance of $S+N$ SC receivers are examined and the performance of $S+N$ SC is compared to classical SC. Our analytical results are verified using Monte Carlo simulation results. Note, that the equally correlated model can be used as a worst case benchmark or as a rough approximation by replacing every non-diagonal element in the correlation matrix ($\rho_{ij}, i \neq j$) with the average value of ρ_{ij} [20]. The equally correlated model has been used to model a set of closely placed antennas [44]. However, using experimental measurements, Zhang [45] has shown that the correlation model for a set of three equally placed antennas does not follow the equally correlated model, so the equally correlated model must be applied with care. The performance of classical SC over correlated fading channels has been studied in [46]- [53].

The remainder of this chapter is organized as follows. In Section 5.1, average SER expressions are derived for $S+N$ SC Model 1 for the cases of correlated Rayleigh and Rician fading channels. In Section 5.2, average BER expressions are derived for the performance of $S+N$ SC Model 2 in equally correlated Rayleigh and Rician channels. Several numerical examples that compare the performances of the two $S+N$ SC receiver structures with classical SC are presented in Section 5.3 and the validity of the analytical expressions obtained in Sections 5.1 and 5.2 are verified using Monte Carlo simulations. Finally, some conclusions are given in Section 5.4

5.1 Average SER of $S+N$ SC Model 1

The performance of noncoherent MFSK signaling with L branch diversity with $S+N$ SC Model 1 is considered. The structure of the receiver is given in Fig. 4.1 and the

outputs of the square-law detectors are give by

$$X_{i1} = |2E_sG_i + N_{i1}|^2 \tag{5.1}$$

$$X_{im} = |N_{im}|^2, \quad i = 1, \cdots, L, m = 2, \cdots, M \tag{5.2}$$

where $G_i, i = 1, \cdots, L$ are the complex channel gains and $N_{ij}, i = 1, \cdots, L, j = 1, \cdots, M$ are complex Gaussian RVs with variance $4E_sN_0$. Following the analysis in Section 4.1, the average SER can be written as

$$P_s(E) = \Pr[X_{1\max} < X_{2\max}] \tag{5.3a}$$

$$= \int_0^\infty F_{X_{1\max}}(x) f_{X_{2\max}}(x) dx \tag{5.3b}$$

Noting that the RVs $X_{im}, i = 1, \cdots, L, m = 2, \cdots, M$ are independent and identically chi-squared RVs with common PDF and CDF given by

$$f_X(x) = \frac{1}{4E_sN_0} \exp\left(-\frac{w}{4E_sN_0}\right) \tag{5.4}$$

and

$$F_X(x) = 1 - \exp\left(-\frac{w}{4E_sN_0}\right) \tag{5.5}$$

respectively, we can obtain the PDF of $X_{2\max}$ as

$$f_{X_{2\max}}(x) = \frac{L(M-1)}{4E_sN_0} \exp\left(-\frac{x}{4E_sN_0}\right)\left(1 - \exp\left(-\frac{x}{4E_sN_0}\right)\right)^{LM-L-1}. \tag{5.6}$$

The CDF of $X_{1\max}$ is given by

$$F_{X_{1\max}}(x) = F_{X_{11}, X_{21}, \cdots, X_{L1}}(x, x, \cdots, x) \tag{5.7}$$

where $F_{X_{11}, X_{21}, \cdots, X_{L1}}(x, x, \cdots, x)$ is the joint CDF of the RVs $X_{i1}, i = 1, \cdots, L$. Substituting (5.6) and (5.7) in (5.3b), we obtain a general expression for the average SER of noncoherent MFSK with $S + N$ SC in correlated fading as

$$P_s(E) = \frac{L(M-1)}{4E_sN_0} \int_0^\infty F_{X_{11}, X_{21}, \cdots, X_{L1}}(x, x, \cdots, x) \exp\left(-\frac{x}{4E_sN_0}\right) \times \left(1 - \exp\left(-\frac{x}{4E_sN_0}\right)\right)^{LM-L-1} dx. \tag{5.8}$$

Note that the average BER can now be obtained from the average SER using $P_b(E) = M/(2(M-1))P_s(E)$. If the branches are independent, $F_{X_{1\max}}(x)$ can be written as the product of the marginal CDFs $F_{X_{i1}}, i = 1, \cdots, L$ and (5.8) reduces to

$$P_s(E) = \frac{L(M-1)}{4E_sN_0} \int_0^\infty \left\{ \prod_{i=1}^{L} F_{X_{i1}}(x) \right\} \exp\left(-\frac{x}{4E_sN_0}\right) \times \left(1 - \exp\left(-\frac{x}{4E_sN_0}\right)\right)^{LM-L-1} dx. \tag{5.9}$$

which is equal to (4.3a).

5.1.1 Rayleigh Fading

Let Σ denote the branch power covariance coefficient matrix, whose elements $\Sigma_{i,j}(i, j = 1, \cdots, L)$ satisfy [43, eq. (2)], i.e.,

$$\Sigma_{i,j} = \frac{\mathbb{E}(|G_i|^2|G_j|^2) - \mathbb{E}(|G_i|^2)\mathbb{E}(|G_j|^2)}{\sqrt{\mathrm{Var}(|G_i|^2)\mathrm{Var}(|G_j|^2)}} = \rho_i\rho_j \tag{5.10}$$

where $G_i, i = 1, \cdots, L$ are the complex channels gains and $\mathbb{E}(X)$ and $\mathrm{Var}(X)$ denote the expected value and the variance of X, respectively. Note that, for $\rho_i = \rho, i = 1, \cdots, L$, (5.10) reduces to the case of equally correlated branches. For Rayleigh fading we write the channel gains, G_i, as [30]

$$G_i = \sqrt{\Omega_i}(\sqrt{1-\rho_i}U_i + \sqrt{\rho_i}U_0 + j(\sqrt{1-\rho_i}V_i + \sqrt{\rho_i}V_0)), \quad i = 1, \cdots, L \tag{5.11}$$

where $j = \sqrt{-1}$, U_i and $V_i, i = 0, \ldots, L$ are *independent* zero-mean Gaussian RVs with variance $\frac{1}{2}$, $0 \leq \rho_i < 1$ and $\Omega_i = E[|G_i|^2]$ is the average fading power on the ith channel. Note that one can show that $|G_i|$ are Rayleigh distributed and that the branch power covariance matrix will follow (5.10). Furthermore, one can show that the cross-correlation between any G_i and G_j is $\sqrt{\rho_i\rho_k} = E[G_iG_k^*]/\sqrt{E[|G_i|^2]E[|G_k|^2]}$.

Using (5.11), we can write X_{i1} defined in (5.1) as

$$X_{i1} = (2E_s\sqrt{\Omega_i}(\sqrt{1-\rho_i}U_i + \sqrt{\rho_i}U_0) + N_{11}^I)^2 + (2E_s\sqrt{\Omega_i}(\sqrt{1-\rho_i}V_i + \sqrt{\rho_i}V_0) + N_{11}^Q)^2 \tag{5.12}$$

where N_{11}^I and N_{11}^Q are zero-mean Gaussian RVs with variance $2E_bN_0$. Define $Z = U_0^2 + V_0^2$. Then assuming that U_0 and V_0 are fixed, one can show that the RVs X_{i1} conditioned on Z are independent and their conditional CDFs, $F_{X_{i1}|Z}(x)$, are given by

$$F_{X_{i1}|Z}(x) = 1 - Q_1\left(\sqrt{\frac{2\bar{\gamma}_i\rho_i z}{1+\bar{\gamma}_i(1-\rho_i)}}, \sqrt{\frac{x}{2E_sN_0(1+\bar{\gamma}_i(1-\rho_i))}}\right) \tag{5.13}$$

where $\bar{\gamma}_i$ is the average SNR on the ith branch. Thus, the joint CDF of $X_{i1}, i = 1, \cdots, L$ conditioned on the RV Z can be written as the product of the marginal CDFs conditioned on the RV Z, i.e.,

$$F_{X_{11},X_{21},\cdots,X_{L1}|Z}(x_1, x, \cdots, x_L) = \prod_{i=1}^{L} F_{X_{i1}|Z}(x_i|z). \tag{5.14}$$

The RV Z is central chi-squared with two degrees of freedom and its PDF is given by

$$f_Z(z) = \exp(-z). \tag{5.15}$$

Using (5.14) and (5.15), we can now obtain the joint CDF of $X_{i1}, i = 1, \cdots, L$ as

$$F_{X_{11},X_{21},\cdots,X_{L1}}(x_1, x, \cdots, x_L) = \int_0^\infty \left[\prod_{i=1}^{L} F_{X_{i1}|Z}(x_i|z)\right] f_Z(z)dz \tag{5.16a}$$

$$= \int_0^\infty \left[\prod_{i=1}^{L}\left(1 - Q_1\left(\sqrt{\frac{2\bar{\gamma}_i\rho_i z}{1+\bar{\gamma}_i(1-\rho_i)}}, \sqrt{\frac{x_i}{2E_sN_0(1+\bar{\gamma}_i(1-\rho_i))}}\right)\right)\right] \times \exp(-z)dz. \tag{5.16b}$$

Substituting (5.16b) in (5.8) and using a simple change of variable, the average SER of noncoherent MFSK with $S+N$ SC Model 1 operating with nonidentically distributed

correlated Rayleigh fading branches becomes

$$P_s(E) = L(M-1)\int_0^\infty \int_0^\infty \left[\prod_{i=1}^{L}\left(1 - Q_1\left(\sqrt{\frac{2\bar{\gamma}_i\rho_i z}{1+\bar{\gamma}_i(1-\rho_i)}}, \sqrt{\frac{2x}{(1+\bar{\gamma}_i(1-\rho_i))}}\right)\right)\right] \times \exp(-x-z)\left(1-\exp(-x)\right)^{LM-L-1} dzdx. \tag{5.17}$$

For the important case of dual-branch diversity, after much mathematical manipulation and integral evaluations, (5.17) reduces to a closed-form expression given by

$$P_s(E) = 2(M-1)\sum_{i=0}^{2M-3}\binom{2M-3}{i}(-1)^i\left[\frac{1}{i+1} - \frac{1}{2(i+1+A_1)} \times \left(1 + \frac{A_2 - A_3 + 2(i+1+A_1)}{\sqrt{(A_2+A_3+2(i+1+A_1))^2 - 4A_2A_3}}\right) - \frac{1}{2(i+1+A_4)} \times \left(1 - \frac{A_5 - A_6 + 2(i+1+A_4)}{\sqrt{(A_5+A_6+2(i+1+A_4))^2 - 4A_5A_6}}\right)\right] \tag{5.18a}$$

where $\Sigma_{12} = \rho^2$ and

$$A_1 = \frac{1}{1+\bar{\gamma}_1} \tag{5.18b}$$

$$A_2 = \frac{2(1+\bar{\gamma}_1)}{\bar{\gamma}_1\bar{\gamma}_2(1-\rho^2) + \bar{\gamma}_1 + \bar{\gamma}_2 + 1} \tag{5.18c}$$

$$A_3 = \frac{2\bar{\gamma}_1\bar{\gamma}_2\rho^2}{(\bar{\gamma}_1\bar{\gamma}_2(1-\rho^2) + \bar{\gamma}_1 + \bar{\gamma}_2 + 1)(1+\bar{\gamma}_1)} \tag{5.18d}$$

$$A_4 = \frac{1}{1+\bar{\gamma}_2} \tag{5.18e}$$

$$A_5 = \frac{2\bar{\gamma}_1\bar{\gamma}_2\rho^2}{(\bar{\gamma}_1\bar{\gamma}_2(1-\rho^2) + \bar{\gamma}_1 + \bar{\gamma}_2 + 1)(1+\bar{\gamma}_2)} \tag{5.18f}$$

$$A_6 = \frac{2(1+\bar{\gamma}_2)}{\bar{\gamma}_1\bar{\gamma}_2(1-\rho^2) + \bar{\gamma}_1 + \bar{\gamma}_2 + 1}. \tag{5.18g}$$

The derivation of (5.18) is given in Appendix B.

5.1.2 Rician Fading

In the case of Rician fading, we consider the case of equally correlated branches and we represent the channel gains as [20]

$$G_i = \sqrt{1-\rho}U_i + \sqrt{\rho}U_0 + m_1 + j(\sqrt{1-\rho}V_i + \sqrt{\rho}V_0 + m_2) \tag{5.19}$$

where $0 \leq \rho < 1$ and U_i and V_i are independent zero-mean Gaussian RVs with variance $\sigma^2 = \Omega/(2(K+1))$, and where $K = (m_1^2+m_2^2)/(2\sigma^2)$ is the Rician factor [4]. Using the representation given in (5.19), one can show that the fading correlation between G_1 and G_2 is equal to ρ and $E[|G_i|^2] = \Omega, i = 1, \cdots, L$, i.e., the branches are identically distributed. In addition, the power correlation between $|G_i|^2$ and $|G_j|^2$ $(i \neq j)$ can be obtained as [20]

$$\rho_\eta = \rho\frac{2K+\rho}{2K+1}. \tag{5.20}$$

Define $Z = (U_0 + \frac{m_1}{\sqrt{\rho}})^2 + (V_0 + \frac{m_2}{\sqrt{\rho}})^2$. Then assuming that Z is fixed, one can show, after some mathematical simplification, that the conditional CDF of $X_{i1}, i = 1, \cdots, L$ given Z, i.e., $F_{X_{i1}|Z}(x)$, can be written as

$$F_{X_{i1}|Z}(x) = 1 - Q_1\left(\sqrt{\frac{2\bar{\gamma}\rho(1+K)z}{1+K+\bar{\gamma}(1-\rho)}}, \sqrt{\frac{(1+K)x}{2E_sN_0(1+K+\bar{\gamma}(1-\rho))}}\right). \tag{5.21}$$

Note that because the branches are identically distributed $F_{X_{i1}|Z}(x)$ is independent of i. Using (5.21) and the PDF of Z given by

$$f_Z(z) = (K+1)\exp\left(-\frac{K}{\rho} - (K+1)z\right) I_0\left(2\sqrt{\frac{K(K+1)z}{\rho}}\right) \tag{5.22}$$

we obtain the joint CDF of $X_{i1}, i = 1, \cdots, L$ as

$$F_{X_{11},X_{21},\cdots,X_{L1}}(x, x, \cdots, x) = (K+1)\exp\left(-\frac{K}{\rho}\right) \times \int_0^\infty \exp\left(-(K+1)z\right) I_0\left(2\sqrt{\frac{K(K+1)z}{\rho}}\right) \times \left(1 - Q_1\left(\sqrt{\frac{2\bar{\gamma}\rho(1+K)z}{1+K+\bar{\gamma}(1-\rho)}}, \sqrt{\frac{(1+K)x}{2E_sN_0(1+K+\bar{\gamma}(1-\rho))}}\right)\right)^L dz. \tag{5.23}$$

The average SER of noncoherent MFSK with $S+N$ SC Model 1 in identically distributed equally correlated Rician fading can now be obtained by substituting (5.21) in (5.8) as

$$P_s(E) = L(K+1)(M-1)\exp\left(-\frac{K}{\rho}\right)\int_0^\infty\int_0^\infty (1-\exp(-x))^{LM-L-1} \times \exp\left(-(K+1)z - x\right) I_0\left(2\sqrt{\frac{K(K+1)z}{\rho}}\right) \times \left(1 - Q_1\left(\sqrt{\frac{2\bar{\gamma}\rho(1+K)z}{1+K+\bar{\gamma}(1-\rho)}}, \sqrt{\frac{2(1+K)x}{(1+K+\bar{\gamma}(1-\rho))}}\right)\right)^L dzdx. \tag{5.24}$$

Note that eq. (5.24) is valid for $\rho > 0$ as we have used (5.22) to obtain (5.24) which implicitly assumes that $\rho > 0$. For $\rho = 0$, which corresponds to independent fading branches, the average SER is given in [54, eq. (11)].

5.2 Average BER of $S+N$ SC Model 2

The receiver structure of $S+N$ SC Model 2 is depicted in Fig. 4.2 and the outputs of the square-law detectors are given by

$$X_{i1} = |2E_bG_i + N_{i1}|^2 \tag{5.25}$$

$$X_{i2} = |N_{i2}|^2, \quad i = 1, \cdots, L \tag{5.26}$$

where E_b denotes the energy per bit, N_{i1} and $N_{i2}, i = 1, \cdots, L$ are i.i.d zero-mean complex Gaussian RVs with variance $4E_bN_0$ and $G_i, i = 1, \cdots, L$ denote the complex channel gains.

As discussed in Section 4.2, the receiver bases its decision on the decision statistics $X_i = X_{i1} - X_{i2}$, i.e., a summing process occurs on each diversity branch before data detection. The receiver will make an error if from the L statistics X_i, the one with the largest magnitude is negative. Therefore, we can write the average BER as

$$P_b = \sum_{i=1}^{L} \Pr\left(\max_{j\neq i} |X_j| < |X_i|, X_i < 0\right) \tag{5.27a}$$

$$= \sum_{i=1}^{L} \Pr\left(\max_{j\neq i} |X_j| + X_i < 0\right) \tag{5.27b}$$

$$= \sum_{i=1}^{L} F_{W_i}(0) \tag{5.27c}$$

where $W_i = X_i + Y_i$ and $Y_i = \max_{j\neq i} |X_j|$. The CDF of W_i, $F_{W_i}(w)$, calculated at $w = 0$ can be written as

$$F_{W_i}(0) = \int_{x=-\infty}^{\infty} \int_{y=-\infty}^{-x} f_{X_i,Y_i}(x, y) dy dx. \tag{5.28}$$

To continue, assume that the RVs X_i are independent given a RV Z. Then, because functions of independent RVs are also independent, we conclude that X_i and Y_i given Z are also independent RVs and thus, $f_{X_i,Y_i|Z}(x, y|z) = f_{X_i|Z}(x) f_{Y_i|Z}(y)$. Noting that $f_{X_i,Y_i}(x, y) = \int_0^{\infty} f_{X_i,Y_i|Z}(x, y) f_Z(z) dz$, we can write (5.28) as

$$F_{W_i}(0) = \int_{x=-\infty}^{\infty} \int_{y=-\infty}^{-x} \int_0^{\infty} f_{X_i|Z}(x) f_{Y_i|Z}(y) f_Z(z) dz dy dx \tag{5.29a}$$

$$= \int_0^{\infty} f_Z(z) \left(\int_{x=-\infty}^{\infty} f_{X_i|Z}(x) F_{Y_i|Z}(-x) dx \right) dz \tag{5.29b}$$

$$= \int_0^{\infty} f_Z(z) \left(\int_{x=0}^{\infty} f_{X_i|Z}(-x) F_{Y_i|Z}(x) dx \right) dz. \tag{5.29c}$$

Next, we calculate $F_{Y_i|Z}(x)$ as

$$F_{Y_i|Z}(x) = \prod_{\substack{j=1 \\ j\neq i}}^{L} \left(F_{X_j|Z}(x) - F_{X_j|Z}(-x)\right) \tag{5.30}$$

where we have used the fact that the RVs X_j are independent given Z. Combining (5.30) and (5.29c) and the result in (5.27c), we obtain the average BER of noncoherent BFSK with $S+N$ SC Model 2 as

$$P_b(E) = \sum_{i=1}^{L} \int_0^{\infty} \int_0^{\infty} \prod_{\substack{j=1 \\ j\neq i}}^{L} \left(F_{X_j|Z}(x) - F_{X_j|Z}(-x)\right) f_{X_i|z}(-x) f_Z(z) dx dz. \tag{5.31}$$

We now obtain analytical expressions for $F_{X_i|Z}(x)$, for the cases of Rayleigh and Rician fading channels. Using these expressions we can obtain analytical expressions for the average BER of noncoherent BFSK $S+N$ SC Model 2 in these fading scenarios.

5.2.1 Rayleigh Fading

In this case, using (5.11), we can write X_i as

$$\begin{aligned} X_i = &(2E_b\sqrt{\Omega_i}(\sqrt{1-\rho_i}U_i + \sqrt{\rho_i}U_0) + N_{i1}^I)^2 \\ &+ (2E_b\sqrt{\Omega_i}(\sqrt{1-\rho_i}V_i + \sqrt{\rho_i}V_0) + N_{i1}^Q)^2 - |N_{2i}|^2. \end{aligned} \tag{5.32}$$

As in the previous section, define $Z = U_0^2 + V_0^2$. Then, assuming Z is fixed, it is easy to see that X_i is the difference of a non-central and a central chi-squared RV. Using [13, eq. (51)], we can obtain the conditional CDF of X_i given Z as

$$F_{X_i|Z}(x) = \begin{cases} \Phi_1(\bar{\gamma}_i, \rho_i, z) \exp\left(\frac{x}{4E_bN_0}\right), & x < 0 \\ 1 - Q_1\left(\sqrt{\Phi_2(\bar{\gamma}_i, \rho_i, z)}, \sqrt{\dfrac{x}{2E_bN_0(1+(1-\rho_i)\bar{\gamma}_i)}}\right) & \\ +\Phi_1(\bar{\gamma}_i, \rho_i, z) \exp\left(\frac{x}{4E_bN_0}\right) \times & \\ Q_1\left(\sqrt{\Phi_3(\bar{\gamma}_i, \rho_i, z)}, \sqrt{\dfrac{\Phi_4(\bar{\gamma}_i, \rho_i, z)x}{4E_bN_0}}\right), & x > 0 \end{cases} \tag{5.33a}$$

where

$$\Phi_1(\bar{\gamma},\rho,z) = \frac{1}{2+(1-\rho)\bar{\gamma}}\exp\left(-\frac{\bar{\gamma}\rho z}{2+(1-\rho)\bar{\gamma}}\right) \tag{5.33b}$$

$$\Phi_2(\bar{\gamma},\rho,z) = \frac{2\rho\bar{\gamma}z}{(1+(1-\rho)\bar{\gamma})} \tag{5.33c}$$

$$\Phi_3(\bar{\gamma},\rho,z) = \frac{2\rho\bar{\gamma}z}{(1+(1-\rho)\bar{\gamma})(2+(1-\rho)\bar{\gamma})} \tag{5.33d}$$

$$\Phi_4(\bar{\gamma},\rho,z) = 2\frac{2+(1-\rho)\bar{\gamma}}{1+(1-\rho)\bar{\gamma}}. \tag{5.33e}$$

From (5.33), we obtain $f_{X_i|Z}(x)$ for negative arguments as

$$f_{X_i|Z}(x) = \frac{1}{4E_bN_0}\Phi_1(\bar{\gamma}_i,\rho_i,z)\exp\left(\frac{x}{4E_bN_0}\right), x<0. \tag{5.34}$$

Substituting (5.33) and (5.34) in (5.31), we obtain the average BER of BFSK with $S+N$ SC Model 2 as

$$\begin{aligned} P_b(E) = \sum_{i=1}^{L}\int_0^\infty\int_0^\infty \Phi_1(\bar{\gamma}_i,\rho_i,z) \\ \times\prod_{\substack{j=1\\ j\neq i}}^{L}\left\{1-Q_1\left(\sqrt{\Phi_2(\bar{\gamma}_j,\rho_j,z)},\sqrt{\frac{2x}{(1+(1-\rho_j)\bar{\gamma}_j}}\right)+\Phi_1(\bar{\gamma}_j,\rho_j,z)\exp(x)\right. \\ \left.\times Q_1\left(\sqrt{\Phi_3(\bar{\gamma}_j,\rho_j,z)},\sqrt{\Phi_4(\bar{\gamma}_j,\rho_j,z)x}\right)-\Phi_1(\bar{\gamma}_j,\rho_j,z)\exp(-x)\right\} \\ \times\exp(-x-z)dxdz. \end{aligned} \tag{5.35}$$

For dual-branch diversity, after many mathematical manipulations, a simple closed-form expression is derived for the average BER of noncoherent BFSK with $S+N$ SC Model 2 as

$$P_b(E) = \frac{8+5\bar{\gamma}_1+5\bar{\gamma}_2+3\bar{\gamma}_1\bar{\gamma}_2(1-\rho^2)}{(4+2\bar{\gamma}_1+2\bar{\gamma}_2+\bar{\gamma}_1\bar{\gamma}_2(1-\rho^2))^2}. \tag{5.36}$$

5.2.2 Rician Fading

Using the representation of the complex channel gains in (5.19), and assuming that $Z = (U_0 + m_1/\sqrt{\rho})^2 + (V_0 + m_2/\sqrt{\rho})^2$ is fixed, one can show, similar to the case of Rayleigh fading, that X_i conditioned on Z is the difference between a noncentral chi-squared and a noncentral chi-squared RV. Hence, using [13, eq. (51)], and after some mathematical manipulations, $F_{X_i|Z}(x)$ can be obtained as

$$F_{X_i|Z}(x) = \begin{cases} H_1(\bar{\gamma}, K, \rho, z) \exp\left(\frac{w}{4E_bN_0}\right), & x < 0 \\ 1 - Q_1\left(\sqrt{H_2(\bar{\gamma}, K, \rho, z)}, \sqrt{H_3(\bar{\gamma}, K, \rho)\frac{w}{2E_bN_0}}\right) & \\ + H_1(\bar{\gamma}, K, \rho, z) \exp\left(\frac{w}{4E_bN_0}\right) \times & \\ Q_1\left(\sqrt{H_4(\bar{\gamma}, K, \rho, z)}, \sqrt{H_5(\bar{\gamma}, K, \rho)\frac{w}{2E_bN_0}}\right), & x > 0 \end{cases} \tag{5.37a}$$

where

$$H_1(\bar{\gamma}, K, \rho, z) = \frac{1+K}{2(1+K) + \bar{\gamma}(1-\rho)} \exp\left(-\frac{\bar{\gamma}\rho(1+K)z}{2(1+K) + \bar{\gamma}(1-\rho)}\right) \tag{5.37b}$$

$$H_2(\bar{\gamma}, K, \rho, z) = \frac{2\bar{\gamma}\rho(1+K)z}{1+K+\bar{\gamma}(1-\rho)} \tag{5.37c}$$

$$H_3(\bar{\gamma}, K, \rho) = \frac{2(1+K)}{1+K+\bar{\gamma}(1-\rho)} \tag{5.37d}$$

$$H_4(\bar{\gamma}, K, \rho, z) = \frac{2\bar{\gamma}\rho(1+K)^2 z}{(1+K+\bar{\gamma}(1-\rho))(2(1+K)+\bar{\gamma}(1-\rho))} \tag{5.37e}$$

$$H_5(\bar{\gamma}, K, \rho) = \frac{2(2(1+K)+\bar{\gamma}(1-\rho))}{1+K+\bar{\gamma}(1-\rho)}. \tag{5.37f}$$

Note that because the branches are identically distributed $F_{X_i|Z}(x)$ does not depend on i. From (5.37), we obtain the conditional PDF of X_i given Z for negative arguments as

$$f_{X_i|Z}(x) = \frac{1}{4E_bN_0} H_1(\bar{\gamma}, K, \rho, z) \exp\left(\frac{w}{4E_bN_0}\right), \quad x < 0. \tag{5.38}$$

Substituting (5.37) and (5.38) in (5.31), The average BER of noncoherent BFSK with $S+N$ SC Model 2 in identically distributed equally correlated Rician fading is

obtained as

$$P_b(E) = L(K+1)\int_0^{\infty}\int_0^{\infty} H_1(\bar{\gamma},K,\rho,z)\Bigg[1 - Q_1\left(\sqrt{H_2(\bar{\gamma}_i,K,\rho,z)},\sqrt{H_3(\bar{\gamma},K,\rho)x}\right)$$
$$+ \exp(x)H_1(\bar{\gamma},K,\rho,z)Q_1\left(\sqrt{H_4(\bar{\gamma}_i,K,\rho,z)},\sqrt{H_5(\bar{\gamma},K,\rho)x}\right)$$
$$- H_1(\bar{\gamma},K,\rho,z)\exp(-x)\Bigg]^{L-1}\exp\left(-\frac{K}{\rho} - (K+1)z - x\right)$$
$$\times I_0\left(2\sqrt{\frac{K(K+1)z}{\rho}}\right)dxdz, \quad \rho > 0. \tag{5.39}$$

For $\rho = 0$, the average BER is given in [54, eq. (24)]. In the important case of dual-branch diversity, using [18, eqs. (B.27) and (B.31)] and similar to the procedure presented in the Appendix, (5.39) reduces to

$$P_b(E) = \frac{B_0 B_1}{B_1+2}\exp\left(-\frac{B_2}{B_1+2}\right) + \frac{B_3(4+2B_4-B_5)}{2B_5} \tag{5.40a}$$

where

$$B_0 = \frac{2(K+1)}{2K+2+\bar{\gamma}}\exp\left(-\frac{K\bar{\gamma}}{2K+2+\bar{\gamma}}\right) \tag{5.40b}$$
$$B_1 = \frac{2(K+1)(2K+2+\bar{\gamma})}{\bar{\gamma}^2(1-\rho^2)+3\bar{\gamma}(1+K)+2(1+K)^2} \tag{5.40c}$$
$$B_2 = \frac{2K\bar{\gamma}(2(1+K)+\bar{\gamma}(1-\rho))^2}{(2K+2+\bar{\gamma})(\bar{\gamma}^2(1-\rho^2)+3\bar{\gamma}(1+K)+2(1+K)^2)} \tag{5.40d}$$
$$B_3 = \frac{2(1+K)^2}{(2(1+K)+\bar{\gamma}(1+\rho))(2(1+K)+\bar{\gamma}(1-\rho))} \times \exp\left(-\frac{2K\bar{\gamma}}{2(K+1)+\bar{\gamma}(1+\rho)}\right) \tag{5.40e}$$
$$B_4 = \frac{2K\bar{\gamma}(K+1)(2(1+K)+\bar{\gamma}(1-\rho))}{(2(1+K)+\bar{\gamma}(1+\rho))(\bar{\gamma}^2(1-\rho^2)+3\bar{\gamma}(1+K)+2(1+K)^2)} \tag{5.40f}$$
$$B_5 = \frac{2(2(1+K)+\bar{\gamma}(1+\rho))(2(1+K)+\bar{\gamma}(1-\rho))}{\bar{\gamma}^2(1-\rho^2)+3\bar{\gamma}(1+K)+2(1+K)^2}. \tag{5.40g}$$

5.3 Numerical Examples

In this section, we give some numerical examples to show the effects of correlation, average fading power imbalance and fading parameter on the performance of $S+N$ SC receivers. Furthermore, we compare the performance of $S+N$ SC Model 1 and $S+N$ SC Model 2 to that of classical SC. Monte Carlo simulation results are presented to confirm the validity of our analytical expressions.

Fig. 5.1 shows the average BER of QFSK as a function of the average SNR per bit per branch of $S+N$ Model 1 and classical SC in equally correlated identically distributed Rician fading for $K=4$ and $\rho=0.5$ for several values of diversity order $L=2,4$ and 6. Fig. 5.1 shows that similar to the case of independent fading [54], the performance of $S+N$ SC is superior to the performance of classical SC for the range of SNR given. Also note that as the number of diversity branches increases, the performance gap between $S+N$ SC Model 1 and classical SC increases. For example, at an average BER of 10^{-4} the SNR gap between $S+N$ SC Model 1 and classical SC is 0.33 dB, 0.83 dB and 1.10 dB for $L=2,4$ and 6, respectively.

In Fig. 5.2, the effect of fading parameter on the relative performance of $S+N$ SC Model 1 is compared to that of classical SC in equally correlated Rician fading. Fig. 5.2 shows the average BER of QFSK with 3-branch diversity in equally correlated Rician fading for $K=0,5$ and $\rho=0.6$. It can be seen from Fig. 5.2 that the SNR gap between the two SC schemes increases as the channel becomes less faded. For example, for an average BER of 10^{-3} the SNR gap between $S+N$ SC Model 1 and classical SC is 0.56 dB, 0.69 dB and 1.17 dB for $K=0,5$ and 10, respectively.

In Fig. 5.3, the average BER of MFSK with $S+N$ SC and classical SC in Rayleigh fading is plotted as a function of the average SNR per bit of the first branch $\bar{\gamma}_1$ for an exponentially decaying multipath intensity profile ($\bar{\gamma}_i = \bar{\gamma}_1 \exp(-\beta(i-1))$, $i=$

$1, \cdots, L$ where β is the average power decay factor) for $\beta = 0.5$ and $[\rho_1, \cdots, \rho_4] = [0.3, 0.5, 0.7, 0.9]$. Both theoretical and simulation results are presented. The equation used to plot the curves for classical SC is

$$P_s(E) = \sum_{n=1}^{M-1} \binom{M-1}{n} \frac{(-1)^{n+1} n \log_2(M)}{(n+1)^2} \int_0^\infty \int_0^\infty \exp\left(-\frac{n \log_2(M)\gamma}{n+1} - t\right) \times \prod_{i=1}^{L} \left(1 - Q_1\left(\sqrt{\frac{2\rho_i t}{1-\rho_i}}, \sqrt{\frac{2\gamma}{\bar{\gamma}_i(1-\rho_i)}}\right)\right) d\gamma dt. \tag{5.41}$$

Note that eq. (5.41) is derived using similar techniques to that of [43] and generalizes the result given in [43, eq. (23)] for Rayleigh fading to include the effect of average fading power imbalance. Fig. 5.3 indicates that the performance gap between $S + N$ SC Model 1 and classical SC remains almost constant for different values of modulation order.

Fig. 5.4 shows the average BER of 4-branch QFSK with $S + N$ SC Model 1 and classical SC in correlated Rayleigh fading for several values of average decay factor $\beta = 0, 0.5$ and 1 with $[\rho_1, \cdots, \rho_4] = [0.3, 0.5, 0.7, 0.9]$. Note that the performance of classical SC relative to the performance of $S + N$ SC is a function of the average decay factor. For example, while for $\beta = 0$, $S + N$ SC outperforms classical SC for the range of SNR given, for $\beta = 1$, classical SC outperforms $S + N$ SC for the range of 0 to 10 dB. This phenomena can be explained as follows. When the average SNR is small, the noise term is dominant and the $S + N$ SC receiver is practically choosing the branch that is mostly affected by noise and thus its performance is inferior to the classical SC receiver which selects the branch with the largest SNR. However, when the SNR is large, the $S + N$ SC receiver yields a better error performance than that of the classical SC receiver because with the former system there is opportunity for at least one sample to be better (less noisy) than the average of the samples [7]. Notice that for $\beta = 0$, $S + N$ SC outperforms classical SC in the range of SNR given but as

the channel becomes more faded (β increases) and for small SNR, the noise term is again dominant and the $S+N$ SC receiver is more likely to make errors compared to the classical SC receiver.

In Fig. 5.5, the average BER of BFSK with $S+N$ SC Model 1 is compared to the average BER of $S+N$ SC Model 2 in correlated Rayleigh fading for $L=3$, $[\rho_1, \rho_2, \rho_3] = [0.55, 0.85, 0.25]$ and for several values of the average decay factor $\beta = 0, 0.6$ and 1.2. The analytical and simulation results are in excellent agreement. Fig. 5.5 shows that the average SNR difference between $S+N$ SC Model 1 and $S+N$ SC Model 2 does not change significantly with β at small average BERs. However, at large average BERs the difference in the average SNR between the two receivers is larger for smaller values of β.

In Fig. 5.6, the performances of 4-branch BFSK with $S+N$ SC Model 1 and Model 2 are compared to the performance of classical SC in equally correlated Rician fading with $K=5$ and for several values of $\rho = 0.2, 0.4$ and 0.6. Fig. 5.6 shows that $S+N$ SC Model 2 outperforms both $S+N$ SC Model 1 and classical SC. Fig. 5.6 also shows that the performance gap between $S+N$ SC Model 1 and $S+N$ SC Model 2 increases as ρ increases. For example, at an average BER of 10^{-4}, the SNR difference between $S+N$ SC Model 1 and $S+N$ SC Model 2 is 0.16 dB, 0.65 dB and 0.99 dB for $\rho = 0.2$, 0.4 and 0.6, respectively. The SNR difference between classical SC and $S+N$ SC Model 1 and Model 2 also increases as the correlation among the diversity branches increases. For example, for an average BER of 10^{-4}, the SNR difference between $S+N$ SC Model 2 and classical SC is 1.17 dB, 1.38 dB and 1.56 dB for $\rho = 0.2, 0.4$ and 0.6, respectively.

Finally, in Fig. 5.7 the average BER of BFSK with classical SC, $S+N$ SC Model 1 and $S+N$ SC Model 2 is plotted as a function of average SNR per bit per branch

in equally correlated Rician fading with $K = 10$ and $\rho = 0.6$ for several values of $L = 2, 3$ and 4. Fig. 5.7 shows that the average SNR gap between classical SC with $S+N$ SC Model 1 and Model 2 increases as L increases. For example, for an average BER of 10^{-4} the SNR difference between $S+N$ SC Model 2 and classical SC is 1.44 dB, 2.06 dB and 2.43 dB for $L = 2$, 3 and 4, respectively. Fig. 5.7 also shows that the SNR gap between $S+N$ SC Model 2 and $S+N$ SC Model 1 increases as L increases.

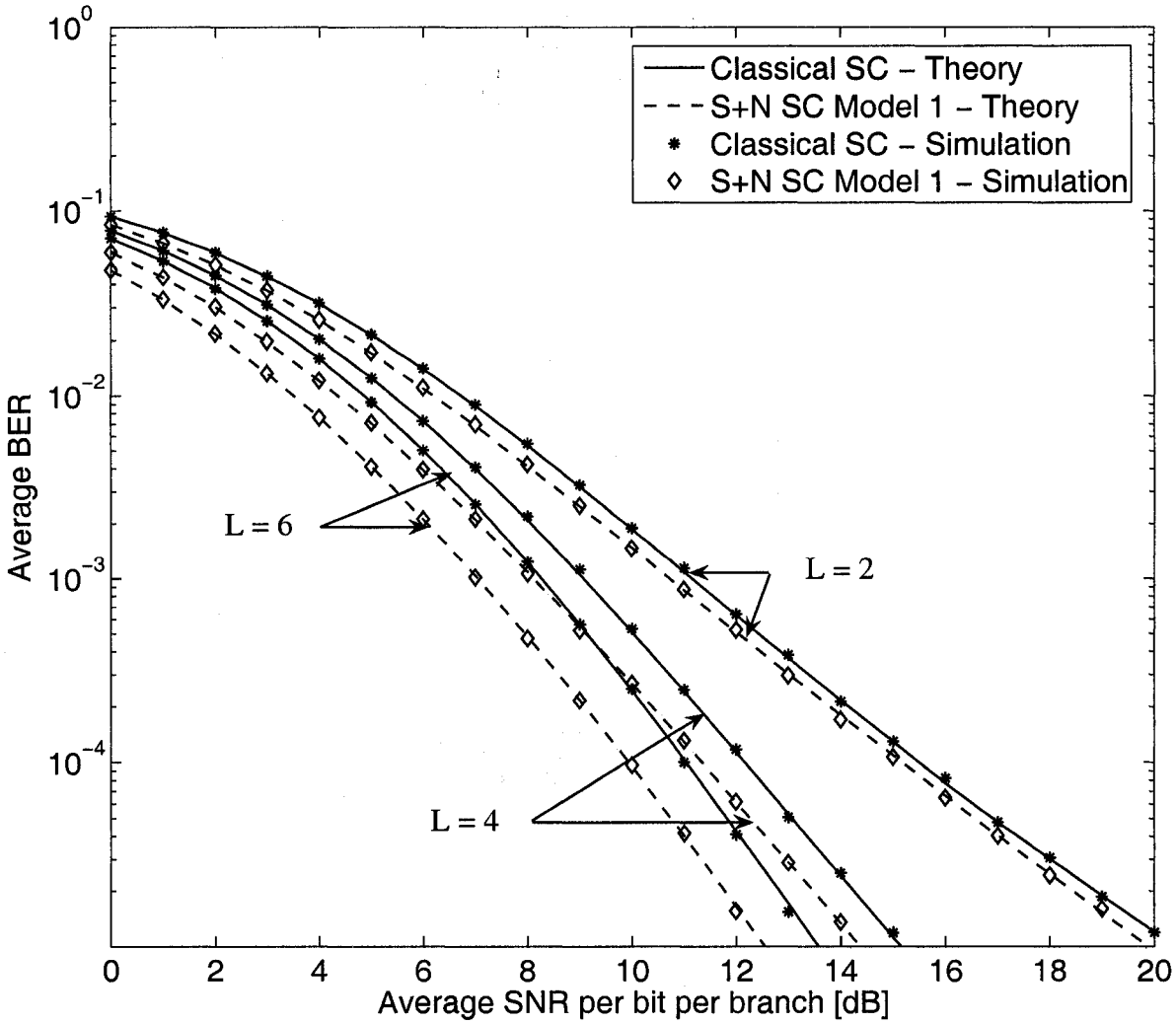

Figure 5.1: The average BER of QFSK with $S + N$ SC Model 1 and classical SC as a function of average SNR per bit per branch in equally correlated identically distributed Rician fading for $K = 4$, $\rho = 0.5$ and $L = 2, 4$ and 6.

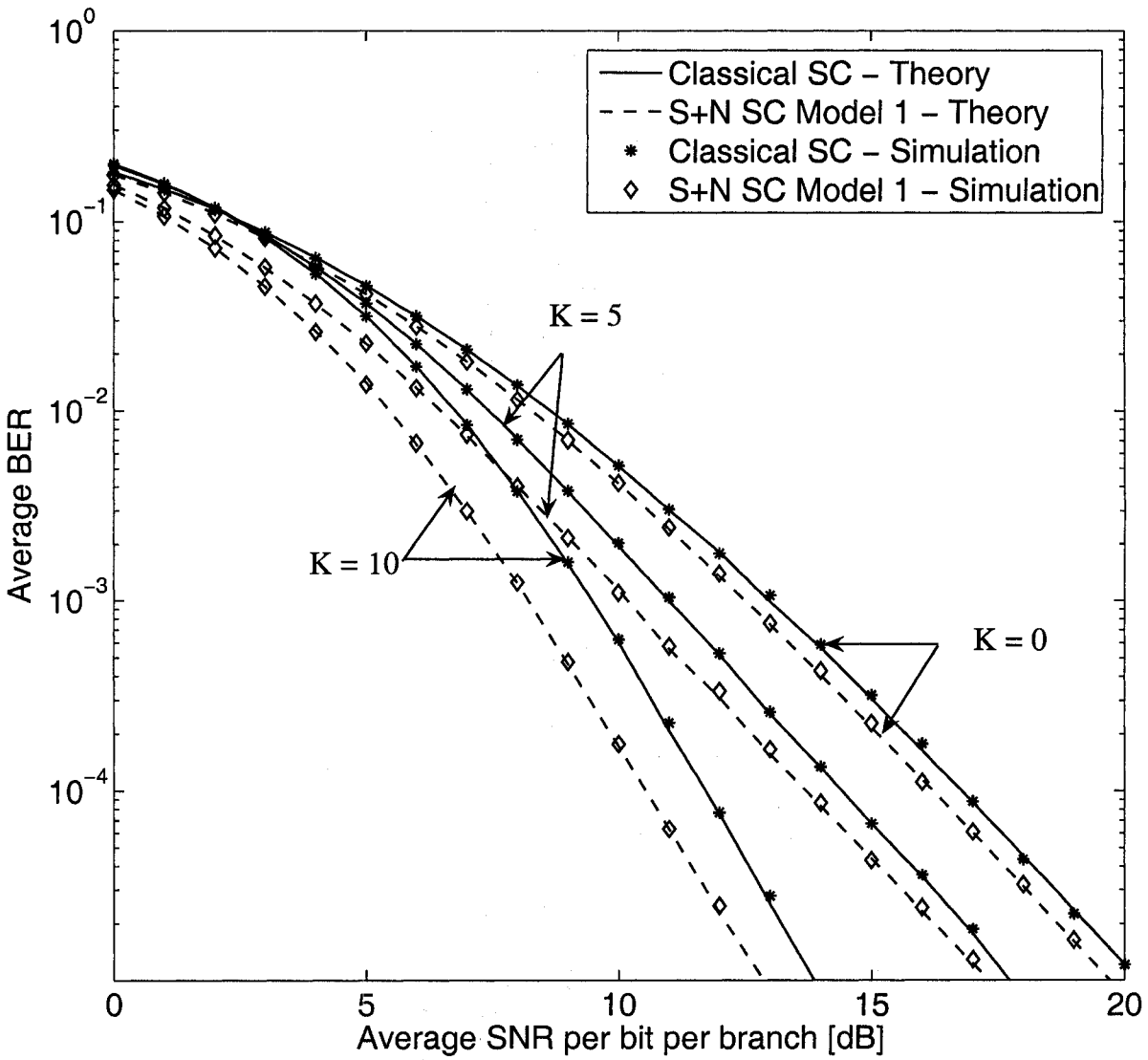

Figure 5.2: The average BER of QFSK with $S+N$ SC Model 1 and classical SC as a function of average SNR per bit per branch in equally correlated Rician fading for $K = 0, 5, 10$ and $\rho = 0.6$.

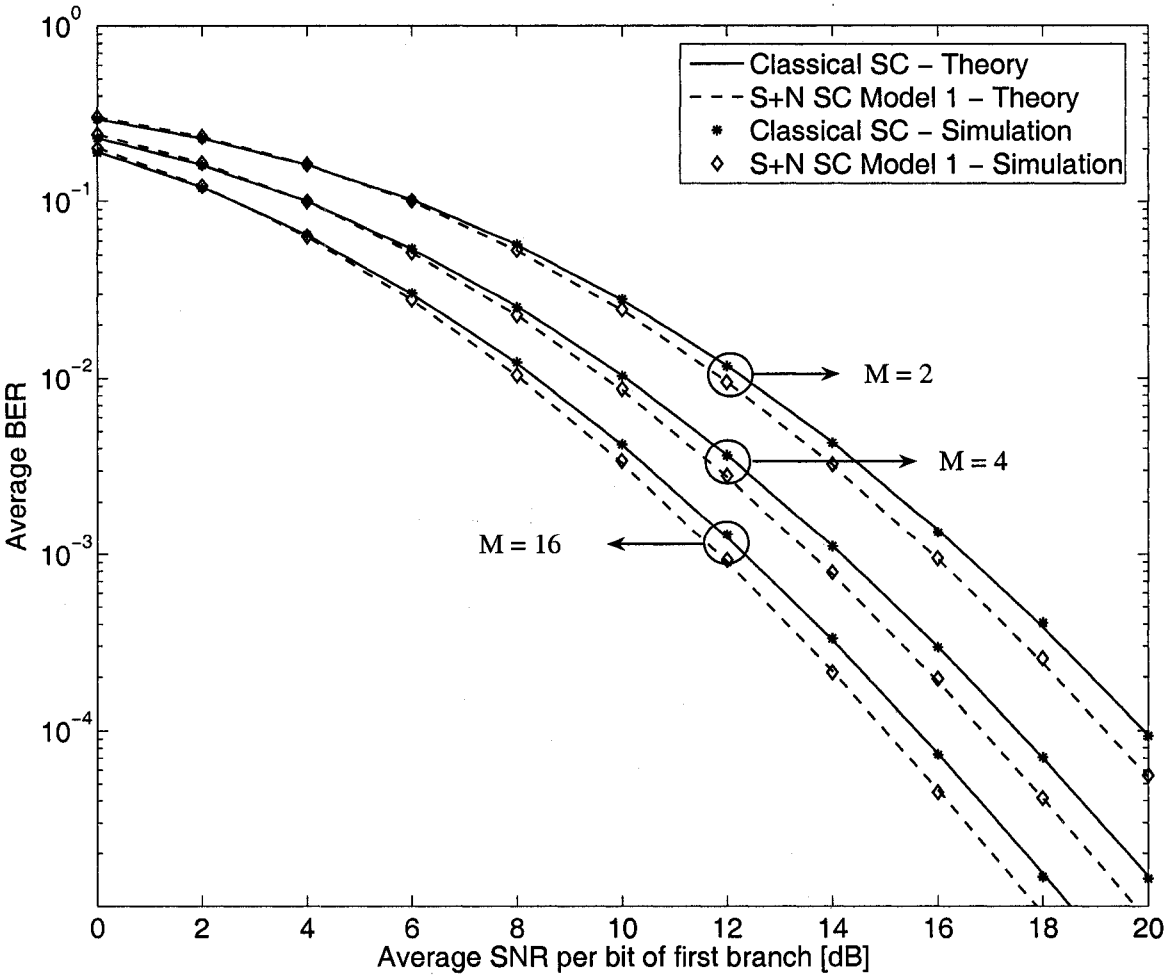

Figure 5.3: The average BER of 4-branch MFSK with $S+N$ SC Model 1 and classical SC as a function of average SNR per bit per branch in correlated Rayleigh fading with $M = 2, 4$ and 16.

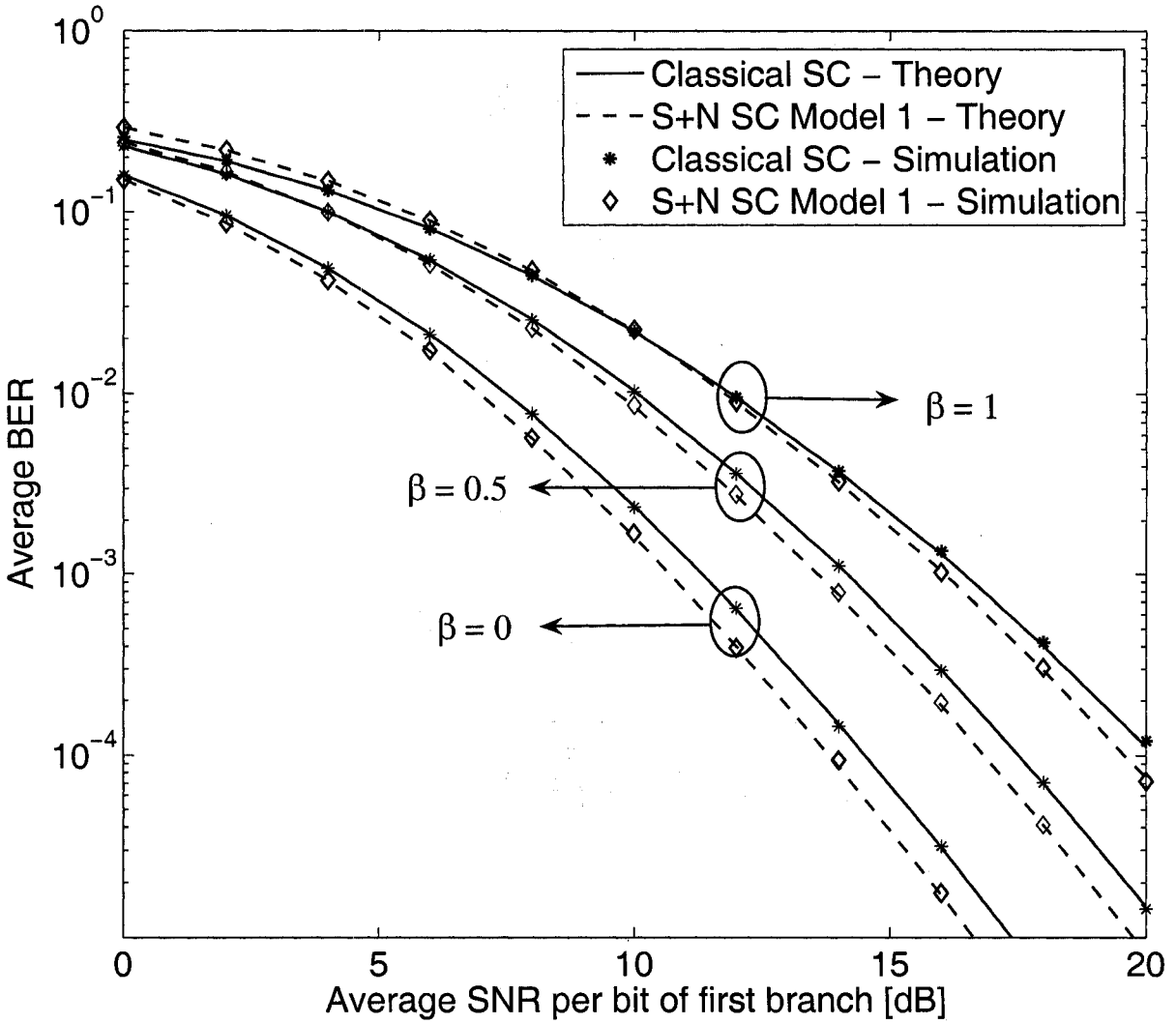

Figure 5.4: The average BER of QFSK with $S+N$ SC Model 1 and classical SC as a function of the average SNR per bit of the first branch in correlated Rayleigh fading with $\beta = 0, 0.5$ and 1.

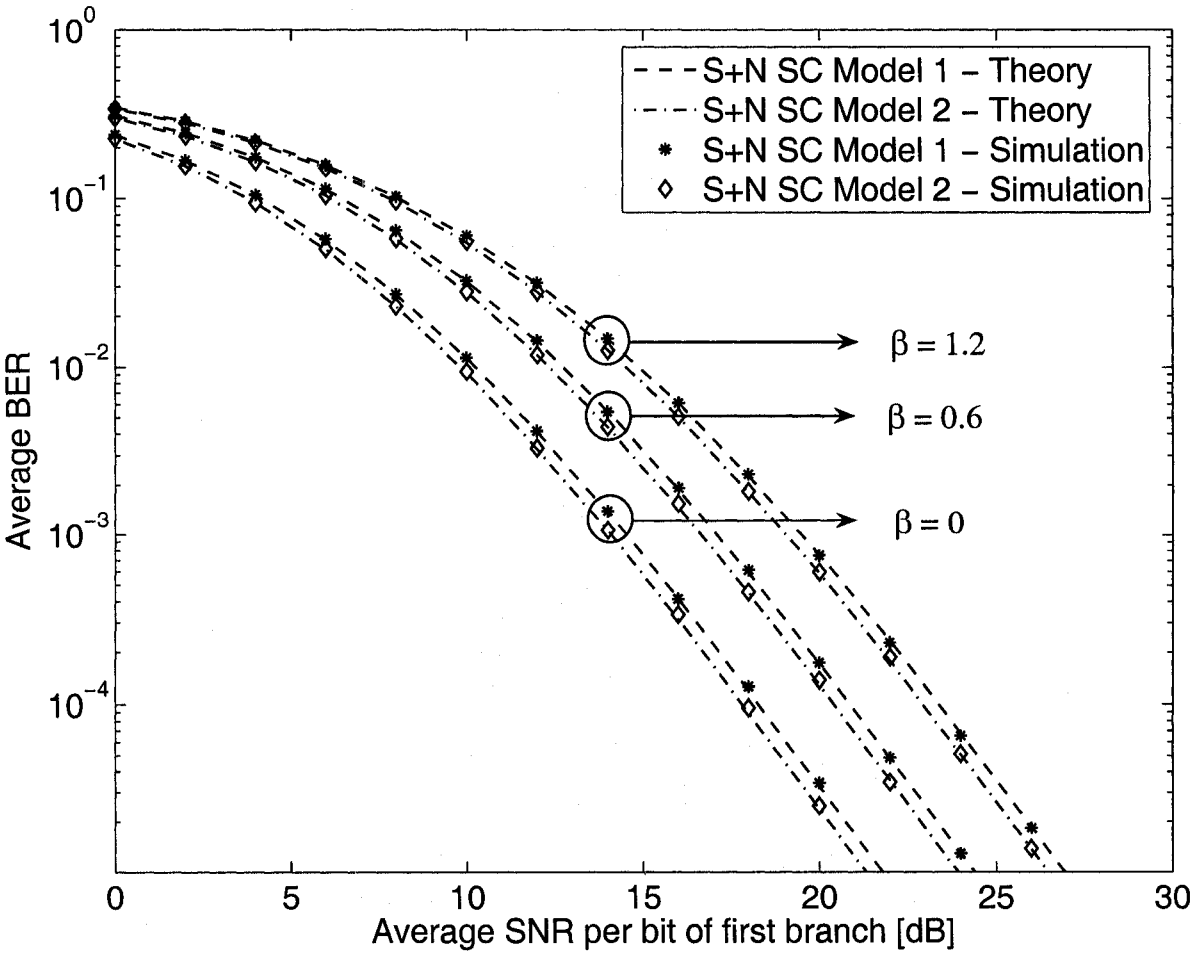

Figure 5.5: The average BER of 3-branch BFSK with $S+N$ SC Model 1 and $S+N$ SC Model 2 in correlated Rayleigh fading for several values of average decay factor $\beta = 0, 0.6$ and 1.2.

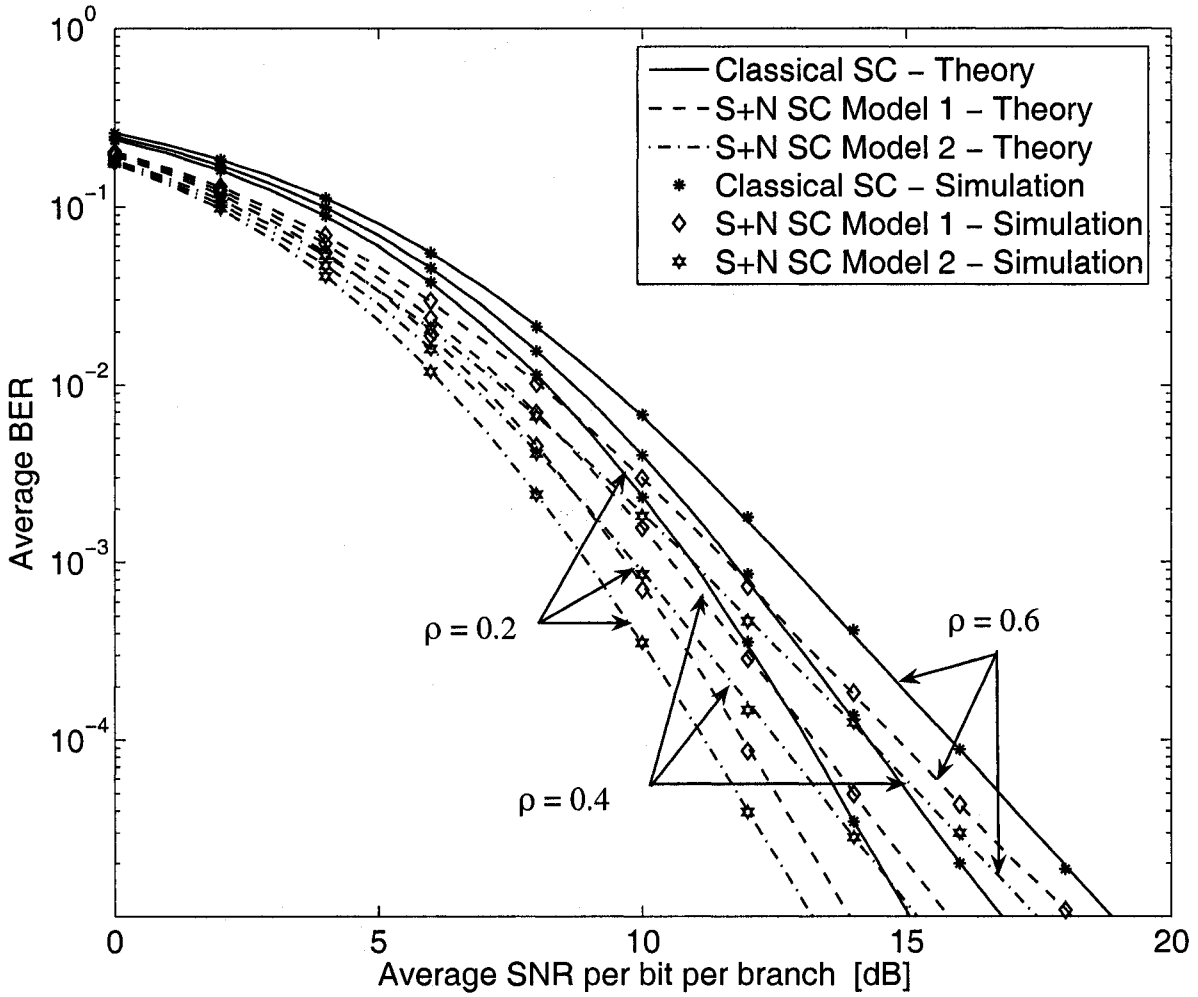

Figure 5.6: The average BER of 4-branch BFSK with $S+N$ SC Model 1, $S+N$ SC Model 2 and classical SC as a function of average SNR per bit per branch in equally correlated Rician fading with $K = 5$ and $\rho = 0.2, 0.4$ and 0.6

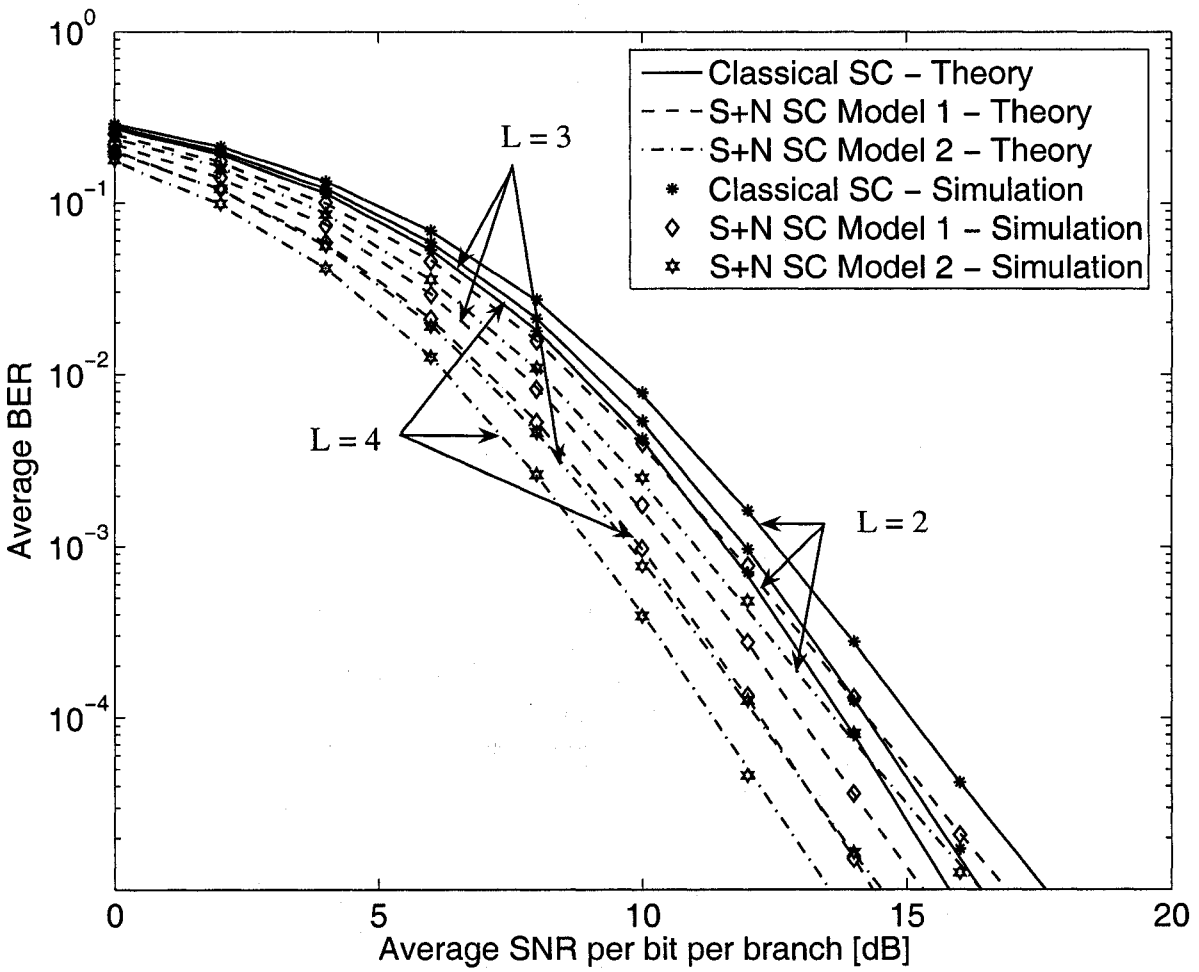

Figure 5.7: The average BER of 2-, 3-, and 4-branch BFSK with classical SC, $S+N$ SC Model 1 and $S+N$ SC Model 2 as a function of average SNR per bit per branch in equally correlated Rician fading with $K = 10$ and $\rho = 0.6$.

5.4 Conclusion

The performances of two $S + N$ SC receivers in correlated Rayleigh fading for a particular correlation structure and in equally correlated Rician fading were analyzed. For each receiver structure, analytical expressions were derived for the average BER. The performances of $S + N$ SC Model 1 and Model 2 receivers were compared to classical SC and the impacts of correlation, modulation order, fading parameter, fading factor and number of diversity branches on the relative performances of $S+N$ SC receivers were studied. It was shown that for Rayleigh fading and with average fading power imbalance, classical SC outperforms $S+N$ SC for small values of average SNR.

Chapter 6

On Decorrelation in Dual-Branch Diversity Systems

6.1 Introduction

It is well known that correlation between the branches of a dual diversity system has a deleterious effect on the performances, outage and average error rate, of the diversity system [32], [55], [56]. Meanwhile, space restrictions may dictate that only correlated diversity branches are available in an application; this is particularly true for a handheld wireless unit. In these cases, correlated dual branches are employed for the gains they provide over a single branch system, even though the gains are reduced relative to independent dual branches. Decorrelation of the correlated branches might be considered to improve the diversity receiver performance. However, results in [57] show that there is no benefit gained from decorrelating correlated branches in an optimal maximal ratio combining (MRC) diversity system . The question remains as to whether the performances of other diversity combining schemes such as selection combining (SC), switch-and-stay combining (SSC), square-law combining (SLC) and equal gain combining (EGC) can be improved by employing decorrelation. In

this regard, complexity plays a crucial role. In general, performing a decorrelation of correlated diversity branches requires complex measurement of channel state information for the diversity branches in order to determine the parameters needed to implement complex matrix transformations to effect the decorrelation. Overall, the system becomes more complex than a MRC diversity system, requiring more channel estimation and more signal processing than an optimal MRC system. Thus, MRC is simply to be preferred and decorrelation is impractical.

In the special case of dual diversity, however, decorrelation can be easily and economically implemented using simple addition and subtraction of the correlated signals without any channel state information, regardless of the value of the correlation coefficient between the branches, provided that the channels have the same average power. If the fading is Rician, or complex Gaussian, the decorrelated branches are independent branches, albeit of different mean powers. The addition of simple, economical adder circuits as signal pre-processing ahead of SC, SSC or EGC diversity combining is both practical and consistent with the otherwise simple and economical implementations of these diversity combining schemes. In this chapter, we examine the use of decorrelation pre-processing with SC, SSC and EGC diversity schemes. The results will show that in the case of dual branch diversity with branches of equal mean powers, decorrelation pre-processing offers worthwhile performance enhancement at little additional cost for SC and SSC diversity systems, but has no value in MRC, EGC and SLC systems.

Many researchers have analyzed the performance of dual-branch diversity systems in independent and correlated fading channels employing several combining schemes such as MRC, EGC, SC and SSC [32], [55], [56], [58]- [67]. The performance of coherent as well as noncoherent and differentially coherent modulation methods have

been analyzed in dual-branch diversity systems. For example, Simon and Alouini presented a unified performance analysis of digital communication systems with dual-branch selective combining diversity over correlated Rayleigh and Nakagami-m fading channels [55]. In this chapter, we propose a simple decorrelator dual-branch diversity receiver structure and we show that the performance of this receiver with SC and SSC is superior to the performance of a conventional SC and SSC receiver, respectively, in correlated Rician and Rayleigh fading.

We assume that the branches have the same average fading power and the branches are generally correlated with correlation coefficient ρ. Slow, flat fading is assumed. In the decorrelator receiver the branches are first decorrelated and then diversity combining is performed on the decorrelated branches. It is shown that to decorrelate the incoming signals, the receiver does not need any information about the signals and the decorrelation can be easily done by adding and subtracting the signals on the two diversity branches. Important performance measures such as the mean output signal-to-noise ratio (SNR), outage probability, average symbol error rate (SER) and average bit error rate (BER) of several modulation schemes of practical interest are computed for each combiner. The performance of the decorrelator diversity receiver with SC and SSC is compared to the performance of the conventional SC and SSC receiver, respectively, and it is shown that the decorrelator receiver has superior performance in terms of the average BER, outage probability and mean output SNR. For example, for binary phase shift keying (BPSK) and at an average BER of 10^{-4}, the SNR improvement of the decorrelator receiver over the conventional receiver is as much as 2.1 dB in correlated Rician fading. The effects of modulation order, correlation and the severity of fading on the relative performances of the conventional and the decorrelator receivers are examined. We note that using the results of [57],

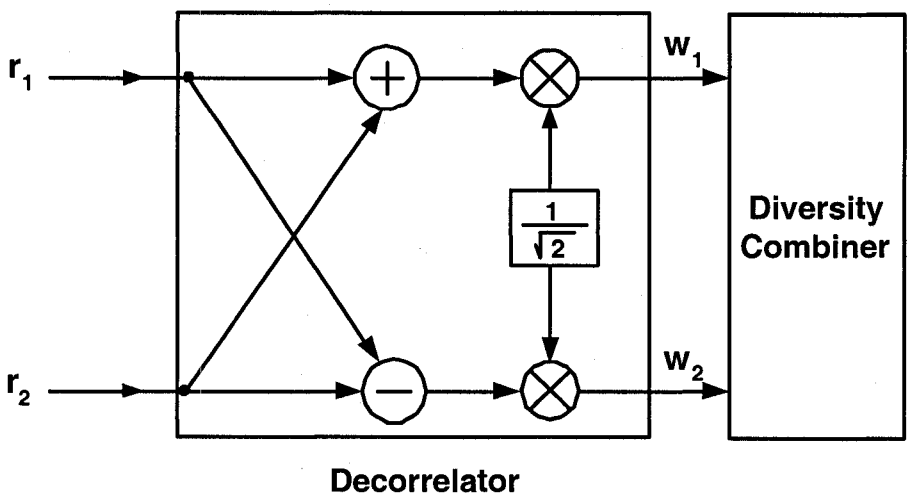

Figure 6.1: The structure of the dual-branch decorrelator receiver.

one can show that the performance of the decorrelator receiver and the conventional receiver with MRC are identical. In this paper we show that the performance of the decorrelator receiver and the conventional receiver are also equivalent when SLC is employed at the receiver. For EGC, we show that the performance of the decorrelator receiver is inferior to the performance of the conventional receiver.

The remainder of this chapter is organized as follows. The system model is presented in Section 6.2. The performances of the decorrelator receiver with SC and SSC are discussed in Sections 6.3 and 6.4, respectively. In Section 6.5, it is proven that the performance of the decorrelator and the conventional receiver with SLC is identical. The performances of the two receivers with EGC are compared in Section 6.6. In Section 6.7, some numerical examples are presented and the performances of the conventional and the decorrelator receiver are compared. Finally, some conclusions are given in Section 6.8.

6.2 System Model

The structure of the decorrelator receiver is shown in Fig. 6.1. Let r_1 and r_2 denote the received base-band equivalent signal samples at the first and second branch, respectively, given by

$$r_1 = G_1 x + N_1 \tag{6.1}$$

$$r_2 = G_2 x + N_2. \tag{6.2}$$

In (6.1) and (6.2) x is the data symbol sample, $G_i, i = 1, 2$ are the complex channel gains and $N_i, i = 1, 2$ are independent complex additive white zero-mean Gaussian noise samples with variance $N_0/2$ per dimension. We assume that the fadings on the branches are identically distributed and the instantaneous and average signal-to-noise ratios on each branch are given by γ and $\bar{\gamma}$, respectively.

Let the fadings on the branches be slow and frequency flat Rician, correlated with correlation coefficient ρ. It is useful in the subsequent development to represent the channel gains as (3.28), which we repeat here for the sake of completeness as

$$G_i = \sqrt{1-\rho} X_i + \sqrt{\rho} X_0 + \nu_1 + j(\sqrt{1-\rho} Y_i + \sqrt{\rho} Y_0 + \nu_2), \quad i = 1, 2 \tag{6.3}$$

where $0 \leq \rho < 1$ and X_i and Y_i are independent zero-mean Gaussian RVs with variance $\sigma^2 = \Omega/(2(K+1))$, and where $K = (\nu_1^2 + \nu_2^2)/(2\sigma^2)$ is the Rician factor. Signal samples r_1 and r_2 are input to the decorrelator. The outputs of the decorrelator, denoted as w_1 and w_2, are given by

$$w_1 = \frac{r_1 + r_2}{\sqrt{2}} = \frac{G_1 + G_2}{\sqrt{2}} x + \frac{N_1 + N_2}{\sqrt{2}} \triangleq \Delta_1 x + v_1 \tag{6.4}$$

$$w_2 = \frac{r_1 - r_2}{\sqrt{2}} = \frac{G_1 - G_2}{\sqrt{2}} x + \frac{N_1 - N_2}{\sqrt{2}} \triangleq \Delta_2 x + v_2. \tag{6.5}$$

Since g_1 and g_2 are complex Gaussian RVs, one can see from the definition of Δ_1 and Δ_2 that these are also complex Gaussian RVs. Furthermore, one can show that

Δ_1 and Δ_2 are uncorrelated and thus independent. Similarly, one can prove that the noise terms v_1 and v_2 are mutually independent Gaussian RVs with variance $N_0/2$ per dimension. Furthermore, it can easily be shown that the noise components v_1 and v_2 are independent of each other and also independent of the signal components in w_1 and w_2. Thus, the decorrelator transforms the two correlated branches into two independent branches. The outputs of the decorrelator are input into a diversity combiner. In the sequel, we analyze the performance of the decorrelator receiver in conjunction with SC and SSC. Important performance measures such as the mean output SNR, outage probability and average SER and average BER of several modulation formats are examined.

6.3 Selection Combining

In selection combining the branch with the largest SNR is chosen for data detection. Let γ_1 and γ_2 denote the instantaneous SNR for w_1 and w_2, respectively. Then, one can show that the CDF of γ_1 and γ_2 are given by

$$F_{\gamma_1}(x) = \left(1 - Q_1\left(\sqrt{\frac{4K}{1+\rho}}, \sqrt{\frac{2(1+K)x}{\bar{\gamma}(1+\rho)}}\right)\right) \tag{6.6}$$

and

$$F_{\gamma_2}(x) = 1 - \exp\left(-\frac{(1+K)x}{\bar{\gamma}(1-\rho)}\right) \tag{6.7}$$

respectively. Examination of (6.6) shows that (6.4) corresponds to a Rician faded branch with average fading power

$$\bar{\gamma}(1+\rho+2K)/(1+K) \tag{6.8}$$

and Rician factor $2K/(1+\rho)$. Similarly, one can see from (6.7) that (6.5) corresponds to a Rayleigh faded branch with average fading power

$$\bar{\gamma}(1-\rho)/(1+K). \tag{6.9}$$

6.3.1 Output SNR CDF

Noting that the two branches after decorrelation are independent, the CDF of the output SNR can be written as the product of the CDF of the SNRs of the individual branches. Thus, using (6.6) and (6.7), the CDF of the decorrelator receiver with SC, $F_{\gamma_{SC}}(x)$, can be calculated as

$$F_{\gamma_{SC}}(x) = \left(1-\exp\left(-\frac{(1+K)x}{\bar{\gamma}(1-\rho)}\right)\right)\left(1-Q_1\left(\sqrt{\frac{4K}{1+\rho}},\sqrt{\frac{2(1+K)x}{\bar{\gamma}(1+\rho)}}\right)\right). \tag{6.10}$$

6.3.2 Output SNR PDF

Differentiating (6.10) with respect to x, using (3.59) and after some algebraic simplifications, the PDF of the output SNR is obtained as

$$\begin{aligned} f_{\gamma_{SC}}(x) = {} & \frac{(1+K)}{\bar{\gamma}(1-\rho)}\exp\left(-\frac{(1+K)x}{\bar{\gamma}(1-\rho)}\right)\left(1-Q_1\left(\sqrt{\frac{4K}{1+\rho}},\sqrt{\frac{2(1+K)x}{\bar{\gamma}(1+\rho)}}\right)\right) \\ & + \frac{1+K}{\bar{\gamma}(1+\rho)}\left(1-\exp\left(-\frac{(1+K)x}{\bar{\gamma}(1-\rho)}\right)\right)\exp\left(-\frac{2K}{1+\rho}-\frac{(1+K)x}{\bar{\gamma}(1+\rho)}\right) \\ & \times I_0\left(\sqrt{\frac{8K(1+K)x}{\bar{\gamma}(1+\rho)^2}}\right). \end{aligned} \tag{6.11}$$

6.3.3 Output SNR MGF

A closed-form expression for the MGF of γ_{SC} can be obtained as

$$\begin{aligned} \Phi_{SC}(s) = {} & \frac{1+K}{1+K-s\bar{\gamma}(1+\rho)}\exp\left(\frac{2K\bar{\gamma}s}{1+K-s\bar{\gamma}(1+\rho)}\right) \\ & + \frac{\bar{\gamma}s(1-\rho)^2(1+K)}{(2+2K-s\bar{\gamma}(1-\rho^2))(1+K-s\bar{\gamma}(1-\rho)}\exp\left(-\frac{2K(1+K-s\bar{\gamma}(1-\rho))}{2+2K-s\bar{\gamma}(1-\rho^2)}\right). \end{aligned} \tag{6.12}$$

6.3.4 Mean Output SNR

The average output SNR can be obtained from the MGF using

$$\bar{\gamma}_{\text{SC}} = \frac{d\Phi_{\text{SC}}(s)}{ds}\Big|_{s=0}. \tag{6.13}$$

Substituting (6.12) in (6.13) and after some mathematical simplifications, we obtain the average output SNR as

$$\bar{\gamma}_{\text{SC}} = \frac{\bar{\gamma}(1+\rho+2K)}{1+K} + \frac{\bar{\gamma}(1-\rho^2)}{2(1+K)}\exp(-K). \tag{6.14}$$

For conventional dual-branch SC, similar to the procedure in [20, Section V.C], the mean output SNR in correlated Rician fading can be calculated as a two-dimensional integral given by

$$\begin{aligned}\bar{\gamma}_{\text{SC}} = {} & \frac{2(1+K)}{\bar{\gamma}(1-\rho)}\exp\left(-\frac{K}{\rho}\right)\int_0^\infty\int_0^\infty x\left(1-Q_1\left(\sqrt{\frac{2\rho y}{1-\rho}},\sqrt{\frac{2(1+K)x}{\bar{\gamma}(1-\rho)}}\right)\right) \\ & \times\exp\left(-\frac{(1+K)x}{\bar{\gamma}(1-\rho)}-\frac{\rho+1}{\rho-1}y\right)I_0\left(\sqrt{\frac{4\rho(1+K)}{\bar{\gamma}(1-\rho)^2}}\right)I_0\left(\sqrt{\frac{4Ky}{\rho}}\right)dxdy.\end{aligned} \tag{6.15}$$

Note that one can easily calculate the double integral in (6.15) using the Gauss-Laguerre formula [68].

6.3.5 Average Error Rate

One could either use

$$P_e = \int_0^\infty P_s(e|\gamma)f_{\gamma_{\text{SC}}}(\gamma)d\gamma. \tag{6.16}$$

or

$$P_s = -\int_0^\infty P_s'(e|\gamma)F_{\gamma_{\text{SC}}}(\gamma)d\gamma \tag{6.17}$$

to calculate the average SER of various modulation techniques. However, because (6.10) is more compact than (6.11), we use (6.17) to calculate the average SER of

various modulation formats in the sequel. We note that, one could also use the MGF-based approach given in [12] to derive the average SER. As shown in [12] the main step in using the MGF-based approach is expressing the MGF of the combiner output in a form that is both simple and suitable for single integration. Since the MGF of the output combiner has been already derived in (6.12), we can use it to obtain the average SER using the methodology given in [12]. In the sequel, we use (6.17) and the MGF-based approach to derive the average SER of various modulation techniques of practical interest.

1) For coherent BFSK and MPAM the static SER is given in (2.19). Substituting (2.19) in (6.17), the average SER becomes

$$P_s = \frac{a\sqrt{b}}{2\sqrt{2\pi}} \int_0^\infty \frac{1}{\sqrt{\gamma}} \exp\left(-\frac{1}{2}b\gamma\right) F_{\gamma_{SC}}(\gamma) d\gamma. \tag{6.18}$$

where $(a, b) = (1, 2)$ for BPSK, $(a, b) = (1, 1)$ for coherent BFSK and $(a, b) = (2(M-1)/M, 6/(M^2-1))$ for MPAM.

2) For QPSK, MQAM, MSK and coherently detected DPSK, the static SER is given in (2.21). Substituting (2.21) in (6.17), we obtain the average SER as

$$P_s = \sqrt{\frac{b}{2\pi}} \int_0^\infty \frac{1}{\sqrt{\gamma}} \exp\left(-\frac{1}{2}b\gamma\right) \left(\frac{a}{2} - cQ\left(\sqrt{b\gamma}\right)\right) F_{\gamma_{SC}}(\gamma) d\gamma. \tag{6.19}$$

where $(a, b, c) = (2, 2, 1)$ for 4PSK or MSK, $(a, b, c) = (2, 2, 2)$ for coherently detected DPSK and $(a, b, c) = (\frac{4(\sqrt{M}-1)}{\sqrt{M}}, \frac{3\log_2 M}{M-1}, \frac{4(\sqrt{M}-1)^2}{M})$ for MQAM. Substituting (2.21) in (6.17), we obtain the average SER as

3) For $\pi/4$-QDPSK and noncoherent correlated BFSK, the static SER is given in (2.23). Substituting (2.23) in (6.17), the average SER in this case can be obtained using

$$P_s = \frac{a^2 - b^2}{4} \int_0^\infty \exp\left(-\frac{(a^2+b^2)\gamma}{2}\right) I_0(ab\gamma) F_{\gamma_{SC}}(\gamma) d\gamma. \tag{6.20}$$

where $(a,b) = (\sqrt{2-\sqrt{2}}, \sqrt{2+\sqrt{2}})$ and $(a,b) = (\sqrt{\frac{1-\sqrt{1-\lambda^2}}{2}}, \sqrt{\frac{1-\sqrt{1+\lambda^2}}{2}})$ for $\pi/4$-DQPSK and noncoherent correlated BFSK, respectively, and where λ is the correlation between the binary signals in noncoherent correlated BFSK.

Alternatively, using the MGF-based method, the average SER can be obtained by calculating

$$P_s = \frac{1}{4\pi}\int_{-\pi}^{\pi} \Phi_{\text{SC}}\left(-\frac{b^2(1-\zeta)^2}{2(1+2\zeta\sin(\theta)+\zeta^2)}\right)d\theta \tag{6.21}$$

where $\zeta = a/b$.

4) Using the MGF-based approach, the average SER of MFSK can be obtained as

$$P_s = \sum_{n=1}^{M-1} \frac{(-1)^{n+1}\binom{M-1}{n}}{n+1}\Phi_{\text{SC}}\left(\frac{n}{n+1}\right). \tag{6.22}$$

Again, using the MGF-based approach, one can derive the average BER of noncoherent BPSK and DBPSK as

$$P_s = a\Phi_{\text{SC}}(b) \tag{6.23}$$

where $(a,b) = (1/2, 1/2)$ for noncoherent BPSK and $(a,b) = (1/2, 1)$ for DBPSK, respectively.

6.3.6 Outage Probability

The outage probability, P_{out}, is the probability that the instantaneous output SNR falls below a given threshold γ_{th} and is given by

$$P_{\text{out}} = \Pr(\gamma_{\text{SC}} < \gamma_{th}) = F_{\gamma_{\text{SC}}}(\gamma_{th}). \tag{6.24}$$

Using (6.10), the outage probability can be easily computed as

$$P_{\text{out}} = \left(1-\exp\left(-\frac{(1+K)\gamma_{th}}{\bar{\gamma}(1-\rho)}\right)\right)\left(1-Q_1\left(\sqrt{\frac{4K}{1+\rho}}, \sqrt{\frac{2(1+K)\gamma_{th}}{\bar{\gamma}(1+\rho)}}\right)\right). \tag{6.25}$$

The results in this section will be used to examine the performance of dual selection combining with decorrelation in Section 6.4.

6.4 Switch-and-Stay Combining

The structure of the SSC receiver was introduced in Section 2.2. Similar to Section 2.2, we denote the output SNR of the SSC receiver at time $t = nT$ as γ_{SSC}. Then, $\gamma_{\text{SSC}}(n)$ can be written as [17, eq. (3)]

$$\gamma_{\text{SSC}}(n) = \gamma_1(n) \text{ iff} \begin{cases} \gamma_{\text{SSC}}(n-1) = \gamma_1(n-1) & \gamma_1(n) \geq \gamma_T \\ \gamma_{\text{SSC}}(n-1) = \gamma_2(n-1) & \gamma_2(n) < \gamma_T \end{cases} \tag{6.26a}$$

$$\gamma_{\text{SSC}}(n) = \gamma_2(n), \quad \text{as above with interchanging } \gamma_1 \text{ and } \gamma_2. \tag{6.26b}$$

In the following sections, we obtain the output SNR CDF, output SNR PDF and the output SNR MGF of the decorrelator receiver with SSC in correlated Rician fading.

6.4.1 Output SNR CDF

Following the analysis in [14], one can obtain the CDF of the output SNR as

$$F_{\gamma_{\text{SSC}}}(x) = \begin{cases} \dfrac{F_{\gamma_1}(\gamma_T)F_{\gamma_2}(\gamma_T)}{F_{\gamma_1}(\gamma_T)+F_{\gamma_2}(\gamma_T)}\left(F_{\gamma_1}(x)+F_{\gamma_2}(x)\right), & x < \gamma_T \\ \dfrac{F_{\gamma_1}(\gamma_T)F_{\gamma_2}(\gamma_T)}{F_{\gamma_1}(\gamma_T)+F_{\gamma_2}(\gamma_T)}\left(F_{\gamma_1}(x)+F_{\gamma_2}(x)-2\right) & \\ \quad + \dfrac{F_{\gamma_1}(\gamma_T)F_{\gamma_2}(x)+F_{\gamma_1}(x)F_{\gamma_2}(\gamma_T)}{F_{\gamma_1}(\gamma_T)+F_{\gamma_2}(\gamma_T)}, & x \geq \gamma_T \end{cases} \tag{6.27}$$

where $F_{\gamma_1}(\cdot)$ and $F_{\gamma_2}(\cdot)$ are defined in (6.6) and (6.7), respectively.

6.4.2 Output SNR PDF

The PDF of the output combiner can be obtained from the combiner output CDF by differentiation as

$$F_{\gamma_{\text{SSC}}}(x) = \begin{cases} \dfrac{F_{\gamma_1}(\gamma_T)F_{\gamma_2}(\gamma_T)}{F_{\gamma_1}(\gamma_T)+F_{\gamma_2}(\gamma_T)}\left(f_{\gamma_1}(x)+f_{\gamma_2}(x)\right), & x<\gamma_T \\ \dfrac{F_{\gamma_1}(\gamma_T)F_{\gamma_2}(\gamma_T)}{F_{\gamma_1}(\gamma_T)+F_{\gamma_2}(\gamma_T)}\left(f_{\gamma_1}(x)+f_{\gamma_2}(x)\right) & \\ \quad + \dfrac{F_{\gamma_1}(\gamma_T)f_{\gamma_2}(x)+f_{\gamma_1}(x)F_{\gamma_2}(\gamma_T)}{F_{\gamma_1}(\gamma_T)+F_{\gamma_2}(\gamma_T)}, & x\geq\gamma_T \end{cases} \tag{6.28a}$$

where $f_{\gamma_1}(\cdot)$ and $f_{\gamma_2}(\cdot)$ are the PDFs of γ_1 and γ_2 and are calculated using (6.6) and (6.7) as

$$f_{\gamma_1}(x) = \frac{1+K}{\bar{\gamma}(1+\rho)}\exp\left(-\frac{2K}{1+\rho}-\frac{(1+K)x}{\bar{\gamma}(1+\rho)}\right)I_0\left(\sqrt{\frac{8K(1+K)x}{\bar{\gamma}(1+\rho)^2}}\right) \tag{6.28b}$$

and

$$f_{\gamma_2}(x) = \frac{(1+K)}{\bar{\gamma}(1-\rho)}\exp\left(-\frac{(1+K)x}{\bar{\gamma}(1-\rho)}\right) \tag{6.28c}$$

respectively.

6.4.3 Output SNR MGF

Similar to the analysis in the previous section, taking the Laplace transform of (6.28a), we obtain a closed-form expression for the MGF of the output SNR as

$$\Phi_{\text{SSC}}(s) = H_1(s,\gamma_T)G(\gamma_T) + (1-G(\gamma_T))H_2(s,\gamma_T) \tag{6.29a}$$

where $G(\gamma_T)$, $H_1(s,\gamma_T)$ and $H_2(s,\gamma_T)$ are defined as

$$G(\gamma_T) = \frac{F_{\gamma_1}(\gamma_T)}{F_{\gamma_1}(\gamma_T)+F_{\gamma_2}(\gamma_T)}, \tag{6.29b}$$

$$\begin{aligned} H_1(s,\gamma_T) = {} & \frac{(1+K)}{1+K-s\bar{\gamma}(1-\rho)} \\ & \times\left[1-\exp\left(-\frac{\gamma_T(1+K)}{\bar{\gamma}(1-\rho)}\right)+\exp\left(-\frac{\gamma_T(1+K-s\bar{\gamma}(1-\rho))}{\bar{\gamma}(1-\rho)}\right)\right] \end{aligned} \tag{6.29c}$$

and

$$H_2(s,\gamma_T) = \frac{1+K}{1+K-s\bar{\gamma}(1+\rho)} \exp\left(\frac{2sK\bar{\gamma}}{K+1-s\bar{\gamma}(1+\rho)}\right) \left[F_{\gamma_1}(\gamma_T) + Q_1\left(\sqrt{\frac{4K(K+1)}{(1+\rho)(1+K-s\bar{\gamma}(1+\rho))}}, \sqrt{\frac{2\gamma_T(1+K-s\bar{\gamma}(1+\rho)}{\bar{\gamma}(1+\rho)}}\right)\right] \tag{6.29d}$$

respectively.

6.4.4 Mean Output SNR

Using the MGF in (6.29), and after tedious mathematical manipulations, the mean output SNR is derived as

$$\bar{\gamma}_{\text{SSC}} = G(\gamma_T)\left(\frac{\bar{\gamma}(1-\rho)}{1+K} + \gamma_T \exp\left(-\frac{(1+K)\gamma_T}{\bar{\gamma}(1-\rho)}\right)\right) + (1-G(\gamma_T))\left[\frac{(1+\rho+2K)\bar{\gamma}}{1+K} + \exp\left(-\frac{(1+K)\gamma_T}{\bar{\gamma}(1+\rho)} - \frac{2K}{1+\rho}\right)\left\{\gamma_T I_0\left(\sqrt{\frac{8K(1+K)\gamma_T}{\bar{\gamma}(1+\rho)^2}}\right) + \sqrt{\frac{2\bar{\gamma}K\gamma_T}{1+K}} I_1\left(\sqrt{\frac{8K(1+K)\gamma_T}{\bar{\gamma}(1+\rho)^2}}\right)\right\}\right]. \tag{6.30}$$

Note that the mean output SNR is dependent on the switching threshold γ_T. An optimum switching threshold that maximizes the average output SNR can be computed by finding the root of

$$d\bar{\gamma}_{\text{SSC}}/d\gamma_T = 0. \tag{6.31}$$

6.4.5 Average Error Rate

Similar to the analysis in the previous section, one can obtain the average SER of SSC with various modulation schemes of practical interest. For example, the average

SER of noncoherent MFSK can be obtained as

$$P_s = \sum_{n=1}^{M-1} \frac{(-1)^{n+1}\binom{M-1}{n}}{n+1} \Phi_{\text{SSC}}\left(\frac{n}{n+1}\right). \tag{6.32}$$

Note that the average SER is a function of the switching threshold. An optimum switching threshold that minimizes the average SER can be obtained by finding the root of $dP_s/d\gamma_T = 0$. For example, for noncoherent MFSK the optimum switching threshold is the root of

$$\sum_{n=1}^{M-1} \frac{(-1)^{n+1}\binom{M-1}{n}}{n+1} \Phi'_{\text{SSC}}\left(\frac{n}{n+1}\right) = 0. \tag{6.33}$$

In (6.33), $\Phi'_{\text{SSC}}(\cdot)$ is the derivative of $\Phi_{\text{SSC}}(\cdot)$ with respect to γ_T and can be calculated as

$$\Phi'_{\text{SSC}}(s) = G(\gamma_T)H'_1(s,\gamma_T) + (1-G(\gamma_T))H'_2(s,\gamma_T) + G'(\gamma_T)[H_1(s,\gamma_T) - H_2(s,\gamma_T)] \tag{6.34a}$$

where $G'(\gamma_T)$, $H'_1(s,\gamma_T)$ and $H'_1(s,\gamma_T)$ are the derivatives of (6.29b), (6.29c) and (6.29d) with respect to γ_T and are given by

$$G'(\gamma_T) = \frac{f_{\gamma_1}(\gamma_T)F_{\gamma_2}(\gamma_T) - f_{\gamma_2}(\gamma_T)F_{\gamma_1}(\gamma_T)}{(F_{\gamma_1}(\gamma_T) + F_{\gamma_2}(\gamma_T))^2} \tag{6.34b}$$

$$\begin{aligned} H'_1(s,\gamma_T) = \frac{(1+K)}{1+K-s\bar{\gamma}(1-\rho)}\Bigg[&\frac{(1+K)}{\bar{\gamma}(1-\rho)}\exp\left(-\frac{\gamma_T(1+K)}{\bar{\gamma}(1-\rho)}\right) \\ &- \frac{(1+K-s\bar{\gamma}(1-\rho))}{\bar{\gamma}(1-\rho)}\exp\left(-\frac{\gamma_T(1+K-s\bar{\gamma}(1-\rho))}{\bar{\gamma}(1-\rho)}\right)\Bigg] \end{aligned} \tag{6.34c}$$

and

$$\begin{aligned} H'_2(s,\gamma_T) = -\frac{1+K}{(1+K-s\bar{\gamma}(1+\rho)}&\exp\left(\frac{2sK\bar{\gamma}}{(K+1-s\bar{\gamma}(1+\rho))}\right)\Bigg[f_{\gamma_1}(\gamma_T) \\ &+ \frac{(1+K-s\bar{\gamma}(1+\rho)}{\bar{\gamma}(1+\rho)} I_0\left(\frac{8K(K+1)\gamma_T}{\bar{\gamma}(1+\rho)^2}\right) \\ &\times \exp\left(-\frac{2K(K+1)}{(1+\rho)(1+K-s\bar{\gamma}(1+\rho))} - \frac{\gamma_T(1+K-s\bar{\gamma}(1+\rho)}{\bar{\gamma}(1+\rho)}\right)\Bigg] \end{aligned} \tag{6.34d}$$

respectively. Note that, in general, the optimum switching threshold that minimizes the average SER, is different from the optimum switching threshold that maximizes the average output SNR. The results of this section are used in Section 6.7 to examine the performance of SSC diversity with decorrelation.

6.5 Square-Law Combining

In this section, we show that the performances of the decorrelator receiver and the conventional receiver are identical when the combining scheme is SLC. In SLC, the receiver bases it decision on the summation of the outputs of the square-law detectors. For the conventional and the decorrelator receiver, the decision output statistics are given by

$$D_1 = |r_1|^2 + |r_2|^2 \tag{6.35}$$

and

$$D_2 = |w_1|^2 + |w_2|^2 \tag{6.36}$$

respectively. Let

$$r_1 = x_1 + jy_1 \tag{6.37}$$

$$r_2 = x_2 + jy_2. \tag{6.38}$$

Then it is easy to show that $D_1 = x_1^2 + x_2^2 + y_1^2 + y_2^2$. Substituting (6.4) and (6.5) in (6.36), and using (6.37) and (6.38), one can show that $D_2 = D_1$. This proves that the performances of the decorrelator and conventional SLC receivers are identical.

6.6 Equal Gain Combining

In this section, we prove that the mean output SNR of the decorrelator receiver is less than the mean output SNR of the conventional receiver when EGC is employed. For the conventional receiver, using the approach of [69], one can show that the mean output SNR is given by

$$\bar{\gamma}_{\text{EGC}} = \bar{\gamma}\left(1 + \frac{\pi(1-\rho)^2}{4\rho(1+K)} \exp\left(-\frac{K}{\rho}\right) \times \int_0^{\infty} \left[(1+z)I_0\left(\frac{z}{2}\right) + zI_1\left(\frac{z}{2}\right)\right]^2 I_0\left(2\sqrt{\frac{K(1-\rho)z}{\rho^2}}\right) \exp\left(-\frac{z}{\rho}\right)\right) dz. \tag{6.39}$$

Note that (6.39) corrects [69, eq. (36)]. For $K = 0$, the mean output SNR is given as

$$\bar{\gamma}_{\text{EGC}} = \bar{\gamma}\left(1 + \frac{\pi}{4} \cdot {}_2F_1(-\frac{1}{2}, -\frac{1}{2}; 1; \rho^2)\right) \tag{6.40}$$

where ${}_2F_1(a, b; c; z)$ is the Gauss hypergeometric function defined in [19, eq. (9-100)].

For the decorrelator receiver, one can show that the mean output SNR is given by

$$\bar{\gamma}_{\text{EGC}} = \bar{\gamma}\left(1 + \frac{\pi\sqrt{1-\rho^2}}{4(1+K)} \exp\left(-\frac{K}{1+\rho}\right) \times \left[\frac{1+2K+\rho}{1+\rho} I_0\left(\frac{K}{1+\rho}\right) + \frac{2K}{1+\rho} I_1\left(\frac{K}{1+\rho}\right)\right]\right) \tag{6.41}$$

which, in the case of Rayleigh fading ($K = 0$), reduces to

$$\bar{\gamma}_{\text{EGC}} = \bar{\gamma}\left(1 + \frac{\pi}{4}\sqrt{1-\rho^2}\right). \tag{6.42}$$

Comparing (6.40) with (6.42), one can prove that for Rayleigh fading the mean output SNR of the decorrelator receiver is always less than the mean output SNR of the conventional receiver. For Rician fading, Fig. 6.2 shows the normalized mean output SNRs ($\bar{\gamma}_{\text{EGC}}/\bar{\gamma}$) of the decorrelator receiver and the conventional receiver as a function

of ρ for several values of K. Fig. 6.2 shows that the mean output SNR of the decorrelator receiver is less that the mean output SNR of the conventional receiver for all values of ρ. Thus, one can conclude that the performance of the decorrelator receiver with EGC is inferior to the performance of the conventional EGC receiver. An interesting behaviour shown in Fig. 6.2 is that the mean output SNR of the decorrelator EGC receiver decreases as K increases while the mean output SNR of the conventional EGC receiver increases as the channel becomes less faded. We also note that numerical results show that when K approaches infinity (6.39) approaches $2\bar{\gamma}$ while (6.41) approaches $\bar{\gamma}$.

6.7 Numerical Examples

In this section, we give some numerical examples to compare the performance of the decorrelator SC and SSC receivers with conventional SC and SSC receivers, respectively. Fig. 6.3 shows the average BER of BPSK for the conventional and the decorrelator SC receivers as a function of the average SNR per bit per branch in correlated Rician fading with $\rho = 0.55$ and for several values of $K = 0, 5$ and 10. Note that for $K = 0$, which corresponds to Rayleigh fading, the performance of the two receivers are almost identical and the decorrelator receiver performs slightly better than the conventional receiver for small values of SNR. However, in Rician fading, the performance of the decorrelator receiver is significantly better than the performance of the conventional receiver and the performance improves as the channel becomes less faded (K increases). For example, Fig. 6.3 shows that for $K = 10$ and for an average BER of 10^{-3}, the average SNR difference between the conventional and the decorrelator receiver is 2.1 dB. Fig. 6.4 studies the effect of correlation on the

relative performance of the conventional and the decorrelator receiver in correlated Rician fading with $K = 5$ and 10 for $\rho = 0.1, 0.4$ and 0.8. Fig. 6.4 shows that the decorrelator receiver outperforms the conventional receiver for the whole range of SNR. For example, at an average BER of 10^{-4}, the SNR gain of decorrelator receiver over the conventional receiver is 0.77 dB, 0.54 dB and 0.63 dB for $\rho = 0.1$, $\rho = 0.4$ and $\rho = 0.8$, respectively.

The outage probabilities of the conventional and the decorrelator SC receivers in correlated Rician fading are plotted in Figs. 6.5 and 6.6 for several values of K and ρ as a function of the normalized threshold SNR. Both figures show that the outage probability of the decorrelator receiver is much less than the outage probability of the conventional receiver. For example, Fig. 6.5 shows that for a normalized threshold SNR of -4 dB and for $K = 10$, the outage probability of the conventional and the decorrelator receiver are 0.0115 and 0.0019, respectively which means that the outage probability of the decorrelator receiver is one-sixth of that of the conventional receiver. Note also that Fig. 6.5 indicates that as K increases and for a given normalized threshold SNR, the difference between the outage performance of the two receivers increases.

In Fig. 6.7 the mean output SNR of the conventional and the decorrelator SC receivers in correlated Rician fading with $\rho = 0.5$ have been plotted for several values of $K = 0, 5$ and 10. Fig. 6.7 indicates that unlike the conventional SC receiver where the mean output SNR decreases as K increases [1], the mean output SNR increases as K increases in the decorrelator SC receiver.

[1]This behaviour may seem unexpected. However, a similar behaviour is observed and explained in [60].

Fig. 6.8 shows the average BER of QFSK with the conventional and the decorrelator SSC receiver as a function of average SNR per bit per branch in correlated Rician fading with $\rho = 0.6$ and $K = 0, 5$ and 10. To plot the curves in Fig. 6.8, for each value of SNR, the optimum switching threshold the minimizes the average BER has been used. Fig. 6.8 shows that the performance of the decorrelator receiver is superior to the performance of the conventional receiver and the performance gap increases as K increases. For example, at an average BER of 10^{-4} the SNR gap between the conventional and the decorrelator receiver is 2.83 dB and 1.11 dB for $K = 5$ and $K = 10$, respectively. For $K = 0$, the performance of the two receivers are almost identical for moderate to large values of average SNR. For small values of average SNR, however, the decorrelator receiver performs slightly better.

The dependence of the average BER of QFSK with the decorrelator receiver in correlated Rician fading, on the switching threshold is studied in Fig. 6.9 for several values of $\bar{\gamma}$ and ρ. Fig. 6.9 shows that for a fixed $\bar{\gamma}$, the optimum switching threshold increases as ρ decreases. This is similar to the dependency of the conventional SSC receiver found in [32, Fig. 4]. Fig. 6.9 also indicates that for a fixed ρ, the optimum switching threshold increases as $\bar{\gamma}$ increases, which is again similar to the behaviour of the conventional SSC receiver found in [32, Fig. 4]. Despite these similarities, comparing Fig. 6.9 with [32, Fig. 4] shows that the average BER of the decorrelator receiver is more sensitive to the changes in switching threshold than the conventional SSC receiver, particularly for small values of $\bar{\gamma}$.

The effect of modulation order M on the average BER of MFSK with the decorrelator and the conventional SSC receiver is studied in Fig. 6.10 for several values of $M = 2, 4$ and 16. Again, similar to Fig. 6.10, for each SNR value, the optimum switching threshold that minimizes the average BER is computed. Fig. 6.10 shows

that for a given average BER the performance gap between the two receivers does not change significantly with M. For example, at an average BER of 10^{-3}, the SNR gap between the two receivers is 1.44 dB, 1.05 dB and 1.19 dB for $M = 2$, 4 and 16, respectively.

Finally, the mean output SNRs of the conventional and the decorrelator receiver with SSC in correlated Rician fading with $K = 10$ are compared in Fig. 6.11 for several values of correlation $\rho = 0.15, 0.45$ and 0.75. Fig. 6.11 shows that unlike the conventional SSC receiver and for a fixed average SNR, the mean output SNR of the decorrelator SSC receiver increases as the channel becomes less faded. Fig. 6.11 also indicates that mean output SNR of the decorrelator receiver is much larger than that of the conventional receiver. For each value of average SNR in Fig. 6.11, the optimum switching threshold that maximizes the mean output SNR has been computed. These optimum switching thresholds have been calculated by obtaining the roots of (6.31) numerically. Fig. 6.11 shows that the mean output SNR of the decorrelator SSC receiver is less sensitive to the changes in the correlation than the mean output SNR of the conventional SSC receiver for small to medium average SNR.

An interesting behaviour evidenced in Figs. 6.4, 6.6 and 6.11 is that the performance of the decorrelator receiver improves with increasing correlation coefficient while that of the conventional receiver degrades with increasing correlation coefficient. This happens because the correlation increases the SNR of the stronger decorrelated branch (see eq. (6.8)) while decreasing the SNR of the weaker decorrelated branch (see eq. (6.9)), so that the effective SNR of the selected branch generally improves with increasing correlation.

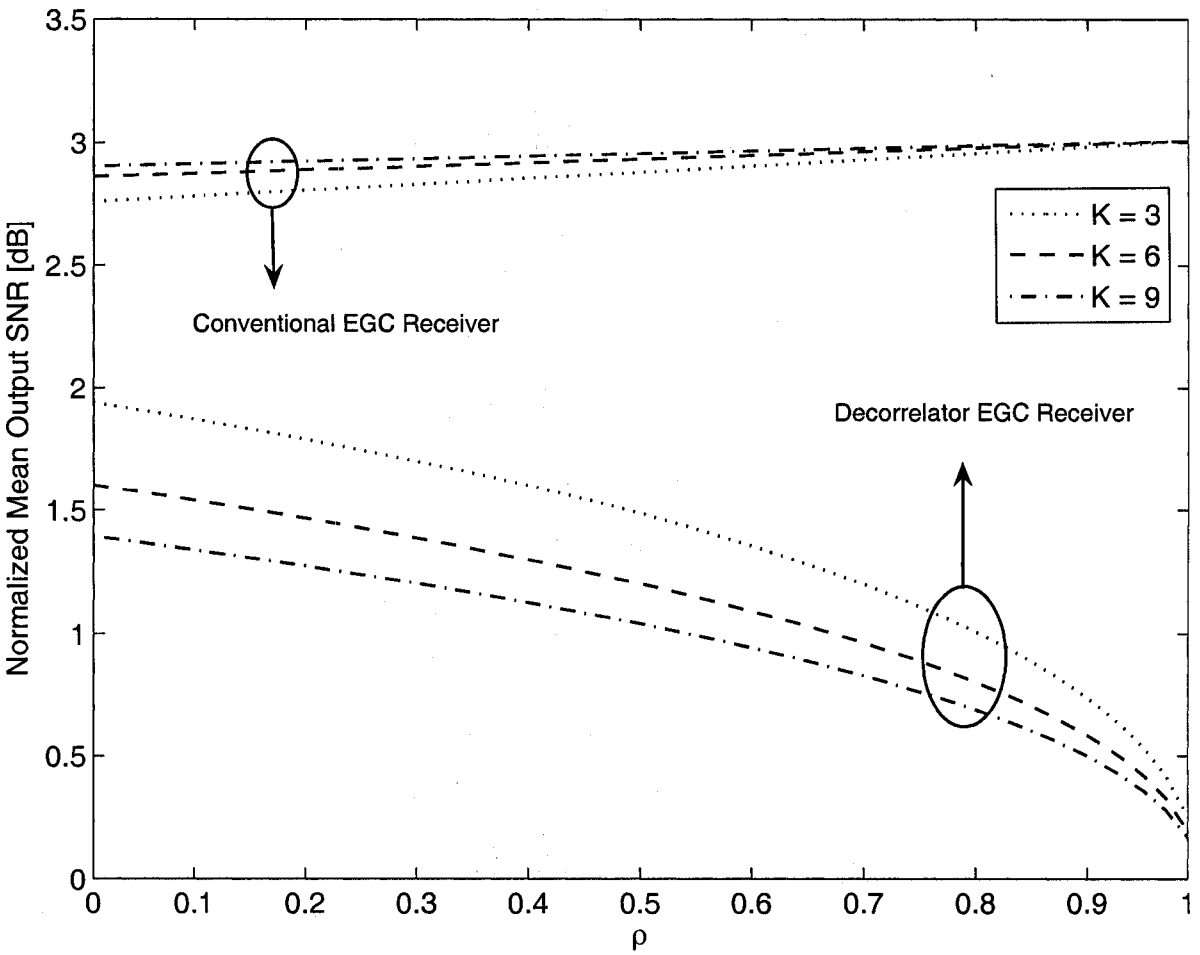

Figure 6.2: The normalized mean output SNRs of the conventional and decorrelator EGC receivers as a function of the correlation, ρ, for $K = 3, 6$ and 9.

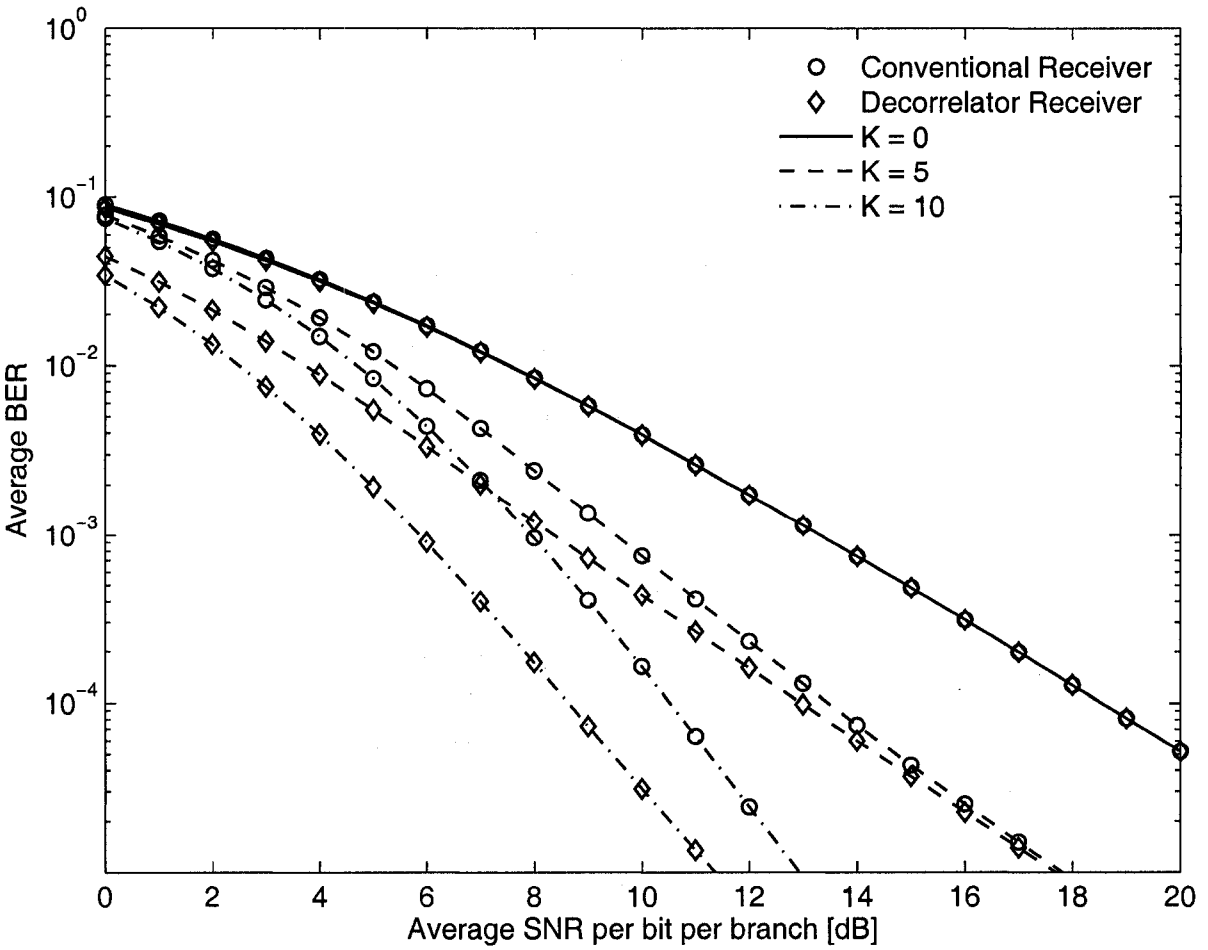

Figure 6.3: The average BER of BPSK for the conventional and decorrelator SC receivers as a function of the average SNR per bit per branch in correlated Rician fading with $\rho = 0.55$ for $K = 0, 5$ and 10.

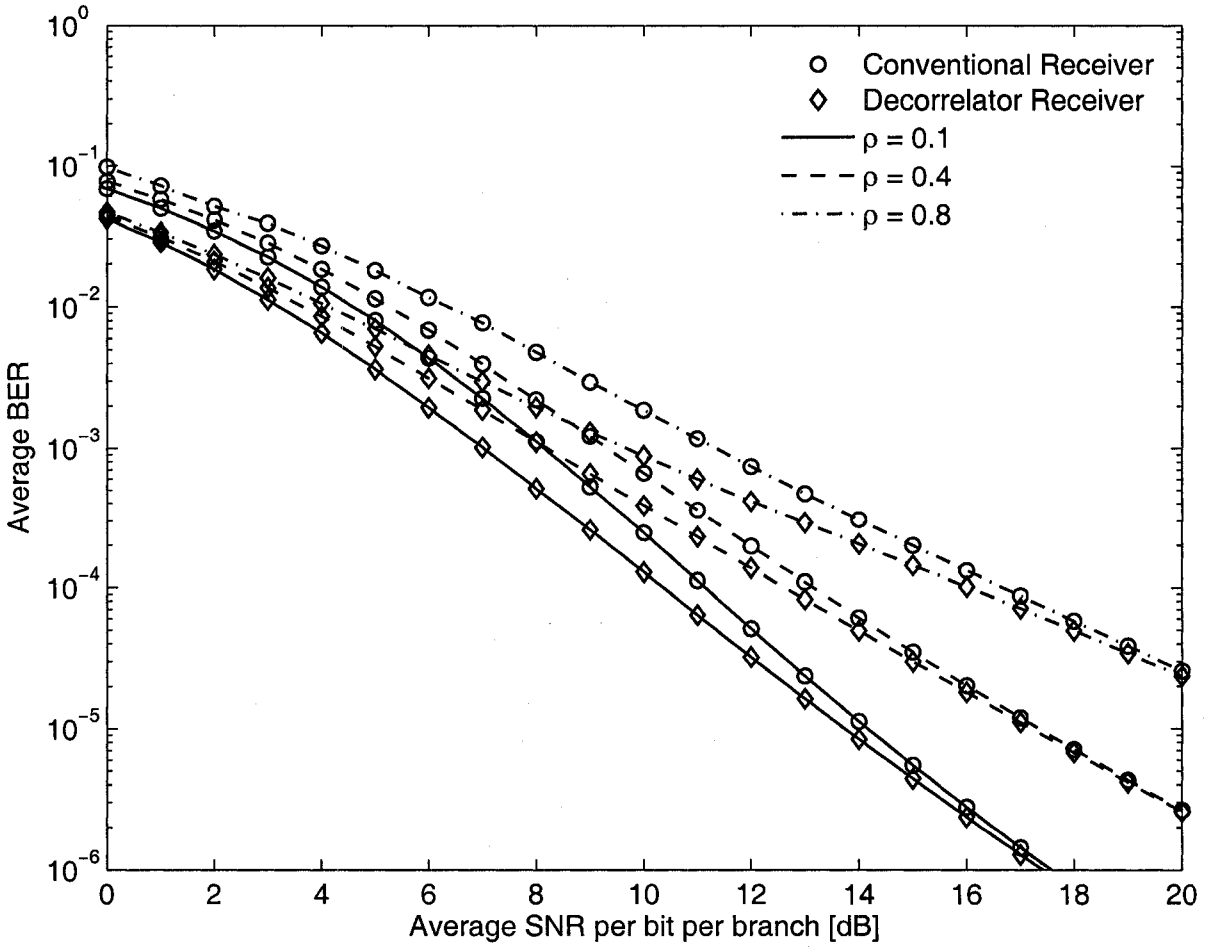

Figure 6.4: The average BER of BPSK for the conventional and the decorrelator SC receivers as a function of the average SNR per bit per branch in correlated Rician fading with $K = 5$ for $\rho = 0.1, 0.5$ and 0.9.

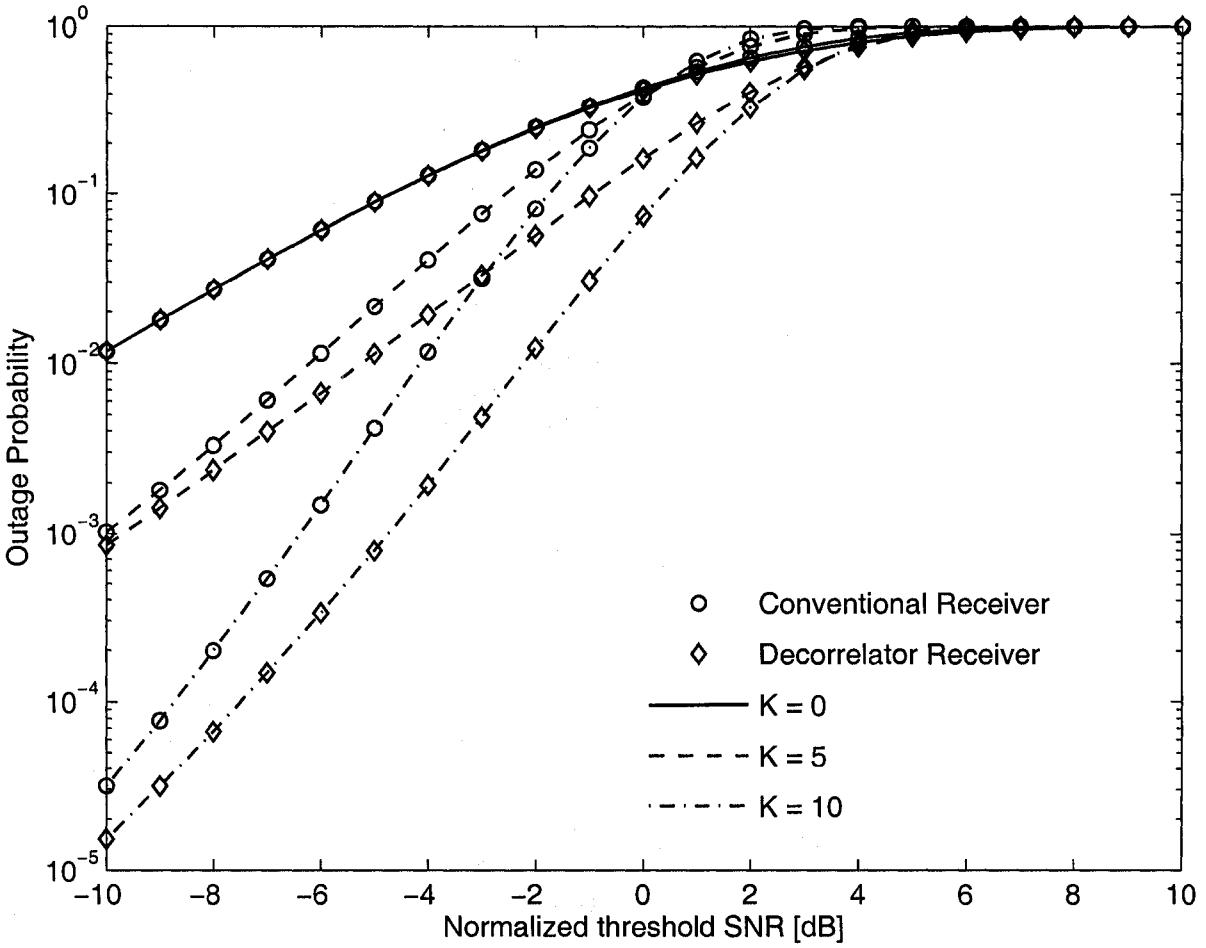

Figure 6.5: The outage probability of conventional and decorrelator SC receivers as a function of the average SNR per branch in correlated Rician fading with $\rho = 0.5$ for $K = 0, 5$ and 10.

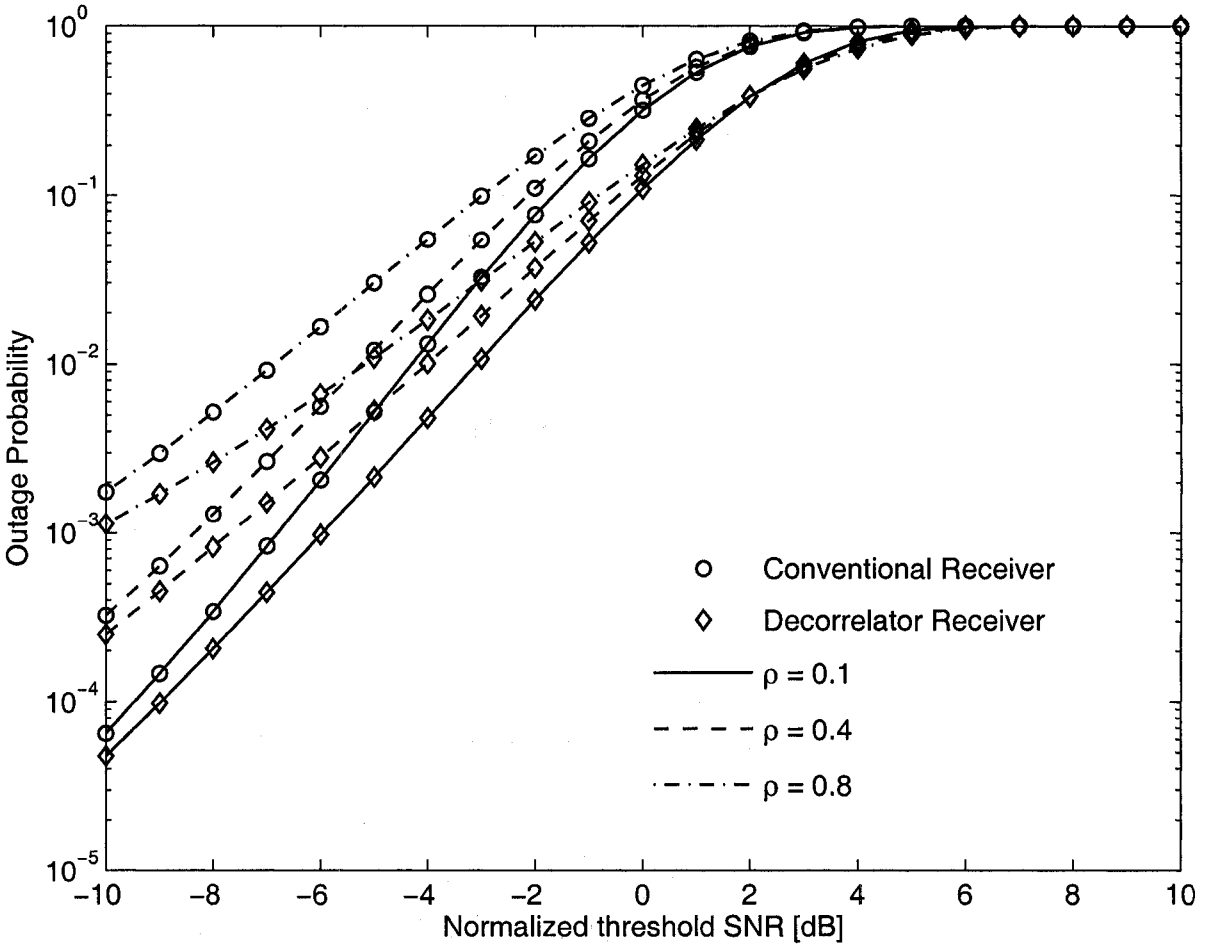

Figure 6.6: The outage probability of conventional and decorrelator SC receivers as a function of the average SNR per branch in correlated Rician fading with $K = 6$ for $\rho = 0.1, 0.4$ and 0.8.

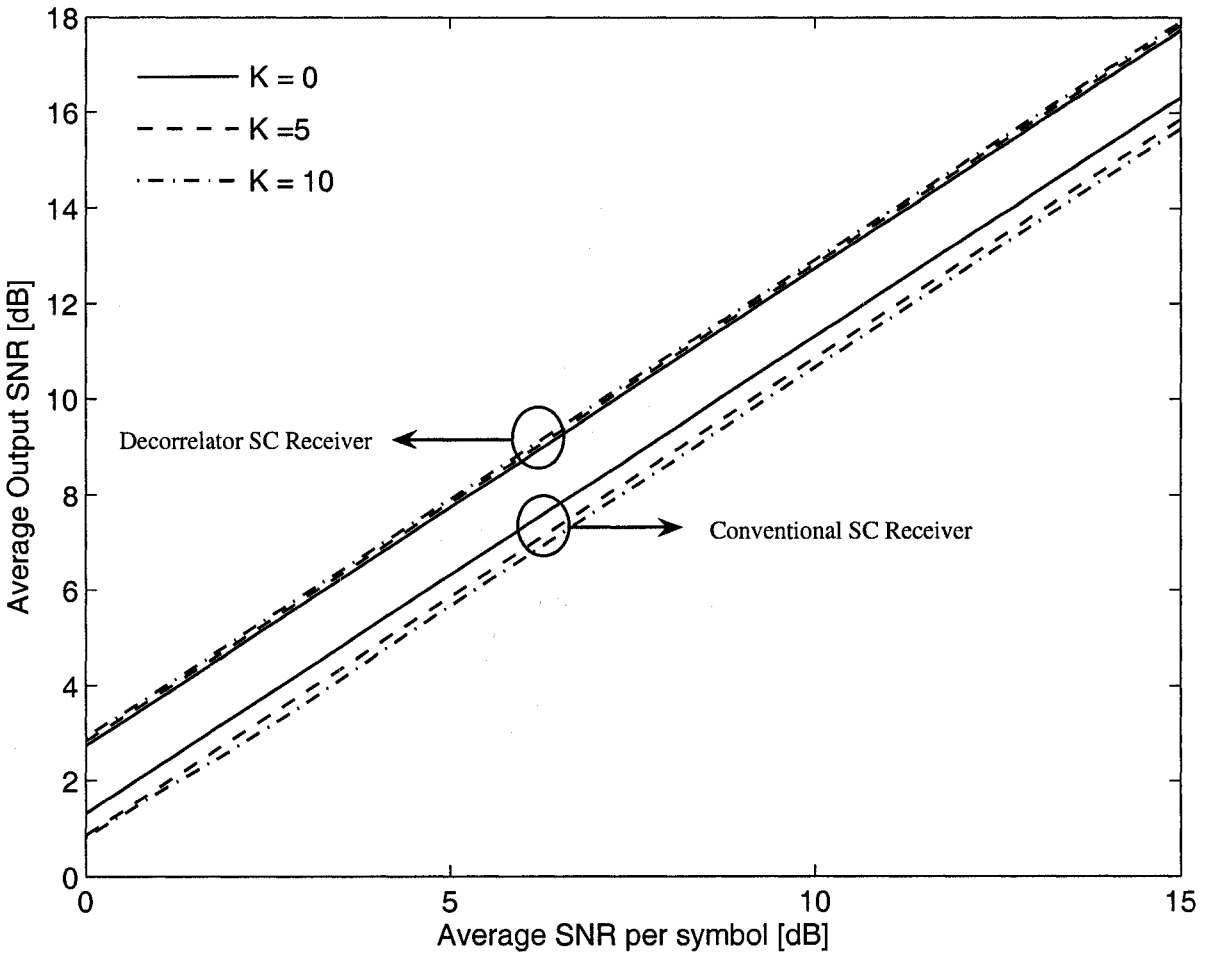

Figure 6.7: The average output SNR of the conventional and the decorrelator receivers in correlated Rician fading with $\rho = 0.5$ for $K = 0, 5$ and 10.

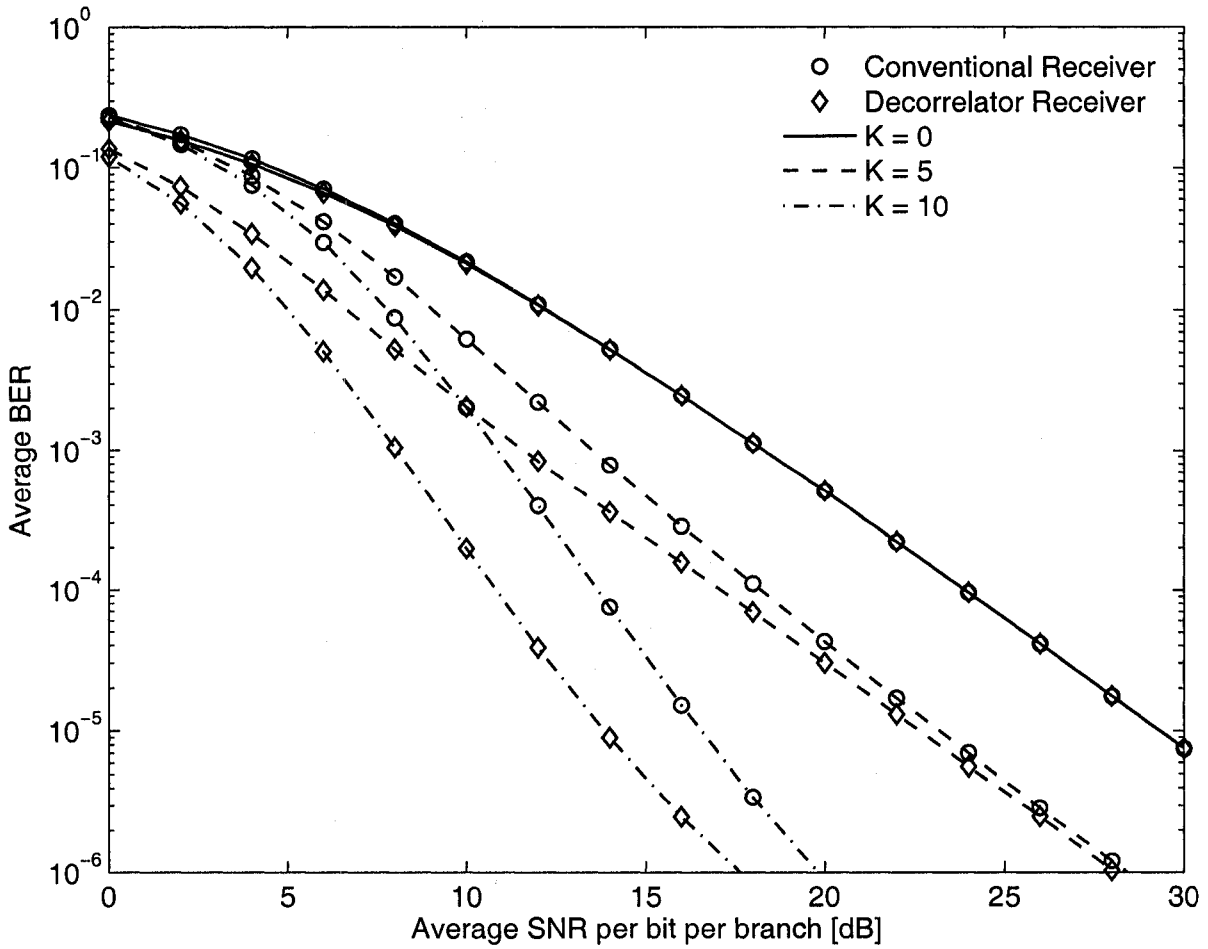

Figure 6.8: The average BER of QFSK for the conventional and decorrelator SSC receivers in correlated Rician fading with $\rho = 0.6$ for $K = 0, 5$ and 10.

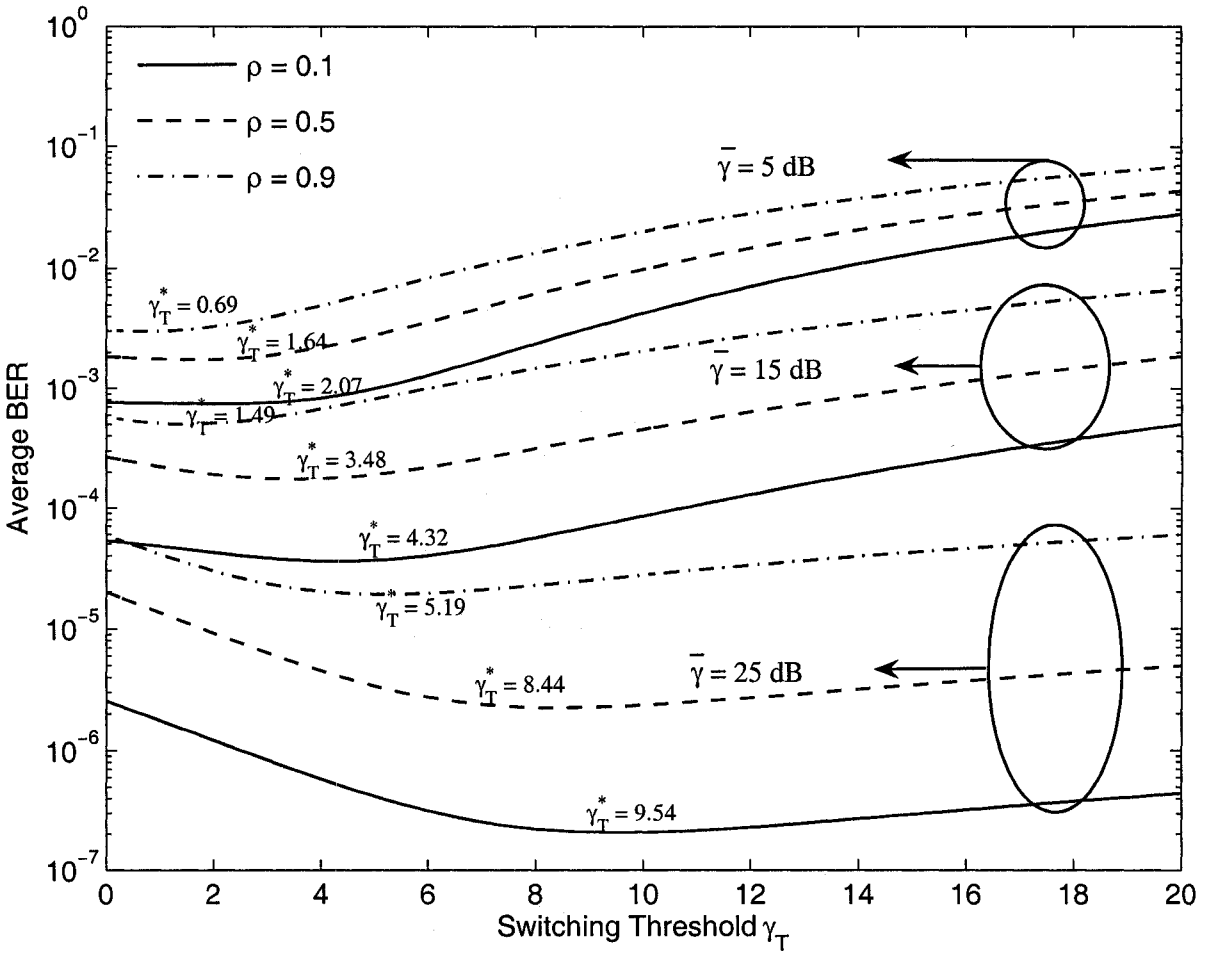

Figure 6.9: The average BER of QFSK for the decorrelator SSC receiver as a function of the switching threshold in correlated Rician fading with $K = 5$ and $\rho = 0.1, 0.5$ and 0.9 for $\bar{\gamma} = 10, 15$ and 25 dB.

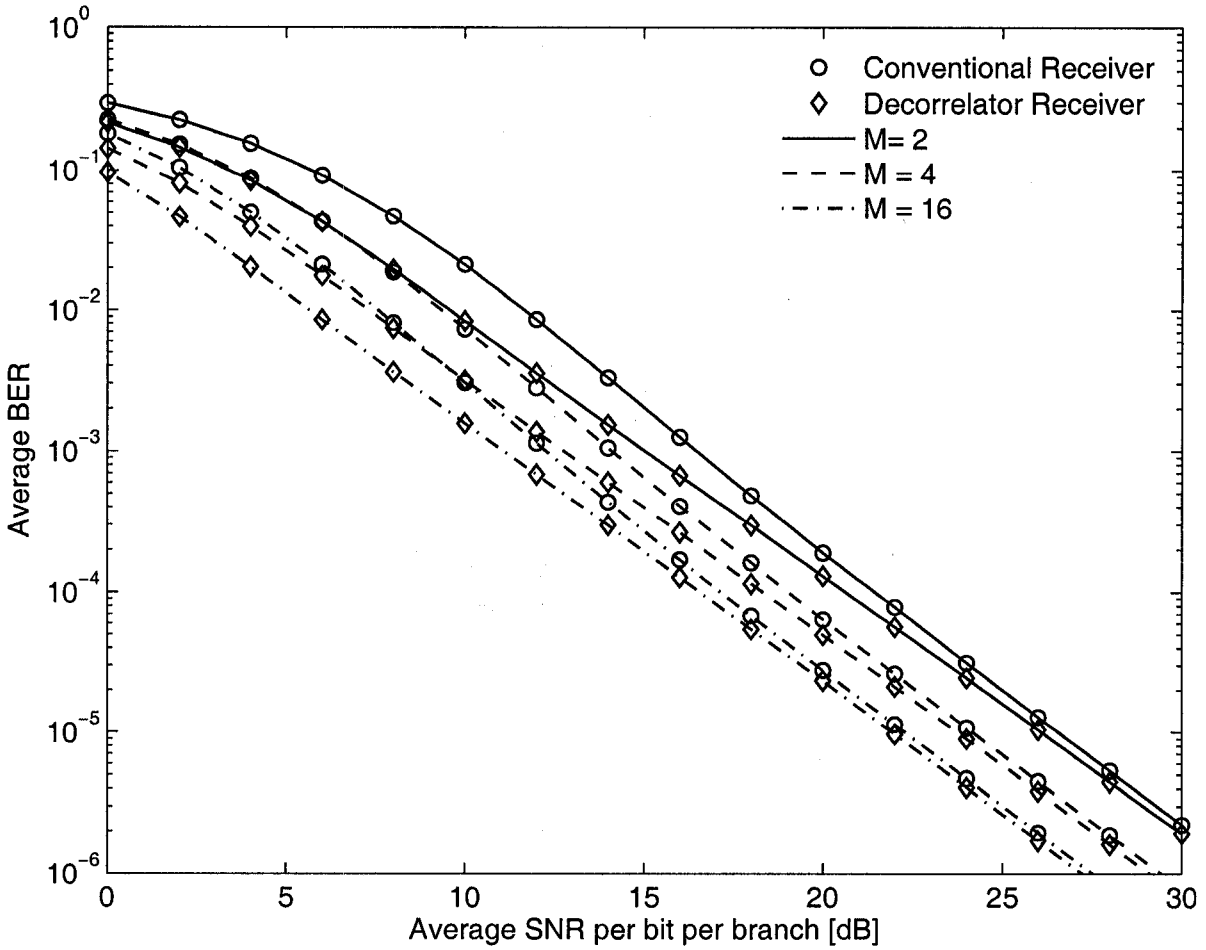

Figure 6.10: The average BER of MFSK for the conventional and the decorrelator SSC receivers in correlated Rician fading with $\rho = 0.6$ and $K = 4$ for $M = 2, 4$ and 16.

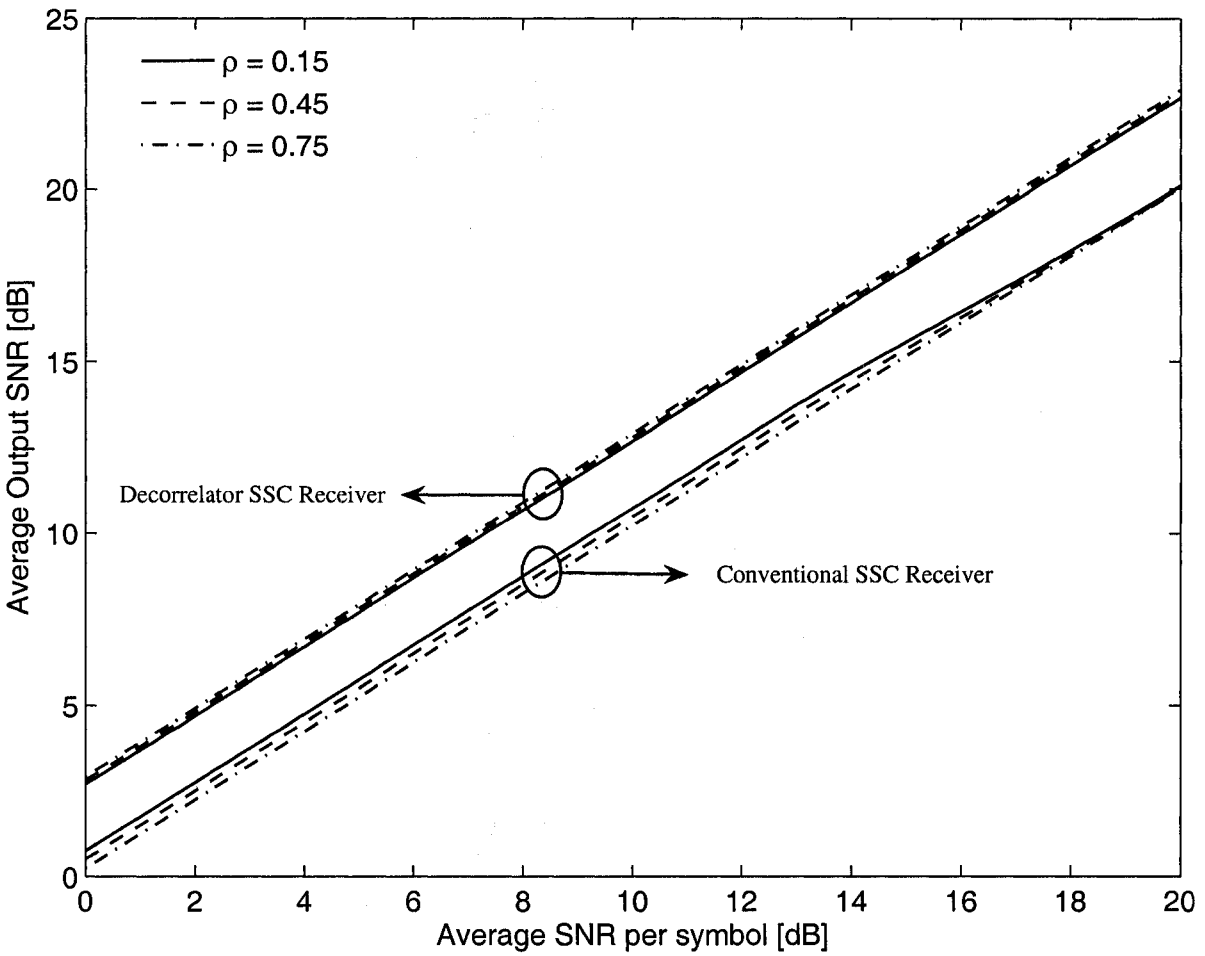

Figure 6.11: The average output SNR of the conventional and the decorrelator SSC receivers as a function of the average SNR per symbol in correlated Rician fading with $K = 10$ for $\rho = 0.15, 0.45$ and 0.75.

6.8 Conclusion

The benefit of implementing decorrelation prior to the employment of SC and SSC diversity was analyzed in correlated Rayleigh and Rician fading channels for dual-branch diversity. The performance of a dual-branch decorrelator receiver in conjunction with SC and SSC was analyzed in correlated Rayleigh and Rician fading channels. Important performance measures such as the average BER of several modulations of practical interest, mean output SNR and outage probability were computed for each diversity receiver. It was shown that the performances of the decorrelator SC and SSC receivers are superior to the performances of the conventional SC and SSC receivers in correlated Rician fading, respectively, and that the average SNR gain can be as much as 2.83 dB. Similarly the outage probability of the decorrelator receiver was shown to be reduced by as much as one-sixth relative to the outage probability of the conventional receiver in some scenarios.

Chapter 7

Conclusion

In this chapter, we summarize the contributions of this thesis. We also give some suggestions for future research.

7.1 Conclusions

1. The performance of dual-branch SSC in correlated Rician fading channels was studied. Analytical expressions for the average SER of various modulation formats of practical interest, outage probability and mean output SNR were derived.

2. The performances of two-dual branch postdetection SSC receivers in correlated Rayleigh and Rician fading channels were analyzed. For each receiver structure analytical expressions were derived for the average BER and average SER of noncoherent BFSK and noncoherent MFSK in correlated Rayleigh and Rician fading. These analytical expressions are obtained in closed-form and are easy-to-compute. For Rayleigh fading, the impact of fading power imbalance on the performance of postdetection SSC receivers was studied.

3. The effects of important parameters, such as the correlation coefficient, fading

power imbalance and fading factor, on the performances of postdetection SSC receivers were analyzed.

4. The performances of predetection and postdetection SSC receivers were compared. It was shown that postdetection SSC outperforms predetection SSC for any given average SNR.

5. The performances of two $S+N$ SC receivers with noncoherent MFSK and noncoherent BFSK in i.n.d Rician, Nakagami and Rayleigh fading channels were computed as single integrals with finite integration limits. The performances of $S+N$ SC receivers were compared with the performance of classical SC and it was observed that, unlike as suggested by previously published results, the performances of $S+N$ SC receivers are not always superior to the performance of classical SC.

6. It was shown that increasing the number of diversity branches in a $S+N$ SC receiver does not decrease the average SER if the system is operating in the low SNR regime.

7. Tractable analytical expressions have been derived for the average SER of noncoherent BFSK and noncoherent MFSK with L branch $S+N$ SC in correlated Rician fading. The performances of $S+N$ SC receivers in correlated Rayleigh fading were also studied. The correlation model used for Rayleigh fading is more general than the equally correlated case and includes it as a special case.

8. The effects of important measures such as correlation and average power decay factor on the performances of $S+N$ SC receivers were studied.

9. A new dual-branch decorrelator receiver was introduced and its performance in

correlated Rician fading was analyzed. It was shown that the decorrelation process does not require knowledge of the fading statistics and can be performed by the addition and subtraction of the incoming signals. It was shown that the decorrelator receiver, when combined with classical SC and SSC, can improve the system performance by as much as 2.83 dB in SNR.

10. The outage probability and the mean output SNR of the SC and SSC decorrelator receivers were computed and it was shown that the outage probability of the decorrelator receiver can be reduced by as much as one-sixth of the outage probability of the conventional SC and SSC receivers.

11. The performance of SLC and EGC when combined with the decorrelator receiver were analyzed and it was shown that for SLC, the decorrelator and the conventional receiver have the same performance. For EGC, it was proved that the decorrelator receiver has negative benefit and its performance is inferior to the performance of the conventional receiver.

7.2 Suggestions for Future Research

1. Recently, there has been much interest in the performance of generalized selection combining (GSC) diversity systems where a subset of diversity branches are selected for processing [70]- [79]. In all these GSC systems, the criterion used to select a branch is a function of the SNRs on the branches. In a GSC diversity system, from the available L branches, L_c branches are chosen whose SNRs satisfy the system requirement. For example in hybrid-selection/maximum ratio combining (H-S/MRC) the L_c branches having the largest SNRs are chosen and combined using a maximum ratio combiner. This requires the receiver to estimate

the channel gains on all the diversity branches. For coherent modulation formats, the receiver needs these estimates for data detection. For example in MRC, the branches are co-phased and weighted proportional to their SNRs to form the output statistics. For noncoherent and differentially coherent modulations, the information of the channel gain is only used to choose the branches and is not used in the data detection process. For noncoherent modulation formats, the L_c branches having the largest SNRs are combined using an equal gain combiner. We refer to these combining systems as SC/EGC in the sequel. Note that the performance of SC/EGC in i.i.d and i.n.d fading channels has been well studied in the literature. For example, in [79] the authors have derived the performance of SC/EGC in i.n.d generalized fading channels for binary noncoherent and differentially coherent modulation formats.

Instead of using the SNR on the branches as a measure of choosing a branch, one may select a branch whose matched filter output satisfies a given condition. For example, as shown in the previous sections, in $S+N$ SC, the branch having the largest sample at the output of the matched filter is chosen for data recovery. This combining technique will alleviate the need for estimating the channel gains. Now consider a noncoherent or differentially coherent system where the L_c branches having the largest matched filter outputs are selected and combined using EGC to form the output statistics. We refer to this combining scheme as $S+N$/EGC.

Although the performance of SC/EGC systems is well studied in the literature, there is little work on the performance analysis of $S+N$/EGC systems in fading channels [80]. In [80], the average BER of a M-ary orthogonal NCFSK with $S+N$/EGC is studied in L branch i.i.d Rayleigh fading channels where for each of the M hypothesis, the receiver combines the L_c largest outputs among the L available

square-law detectors. The results in [80] are limited to the case of i.i.d Rayleigh fading channels. Furthermore, no comparison between $S+N$/EGC and SC/EGC is given in [80]. An investigation of the performance of M-ary noncoherent NCFSK with $S+N$/EGC in i.n.d fading channels is needed. Other fading models such as Nakagami-m and Rician fading can be considered. In addition, it is of interest to study the performance of $S+N$/EGC receivers in correlated fading channels.

2. The performance of the decorrelator receiver was examined when the branches are identically distributed. A topic for future research is to study the performance of the dual-branch decorrelator receiver when there is average fading power imbalance.

3. The performance of $S+N$ SC receivers was analyzed in equally correlated Rician fading channels. It is of interest to study the performance of $S+N$ SC receivers when the correlation model is more general than the equally correlated case.

References

[1] D. G. Brennan, "Linear Diversity Combining Techniques," *Proc. of the IRE*, vol. 46, pp. 1075–1102, Jun. 1959.

[2] B. Sklar, "Rayleigh Fading Channels in mobile Digital communication systems part I : Characterization," *IEEE Commun. Magazine*, vol. 35, pp. 90–100, Jul. 1997.

[3] B. Sklar, "Rayleigh Fading Channels in mobile Digital Communication Systems Part II : Mitigation," *IEEE Commun. Magazine*, vol. 35, pp. 102–109, Jul. 1997.

[4] G. L. Stuber, *Principles of Mobile Communication*, 2nd ed. Norwell, MA: Kluwer Academic Publishers, 2001.

[5] W. C. Jakes, *Microwave Mobile Communications*. New York: IEEE press, reprint, 1974.

[6] J. D. Parsons, *The Mobile Radio Propagation Channel*, 2nd ed. New York: McGraw-Hill, 2000.

[7] E. A. Neasmith and N. C. Beaulieu, "New Results on Selection Diversity," *IEEE Trans. Commun.*, vol. 46, pp. 695–704, May 1998.

[8] J. M. Wozencraft and I. M. Jacobs, *Principles of Communication Engineering*. New York: John Wiley and Sons, 1965.

[9] J. K. Cavers and P. Ho, "Switching Rate and Dwell Time in M-of-N Selection Diversity," *IEEE Trans. on Wireless Commun.*, vol. 6, pp. 1218–1223, Apr. 2007.

[10] J. K. Cavers and P. Ho, "Switching Rate and Dwell Time of Hybrid Selection-Maximal Ratio Combining in Rayleigh Fading Channels," in *Proc. IEEE Veh. Technol. Conf.*, Melbourne, Australia, May 2006, vol. 4, pp. 1650–1654.

[11] N. C. Beaulieu, "Switching Rates of Dual Selection Diversity and Dual Switch-and-Stay Diversity," *to appear in IEEE Trans. Commun.*, 2007.

[12] M. K. Simon and M.-S. Alouini, *Digital Communication over Fading Channels: A Unified Approach to Performance Analysis.* New York: Wiley, 2000.

[13] M.-S. Alouini and M. K. Simon, "Postdetection Switched Combining- A Simple Diversity Scheme With Improved BER Performance," *IEEE Trans. Commun.*, vol. 51, pp. 1591–1602, Sep. 2003.

[14] Y.-C. Ko, M.-S. Alouini, and M. K. Simon, "Analysis and optimization of switched diversity systems," *IEEE Trans. Veh. Technol.*, vol. 49, pp. 1569–1574, Sep. 2000.

[15] C. Tellambura, A. Annamalai, and V. K. Bhargava, "Unified analysis of switched diversity systems in independent and correlated fading channels," *IEEE Trans. Commun.*, vol. 49, pp. 1955–1965, Nov. 2001.

[16] A. A. Abu-Dayya and N. C. Beaulieu, "Switched Diversity on Microcellular Ricean Channels," *IEEE Trans. Veh. Technol.*, vol. 43, pp. 970–976, Nov. 1994.

[17] A. A. Abu-Dayya and N. C. Beaulieu, "Analysis of Switched Diveristy Systems of Generalized fading Channels," *IEEE Trans. Commun.*, vol. 42, pp. 2959–2966, Nov. 1994.

[18] M. K. Simon, *Probability Distributions Involving Gaussian Random Variables: A Handbook for Engineers and Scientists.* Boston: Kluwer Academic Publishers, 2002.

[19] I. S. Gradshteyn and I. M. Ryzhik, *Table of Intergrals, Series and Products*, 6th ed. San Diego, CA: Academic Press, 2000.

[20] Y. Chen and C. Tellambura, "Distribution functions of selection combiner output in equally correlated Rayleigh, Rician, and Nakagami-m fading channels," *IEEE Trans. Commun.*, vol. 52, pp. 1948–1956, Nov. 2004.

[21] J. G. Proakis, *Digital Communications*, 2nd ed. New York: McGraw-Hill, 1989.

[22] M. Blanco and K. Zdunek, "Performance and optimization of switched diversity systems for the detection of signal with Rayleigh fading," *IEEE Trans. Commun.*, vol. COM-27, pp. 1887–1895, Dec. 1979.

[23] A. Rustako, Y. Yeh, and R. Murray, "Performance of feedback and switch space diversity 900 MHz FM mobile radio systems with Rayleigh fading," *IEEE Trans. Commun.*, vol. COM-21, pp. 1257–1268, Nov. 1973.

[24] F. Adachi, T. Hattori, K. Hirade, and T.Kamata, "A periodic switching diversity technique for a digital FM land mobile radio," *IEEE Trans. Veh. Technol.*, vol. VT-27, pp. 211–219, Nov. 1978.

[25] F. Adachi, "Periodic switching diversity effect on co-channel interference performance of a digital FM land mobile radio," *IEEE Trans. Veh. Technol.*, vol. VT-27, pp. 220–223, Nov. 1978.

[26] H.-C. Yang, M.-S. Alouini, and M. K. Simon, "Average error rate of NCFSK with multi-branch post-detection switched diversity," in *Proc. IEEE VEhicular Technology Conf. (VTC'02-Fall)*, Vancouver, BC, Canada, Sep. 2002, vol. 1, pp. 366–370.

[27] M. K. Simon and M.-S. Alouini, "Probability of Error for noncoherent M-ary orthogonal FSK With Post-detection Switched Combining," *IEEE Trans. Commun.*, vol. 51, pp. 1456–1462, Sep. 2003.

[28] S. Haghani and N. C. Beaulieu, "Revised Analyses of Postdetection Switched Combining in Nakagami-m Fading," *IEEE Trans. Commun.*, vol. 53, pp. 1587–1594, Sep. 2005.

[29] S. Haghani and N. Beaulieu, "Revised Analyses of Postdetection Switch-and-Stay Diversity in Rician Fading," *IEEE Trans. Commun.*, pp. 1175–1178, Jul. 2006.

[30] Y. L. Tong, *The Multivariate Normal Distribution.* New York: Springer-Verlog, 1990.

[31] V. A. Aalo, "Performance of maximal-ratio diversity systems in a correlated Nakagami-fading environment," *IEEE Trans. Commun.*, vol. 43, pp. 2360–2369, Aug. 1995.

[32] S. Haghani and N. C. Beaulieu, "Predetection Switched Combining in Correlated Rician Fading," *to appear in IEEE Trans. on Wireless Commun.*, 2007.

[33] G. Chyi, J. G. Proakis, and C. M. Keller, "On the symbol error probability of maximum-selection diversity reception schemes over a Rayleigh fading channel," *IEEE Trans. Commun.*, vol. 37, pp. 79–83, Jan. 1989.

[34] R. Annavajjala, A. Chockalingam, and L. B. Milstein, "Further Results on Selection Combining of Binary NCFSK Signals in Rayleigh Fading Channels," *IEEE Trans. Commun.*, vol. 52, pp. 939–952, Jun. 2004.

[35] A. Papoulis and S. U. Pillai, *Probability, Random Variables and Stochastic Processes*, 4th ed. New York, USA: McGraw-Hill, 2002.

[36] A. H. Nuttall, "Some Integrals Involving the Q_M Function," *IEEE Trans. Inform. Theory*, vol. 37, pp. 95–96, Jan. 1975.

[37] S. Haghani and N. C. Beaulieu, "M-ary NCFSK with $S + N$ Selection Combining in Rician Fading," *IEEE Trans. on Commun.*, pp. 491–498, Mar. 2006.

[38] S. Haghani and N. C. Beaulieu, "SER of M-ary NCFSK with $S + N$ Selection Combining in Nakagami Fading for Integer m," *IEEE Trans. on Wireless Commun.*, pp. 3050–3055, 2006.

[39] M. K. Simon and M.-S. Alouini, "Average Bit-Error Probability Performance for Optimum Diversity Combining of Noncoherent FSK Over Rayleigh Fading Channels," *IEEE Trans. Commun.*, vol. 51, pp. 566–569, Apr. 2003.

[40] C. M. Lo and W. H. Lam, "Average SER for M-ary modulation systems with space diversity over independent and correlated Nakagami-m fading channels," *IEE Commun. Proc.*, vol. 148, pp. 377–384, Dec. 2001.

[41] P. M. Hahn, "Theoretical Diversity Improvement in Multiple Frequency Shift Keying," *IRE Trans. Commun. System.*, vol. 37, pp. 177–184, Jun. 1962.

[42] A. Annamalai and C. Tellambura, "A Moment-Generating Function (MGF) Derivative-Based Unified Analysis of Incoherent Diversity Reception of M-ary Orthogonal Signals over Independent and Correlated Fading Channels," *International Journal of Wireless Information Networks*, vol. 10, pp. 41–56, Jan. 2003.

[43] X. Zhang and N. C. Beaulieu, "Performance Analysis of Generalized Selection Combining in Generalized Correlated Nakagami-m Fading," *IEEE Trans. Commun.*, pp. 2103–2112, Nov. 2006.

[44] V. A. Aalo, "Performance of maximal-ratio diversity systems in a correlated Nakagami-fading environment," *IEEE Trans. Commun.*, vol. 43, pp. 2360–2369, Aug. 1995.

[45] Q. T. Zhang, "Maximal-ratio combining over Nakagami fading channels with an arbitrary branch covariance matrix," *IEEE Trans. Veh. Technol.*, vol. 48, pp. 1141–1150, Jul. 1999.

[46] M. Schwartz, W. R. Bennett, and S. Stein, *Communications Systems and Techniques*. New York: McGraw-Hill, 1966.

[47] Y.-C. Ko, M.-S. Alouini, and M. K. Simon, "Average SNR of dual selection combining over correlated Nakagami-m fading channels," *IEEE Commun. Lett.*, vol. 4, pp. 12–14, Jan. 2000.

[48] D. A. Zogas, G. K. Karagiannidis, and S. A. Kotsopoulos, "On the average output SNR in selection combining with three correlated branches over Nakagami-m fading channels," *IEEE Trans. on Wireless Commun.*, vol. 3, pp. 25–28, Jan. 2004.

[49] G. K. Karagiannidis, D. A. Zogas, and S. A. Kotsopoulos, "Performance analysis of triple selection diversity over exponentially correlated Nakagami-m fading channels," *IEEE Trans. Commun.*, vol. 51, pp. 1245–1248, Aug. 2003.

[50] O. C. Ogweje and Q. T. Zhang, "Performance of Selection Diversity System in Correlated Nakagami fading," in *Proc. IEEE Vehicular Technology Conf.*, New York, USA, 1997, pp. 1488–1492.

[51] M. K. Simon and M.-S. Alouini, "A unified performance analysis of digital communication with dual selective combining diversity over correlated Rayleigh and Nakagami-m fading channels," *IEEE Trans. Commun.*, vol. 47, pp. 33–44, Jan. 1999.

[52] Q. T. Zhang and H. G. Lu, "A general analytical approach to multi-branch selection combining over various spatially correlated fading channels," *IEEE Trans. Commun.*, vol. 50, pp. 1066–1073, Jul. 2002.

[53] Y. Chen and C. Tellambura, "Performance Analysis of Three-Branch Selection Combining Over Arbitrarily Correlated Rayleigh-Fading Channels," *IEEE Trans. on Wireless Commun.*, vol. 4, pp. 861–865, May 2005.

[54] S. Haghani and N. C. Beaulieu, "M-ary NCFSK with $S + N$ Selection Combining in Rician Fading," *IEEE Trans. Commun.*, vol. 54, pp. 491–498, Mar. 2006.

[55] M. K. Simon and M.-S. Alouini, "A Unified Performance Analysis of Digital Communication with Dual Selective Combining Diversity over Correlated Rayleigh and Nakagami-m Fading Channels," *IEEE Trans. on Commun.*, vol. 47, pp. 33–43, Jan. 1999.

[56] C. Tellambura, A. Annamalai, and V. K. Bhargava, "Closed form and infinite series solutions for the MGF of a dual-diversity selection combiner output in bivariate Nakagami fading," *IEEE Trans. Commun.*, vol. 51, pp. 539–542, Apr. 2003.

[57] X. Dong and N. C. Beaulieu, "Optimal maximal ratio combining with correlated diversity branches," *IEEE Commun. Lett.*, vol. 6, pp. 22–24, Apr. 2002.

[58] K. Dietze, C. B. Dietrich, and W. L. Stutzman, "Analysis of a two-branch maximal ratio and selection diversity system with unequal SNRs and correlated inputs for a Rayleigh fading channel," *IEEE Trans. on Wireless Commun.*, vol. 1, pp. 274–281, Apr. 2002.

[59] V. Veeravalli, "On performance analysis for signaling on correlated fading channels ," *IEEE Trans. Commun.*, vol. 49, pp. 1879–1883, Nov. 2001.

[60] Y.-C. Ko, M.-S. Alouini, and M. K. Simon, "Average SNR of dual selection combining over correlated Nakagami-m fading channels," *IEEE Commun. Lett.*, vol. 4, pp. 12–14, Jan. 2000.

[61] D. A. Zogas and G. K. Karagiannidis, "Infinite-series representations associated with the bivariate Rician distribution and their applications," *IEEE Trans. Commun.*, vol. 53, pp. 1790–1794, Nov. 2005.

[62] N. Sagias, G. K. Karagiannidis, D. A. Zogas, P. T. Mathiopoulos, and G. S. Tombras, "Performance analysis of dual selection diversity in correlated Weibull fading channels," *IEEE Trans. on Commun.*, vol. 52, pp. 1063–1067, Jul. 2004.

[63] G. Karagiannidis, "Performance analysis of SIR-based dual selection diversity over correlated Nakagami-m fading channels," *IEEE Trans. Veh. Technol.*, vol. 52, pp. 1207–1216, Sep. 2003.

[64] F. Adachi, K. Ohno, and M. Ikura, "Postdetection selection diversity reception with correlated, unequal average power Rayleigh fading signals for $\pi/4$-shift QDPSK mobile radio," *IEEE Trans. Veh. Technol.*, vol. 41, pp. 199–210, May 1992.

[65] P. S. Bithas, G. K. Karagiannidis, N. C. Sagias, and D. A. Z. P. M. P.T., "Dual-Branch Diversity Receivers over Correlated Rician Fading Channels," in *Proc. IEEE Veh. Technol. Conf.*, Sep. 2005, vol. 4, pp. 2642–2646.

[66] G. M. Vitetta, U. Mengali, and D. P. Taylor, "An error probability formula for noncoherent orthogonal binary FSK with dual diversity on correlated Rician channels," *IEEE Commun. Lett.*, vol. 3, pp. 43–45, Feb. 1999.

[67] P. K. Mallik, M. Z. Win, and J. H. Winters, "Performance of dual-diversity predetection EGC in correlated Rayleigh fading with unequal branch SNRs," *IEEE Trans. Commun.*, vol. 50, pp. 43–45, Jul. 2002.

[68] H. R. Schwarz, *Numerical analysis : a comprehensive introduction.* New York: Wiley, 1989.

[69] Y. Chen and C. Tellambura, "Moment Analysis of the Equal Gain Combiner Output in Equally Correlated Fading Channels," *IEEE Trans. Veh. Technol.*, vol. 54, pp. 1971–1979, Nov. 2005.

[70] T. Eng, N. Kong, and L. B. Milstein, "Comparison of diversity combining techniques for Rayleigh-fading channels," *IEEE Trans. Commun.*, vol. 44, pp. 1117–1129, Sep. 1996.

[71] N. Kong and L. B. Milstein, "Average SNR of a generalized diversity selection combining scheme," *IEEE Commun. Lett.*, vol. 3, pp. 57–59, Mar. 1999.

[72] M. Z. Win and J. H. Winters, "Virtual branch analysis of symbol error probability for hybrid selection/maximal-ratio combining in Rayleigh fading," *IEEE Trans. Commun.*, vol. 49, pp. 1926–1934, Nov. 2001.

[73] M.-S. Alouini and M. K. Somon, "An MGF-based performance analysis of generalized selection combining over Rayleigh fading channels," *IEEE Trans. Commun.*, vol. 48, pp. 401–415, Mar. 2000.

[74] M. Z. Win and J. H. Winters, "Analysis of hybrid selection/maximal-ratio combining in Rayleigh fading," *IEEE Trans. Commun.*, vol. 47, pp. 1773–1776, Dec. 1999.

[75] A. Annamalai, G. K. Deora, and C. Tellambura, "Unified analysis of generalized selection diversity with normalized threshold test per branch," in *Proc. IEEE Wireless Commununications Networking Conf.*, New Orleans, USA, Mar. 2003, pp. 752–756.

[76] N. Kong and L. Milstein, "SNR of generalized diversity selection combining with nonidentical Rayleigh fading statistics," *IEEE Trans. Commun.*, vol. 48, pp. 1266–1271, Aug. 2000.

[77] M. K. Simon and M.-S. Alouini, "A compact performance analysis of generalized selection combining with independent but nonidentically distributed Rayleigh fading paths," *IEEE Trans. Commun.*, vol. 50, pp. 1409–1412, Sep. 2002.

[78] Y. Chen and T. Tellambura, "A new hybrid generalized selection combining scheme and its performance over fading channels," in *Proc. Wireless Communication and Networking Conf.*, Atlanta, USA, Mar. 2004, vol. 2, pp. 926–931.

[79] A. Annamalai, G. K. Deora, and C. Tellambura, "Theoretical diversity improvement in GSC(N, L) receiver with nonidentical fading statistics," *IEEE Trans. Commun.*, vol. 53, pp. 1027–1035, Jun. 2005.

[80] A. Ramesh, A. Chockalingam, and L. B. Milstein, "Performance analysis of generalized selection combining of M-ary NCFSK signals in Rayleigh fading channels," in *Proc. IEEE International Conf. on Communications*, May 2003, vol. 4, pp. 2773–2778.

[81] M. Z. Win and R. K. Mallik, "Error Analysis of Noncoherent M-ary FSK with Postdetection EGC over Correlated Nakagami and Rician Channels," *IEEE Trans. Commun.*, vol. 50, pp. 378–383, Mar. 2002.

[82] S. Haghani and N. C. Beaulieu, "Revised Analyses of Postdetection Switched Combining in Nakagami-m Fading," *IEEE Trans. Commun.*, pp. 1587–1594, Sep. 2005.

[83] A. Annamalai and C. Tellambura, "Error Rates for Namakami-m Fading Multichannel Reception of Binary and M-ary Signals," *IEEE Trans. Commun.*, vol. 49, pp. 58–68, Jan. 2001.

[84] J. F. Weng and S. H. Leung, "Analysis of M-ary FSK square law combiner under Nakagami fading conditions," *Electron. Lett.*, vol. 33, pp. 1671–1673, Sep. 1997.

[85] M. K. Simon and M.-S. Alouini, "Bit Error Probability of Noncoherent M-ary Orthogonal Modulation over Generalized Fading Channels," *Journal of Communication and Networks*, vol. 1, pp. 111–117, Jun. 1999.

[86] V. Aalo, O. Ugweje, and R. Sudhakar, "Perfromance analysis of a DS/CDMA system with noncoherent M-ary orthogonal modulation in Nakagami fading," *IEEE Trans. on Vehicular Technol.*, vol. 47, pp. 20–29, Feb. 1998.

[87] P. Y. Kam, "Error Probabilities of MDPSK Over the Nonselective Rayleigh Fading Channel with Diversity Reception," *IEEE Trans. Commun.*, vol. 51, pp. 220–224, Feb. 1991.

[88] A. A. Abu-Dayya and N. C. Beaulieu, "Micro- and macrodiversity NCFSK (DPSK) on shadowed Nakagami-fading channels," *IEEE Trans. Commun.*, vol. 42, pp. 2693–2702, Sep. 1994.

[89] P. Y. Kam, T. P. Soh, and C. S. Ng, "Further Results on the Bit Error Probabilities of MDPSK over Nonselective Rayleigh Fading Channel with Diversity Reception," *IEEE Trans. Commun.*, vol. 43, pp. 2732–2741, Nov. 1995.

[90] C. M. Lo and W. H. Lam, "Probability of Symbol Error for MPSK, MDPSK and Noncoherent MFSK with MRC and SC Space Diversity in Nakagami-m Fading Channel," in *Proc. Wireless Communication and Networking Conf.*, Chicago, IL, Sep. 2000, vol. 3, pp. 23–28.

[91] H. Fu and P. Y. Kam, "Performance Comparison of Selection Combining Schemes for Binary DPSK on Nonselective Rayleigh-Fading Channels With Interference," *IEEE Trans. Wireless Commun.*, vol. 51, pp. 192–201, Jan. 2005.

[92] P. J. Crepeau, "Uncoded and Coded Performance of MFSK and DPSK in Nakagami Fading Channels," *IEEE Trans. Commun.*, vol. 40, pp. 487–493, Mar. 1992.

[93] U. Charash, "Reception through Nakagami fading multipath channels with random delays," *IEEE Trans. Commun.*, vol. 27, pp. 657–670, Apr. 1979.

[94] G. F. Montgomery, "Message error in diversity frequency-shift reception," *Proc. IRE.*, vol. 42, pp. 1184–1187, Jul. 1954.

[95] F. Patenaude, J. H. Lodge, and J.-Y. Chouinard, "Noncoherent Diversity Reception Over Nakagami-Fading Channels," *IEEE Trans. Commun.*, vol. 46, pp. 985–991, Aug. 1998.

[96] J. F. Weng and S. H. Leung, "Analysis of DPSK with equal gain combining in Nakagami fading channels," *Electron. Lett.*, vol. 33, pp. 654–656, Apr. 1997.

[97] S. Haghani and N. C. Beaulieu, "Symbol error rate performance of m-ary ncfsk with $s + n$ selection combining in rician fading," in *Proc. IEEE International Conf. on Communications*, Seoul, Korea, 16-20 May 2005, vol. 4, pp. 2500–2505.

[98] Y.-C. Ko and T. Luo, "Effect of Noise Imbalance on Dual-MRC over Rayleigh Fading Channels," *IEEE Trans. on Wireless Commun.*, vol. 5, pp. 514–518, Mar. 2006.

[99] S. Okui, "Probability of co-channel interference for selection diversity reception in the Nakagami m-fading channel," *Proc. Inst. Elec. Eng.*, vol. 139, pp. 91–94, Feb. 1992.

[100] G. Fedele, I. Izzo, and M. Tanda, "Dual diversity reception of m-ary DPSK signals over Nakagami fading channels," in *Proc. IEEE Int. Symp. Personal, Indoor, and Mobile Communications PIMRC'95*, Toronto, ON, Sep. 1995, pp. 1195–1201.

[101] S. Haghani and N. Beaulieu, "Predetection switched combining in correlated Rician fading," *submitted to IEEE Trans. on Wireless Commun.*, vol. 38, pp. 565–567, May 1990.

[102] Y. Ma and Q. T. Zhang, "Accurate Evaluation for MDPSK With Noncoherent Diversity," *IEEE Trans. Commun.*, vol. 50, pp. 1189–1200, Jul. 2002.

[103] Y. Ma and T. J. Lim, "Bit Error Probability for MDPSK and NCFSK over Arbitrary Rician Fading Channels," *IEEE J. Select. Areas Commun.*, vol. 18, pp. 2179–2189, Nov. 2000.

[104] S. Zhang, J. Wang, P. Y. Kam, and P. Ho, "Bit Error Probabilities of MDPSK over Correlated Nonselective Rayleigh Fading Channel With Diversity Reception," in *Proc. Int. Conf. on Commun. Syst.*, Nov. 2002, vol. 1, pp. 539–543.

[105] M. A. Smadi and V. K. Prabhu, "Postdetection EGC Diversity Receivers for Binary and Quaternary DPSK Systems Over Fading Channels," *IEEE Trans. Veh. Technol.*, vol. 54, pp. 1030–1036, May 2005.

[106] M. Nakagami, "The m-distribution- A General Formula of Intensity Distribution of Rapid Fading," in *Statistical Methods of Radio Wave Propagation*, W. G. Hoffman, Ed. Oxford, U.K., 1960.

[107] H. Fu and P. Y. Kam, "Performance of Optimum and Suboptimum Combining Diversity Reception for Binary DPSK over Independent, Nonidentical Rayleigh Fading Channels," Seoul, Korea, May 2005.

[108] J. W. Craig, "A new simple and exact result for calculating the probability of error for two-dimensional signaling constellation," in *Proc. IEEE Military Conf. MILCOM 91*, May 1991, vol. Boston, MA, pp. 25.5.1–25.5.5.

[109] X. Dong, N. C. Beaulieu, and P. H. Wittke, "Error probabilities of two-dimensional m-ary signaling in fading," *IEEE Trans. Commun.*, vol. 47, pp. 352–355, Mar. 1999.

[110] X. Dong, N. C. Beaulieu, and P. H. Wittke, "Signaling constellations for fading channels," *IEEE Trans. Commun.*, vol. 47, pp. 703–714, May 1999.

[111] W. T. Webb and R. Steele, "Variable rate QAM for Mobile Radio," *IEEE Trans. Commun.*, vol. 43, pp. 2223–2230, Jul. 1995.

[112] W. T. Webb, "Spectrum efficiency of Multilevel Modulation Schemes in Mobile Radio Communications," *IEEE Trans. Commun.*, vol. 43, pp. 2344–2349, Aug. 1995.

[113] J. Lu, T. Tjhung, and C. Chai, "Error Probability Performance of L-Branch Diversity Reception of MQAM in Rayleigh Fading," *IEEE Trans. Commun.*, vol. 46, Feb. 1998.

[114] M.-S. Alouini and A. Goldsmith, "A unified approach for calculating error rates of linearly modulated signals over generalized fading channels," *Proc. Int. Conf. on Commun.*, vol. 1, pp. 459–463, Jun. 1998.

[115] L. R. Kahn, "Ratio Squarer," *Proc. IRE (Corresp.)*, vol. 42, pp. 1954, Nov. 1954.

[116] H. A. Abdel-Ghaffar and S. Pasupathy, "Asymptotic Performance of M-ary and Binary Signals over Multipath/Multichannel Rayleigh and Ricean Fading," *IEEE Trans. Commun.*, vol. 48, Nov. 1995.

[117] X. Dong and N. C. Beaulieu, "New Analytical Expressions for Probability of Error for classes of orthogonal signals in Rayleigh fading," in *Globecom'99*, Dec. 1999, vol. Rio de Janeiro, Brazil, pp. 2528–2533.

[118] A. Annamalai, C. Tellambura, and V. K. Bhargava, "Exact evaluation of maximal-ratio and equal-gain diversity receivers for M-ary QAM on Nakagami fading channels," *IEEE Trans. Commun.*, vol. 47, pp. 1335–1344, Sep. 1999.

[119] E. Kreyszig, *Advanced Engineering Mathematics*, 4th ed. New York, USA: John Wiley & Sons, 1979.

[120] T. M. Apostol, *Mathematical Analysis*, 2nd ed. Reading, Massachusettes: Addison-Wesley, 1974.

[121] G. Hardy, J. Littlewood, and G.Pólya, *Inequalities*, 2nd ed. Cambridge, UK: Cambridge University Press, 1952.

[122] L. Hanzo, T. Webb, and T. Keller, *Single- and Multi-carrier Quadrature Amplitude Modulation: Principles and Applications for Personal Communications, WLANs and Broadcasting.* Chinchester, UK: Wiley, 2002.

[123] B. P. Lahti, *Modern Digital and Analog Communication System*, 3rd ed. Oxford: Oxford University Press, 1998.

[124] T. S. Rappaport, *Wireless Communications Principles and Practice*, 2nd ed. New Jersey: Prentice Hall PTR, 2002.

[125] S. Ross, *A First Course in Probability*, 6th ed. Upper Saddle River, NJ: Prentice Hall, 2002.

[126] M. K. Simon, S. M. Hinedi, and W. C. Lindsey, *Digital Communication Techniques: Signal Design and Detection.* Upper Saddle River, NJ: Prentice Hall, 1995.

[127] F. Xiong, *Digital Modulation Techniques.* 685 Canton St. MA 02062: Artech House Inc., 2000.

[128] M. J. Gans, "A Power-Spectral Theory of Propagation in the mobile radio environment," *IEEE Trans. Veh. Tech.*, vol. 80, no. VT-16, pp. 27–38, Feb. 1972.

[129] S. O. Rice, "Mathematical Analysis of Random Noise," *Bell System Tech. J.*, vol. 23, pp. 282–332, Jul. 1944.

[130] H. Erben, S. Zeisberg, and H. Nuszkowski, "BER performance of a hybrid SC/MRC 2DPSK RAKE receiver in realistic mobile channels," in *Proc. Annual Int. Veh. Tech. Conf.*, Stockhom, Sweden, Jun. 1994, vol. 2, pp. 738–741.

[131] M. Z. Win and R. A. Schultz, "On the energy capture of ultra-wide bandwidth signals in dense multipath environments," *IEEE Commun. Lett.*, vol. 2, pp. 245–247, Sep. 1998.

[132] M. Z. Win and Z. A. Kostić, "Impact of spreading bandwidth on Rake reception in dense multipath channels," in *Proc. 8th Comm. Theory Mini Conf.*, Vancouver, Canada, Jun. 1999, vol. 2, pp. 78–82.

[133] M. Z. Win and Z. A. Kostić, "Virtual path analysis of selective Rake receiver in dense multipath channels," *IEEE Commun Lett.*, vol. 3, pp. 308–310, Nov. 1999.

[134] M. Z. Win, G. Chrisikos, and N. R. Sollenberger, "Performance of Rake reception in dense multipath channels: Implications of spreading bandwidth and selection diversity order," *IEEE J. Select. Areas Commun.*, vol. 18, pp. 1516–1525, Aug. 2000.

[135] N. Kong and L. B. Milstein, "Combined average SNR of a generalized diversity selection combining scheme," in *Proc. IEEE Int. Conf. on Commun.*, Atlanta, GA, Jun. 1998, vol. 3, pp. 1556–1560.

[136] M. Z. Win and J. H. Winters, "Analysis of hybrid selection/maximal-ratio combining of diversity branches with unequal SNR in Rayleigh fading," in *Proc. 49th Annual Int. Veh. Technol. Conf.*, Houston, TX, May 1999, vol. 1, pp. 215–220.

[137] M. Z. Win and J. H. Winters, "Analysis of hybrid selection/maximal-ratio combining in Rayleigh fading," in *Proc. IEEE Int. Conf. on Commun.*, Vancouver, Canada, Jun. 1999, vol. 1, pp. 6–10.

[138] M. K. Simon and D. Divsalar, "Some new twists to problems involving the Gaussian probability integral," *IEEE Trans. Commun.*, vol. 46, pp. 200–210, February 1998.

Appendix A

In this appendix, we derive (3.52). The main step in deriving (3.52) is to simplify the integrals

$$J_k = \int_{w_{T_i}}^{\infty} f_{W_{i1}}(w)[F_{W_{i2}}(w)]^{M-1}dw, \quad k = 1, 2 \tag{A.1}$$

and

$$L_k = \int_0^{\infty} \left\{ \int_0^{\infty} F_{W_{i1}|Z}(w_{T_i}) F_{W_{\bar{i}1}|Z}(w) f_Z(z) dz \right\} (F_{W_{i2}}(w))^{M-2} f_{W_{i2}}(w) dw, \quad k = 1, 2 \tag{A.2}$$

that appear in (3.45). These integrals are simplified below for $k = 1$. Similar results can be obtained for $k = 2$. Substituting (3.49) and (3.50) in (A.1), and using standard integration techniques we obtain a closed-form expression for J_1 as

$$J_1 = \sum_{i=0}^{M-1} \binom{M-1}{i} \frac{(-1)^i}{1 + i(1 + \bar{\gamma}_1)} \exp\left(- \frac{\eta_{T_1} \bar{\gamma}_1 (1 + i(1 + \bar{\gamma}_1))}{4(1 + \bar{\gamma}_1)} \right). \tag{A.3}$$

Next we calculate I_1. Substituting (3.12), (5.13), (3.50) and (3.51) in (A.2) and using the change of variable $y = w/(4E_s N_0)$ we obtain

$$\begin{aligned} L_1 = \int_0^{\infty} \int_0^{\infty} & \left[1 - Q_1\left(\sqrt{a_1 z}, \sqrt{b_1} \right) \right] \left[1 - Q_1\left(\sqrt{a_2 z}, \sqrt{b_2 w} \right) \right] \\ & \times (1 - \exp(-y))^{M-2} \exp(-y) \exp(-z) dz dy \end{aligned} \tag{A.4}$$

where for notational simplicity we have defined $a_1 = 2\bar{\gamma}_1 \rho / (1 + \bar{\gamma}_1 (1 - \rho))$, $b_1 = \eta_{T_1} \bar{\gamma}_1 / (2(1 + \bar{\gamma}_1 (1 - \rho)))$, $a_2 = 2\bar{\gamma}_2 \rho / (1 + \bar{\gamma}_2 (1 - \rho))$ and $b_2 = 2/(1 + \bar{\gamma}_2 (1 - \rho))$.

Next, expanding $(1-\exp(-y))^{M-2}$ in the above equation, (A.4) can be written as

$$L_1 = \sum_{i=0}^{M-2} (-1)^i (L_{11} + L_{12} + L_{13} + L_{14}) \tag{A.5a}$$

where

$$L_{11} = \int_0^\infty \int_0^\infty \exp(-z)\exp(-(1+i)y)dzdy \tag{A.5b}$$

$$L_{12} = \int_0^\infty \int_0^\infty Q_1\left(\sqrt{a_1 z}, \sqrt{b_1}\right)\exp(-z)\exp(-(1+i)y)dzdy \tag{A.5c}$$

$$L_{13} = \int_0^\infty \int_0^\infty Q_1\left(\sqrt{a_2 z}, \sqrt{b_2 y}\right)\exp(-z)\exp(-(1+i)y)dzdy \tag{A.5d}$$

$$L_{14} = \int_0^\infty \int_0^\infty Q_1\left(\sqrt{a_1 z}, \sqrt{b_1}\right) Q_1\left(\sqrt{a_2 z}, \sqrt{b_2 y}\right)\exp(-z)\exp(-(1+i)y)dzdy. \tag{A.5e}$$

Using standard integration techniques, L_{11} can be calculated as

$$L_{11} = \frac{1}{i+1}. \tag{A.6}$$

For L_{12}, using [18, eq. (B.28)] we obtain

$$L_{12} = \frac{1}{i+1}\exp\left(\frac{b_1}{2+a_1}\right). \tag{A.7}$$

Similarly, using [18, eq. (B.28)] one obtains a closed-form expression for L_{13} as

$$L_{13} = \frac{2+a_2}{(i+1)(2+a_2)+b_2}. \tag{A.8}$$

To calculate L_{14}, using [18, eq. (B.42)] we first integrate over z to obtain

$$\begin{aligned} L_{14} = \int_0^\infty \Bigg\{ & \exp\left(-\frac{b_1}{a_1+2}\right)\left[1 - Q_1\left(\sqrt{\frac{b_2(a_1+2)y}{a_1+a_2+2}}, \sqrt{\frac{a_1 a_2 b_1}{(a_1+2)(a_1+a_2+2)}}\right)\right] \\ & + \exp\left(-\frac{b_2 y}{a_2+2}\right) Q_1\left(\sqrt{\frac{a_1 a_2 b_2 y}{(a_2+2)(a_1+a_2+2)}}, \sqrt{\frac{b_1(a_2+2)}{a_1+a_2+2}}\right)\Bigg\} \\ & \times \exp(-(i+1)y)dy. \end{aligned} \tag{A.9}$$

Next, using [18, eq. (B.28)] twice and after some mathematical manipulation, (A.9) reduces to

$$L_{14} = \frac{1}{i+1}\exp\left(-\frac{b_2}{a_2+2}\right)\left[1-\exp\left(-\frac{(i+1)A_2}{a_1+2(i+1)}\right)\right] + \frac{1}{2A_5}\exp\left(-\frac{A_4A_5}{A_3+2A_5}\right) \tag{A.10a}$$

where

$$A_1 = \frac{b_2(a_1+2)}{a_1+a_2+2} \tag{A.10b}$$

$$A_2 = \frac{a_1a_2b_1}{(a_1+2)(a_1+a_2+2)} \tag{A.10c}$$

$$A_3 = \frac{a_1a_2b_2}{(a_2+2)(a_1+a_2+2)} \tag{A.10d}$$

$$A_4 = \frac{b_1(a_2+2)}{a_1+a_2+2} \tag{A.10e}$$

$$A_5 = i+1+\frac{b_2}{a_2+2}. \tag{A.10f}$$

Finally, combining (A.6)-(A.8) and (A.10) and after some mathematical manipulations we obtain

$$L_1 = \sum_{i=0}^{M-2} \frac{(M-1)\binom{M-2}{i}(-1)^i}{(i+1)((i+1)(1+\bar{\gamma}_2)+1)} \times \left[1-\exp\left(-\frac{\bar{\gamma}_1\eta_{T_1}(i\bar{\gamma}_2+\bar{\gamma}_2+i+2)}{4(\bar{\gamma}_1\bar{\gamma}_2(1-\rho^2)(i+1)+2(1+\bar{\gamma}_1)+(\bar{\gamma}_1+\bar{\gamma}_2)(i+1)+i-\bar{\gamma}_1)}\right)\right]. \tag{A.11}$$

Appendix B

In this appendix, we derive (5.18). Substituting $L = 2$ in (5.17) and expanding the term

$(1 - \exp(-x))^{2M-3}$, we obtain

$$\mathcal{J} = 2(M-1)\sum_{i=0}^{2M-3}\binom{2M-3}{i}(-1)^i\left(\mathcal{J}_1 + \mathcal{J}_2 + \mathcal{J}_3 + \mathcal{J}_4\right) \tag{B.12a}$$

where

$$\mathcal{J}_1 = \int_0^\infty \int_0^\infty \exp(-z)\exp(-(1+i)x)dzdx \tag{B.12b}$$

$$\mathcal{J}_2 = \int_0^\infty \int_0^\infty Q_1\left(\sqrt{a_1 z}, \sqrt{b_1 x}\right)\exp(-z)\exp(-(1+i)x)dzdx \tag{B.12c}$$

$$\mathcal{J}_3 = \int_0^\infty \int_0^\infty Q_1\left(\sqrt{a_2 z}, \sqrt{b_2 x}\right)\exp(-z)\exp(-(1+i)y)dzdx \tag{B.12d}$$

$$\mathcal{J}_4 = \int_0^\infty \int_0^\infty Q_1\left(\sqrt{a_1 z}, \sqrt{b_1 x}\right)Q_1\left(\sqrt{a_2 z}, \sqrt{b_2 x}\right)\exp(-z)\exp(-(1+i)x)dzdx. \tag{B.12e}$$

and where for notational simplicity we have defined $a_i = 2\bar{\gamma}_i\rho_i/(1+\bar{\gamma}_i(1-\rho_i)), i = 1,2$ and $b_i = 2/(1+\bar{\gamma}_i(1-\rho_i)), i = 1,2$. Using standard integration techniques, $\mathcal{J}_1$ can be calculated as

$$\mathcal{J}_1 = \frac{1}{i+1}. \tag{B.13}$$

For $\mathcal{J}_2$, using [18, eq. (B.28)] we obtain

$$\mathcal{J}_2 = \frac{1}{i+1+A_1} \tag{B.14}$$

where A_1 is defined in (5.18b). Similarly, $\mathcal{J}_3$ reduces to

$$\mathcal{J}_3 = \frac{1}{i+1+A_4} \tag{B.15}$$

where A_4 is defined in (5.18c). To calculate $\mathcal{J}_4$, using [18, eq. (B.42)] we first integrate over z to obtain

$$\begin{aligned}\mathcal{J}_4 = \int_0^\infty \Bigg[& \exp\left(-\frac{b_1 x}{a_1+2}\right)\left\{1 - Q_1\left(\sqrt{\frac{b_2(a_1+2)x}{a_1+a_2+2}}, \sqrt{\frac{a_1 a_2 b_1 x}{(a_1+2)(a_1+a_2+2)}}\right)\right\} \\ & + \exp\left(-\frac{b_2 x}{a_2+2}\right) Q_1\left(\sqrt{\frac{a_1 a_2 b_2 x}{(a_2+2)(a_1+a_2+2)}}, \sqrt{\frac{b_1(a_2+2)x}{a_1+a_2+2}}\right)\Bigg] \\ & \times \exp(-(i+1)x)dx.\end{aligned} \tag{B.16}$$

which can be re-written as

$$\begin{aligned}\mathcal{J}_4 = \int_0^\infty & \exp\left(-(A_1+i+1)x\right)\left[1 - Q_1\left(\sqrt{A_2 x}, \sqrt{A_3 x}\right)\right] \\ & + \exp\left(-(A_4+i+1)x\right) Q_1\left(\sqrt{A_5 x}, \sqrt{A_6 x}\right) dx.\end{aligned} \tag{B.17}$$

Next, using [18, eq. (B48)] twice, (B.17) reduces to

$$\begin{aligned}\mathcal{J}_4 = & \frac{1}{A_1+i+1}\left(1 - \frac{A_2 - A_3 + 2(i+1+A_1)}{2\sqrt{(A_2+A_3+2(i+1+A_1))^2 - 4A_2A_3}}\right) + \frac{1}{2(i+1+A_4)} \\ & \times \frac{A_5 - A_6 + 2(i+1+A_4)}{\sqrt{(A_5+A_6+2(i+1+A_4))^2 - 4A_5A_6}}\end{aligned} \tag{B.18}$$

Finally, substituting (B.13)-(B.15) and (B.18) in (B.12), we obtain (5.18).

Vita

Sasan Haghani

EDUCATION

University of Alberta	M.Sc.	Electrical and Computer Engineering September 2000 – July 2002
Isfahan University of Technology	B.Sc.(First Class)	Electrical and Computer Engineering September 1995 – June 2000

AWARDS

- Alberta Ingenuity Fund Scholarship 2002-07
- Alberta Informatics Circle of Research Excellence (iCORE) Scholarship 2002-07
- J. Gordin Kaplan Graduate Student Award. 2004
- University of Alberta International Student Differential Fee Tuition Waiver 2000-01
- First Rank award in the B.Sc., Isfahan University of Technology, Isfahan, IRAN, 2000.

PUBLICATIONS (Accepted or in print)

1. **S. Haghani** and N. C. Beaulieu, "Accurate Analyses of Postdetection Switch-and-Stay Diversity in Rician Fading," *IEEE Transactions on Communications*, vol. 54, pp. 1175-1178, Jul. 2006.

2. **S. Haghani** and N. C. Beaulieu, "M-ary NCFSK with S+N Selection Combining in Rician fading," *IEEE Transactions on Communications*, vol. 54, pp. 491-498, Mar. 2006.

3. **S. Haghani** and N. C. Beaulieu, "Revised Analyses of Postdetection Switched Combining in Nakagami-m Fading," *IEEE Transactions on Communications*, vol. 53, pp. 1587-1594, Sep. 2005.

4. **S. Haghani**, N. C. Beaulieu and M. Z. Win, "Penalty of Hybrid Diversity for Two-Dimensional Signaling in Rayleigh Fading," *IEEE Transactions on Communications*, vol. 52, pp. 694-697, May 2004.

5. **S. Haghani** and N. C. Beaulieu, "Symbol error probability of low-order orthogonal signalings in Rayleigh fading with general diversity combining," *IEEE Communications Letters*, vol. 6, pp. 520 -522, , Dec. 2002,

6. **S. Haghani**, N. C. Beaulieu and M. Z. Win, "Penalty of Hybrid Diversity with Uncoded Modulation in Slow Rayleigh Fading," *IEEE Transactions on Wireless Communications*, vol. 5, Issue 9, pp. 2363-2368, Sep. 2006.

7. **S. Haghani** and N. C. Beaulieu, "SER of M-ary NCFSK with S+N Selection Combining in Nakagami Fading with Integer m," *IEEE Transactions on Wireless Communications*, vol. 5, Issue 11, pp. 3050-3055, Nov. 2006.

8. **S. Haghani** and N. C. Beaulieu, "Predetection Switched Combining in Correlated Rician Fading," accepted in *IEEE Transactions on Wireless Communications* as a Transactions Letter, May 2006.

9. **S. Haghani** and N. C. Beaulieu, "Performance of Two Dual-Branch Postdetection Swith-and-Stay Combining Schemes in Correlated Rayleigh and Rician Fading," accepted in *IEEE Transactions on Communications* as a Transactions Paper, Oct. 2006.

10. **S. Haghani** and N.C. Beaulieu, "Performance Analysis of S+N Selection Diversity Receivers in Correlated Rayleigh and Rician Fading", accepted in *IEEE Transactions on Wireless Communications* as a Transactions Paper, Oct. 2006.

11. **S. Haghani**, N. C. Beaulieu and M.Z. Win, "The Penalty of Hybrid Diversity with I.I.D Rayleigh Fading," in *Proc. IEEE International Symposium on Advances in Wireless Communications*,

Victoria, BC, Canada, Sep. 2002, pp. 87-88, Invited paper.

12. **S. Haghani** and N. C. Beaulieu, "SEP of Low-Order Orthogonal Signalings with General Diversity Combining," in *Proc. IEEE International Symposium on Advances in Wireless Communications*, Victoria, BC, Canada, Sep. 2002, pp. 133-134.

13. **S. Haghani**, N. C. Beaulieu and M. Z. Win, "Bounds to the Error Probability of Hybrid Diversity Two-Dimensional Signaling," in *Proc. IEEE Global Telecommunications Conference*, Taipei, Taiwan, Nov. 2002, vol. 2, pp. 1408-1414.

14. **S. Haghani**, N. C. Beaulieu and M. Z. Win, "SNR Penalty of Hybrid Diversity Combining in Rayleigh Fading", in *Proc. IEEE International Conf. on Communications*, Anchorage, AK, USA, May 2003, vol. 4, pp. 2800-2804.

15. **S. Haghani** and N. C. Beaulieu, "Postdetection Switch-and-Stay Combining in Nakagami-m Fading", in *Proc. IEEE Vehicular Technology Conf.*, Los Angeles, CA, USA, Sep. 2004, vol. 3, pp. 1781-1785.

16. **S. Haghani** and N. C. Beaulieu, "Performance of Binary NCFSK with Dual-Branch S+N Selection Combining in Rician and Nakagami-m Fading", in *Proc. IEEE Global Communications Conf.*, Dallas, TX, USA, Nov.-Dec. 2004, vol. 5, pp. 2848-2853.

17. **S. Haghani** and N. C. Beaulieu, "Postdetection Switch-and-Stay Combining in Rician Fading", in *Proc. IEEE Wireless Communications Networking Conf.*, New Orleans, LA, USA., Mar. 2005, vol. 2, pp. 872-876.

18. **S. Haghani** and N. C. Beaulieu, "Symbol error rate performance of M-ary NCFSK with S+N Selection Combining in Rician Fading," in *Proc. IEEE International Conf. on Communications,* Seoul, Korea, May 2005, vol. 4, pp. 2500-2505.

19. **S. Haghani** and N. C. Beaulieu, "Error rate of S+N Selection Combining M-ary NCFSK in Nakagami fading," in *Proc. IEEE Global Communications Conf.*, St. Louis, MO, USA, Nov.-Dec. 2005, vol. 3, pp. 1223-1228.

20. **S. Haghani** and N. C. Beaulieu, "BER of BFSK with postdetection switched combining in correlated Rayleigh fading," in *Proc. IEEE International Conf. on Communications*, Istanbul, Turkey, Jun. 11-15, 2006, vol. 11, pp. 5140-5144.

21. **S. Haghani** and N. C. Beaulieu, "Optimization of Predetection Switched Combining in Correlated Rician Fading," to appear in the *Proc. IEEE Vehicular Technology Conf.*, Montreal, Canada, Sept. 25-29 2006.

22. **S. Haghani** and N. C. Beaulieu, "M-ary NCFSK with S+N Selection Diversity in Correlated Rayleigh Fading," accepted for presentation in the 2007 *IEEE Vehicular Technology Conf.* Dublin, Ireland, Apr. 2007.

23. **S. Haghani** and N. C. Beaulieu, "BER of MFSK With Postdetection Switch-and-Stay Combining in Correlated Rayleigh and Rician Fading," accepted for presentation in the 2007 *IEEE International Conf. on Communications,* Glasgow, Scotland,, Jun. 2007.